THE UNIVERSITY *of* EDINBURGH

Spatial Modulation: Theory to Practice

Abdelhamid Younis

A thesis submitted for the degree of Doctor of Philosophy.
The University of Edinburgh.
November 2013

Abstract

" The educated man sees with both heart and mind: the ignoramus sees only with his eyes....." (Ali Bin Aby-Talib (r.a))

Spatial modulation (SM) is a transmission technique proposed for multiple–input multiple–output (MIMO) systems, where only one transmit antenna is active at a time, offering an increase in the spectral efficiency equal to the base–two logarithm of the number of transmit antennas. The activation of only one antenna at each time instance enhances the average bit error ratio (ABER) as inter–channel interference (ICI) is avoided, and reduces hardware complexity, algorithmic complexity and power consumption. Thus, SM is an ideal candidate for large scale MIMO (tens and hundreds of antennas). The analytical ABER performance of SM is studied and different frameworks are proposed in other works. However, these frameworks have various limitations. Therefore, a closed–form analytical bound for the ABER performance of SM over correlated and uncorrelated, Rayleigh, Rician and Nakagami–m channels is proposed in this work. Furthermore, in spite of the low–complexity implementation of SM, there is still potential for further reductions, by limiting the number of possible combinations by exploiting the sphere decoder (SD) principle. However, existing SD algorithms do not consider the basic and fundamental principle of SM, that at any given time, only one antenna is active. Therefore, two modified SD algorithms tailored to SM are proposed. It is shown that the proposed sphere decoder algorithms offer an optimal performance, with a significant reduction of the computational complexity. Finally, the logarithmic increase in spectral efficiency offered by SM and the requirement that the number of antennas must be a power of two would require a large number of antennas. To overcome this limitation, two new MIMO modulation systems generalised spatial modulation (GNSM) and variable generalised spatial modulation (VGSM) are proposed, where the same symbol is transmitted simultaneously from more than one transmit antenna at a time. Transmitting the same data symbol from more than one antenna reduces the number of transmit antennas needed and retains the key advantages of SM.

In initial development simple channel models can be used, however, as the system develops it should be tested on more realistic channels, which include the interactions between the environment and antennas. Therefore, a full analysis of the ABER performance of SM over urban channel measurements is carried out. The results using the urban measured channels confirm the theoretical work done in the field of SM. Finally, for the *first* time, the performance of SM is tested in a practical testbed, whereby the SM principle is validated.

Declaration of originality

I hereby declare that the research recorded in this thesis and the thesis itself was composed and originated entirely by myself in the School of Engineering at The University of Edinburgh.

The exceptions to the above is, as part of the beyond 4G, UK-China bridges project:

- The outdoor urban MIMO channel measurements were provided by Dr. William Thompson and Prof. Mark Beach, university of Bristol.
- The MATLAB code used for the digital signal processing of the experimental data was developed jointly with Dr. Nikola Serafimovski and Dr. Raed Mesleh.
- The data used to obtain the channel statistics was collected by Dr. Pat Chambers, Heriot-Watt university

Abdelhamid Younis

Acknowledgements

“ Praise be to Allah, the Cherisher and Sustainer of the worlds;”

My deepest gratitude goes to my family for their unflagging love and support throughout my life; this thesis would have been impossible without them. I am indebted to my parents, Houssein Alhassi and Mareia Alabar, for their care, love, knowledge and support.

I offer my sincerest gratitude to my supervisor, Professor Harald Haas, for his support, patient, encouragement and advice throughout my PhD. His huge enthusiasm on research and fathomless knowledge in many areas has deeply inspired me. I fully appreciate his continuous support and encouragements, especially during my difficult times in work and life.

My sincere thanks go to Dr. Raed Mesleh and Dr. Sinan Sinanović, for their encouragement, assistance, and insightful comments. My thanks also go to Tessa Grafen for her comments and assistance in pointing out the linguistic errors.

Last but not least, I would like to thank my life–long friends for tirelessly supporting me in their own magical ways throughout my studies

“ Those who do not thank people, they do not thank Allah ”

(The Prophet Muhammad (pbuh))

Contents

List of figures

List of tables

Acronyms and abbreviations

1G	first generation
2G	second generation
3G	third generation
3GPP	third generation partnership project
4G	fourth generation
ABER	average bit error ratio
AMPS	advance mobile telephone systems
AWGN	additive white Gaussian noise
B4G	beyond 4G
BPSK	binary phase shift keying
CDF	cumulative distribution function
CDMA	code–division multiple access
CP	cyclic prefix
CSI	channel state information
D–AMPS	digital advanced mobile phone services
D–BLAST	diagonal Bell Labs layered space–time
DL	downlink
DSP–Tx	digital signal processing at the transmitter
DSP–Rx	digital signal processing at the receiver
E–DCH	enhanced dedicated channel
EGC	equal gain combining
FBE–SM	fractional bit encoding spatial modulation
FDD	frequency division duplex
FDMA	frequency–division multiple access

FEC	forward error correction
FIR	finite impulse response
FO	frequency offset
GPRS	general packet radio service
GNSM	generalised spatial modulation
GSSK	generalised space shift keying
HSDPA	high speed downlink packet access
HSUPA	high speed uplink packet access
IAS	inter-antenna synchronization
ICI	inter–channel interference
IFI	inter–frame interference
IF	intermediate frequency
i.i.d.	identical and independently distributed
IGCH	information-guided channel hopping
IMT–2000	international mobile telecommunications 2000 project
IMT–Advanced	international mobile telecommunications–advanced
ISI	inter-symbol interference
ITU	international telecommunications union
ITU–R	radio communications sector of ITU
LDC	linear dispersion codes
LED	light–emitting diode
LEDs	light–emitting diodes
LoS	line of sight
LS	least squares
LTE	Long Term Evolution
MGF	moment-generation function
MISO	multiple–input single–output
MIMO	multiple–input multiple–output
ML	maximum–likelihood

MMSE	minimum mean squared error
MRC	maximal ratio combining
MRRC	maximum receive ratio combining
NAS	network attached storage
NI	National Instruments
NLoS	non–line of sight
NMP	Nordic Mobile Phone
NMT	Nippon Mobile Telephone
OFDM	orthogonal frequency division multiplexing
OFDMA	orthogonal frequency division multiple access
OLT	Offentlig Landmobil Telefoni
OSM	optical spatial modulation
OW	optical wireless
PAM	pulse amplitude modulation
PA	power amplifier
PEP	pairwise error probability
PDC	personal digital cellular
PDF	probability distribution function
PI	power imbalance
PPM	pulse position modulation
PXIe–Tx	National Instruments (NI)–PXIe chassis at the transmitter
PXIe–Rx	National Instruments (NI)–PXIe chassis at the receiver
QAM	quadrature amplitude modulation
QPSK	quadrature phase shift keying
QoS	quality of service
RF	radio frequency
RRC	root raised cosine
RV	random variable

SISO	single–input single–output
SC	spatial correlation
SCM	selection combining
SD	sphere decoder
SDMA	space–division multiple access
SIMO	single–input multiple–ouput
SM	spatial modulation
SM–Rx	spatial modulation Receiver–centric SD
SM–Tx	spatial modulation Transmit–centric SD
SM–TC	spatial modulation with trellis coding
SMX	spatial multiplexing
SNR	signal to noise ratio
SSK	space shift keying
STC	space–time coding
STBC	space–time block coding
STBC–SM	space–time block coding spatial modulation
STTC	space–time trellis coding
TACS	total access communication system
TCM	trellis coded modulation
TCSM	trellis coded spatial modulation
TDD	time division duplex
TDMA	time–division multiple access
TuCM	turbo coded modulation
UL	user equipment
UL	uplink
UMTS	universal mobile telephone system
V–BLAST	vertical Bell Labs layered space–time
VGSM	variable generalised spatial modulation
VoIP	voice over internet protocol
WARC	world administrative radio conference
WiFi	wireless fidelity

Nomenclature

$\otimes$	Kronecker product
$\mathrm{tr}(\cdot)$	Trace function
$\binom{\cdot}{\cdot}$	The binomial operation
$\lfloor \cdot \rfloor$	The flooring operation
$\tilde{(\cdot)}$	Mean of an arbitrary random variable
$[\cdot]^T$	The transpose operation
$[\cdot]^H$	The Hermitian
$\|\cdot\|_{\mathrm{F}}$	Frobenius norm
$\hat{\cdot}$	Estimated symbol
$\mathrm{E}\{\cdot\}$	Expectation operation
$\mathrm{Re}\{\cdot\}$	Real part of a complex variable
$\mathrm{Im}\{\cdot\}$	Imaginary part of a complex variable
$\mathrm{vec}(\mathbf{B})$	Vectorization operator, where the columns of the matrix $\mathbf{B}$ are stacked in a column vector
$N(\mathbf{x}_t, \mathbf{x})$	The number of bits in error between the transmitted vector $\mathbf{x}_t$ and $\mathbf{x}$
$\bar{\bar{a}}$	Cardinality of a
$\mathbf{0}_{p\times q}$	A $p \times q$ matrix with all–zero entries
$\mathbf{1}_{p\times q}$	A $p \times q$ matrix with all–one entries
$\mathbf{I}_n$	An $n \times n$ identity matrix
E_s	Average energy per transmission
η	Spectral Efficiency
η_ℓ	Number of bits sent in the spatial domain
η_s	Number of bits sent in the constellation domain
M	Constellation size
N_t	Number of transmit antennas
N_r	Number of receive antennas
N_u	Number of active antennas
ℓ_t	Active transmit antenna
s_t	Transmitted symbol

$\mathcal{Q}^{\eta}$	A 2^{η} space containing all possible $(N_t \times 1)$ transmitted vectors
$\mathbf{H}$	An $N_r \times N_t$ multiple–input multiple–output (MIMO) fading channel
$\mathbf{h}_{n_t}$	The n_t–th column of $\mathbf{H}$
h_{n_r,n_t}	The n_r–th entry of $\mathbf{h}_{n_t}$
$\mathbf{H}'$	An $N_r \times N_t$ matrix whose entries are modelled as complex identical and independently distributed (i.i.d.) Gaussian random variables with zero–mean and unit–variance
$\mathbf{L}_{\mathbf{H}}$	Covariance matrix of $\mathbf{H}$
$\mathbf{y}$	Received vector
y_r	The received signal at the receive antenna r
$\mathbf{n}$	additive white Gaussian noise (AWGN) vector
σ_n^2	Noise variance
K	Rician factor
m	m factor for Nakagami–m
$\mathbf{R}_{\text{Tx}}$	Transmitter correlation matrix
$\mathbf{R}_{\text{Rx}}$	Receiver correlation matrix
$\mathbf{R}_c$	Exponential decay model
β	The correlation decay coefficient
β_t	The correlation decay coefficient at the transmitter
β_r	The correlation decay coefficient at the receiver
$\Pr_{\text{error}}$	The conditional pairwise error probability (PEP) of deciding on $\mathbf{x}$ given that $\mathbf{x}_t$ is transmitted
$Q(\cdot)$	The Q–function
$\Phi(\cdot)$	The moment-generation function (MGF)
C	Computational Complexity
$\mathcal{C}_{\text{rel}}$	Relative computational complexity
R	Radius of sphere decoder (SD)
Θ_R	The subset of points (ℓ, s) for $\ell \in \{1, 2, \ldots N_t\}$ and $s \in \{s_1, s_2, \ldots s_M\}$ in the transmit search space that lie inside a sphere with radius R and centred around the received signal

$\gamma(c, d)$	The lower incomplete gamma function
$\Gamma(c)$	The gamma function
$I_0(\cdot)$	The modified Bessel function of the first kind with order zero
Υ	Transmit–antennas which are active for transmission
Υ^i	The index of the i–th antenna in Υ
f_D	Doppler shift
v	The velocity of the moving node
θ	The angle between the signal and the direction of the moving node
λ	The wavelength
c	The speed of light
f_c	The carrier frequency
T_c	The coherence time
$f_D^{\max}$	The maximum Doppler shift
B_c	The coherence bandwidth
f_s	Sample rate
Θ_{n_t}	The pilot sequence transmitted from antenna n_t
$\alpha_{(r,n_t)}$	The channel attenuation coefficient from receive antenna r to transmit antenna n_t

Chapter 1
Introduction

1.1 Introduction, Motivations and Contributions

Multiple–input multiple–output (MIMO) systems offer a significant increase in spectral efficiency in comparison to single antenna systems [1]. An example is spatial multiplexing (SMX) [2], which transmits simultaneously over all the transmit antennas. This method achieves a spectral efficiency that increases linearly with the number of transmit antennas. However, with the exponential increase in wireless data traffic, a large number of transmit antennas (large scale MIMO) should be used [3]. Large scale MIMO systems studied in [4, 5, 6, 7, 8], offer a higher data rate and better average bit error ratio (ABER). However, this comes with the expense of an increase in:

1. Computational complexity, where SMX–maximum–likelihood (ML) optimum receiver searches across all possible combinations, and tries to resolve the inter–channel interference (ICI), caused by transmitting from all antennas simultaneously on the same frequency. The sphere decoder (SD) is proposed to reduce the complexity of the SMX–ML while retaining a near optimum performance [9, 10, 11]. The SD reduces the complexity of the ML decoder by limiting the number of possible combinations. Only those combinations that lie within a sphere centred at the received signal are considered. However, even though SMX–SD offers a large reduction in complexity compared to SMX–ML, it still has a high complexity as it does not avoid ICI.

2. Hardware complexity: In SMX the number of radio frequency (RF) chains is equal to the number of transmit antennas. From [12], RF chains are circuits that do not follow Moore's law in progressive improvement. Therefore, increasing the number of transmit antennas and consequently the number of RF chains increases significantly the cost of real system implementation [13].

3. Energy consumption: RF chains contain Power Amplifiers (PAs) which are responsible for 50–80% of the total power consumption in the transmitter [14]. Therefore, increasing the number of RF chains results in a decrease in the energy efficiency [13].

Thus, SMX may not always be feasible and a more energy efficient and low complexity solution should be considered.

Spatial modulation (SM) is a transmission technology proposed for MIMO wireless systems. It aims to increase the spectral efficiency, of single–antenna systems while avoiding ICI [15].

This is attained through the adoption of a new modulation and coding scheme, which foresees: i) the activation, at each time instance, of a single antenna that transmits a given data symbol (*constellation symbol*), and ii) the exploitation of the spatial position (index) of the active antenna as an additional dimension for data transmission (*spatial symbol*) [16]. Both the *constellation symbol* and the *spatial symbol* depend on the incoming data bits. An overall increase by the base–two logarithm of the number of transmit–antennas of the spectral efficiency is achieved. Note that the number of transmit antennas must be a power of two. The receiver applies the Maximum Likelihood optimum decoder for SM (SM–ML), which performs an exhaustive search over the whole *constellation symbol* and *spatial symbol* space [17]. Activating only one antenna at a time means that only one radio frequency (RF) chain is needed, which significantly reduces the hardware system [18]. Moreover, as only one RF chain is needed, SM offers a reduction in the energy consumption which scales linearly with the number of transmit antennas [13, 19]. Furthermore, the computational complexity of SM–ML is equal to the complexity of single–input multiple–ouput (SIMO) systems, *i.e.* the complexity of SM–ML depends only on the spectral efficiency and the number of receive antennas, and does not depend on the number of transmit antennas. Accordingly, SM appears to be a good candidate for large scale MIMO [20, 21, 22, 23].

The analytical ABER performance of SM over different fading channels has been studied by many researchers. The analytical ABER performance of SM over Rayleigh fading channels is studied in [16, 17, 24]. In [16], the authors studied a suboptimal receiver design, and the symbol error probability is computed by resorting to numerical integrations, which are not easy to compute [20]. In [17], the analytical ABER performance of the ML receiver for SM is studied, and an analytical upper bound is derived. However, from [25], the bound is rather weak. The first closed form upper bound for the ABER performance of SM over Rayleigh channels is proposed in [24]. However, it is only applicable for 1) Rayleigh fading, 2) channels with correlation on the transmitter side only.

The authors in [20] studied the analytical ABER performance of SM over correlated Rician channels, however, the proposed upper bounds are complicated and not easy to compute. Furthermore, the work in [16] is extended to Nakagami–m fading channels in [26, 27], however, 1) it is for suboptimal receivers. 2) it is semi–analytical. 3) correlation is taking into account only for the detection of the constellation symbol [28]. Moreover, the authors in [20, 29, 30], studied the analytical ABER performance of SM over correlated and uncorrelated Nakagami–m fading channels using ML optimal receiver. The authors assumed that

the phase of the Nakagami–m fading channel is a uniformly distributed random variable (RV). However, in [31, 32, 33], it is shown that apart from the very special case of $m = 1$, where Nakagami–m fading corresponds to a Rayleigh fading, the phase of Nakagami–m distribution is not uniform. Hence, the bounds stated in [20, 29, 30] will not hold strictly.

Thus, to the best of the authors' knowledge, there is no tight closed form model for the ABER performance of SM over correlated and uncorrelated generalised fading channels. In this work, a tight closed form bound to compute the ABER for SM over correlated and uncorrelated generalised fading channels is provided. Comparing the framework with Monte Carlo simulations and state–of–the–art literature, it is shown that the new bound:

1. offers an accurate estimation of the ABER;
2. provides an easy–to-calculate closed–form upper bound;
3. is applicable for correlated Rayleigh, Rician and Nakagami–m channels.

Furthermore, the performance of SM is compared with the performance of SMX. It is shown that SM offers nearly the same or slightly better ABER performance than SMX for small scale MIMO. However, SM offers a larger reduction in ABER for large scale MIMO. Moreover, the computational complexity of SM–ML is studied and it is shown that it is equal to the complexity of single–antenna systems. This means that the complexity of SM–ML neither depends on the number of transmit antennas, nor the signal constellation size. Therefore SM is a good candidate for large scale MIMO.

In spite of the low–complexity implementation of SM, there is still potential for further reductions, by limiting the number of possible transmitted *spatial symbol* and *constellation symbol* combinations using the SD principle. However, existing SD algorithms in the literature do not consider the basic and fundamental principle of SM, that at any given time only one antenna is active [9, 10, 11]. Therefore, they cannot be applied to SM, and two modified SD algorithms based on the tree search structure that are tailored to SM are proposed. The first SD is called Receiver–centric SD (Rx–SD). It aims at reducing the complexity from combining the received signal by each receive antenna at the receiver, as long as the Euclidean distance from the received point is less than a given radius. This SD–based detector is especially suitable when the number of receive–antennas is very large. It reduces the size of the search space related to the multiple antennas at the receiver (this search space is denoted by "receive search space"). It will be shown later that there is no loss in either the diversity order or the coding gain, *i.e.* the

ABER is very close to that of the ML detector. However, its main limitation is that it does not reduce the search space related to the number of possible transmitted points (this search space is denoted by "transmit search space"). This prevents the detector from achieving a significant reduction in computational complexity when a high data rate is required.

The second SD is called Transmit–centric (Tx–SD). The Tx–SD algorithm aims at reducing the transmit search space, by examining only those *spatial symbol* and *constellation symbol* combinations that lie inside a sphere with a given radius. However, it is limited to the non–underdetermined MIMO setup ($N_t \leq N_r$), where N_t and N_r are the number of transit and receiver antennas respectively. In [34, 35], it is shown that Tx–SD in [36] can still be used for the case of $(2N_r - 1) \geq N_t > N_r$, where it is referred to as E–Tx–SD. Moreover, in [34, 35] a detector for the case of $N_t > N_r$ referred to as G–Tx–SD is proposed. By using the division algorithm the G–Tx–SD technique [34]: 1) Divides the set of possible antennas to a number of subsets. 2) Performs E–Tx–SD over each subset. 3) Takes the minimum solution of all the sets. However, a simple solution is proposed in this thesis, where all that is needed is to set a constant φ to 0 for $N_t \leq N_r$ and $\varphi = \sigma_n^2$ for $N_t > N_r$, where σ_n^2 is the noise variance. In [34, 35], the normalised expected number of nodes visited by the Tx–SD algorithm is used to compare its complexity with the complexity of the SM–ML. This does not take into account the pre–computations needed by the Tx–SD. In this work, when comparing the complexity of Tx–SD with the complexity of SM–ML and Rx–SD, the pre–computations needed by the Tx–SD are taken into account. Because of those pre–computations, the Tx-SD is not always the best solution, whereas in some cases it is even more complex than SM–ML.

In this work, a careful study of the performance of these two detectors, along with an accurate comparison of their computational complexity is provided. Numerical results show that the proposed solutions provide a substantial reduction in computational complexity with respect to the SM–ML decoder, and no loss in the ABER performance. A closed form expression for the ABER performance of SM–SD is derived, where it is shown that by using it, the initial radius can be chosen such that SM–SD gives an optimal performance. Furthermore, it is shown that SM–Rx is less complex than SM–Tx for lower spectral efficiencies, while SM–Tx is the best solution for higher spectral efficiencies. Finally, numerical results show that SM with SD offers a significant reduction and nearly the same performance when compared to SMX with ML decoder or SD.

The logarithmic increase in spectral efficiency offered by SM and the requirement that the number of antennas must be a power of two would require a large number of antennas. Fractional

bit encoding spatial modulation (FBE–SM) in [37], is proposed to overcome this limitation by using the theory of modulus conversion. By doing so an arbitrary number of transmit antennas can be used. However, FBE–SM suffers from error propagation. Motivated by that, two new MIMO modulation systems, generalised spatial modulation (GNSM) and variable generalised spatial modulation (VGSM), are proposed in this thesis to overcome the limitation in the number of transmit antennas. In GNSM and VGSM the same symbol is transmitted simultaneously from more than one transmit antenna. Hence, more than one antenna is active and transmits the same symbol at a time. GNSM is first proposed in [38] and in [39], where in [38], GNSM with ML–optimum receiver is proposed, and in [39], GNSM with maximal ratio combining (MRC) sub–optimal receiver is proposed. In GNSM the number of active antennas is constant. However, in VGSM the number of active antennas varies from only one active antenna at a time to all antennas being active and transmitting the same symbol. As a result, the number of transmit antennas required by GNSM and VGSM to achieve a certain spectral efficiency and a constellation size is reduced. For example, for a spectral efficiency of $\eta = 4$ and binary phase shift keying (BPSK) modulations, GNSM and VGSM reduces the number of transmit antennas needed by SM, by (37%) and (50%) respectively. The mapping procedure for GNSM and VGSM after grouping the incoming data sequence in groups of η bits, can be summarised in two points:

1) The first η_ℓ bits determine which antenna combination to activate.

2) The last η_s bits are modulated and transmitted through the active antennas.

Transmitting the same data symbol from the active antennas retains the key advantage of SM, which is the complete avoidance of ICI at the receiver, and consequently keeps the low computational complexity, which is equal to the complexity of SIMO systems. At the receiver three decoders are proposed. The first one is the ML–optimum receiver. The other two SDs are Tx–SD and Rx–SD proposed for SM where in this thesis they are extended to be used for GNSM and VGSM.

In this thesis, a careful study of the performance of both systems, GNSM and VGSM, using the three proposed detectors, along with an accurate comparison of their computational complexity is provided. Moreover, a tight closed form expression for the ABER performance of GNSM and VGSM, over correlated and uncorrelated Rayleigh and Rician fading channels is derived. Results show that the proposed schemes, VGSM and GNSM, use a much smaller number of antennas than SM and have significantly lower computational complexity than SMX, while

having a small penalty in the ABER performance. More specifically, VGSM and GNSM reduce the number of transmit antennas by up to (93%) when compared to SM. Furthermore, VGSM and GNSM reduce the computational complexity by at least (40%) when compared to SMX, while having an ABER penalty between $1.5 - 4$ dB. Therefore, the proposed schemes are good candidates for low hardware and computational complexity MIMO solutions.

In this thesis, for the first time real-world channel measurements are used to analyse the performance of SM, where a full analysis of the ABER of SM using measured urban correlated and uncorrelated Rayleigh fading channels is provided. The channel measurements are taken from an outdoor urban MIMO measurement campaign. Moreover, an analytical bound for the ABER of SM is derived and performance results using simulated Rayleigh fading channels are provided. It is shown that the results over the measured urban channels validate the derived analytical bound and the results over the simulated channels. The ABER of SM is compared with the performance of SMX using the measured urban channels for small and large scale MIMO. It is shown that SM offers nearly the same or a slightly better performance than SMX for small scale MIMO. However, SM offers large reduction in ABER for large scale MIMO.

Furthermore, for the first time in the world, the performance of SM is tested on a practical testbed and compared with that for SMX, where National Instruments (NI) testbeds are used. In particular, NI–PXIe–1075 chassis for transmitter and receiver side are used [40]. The design of the testbed, hardware and software, is explained in detail along with the transmission chain. The effect of the physical environment on the channel coefficients is studied, where it is shown that the effects can be modelled as a power imbalance (PI) between the various link pairs in the channel. Moreover, an analytical upper bound for the ABER performance of SM over Rician channels with PI is derived, and compared to the experimental and computer simulation results, where the experimental results validate the analytical bound as well as the computer simulations. Finally the performance of SM is compared with the theoretical and experimental results of SMX.

1.2 Thesis layout

The layout of the thesis can be summarised as follows:

Chapter 2 In this chapter, the key concepts in relation to wireless communications and SM are summarised. The chapter starts with an overview of the history of wireless communications, then introduced MIMO communication systems. In particular, the different types of MIMO transmission systems and channel environments are discussed, along with small–scale propagation models. Furthermore, the idea of SMX, and its advantages and disadvantages is reviewed. After that SM is proposed, and its advantages compared to SMX, along with its limitations, are discussed. Finally, an overview of the latest research in SM is presented.

Chapter 3 In this chapter, an accurate closed–form framework to compute the ABER for SM over correlated and uncorrelated generalised fading channels is provided. Furthermore, the performance of SM is compared with the performance of SMX. It is shown that SM offers nearly the same or slightly better performance than SMX for small scale MIMO. However, SM offers a larger reduction in ABER for large scale MIMO. Finally, the computational complexity of SM–ML is studied and it is shown that it is equal to the complexity of SIMO systems.

Chapter 4 In this chapter, SD algorithms for SM are developed to reduce the computational complexity of ML detectors. Two SDs specifically designed for SM are proposed and analysed in terms of ABER and computational complexity. Using Monte Carlo simulations and mathematical analysis, it is shown that by carefully choosing the initial radius the proposed SD algorithms offer the same ABER as ML detection, with a significant reduction of the computational complexity. A tight closed form expression for the ABER performance of SM–SD is derived, along with an algorithm for choosing the initial radius which provides optimum performance. Also, it is shown that none of the proposed SDs is always superior to the others, but the best SD to use depends on the target spectral efficiency. Finally, the performance of SM–SDs are compared to SMX, applying ML decoder and applying SD. It is shown that for the same spectral efficiency, SM–SD offers up to 84% reduction in complexity compared to SMX–SD, with up to 1 dB better ABER performance than SMX–ML decoder.

Chapter 5 In this chapter, GNSM and VGSM along with three receivers are presented. The first receiver is based on ML principle, and the last two receivers, Tx–SD and Rx–SD, are based on the SM–SD principle presented in Chapter 4. The performance of GNSM and VGSM is analysed, and a tight bound on the ABER performance over correlated and uncorrelated Rayleigh and Rician channels is derived. Furthermore, the performance of GNSM and VGSM is validated through Monte Carlo simulations and compared to the performance of SM and SMX, where it is shown that the proposed schemes, GNSM and VGSM, use a much smaller number of transmit antennas than SM and have a significantly lower computational complexity than SMX, while having a small penalty in the ABER performance.

Chapter 6 In this chapter, for the first time real-world channel measurements are used to analyse the performance of SM, where a full analysis of the ABER of SM using measured urban correlated and uncorrelated Rayleigh fading channels is provided. The channel measurements are taken from an outdoor urban MIMO measurement campaign. Moreover, performance results using simulated Rayleigh fading channels are provided and compared with the analytical bound for the ABER of SM, and the ABER results using the measured urban channels. It is shown that the results using the measured urban channels validate the derived analytical bound and the ABER results using the simulated channels. Finally, the ABER of SM is compared with the performance of SMX using the measured urban channels for small and large scale MIMO. It is shown that SM offers nearly the same or a slightly better performance than SMX for small scale MIMO. However, SM offers a large reduction in the ABER performance for large scale MIMO.

Chapter 7 In this chapter, for the first time in the world the performance of SM is tested on a practical system, where NI testbeds are used. In particular, NI–PXIe–1075 chassis for transmitter and receiver side are used. The design of the testbed, hardware and software, is explained in details along with the transmission chain. The effect of the physical environment on the channel coefficients is studied, where it is shown that it can be modelled as a PI between the various link pairs in the channel. Moreover, computer simulation results are provided and compared with the analytical ABER upper bound, and the experimental results. The experimental results validate the analytical bound as well as the computer simulations.

Chapter 8 This chapter contains the conclusion for the above chapters, a discussion of the limitations and directions for potential future research.

Chapter 2
Background

2.1 History of Wireless Communications

The development of wireless communications began in 1820 after Oersted demonstrated that an electric current produces a magnetic field. After that, in 1831, Michael Faraday showed that a changing magnetic field produces an electric field. From that James Clerk Maxwell in 1864 predicted the existence of electromagnetic radiation and formulated the basic theory of electromagnetics, which formed the basis of wireless technology [41]. Later on, in 1887, Heinrich Hertz verified Maxwell's theory experimentally. Oliver Lodge in 1894 invented the coherer. The coherer is a sensitive device that detect radio signals. It was used to demonstrate wireless communication at a 150 yards distance. However, it was not until Guglielmo Marconi in 1895, that the first radio signal transmission was demonstrated at a distance of approximately 2 km. Later, in 1897, Marconi patented a radio telegraph system and founded the Wireless Telegraph and Signal Company [42,43]. Morse–coded ON–OFF keying was used in mobile radio communications until the 1920s [44]. They were first installed and used in transatlantic ocean vessels to send distress calls, and were even used on the well-known *Titanic* [45]. On the 7th of April 1928 the Detroit Police Department installed the first one–way radio communication system, developed by the department's radio bureau, in its patrol cars [46], while in 1933 the police department in Bayonne, New Jersey, introduced the first two–way mobile radio voice system [47]. In 1948, Calude E. Shannon characterised the limits of reliable communications [48]. Shannon showed that there is a maximum data rate, called channel capacity, for which the error probability is zero, *i.e.* for zero error probability, the data rate has to be lower or equal to the channel capacity [49, 50]. Thus, higher data rates require either more bandwidth or greater signal to noise ratio (SNR) [51]. Since then, wireless systems have been in rapid development to cope with the demand for indoor wireless access to bandwidth–intensive applications such as the Internet, multimedia streaming applications (voice over internet protocol (VoIP)), gaming, and network attached storage (NAS) [52, 53, 54].

The Swedish Mobile Telephone System Administration (Telia, formerly Televerket) was one of the early European mobile communication companies. They put the MTA system created by Ericsson in operation on April 25, 1956. The MTA was a fully automatic, 160 MHz band mobile system using pulsed signalling between the terminal and base station. In 1965, it was upgraded to MTB, where it used dual–tone multi–frequency signalling [55]. In 1966, the first land mobile network in Norway, Offentlig Landmobil Telefoni (OLT), was established, and operated until 1990. In 1981, the OLT was the largest land mobile network in the world with 30,000 mobile subscribers.

First generation (1G) cellular mobile systems were all based on analog frequency modulation. The first fully automatic 1G cellular phone system was nordic mobile phone (NMP), in 1981 [55]. Shortly afterwards, Bell Laboratories invented advance mobile telephone systems (AMPS), where the first commercial AMPS was turned on in Chicago in October 1986 [56,57]. Other early 1G standards are total access communication system (TACS) in United Kingdom, and Nippon Mobile Telephone (NMT) in Japan. Digital second generation (2G) systems, like those based on Global System for Mobile Communications in Europe [58], personal digital cellular (PDC) in Japan, digital advanced mobile phone services (D–AMPS) in the United States, replaced the analog 1G systems, where they enabled improved voice communication, text messaging and access to data networks to go wireless in many of the leading markets [59]. The success of these systems led many researchers to concentrate on improving the performance of wireless communications [60, 61, 62].

The development of the third generation (3G) mobile systems such as universal mobile telephone system (UMTS) and multicarrier CDMA2000 (CDMA2000) [63, 64], along with other wireless systems like general packet radio service (GPRS) and wireless fidelity (WiFi), started after the world administrative radio conference (WARC) of the international telecommunications union (ITU), at its 1992 meeting, identifying the frequencies around 2 GHz that were available for use by future third generation mobile systems. The term 3G was set by the radio communications sector of ITU (ITU–R) through the international mobile telecommunications 2000 project (IMT–2000). Simple requirements for IMT–2000 were defined in 1997 [65]: i) 2048 kbps for indoor office. ii) 384 kbps for outdoor to indoor and pedestrian. iii) 144 kbps for vehicular. iv) 9.6 kbps for satellite. Early 3G systems could not cope at the start with these requirements in practical systems, even though they did in theory [65]. Therefore, researchers focused their efforts on methods to improve the deployed system to cope with the

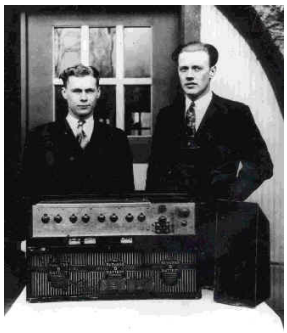

(a) One–way [46]

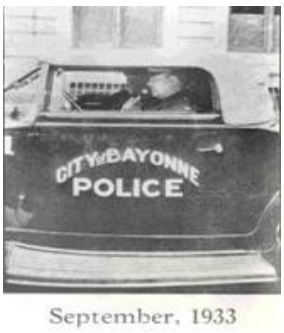

(b) Two–way [47]

Figure 2.1: *First one-way and two–way police radio communications.*

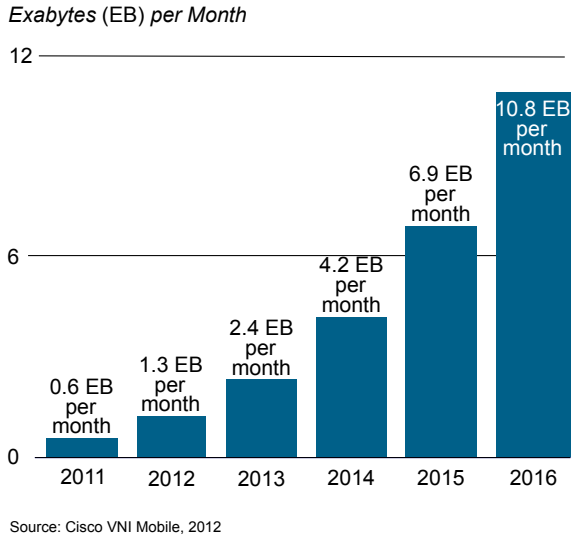

Figure 2.2: *Cisco's forecast for the global demand of mobile data per month [73]*

IMT–2000 requirements and even beyond that. The addition of high speed downlink packet access (HSDPA), enhanced dedicated channel (E–DCH), and high speed uplink packet access (HSUPA) to UMTS introduced 3.5G. Furthermore, the term 3.9G has been widely used to describe IEEE 802.16e standard (Mobile WiMAX), and third generation partnership project (3GPP)'s long term evolution (LTE) [65].

The demand for high data rate and quality of service (QoS) increased due to the convergence of digital wireless networks with the internet, where (as shown in Fig. 2.2) the global demand for data has more than quadrupled since 2011, and it is expected to grow even more. In response to that, the ITU–R initiated fourth generation (4G) mobile systems. As well as that, in 2008, the ITU–R set new requirements for mobile systems named international mobile telecommunications–advanced (IMT–Advanced), where peak data rates of up to 100 Mbps for high mobility and 1 Gbps for low mobility were set to support advanced mobile services and applications [66]. In 2009, six proposals were submitted for IMT–Advanced [67, 68], where all proposals were based on : LTE Advanced by 3GPP [69], and IEEE 802.16m (WiMAX 2) [70]. However, with limited spectrum resources, 4G technologies are expected to make extensive use of multiple–input multiple–output (MIMO) techniques [71], to achieve the minimum target spectral efficiency by the ITU–R [66, 72].

LTE gets its name from the fact that the enhancements are being designed to be competitive for the next decade. In keeping with this, the spectral efficiency targets specified in [74] are 5 bps/Hz in the downlink (DL) and 2.5 bps/Hz in the uplink (UL) For a 20 MHz bandwidth,

this translates to a peak data rate of 100 Mbps and 50 Mbps in the DL and UL respectively, easily rivaling state–of–the–art home broadband speeds. Using orthogonal frequency division multiplexing (OFDM) as a key enabling technology LTE can operate in a wide range of frequency bands and size of spectrum allocations. Therefore, LTE can use spectrum allocations ranging from 1.4 to 20 MHz. Furthermore, LTE systems are envisaged to work seamlessly in either the time division duplex (TDD) or frequency division duplex (FDD) mode, ensuring the implementation of multi–mode user equipment (UE) and making global roaming a true possibility [75, 76].

Using forward error correction (FEC) coding made it possible for single antenna systems to approach Shannon's capacity limit [77, 78, 79]. However, with the demand for high–rate wireless communications, the capacity limit has to be further extended [80, 81]. Fortunately this can be done by the aid of multiple antenna systems [44]. MIMO systems offer a significant increase in spectral efficiency in comparison to single antenna systems [1]. The idea of MIMO systems dates back to 1970, when A.R. Kaye and D.A. George showed that the optimum receiver for pulse amplitude modulation (PAM) signals transmitted over signal antenna systems [82, 83, 84], can be extended to multiple antenna systems [85]. Since then, researchers focused their efforts on finding methods that increase the spectral efficiency, while retaining an optimal average bit error ratio (ABER) performance, and low hardware and software complexity.

2.2 MIMO Communication Systems

In MIMO systems, as shown in Fig. 2.3, the modulated N_t–dimensional vector x is transmitted from all N_t transmit antennas through $N_r \times N_t$ wireless channel with a transfer function $\mathbf{H}$, where N_r is the number of receive antennas. At the receiver, each received signal is constructed from the faded versions of the transmitted signal by using superposition. Thus, the N_r–dimensional receive vector can be written as follows,

$$\mathbf{y} = \mathbf{H}\mathbf{x} + \mathbf{n} \tag{2.1}$$

where $\mathbf{n}$ is the N_r–dimensional additive white Gaussian noise (AWGN).

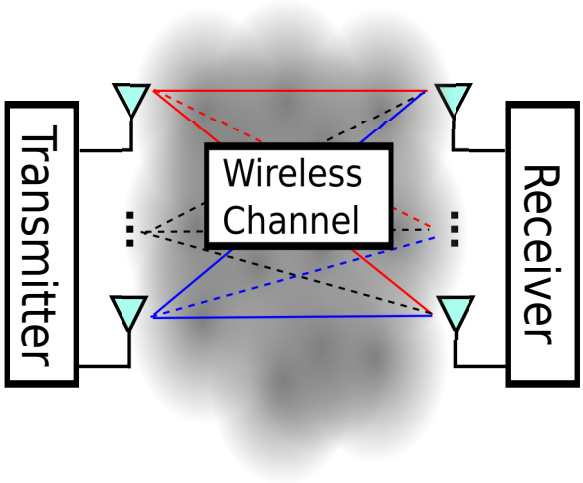

Figure 2.3: *The MIMO system setup [86].*

2.2.1 MIMO Transmission Systems

MIMO transmission systems can be categorised as:

2.2.1.1 Colocated MIMO Systems

Colocated MIMO systems are MIMO systems where the multiple antennas are located at the same transmitter or receiver node. Colocated MIMO systems can be categorised as:

1. *Diversity Techniques* [87, 88]:

   Diversity techniques overcome the poor QoS caused by the fading channel attenuating the signal. This is done by creating independent fading replicas of the same transmitted signal in time, frequency, or spatial domain and both at the transmitter and the receiver [44].

   MIMO diversity techniques can be categorised into:

   (a) *Transmit Diversity*: Transmit diversity is achieved by transmitting copies of the same data symbol over multiple transmit antennas [89].

   (b) *Receiver Diversity*: Receiver diversity is attained simply and without any loss of bandwidth, by having multiple antennas at the receiver [90].

   (c) *Time Diversity*: Time diversity can be achieved by transmitting the same data symbol multiple times, or by assigning redundant bits to the original data bits where they are transmitted at different time instances [78]

(d) *Frequency Diversity*: Frequency diversity can be achieved by sending the same data symbol at different time instants using different transmit frequencies [77].

(e) *Space–time coding (STC)* : In STC systems diversity is achieved by transmitting the same data from different transmit antennas and different time instances [87].

Table 2.1 summarise the different diversity types and gives examples for each type.

Diversity Type	Diversity Technique
Transmit Diversity	Basestation modulation diversity [91] Alamouti scheme [87]
Receiver Diversity	Maximal ratio combining (MRC) [92] Equal gain combining (EGC) [93] Selection combining (SCM) [77]
Time Diversity	FEC [78]
Frequency Diversity	Frequency hopping [77]
Space–time coding	Space–time block coding (STBC) [88, 94, 95] Space–time trellis coding (STTC) [96] Quasi–orthogonal STBC [97] Linear dispersion codes (LDC) [98] Differential space–time coding schemes [99, 100, 101, 102]

Table 2.1: *Summary of the different diversity types*

2. *Multiple Access Techniques:*

   Multiple access techniques are those techniques that enable multiple users to share limited network resources efficiently. Using multiple access the limited bandwidth offered by the telecommunication network can be shared among multiple users fairly, so that no single user spends all available resources [103, 104]. Examples of multiple access techniques are, i) Time–division multiple access (TDMA), ii) frequency–division multiple access (FDMA), iii) code–division multiple access (CDMA), iv) space–division multiple access (SDMA).

3. *Beamforming Techniques:*

   The term beamforming refers to the process of combining signals from different elements, where the signals induced on different elements of an array are combined to form a single output of the array. In other words, beamforming can be used to focus the received beam pattern in the direction of a specified antenna [44, 105, 106, 107].

4. *Spatial Multiplexing Techniques:*

   In spatial multiplexing (SMX) the source data sequence is divided into a number of blocks equal to the number of transmit antennas, then transmitted simultaneously from

all antennas using the same carrier frequency. Hence, the spectral efficiency increases with the increase of the number of transmit antennas. At the receiver, different decoders with trade–offs between the ABER performance and complexity were proposed. Example of SMX decoders are, i) minimum mean squared error (MMSE) [108], ii) diagonal Bell labs layered space–time (D–BLAST) [2], iii) vertical Bell labs layered space–time (V–BLAST) [109], iv) maximum–likelihood (ML) receiver [110], v) sphere decoder (SD) [10, 11].

5. *Space Modulation Techniques:*

   In space modulation at each time instance, only one transmit antenna is active at a time. Thus, information bits can be encoded in: a) The index of the active antenna (*spatial symbol*) [111]. b) The data symbol transmitted from the active antenna (*constellation symbol*) [22, 112]. Hence, the spectral efficiency increases by $\log_2(N_t)$ in comparison to single–input single–output (SISO) systems, where N_t is the number of transmit antennas. Examples of space modulation techniques are, i) spatial modulation (SM) which was first introduced in [15, 16], ii) space shift keying (SSK) [18].

6. *Multifunctional MIMO Techniques:*

   Multifunctional MIMO techniques are the result of combining different MIMO schemes. Consequently, they can attain a combination of diversity gain, beamforming gain, multiplexing gain, and spatial gain. Examples for that are, i) combining SMX with STBC to achieve full multiplexing gain while achieving full diversity gain as shown in [113], ii) space–time block coding spatial modulation (STBC–SM), which is the result of combing SM with with STBC to achieve spatial and diversity gains [114, 115], iii) combining SM with beamforming to achieve spatial and beamforming gains [24].

2.2.1.2 Distributed MIMO Techniques

The basic idea of distributed MIMO, also referred to as cooperative MIMO, goes back to 1971, when Van de Meulen introduced the classic relay channel [116], and the characterisation of the relay channel by Cover and El Gamal [117]. Since then distributed MIMO has attracted much attention [118, 119]. In distributed MIMO the multiple antennas at the front end of the wireless network are distributed among widely separated radio nodes, where each node has only one antenna. The information is sent to the receiver from different nodes at different locations. Hence, a high spatial diversity gain is achieved [120].

2.2.2 MIMO Channel Environment

The propagation environment is the physical medium between the transmit and receive antennas. It consists of every element that effects the propagation of the transmitted signal between the transmitter and the receiver. The propagation environment plays a dominant role in determining the capacity of the MIMO channel. Therefore, modelling of MIMO wireless channels is of paramount importance and has attracted extensive research in the past few years [121, 122, 123].

MIMO channels can be modelled in terms of separation distance between the transmitter and the receiver,

- *Large–scale propagation models:* Models that are designed for MIMO systems with a very large separation between the transmitter and the receiver, hundreds and thousands of meters separation, are called large–scale propagation models [124].

- *Small–scale propagation models:* Models that are designed for MIMO systems with a short separation between the transmitter and the receiver, are called small–scale propagation models [124].

In this thesis, small–scale MIMO channels are considered.

2.2.3 Small–Scale Propagation Models

Small–scale fading models describe the rapid fluctuation of the amplitude of the transmitted signal, which is caused by the interference between more than one copy of the transmitted signal arriving at a slightly different times. These copies are called multipath. Multipath is caused by the presence of reflectors, for example ground and surrounding structures, and has several effects on small scale MIMO systems [125]: i) Rapid changes in signal strength. ii) Random frequency modulation. iii) Time dispersion.

Small–scale fading models are influenced by many factors including,

- *Multipath propagation:* The multipath components are summed constructively and destructively at the receiver, and because of that the received signal might get distorted or fade.

- *Speed of the mobile:* The relative motion between the transmitter and the receiver causes a shift in frequency to each multipath wave. This shift in frequency is called Doppler shift.

- *Speed of surrounding objects:* The speed of the surrounding objects can vary the Doppler shift in time.

- *The transmission bandwidth of the signal:* As it will be shown later, the bandwidth of the transmitted signal determines if the signal is subject to fast or slow, flat or frequency selective fading.

2.2.3.1 Parameters of Small–Scale Propagation Models

Small–scale propagation models have several parameters. Two of them are needed to determine the type of the small–scale fading:

- *Doppler Shift:* The movement of the transmitter or receiver node results in a change in the frequency of the received signal. This change is given by,

$$f_D = \frac{v}{\lambda} \cos\theta \tag{2.2}$$

  where v is the velocity of the moving node, θ is the angle between the signal and the direction of moving node, $\lambda = c/f_c$ is the wavelength, c is the speed of light, and f_c is the carrier frequency.

- *Coherence Time:* The coherence time is the time during which the channel impulse response can be considered static, and it is the time domain dual of Doppler spread,

$$T_c = \frac{1}{{f_D}^{\max}} \tag{2.3}$$

  where $f_D^{\max} = v/\lambda$ is the maximum Doppler shift.

- *Coherence Bandwidth:* It is the range of frequencies over which the channel can be considered static.

2.2.3.2 Types of Small–Scale Fading

Depending on the coherence time and the coherence bandwidth, the transmitted signal will pass through one of four different types of small–scale fading channels [124]: i) Slow flat fading; ii) fast flat fading; iii) slow frequency selective fading; iv) fast frequency selective fading.

Where,

- *Slow fading:* A channel is classified as slow fading when the coherence time is larger than the symbol period, which means that the channel can be considered static during the symbol period.
- *Fast fading:* A channel is a fast fading channel, when the coherence time is smaller than the symbol period. In this case the channel varies within the symbol period.
- *Flat fading:* Flat fading channels are those channels with a coherence bandwidth larger than the bandwidth of the transmitted signal. In the case of flat fading channels the spectral components of the transmitted signal are preserved at the receiver.
- *Frequency selective fading:* Channels with a coherence time smaller than the bandwidth of the transmitted signal are called frequency selective fading channels. In frequency selective fading channels, different spectral components of the transmitted signal experience different fading gains.

For the rest of this thesis, slow flat fading MIMO channels are considered.

2.2.3.3 Slow Flat Fading MIMO Systems

Depending on the nature of the propagation environment, there are different models to describe the behaviour of the MIMO channel. In this thesis, frequency–flat $N_r \times N_t$ MIMO fading channels with a transfer function $\mathbf{H}$ are considered. In particular: Rayleigh Fading, Rician fading, and Nakagami–m fading channels are considered, along with spatial correlation (SC).

- *Rayleigh Fading*

  The Rayleigh distribution is often used to model non–line of sight (NLoS) channels, where the received signal is visualised as a sum of independent vectors with uniformly

distributed phases [126, 127]. Thus, the entries of $\mathbf{H}$ are modelled as complex, identical and independently distributed (i.i.d.) Gaussian random variables with zero mean and unit variance. Furthermore, the amplitude of the channel is distributed according to,

$$p(\vartheta) = 2\vartheta e^{-\vartheta^2} \tag{2.4}$$

where ϑ is the amplitude of the channel, and $p(\cdot)$ is the probability distribution function (PDF).

- *Rician Fading*

  The Rice distribution is often used to model multipath fading channels with a line of sight (LoS) component. From [128, 129] the amplitude of the Rician fading channel is distributed according to,

$$p(\vartheta) = 2(K+1)\vartheta e^{-K-(1+K)\vartheta^2} I_0\left(2\sqrt{K(K+1)}\vartheta\right) \tag{2.5}$$

  where $I_0(\cdot)$ is the modified Bessel function of the first kind with order zero.

  Moreover, the entries of $\mathbf{H}$ are modelled as [130],

$$\mathbf{H} = \sqrt{\frac{K}{1+K}} + \sqrt{\frac{1}{1+K}}\mathbf{H}' \tag{2.6}$$

  where K is the Rician factor, $K/(1+K)$ is the mean power of the LoS component, $1/(1+K)$ is the mean power of the random component, and $\mathbf{H}'$ is a $N_r \times N_t$ matrix whose entries are modelled as complex i.i.d. Gaussian random variables with zero–mean and unit–variance.

- *Nakagami–m Fading*

  Nakagami–m distribution is widely used to describe channels with severe to moderate fading [131]. The main justifications for the use of the Nakagami–m model is, it is good fit to empirical fading data, and it describes well the channel when MRC is used at the receiver [127, 132].

  From [31, 32, 33], for Nakagami–m fading channels the entries of $\mathbf{H}$ for the n_t–th and n_r–th transmit and receive antenna respectively, are modelled as,

$$h_{n_r,n_t} = \sqrt{\sum_{i=1}^{m} |z_i^R|^2} + j\sqrt{\sum_{i=1}^{m} |z_i^I|^2} \tag{2.7}$$

where z_i^R and z_i^R are an i.i.d. Gaussian random variables with zero mean and variance equal to $\sigma_z^2 = (2m)^{-1}$. The envelope of the Nakagami–m fading channel is distributed according to [32],

$$p(\vartheta) = \frac{2m^m \vartheta^{2m-1}}{\Gamma(m)} e^{(-m\vartheta^2)} \tag{2.8}$$

where $\Gamma(\cdot)$ is the gamma function.

Furthermore, the PDF of the phase is [32],

$$p(\theta) = \frac{\Gamma(m)\,|\sin(2\theta)|^{m-1}}{2^m \Gamma^2(m/2)} \tag{2.9}$$

Note, from (2.9) apart from the very special case of $m = 1$, where Nakagami–m fading corresponds to a Rayleigh fading, the phase of Nakagami–m distribution is *not* uniform [32].

- *Spatial Correlation Model (SC)*

  Different channel correlation models were proposed in literature [133, 134] for MIMO systems. In this thesis, the Kronecker channel model is used for its straightforward mathematical description [135, 136],

$$\mathbf{H}_c = \mathbf{R}_{\text{Rx}}^{\frac{1}{2}} \mathbf{H} \mathbf{R}_{\text{Tx}}^{\frac{1}{2}} \tag{2.10}$$

$$= \text{vec}(\mathbf{H})\, \mathbf{R}_s^{\frac{1}{2}} \tag{2.11}$$

  where $\mathbf{H}$ is the uncorrelated channel, which can be NLoS or LoS channels, $\mathbf{R}_{\text{Tx}}$ is the transmitter correlation matrix, $\mathbf{R}_{\text{Rx}}$ is the receiver correlation matrix, $\text{vec}(\mathbf{B})$ is the vectorisation operator, where the columns of the matrix $\mathbf{B}$ are stacked in a column vector, and $\mathbf{R}_s = \mathbf{R}_{\text{Rx}} \otimes \mathbf{R}_{\text{Tx}}$, where $\otimes$ is the Kronecker product.

  Moreover, the correlation matrices are generated using an exponential decay model as shown in [137], for the reason that it is a simple and accurate single parameter correlation model,

$$\mathbf{R}_c = \begin{bmatrix} 1 & r_c & r_c^2 & \cdots & r_c^{n-1} \\ r_c & 1 & r_c & \ddots & \vdots \\ r_c^2 & r_c & 1 & \ddots & r_c^2 \\ \vdots & \ddots & \ddots & \ddots & r_c \\ r_c^{n-1} & \cdots & r_c^2 & r_c & 1 \end{bmatrix} \tag{2.12}$$

where $r_c = \exp(-\beta)$, β is the correlation decay coefficient, and n is the number of antennas.

2.3 Spatial Multiplexing

One of the most promising MIMO techniques to increase the spectral efficiency is SMX [2]. The SMX modulation algorithm can be summarised by:

1. The incoming data bits are divided into a number of sub–streams, equal to the number of transmit antennas. Each sub–stream contains the data bits to be transmitted to a single transmit antenna.
2. Each sub–stream is modulated using any conventional modulation scheme such as quadrature amplitude modulation (QAM).
3. The sub–streams are then transmitted simultaneously from the existing transmit antennas.

Thus a spectral efficiency that increases linearly with the number of transmit antennas is achieved. However, this comes at the expense of an increase in:

1. Computational complexity as the receiver has to resolve the inter–channel interference (ICI) caused by transmitting from all antennas simultaneously.
2. Hardware complexity as the number of radio frequency (RF) chains is equal to the number of transmit antennas.
3. Power Consumption as the power requirements increase linearly with the number of RF chains added [138, 139].

Thus, SMX may not always be practically feasible especially in modern wireless communications where energy efficiency is of great concern. Therefore, solutions need to be found that strike an elegant trade-off between computational complexity, energy efficiency, and spatial multiplexing gain.

2.3.1 Maximum–Likelihood Receiver for SMX

The ML optimum receiver for SMX can be written as,

$$\hat{\mathbf{x}}_t^{(\mathrm{ML})} = \underset{\mathbf{x}\in\mathcal{Q}^m}{\arg\min} \left\{ \|\mathbf{y} - \mathbf{H}\mathbf{x}\|_{\mathrm{F}}^2 \right\} \tag{2.13}$$

where $\mathcal{Q}^m$ is a 2^m space containing all possible $(N_t \times 1)$ transmitted vectors, $\|\cdot\|_{\mathrm{F}}$ is the Frobenius norm, and $\hat{\cdot}$ denotes the estimated spatial and constellation symbols.

2.3.2 Sphere Decoder for SMX

The conventional SD is designed for SMX, where all antennas are active at each time instance [140, 10, 141, 142]. The SD algorithm reduces the number of possible transmitted points $\mathbf{x} \in \mathcal{Q}^m$ to be searched through in (2.13), *i.e.*, the transmit search space, by computing the Euclidean distances only for those points that lie inside a sphere with radius R and centred around the received signal. Hence, (2.13) becomes,

$$\hat{\mathbf{x}}_t^{(\mathrm{SD})} = \underset{\mathbf{x}\in\Theta_R^{\mathrm{SMX}}}{\arg\min} \left\{ \|\mathbf{y} - \mathbf{H}\mathbf{x}\|_{\mathrm{F}}^2 \right\} \tag{2.14}$$

where Θ_R^{SMX} is the subset of points x in the transmit search space that satisfy the condition $R^2 \geq \|\mathbf{y} - \mathbf{H}\mathbf{x}\|_{\mathrm{F}}^2$.

2.4 Spatial Modulation

SM is a transmission technology proposed for MIMO wireless systems. It aims to increase the spectral efficiency of single–antenna systems while avoiding ICI [15]. This is attained as shown in Fig. 2.4, through the adoption of a new modulation and coding scheme which foresees, i) the activation, at each time instance, of a single antenna that transmits a given data symbol (*constellation symbol*), and ii) the exploitation of the spatial position (index) of the active antenna as an additional dimension for data transmission (*spatial symbol*) [16]. Both the *constellation symbol* and the *spatial symbol* depend on the incoming data bits.

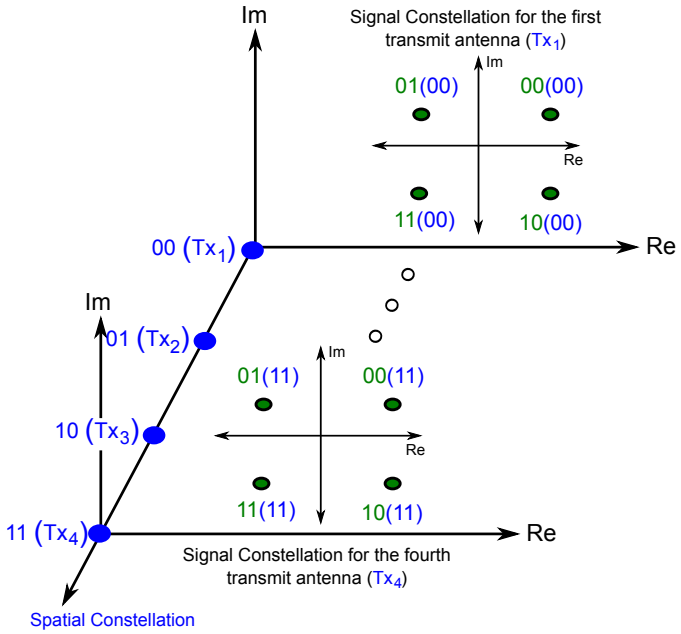

Figure 2.4: *The unique three dimensional constellation diagram for SM. The first two bits from left to right, in the four bit word define the spatial–constellation point which identifies the active antenna. These are shown in parentheses. The remaining two bits determine the signal–constellation point that is to be transmitted [143].*

2.4.1 Operating Principle

The modulation algorithm for SM can be summarised in [112],

1. The incoming data bits are divided into blocks containing $\log_2(N_t)+\log_2(M)$ bits each, where N_t is the number of transmit antennas, and M is the constellation size.

2. The first $\log_2(N_t)$ bits are used to select the antenna which is switched on for data transmission, while the other transmit antennas are kept inactive. In this work, the actual transmit antenna which is active for transmission is denoted by ℓ_t with $\ell_t \in \{1, 2, \ldots, N_t\}$.

3. The second $\log_2(M)$ bits are used to choose a symbol in the signal–constellation diagram. In this work, the actual complex symbol emitted by the transmit antenna ℓ_t is denoted by s_t, with $s_t \in \{s_1, s_2, \ldots, s_M\}$.

Accordingly, the N_t–dimensional transmit vector is:

$$\mathbf{x}_{\ell_t, s_t} = \left[\mathbf{0}_{1\times(\ell_t-1)}, s_t, \mathbf{0}_{1\times(N_t-\ell_t)}\right]^T \tag{2.15}$$

where $[\cdot]^T$ denotes the transpose operation, and $\mathbf{0}_{p\times q}$ is a $p \times q$ matrix with all–zero entries.

An overall increase by the base–two logarithm of the number of transmit–antennas in the spectral efficiency is achieved. Note that the number of transmit antennas must be a power of two. Activating only one antenna at a time means that only one RF chain is needed, which significantly reduces the hardware complexity of the system [18]. It also offers a reduction in the energy needed to power the transmit antennas, as only one antenna needs to be powered at a time, resulting in a very green solution. The energy consumption is independent of the number of transmit antennas which is a very important feature in the context of large (massive) MIMO systems [13]. Moreover, as it will be shown later the computational complexity of SM is equal to the complexity of single–antenna systems, *i.e.* the complexity of SM depends only on the spectral efficiency and the number of receive antennas, and does not depend on the number of transmit antennas. Again, this property makes SM an ideal candidate technology for large scale MIMO.

2.4.2 Maximum–Likelihood Receiver for SM

In SM, only one transmit antenna is active at any given time. Therefore, the optimal receiver in (2.13) can be simplified to,

$$\begin{aligned}\left[\hat{\ell}_t^{(\mathrm{ML})}, \hat{s}_t^{(\mathrm{ML})}\right] &= \underset{\substack{\ell\in\{1,2,\ldots N_t\}\\ s\in\{s_1,s_2,\ldots s_M\}}}{\arg\min} \left\{\left\|\mathbf{y}-\tilde{\mathbf{h}}_\ell s\right\|_{\mathrm{F}}^2\right\} \\ &= \underset{\substack{\ell\in\{1,2,\ldots N_t\}\\ s\in\{s_1,s_2,\ldots s_M\}}}{\arg\min} \left\{\sum_{r=1}^{N_r}\left|y_r-\tilde{h}_{\ell,r}s\right|^2\right\} \end{aligned} \tag{2.16}$$

where y_r is the r–th entry of $\mathbf{y}$.

2.4.3 State-of-the-Art

Space modulation is based on the receiver being able to exploit the distinct received signals from different transmit antennas to distinguish the transmitted information bits [144]. However, the proposed method in [144] has more than one antenna active at a time, thus requiring inter-antenna synchronization (IAS) and more than one RF chain [112]. A year later, the idea of using the index of the antenna to provide multiplexing gain was proposed for the first time in [111]. Independently, a MIMO technique based on the same principle as in [144], called Channel Hopping modulations is introduced in [145, 146], and later on re–named to information-guided channel hopping (IGCH) in [147]. Unlike [144], any number of transmit antennas can be used.

Moreover, it foresaw the activation of a single transmit antenna at a time.

SM was first introduced in [16, 148, 149], it aims at reducing the computational complexity and the number of RF chains needed, while attaining a good end–to–end system performance and high spectral efficiency. This is achieved by activating only a single transmit antenna at each instance to transmit a certain data symbol, where the active antenna index and the data sent depend on the incoming data bits. A simple suboptimal MRC–based detector for SM is proposed in [16], where the index of the active antenna and the transmitted symbol are estimated independently. The performance of this receiver has been studied over correlated and uncorrelated, Rayleigh and Rician channel, with or without antenna coupling, and compared to V–BLAST and Alamouti–STC. The results in [16] showed that SM with maximum receive ratio combining (MRRC), when compared to V–BLAST and Alamouti, offers the same or better ABER performance, and a large reduction in receiver complexity, while attaining the same spectral efficiency. In particular, by activating only one transmit antenna at a time, SM avoids ICI which results in a better ABER and a reduction in complexity when compared to V–BLAST. Furthermore, information bits are conveyed in the index of the active antenna, therefore, a smaller constellation size is needed when compared to Alamouti, and hence, better ABER can be achieved. Later on, the ML–optimum detector for SM is presented in [17], where it is demonstrated that with a slight increase in the complexity, SM–ML can offer a performance gain of 3 dB and 1.5 over i.i.d. Rayleigh channels, when compared to SM–MRC and V–BLAST respectively.

A special case of SM called SSK is proposed in [18], where no symbol is transmitted, and therefore, all the information bits are encoded in the index of the active antenna. In [18], the performance of SSK is analysed comprehensively, where it is shown that the ABER performance of SSK, on the one hand, degrades with the increase of the number of transmit antennas. On the other hand, the ABER performance of SSK improves with the increase of the number of receive antennas. Moreover, the diversity order for SSK over i.i.d. Rayleigh fading channels is derived and shown to be equal to the number of receive antennas [18]. Furthermore, the performance of SSK is compared with the performance of conventional MIMO systems, and shown that it can offer a better ABER. In [150], generalised space shift keying (GSSK) is proposed to reduce the number of transmit antennas needed by SSK where more than one antenna can be active at time. The optimal detector with partial channel state information (CSI) and imperfect channel knowledge is proposed in [151, 152]. A general framework for the performance of SSK over correlated Nakagami–m fading environment is established in [28, 153, 154], and

studied further in [22, 23]. Finally in [155], the performance of SSK is improved by the use of an optimised power allocation.

One of the more comprehensive analyses of SM is presented in [20]. The analytical ABER performance of SM is studied comprehensively over generic fading channels for any MIMO setup, where the effect of fading severity, the achievable diversity gain and the impact of the constellation diagram is derived and analysed. A closed–form expression for the optimisation for the role of the bit mapping in the spatial and signal constellation diagrams is derived. Furthermore, it is shown that for severe fading environments, encoding more bits in the constellation diagram is recommended, however, in less severe fading environments encoding more bits in the the spatial domain is better. The ABER performance of SM is also studied in [29, 156, 30], however, a closed form expression for the ABER performance of SM has not been derived yet.

In [149, 157], the idea of SM is used over orthogonal frequency division multiple access (OFDMA) systems, by activating only one antenna for each sub–channel. By doing so IAS and ICI are avoided. It is shown that SM outperform V–BLAST in terms of the ABER over correlated Rician fading channels with antenna coupling by 7 dB. Furthermore, the hard–decision ML–optimum decoding in [17], is generalised to soft–decision ML detector in [158]. By using the soft–decision ML detector the performance of SM can be improved by up to 3 dB when compared to hard–decision ML detector.

The optimal detector for SM with partial state information, in particular with unknown phase reference at the receiver, is presented in [159]. An analytical framework is derived, and the performance of this detector is compared to the performance of a ML detector with full CSI at the receiver. It is shown that partial CSI at the receiver leads to a sub-optimal receiver design, however, it is a more practical system. The paper also highlights, that unlike ordinary modulation schemes there is a substantial performance loss because the receiver cannot use the phase information for ML detection. It also highlights the importance of accurate channel estimation for efficient operations of SM. The effect of channel estimation error on the performance of SM and space modulation has been studied in [160, 161], and compared to the performance of V–BLAST and Alamouti. It is shown that SM is more robust to channel estimation errors than V–BLAST and Alamouti, because the probability of error is determined by the differences between channels associated with the different transmit antennas instead of the actual channel realisation. Thus, the effect of channel estimations on the performance of space modulation techniques are insignificant [161].

In [25, 130, 162], the performance of SM over correlated channels is enhanced in a novel fashion by using trellis coded modulation (TCM). The novel scheme is called trellis coded spatial modulation (TCSM). In TCSM the transmit antennas are partitioned into sub–sets, such that the spatial spacing between the antennas in each sub–set is maximised. Thus, the effect of the correlation in the channel on the ABER performance of SM is reduced. The ABER performance of TCSM is studied over correlated Rician fading channels, where it is shown that TCSM offers a major improvement when compared to SM, V–BLAST with SD as proposed in [10, 11], and Alamouti with TCM [163] and turbo coded modulation (TuCM) [164]. Another new TCM design for SM called spatial modulation with trellis coding (SM–TC) is proposed in [165], where a soft decision Viterbi decoder is used at the receiver, which is fed with the soft information supplied by the SM–ML decoder. The authors in [165] shows that the SM–TC achieves better ABER performance in terms of the ABER, and a reduced computational complexity, when compared to TCSM, and coded V–BLAST for the same spectral efficiency.

Optical wireless (OW) communications gained new momentum, as light–emitting diodes (LEDs) are expected to be the base for all lighting in the near future. Unlike fluorescent and incandescent light sources, LEDs can be modulated at a high data rate, and they offer a high energy efficiency and reliability [166]. In [167, 168], SM is applied to OW communications. The proposed scheme is called optical spatial modulation (OSM). It offers a power and bandwidth efficient pulse modulation technique for OW communications. In OSM only one light–emitting diode (LED) for an array of LEDs is active and radiating a certain intensity level at each time instant. At the receiver SM is used to detect the index of the active LED, hence an increase in the spectral efficiency by the base 2 logarithm of the number of LEDs is achieved. The effect of the location of the transmit and receive LEDs is studied, and an optimum location is shown. Moreover, it is shown that by aligning the transmitter and the receiver LEDs the performance of OSM in terms of power efficiency and bandwidth is better than on-off keying, pulse position modulation (PPM), and PAM. Moreover, it is shown that the power efficiency can be increased by using receive diversity and/or by using soft and channel hard coding techniques. In addition, in [169], the ABER performance of OSM is enhanced by using TCSM. Lastly, in [170], experimental results demonstrating the practical aspects of applying SM in the optical wireless communications system are shown and studied.

The different SM techniques described in this section are summarised in 2.2. Further information about the development of SM for wireless communications and OW can be found in [44, 112, 166].

Modulation Type	Modulation Techniques
Space Modulation	SM [16, 148, 149] SSK [18] GSSK [150] Channel hopping modulations [145, 146] IGCH [147]
Spatial Modulation	MRC [16] SM–ML optimum detector [17] Soft–decision ML detector [158] Partial state information detector [159]
Coded SM	TCSM [25, 130, 162] SM–TC [165]
Optical Wireless SM	OSM [167, 168] OSM–TCSM [169]

Table 2.2: *Summary of the different SM techniques described in Sec. 2.4.3*

2.5 Summary

In this chapter the key concepts in relation to wireless communications and SM were summarised. The chapter started with an overview of the history of wireless communications, then introduced MIMO communication systems. In particular, the different types of MIMO transmission system, and channel environments were discussed, along with small–scale propagation models. Furthermore, the idea of SMX and its advantages and disadvantages ware reviewed. After that SM was proposed, and its advantages were compared to SMX. Its limitations were also discussed. Finally, an overview of the latest research in SM was presented.

Chapter 3
A Complete Framework for Spatial Modulation

In this chapter, a tight closed–form upper bound to compute the average bit error ratio (ABER) for spatial modulation (SM) over correlated and uncorrelated generalised fading channels is provided. Comparing the framework with Monte Carlo simulations and state–of–the–art literature, it is shown that the new upper bound, 1) offers an accurate estimation of the ABER; 2) provides an easy–to–calculate closed–form upper bound; 3) is applicable for correlated and uncorrelated, Rayleigh, Rician and Nakagami–m channel. Furthermore, the performance of SM is compared with the performance of spatial multiplexing (SMX). It is shown that SM offers nearly the same or slightly better performance than SMX for small scale multiple–input multiple–output (MIMO) systems. However, SM achieves a larger reduction in ABER for large scale MIMO. Finally, the computational complexity of SM–maximum–likelihood (ML) is studied and it is shown that it is equal to the complexity of single–antenna systems, which means that the complexity of SM–ML neither depends on the number of transmit antennas, nor the signal constellation size.

3.1 Introduction

The analytical average bit error ratio (ABER) performance of spatial modulation (SM) over different fading channels is studied by many researchers. The analytical ABER performance of SM over Rayleigh fading channels is studied in [16, 17, 24]. In [16], the authors studied a suboptimal receiver design, and the symbol error probability is computed by resorting to numerical integrations, which are not easy to compute [20]. In [17], the analytical ABER performance of the maximum–likelihood (ML) receiver for SM is studied, and an analytical upper bound is derived. However, [25] shows that the bound is relatively weak. The first closed form upper bound for the ABER performance of SM over Rayleigh fading channels was proposed in [24]. However, 1) the bound is applicable for Rayleigh fading only, and 2) it is only applicable for channels with correlation on the transmitter side.

The authors in [20] studied the analytical ABER performance of SM over correlated Rician channels. However, the proposed upper bounds are mathematically involved and not easy to compute. Furthermore, the work in [16] is extended to Nakagami–m fading channels in [26, 27]. The limitations of [26, 27] are: 1) the bounds are for suboptimal receivers; 2) the approach is semi–analytical; and 3) correlation is only taken into account for the detection of the constellation symbol, where the framework in [16] is used to compute the probability of transmit–antenna detection, which does not take into account correlation [28]. Additional works in [20, 29, 30] study the analytical ABER performance of SM over correlated and uncorrelated Nakagami–m fading channels using ML optimal receiver. It is assumed that the phase of the Nakagami–m fading channel is a uniformly distributed random variable (RV). However, in [31, 32, 33], it is demonstrated that apart from the very special case of $m = 1$, where Nakagami–m fading corresponds to a Rayleigh fading, the phase of Nakagami–m distribution is not uniformly distributed. In all these analysis, the probability distribution function (PDF) of the signal to noise ratio (SNR) at the receiver input considering the specific channel model need to be obtained to derive a closed-form expression of the pairwise error probability (PEP).

Therefore and with respect to current literature, the contributions in this chapter are five folds:

1. A general and tight closed–form expression of the PEP of SM in correlated and uncorrelated channel conditions is derived.

2. The derived expression is applicable for generalised fading channels such as Rayleigh, Rice and Nakagami–m.

3. The general distribution of the Nakagami–m channel, which does not consider the limiting assumption that the phase is uniformly distributed, is considered.

4. An upper bound of the ABER is given and shown to be tight for large range of SNR values.

5. Performance comparison between SM and spatial multiplexing (SMX) is provided.

The remainder of this chapter is organised as follows. The analytical framework for the ABER of SM over correlated and uncorrelated, Rayleigh, Rician and Nakagami–m channels is derived in Section 3.2. The complexity of SM and SMX is discussed and compared in Section 3.3. The results are presented in Section 3.4, and the chapter is concluded in Section 3.5. Note, the operating principle of SM is explained in 2.4.1, the channel model is introduced in 2.2.3.3, and the SM–ML decoder is described in 2.4.2.

3.2 Analytical Upper Bound of the ABER performance of SM

The ABER for SM system can be approximated by using the union bound [110], which can be expressed as follows,

$$\underset{\text{SM}}{\text{ABER}} \leq \frac{1}{2^{\eta}} \sum_{\ell_t, s_t} \sum_{\ell, s} \frac{N\left(\mathbf{x}_{\ell_t, s_t}, \mathbf{x}_{\ell, s}\right)}{\eta} \mathrm{E}_{\mathbf{H}} \left\{ \underset{\text{error}}{\Pr} \right\} \tag{3.1}$$

where $N\left(\mathbf{x}_{\ell_t, s_t}, \mathbf{x}_{\ell, s}\right)$ is the number of bits in error between $\mathbf{x}_{\ell_t, s_t}$ and $\mathbf{x}_{\ell, s}$, $\mathrm{E}_{\mathbf{H}}\{\cdot\}$ is the expectation across the channel $\mathbf{H}$, and $\underset{\text{error}}{\Pr}$ is the conditional PEP of deciding on $\mathbf{x}_{\ell, s}$ given that $\mathbf{x}_{\ell_t, s_t}$ is transmitted,

$$\begin{aligned} \underset{\text{error}}{\Pr} &= \Pr\left(\|\mathbf{y} - \mathbf{H}_c \mathbf{x}_{\ell_t, s_t}\|_{\mathrm{F}}^2 > \|\mathbf{y} - \mathbf{H}_c \mathbf{x}_{\ell, s}\|_{\mathrm{F}}^2 \,\middle|\, \mathbf{H} \right) \\ &= Q\left(\sqrt{\varphi \|\mathbf{H}_c \Psi\|_{\mathrm{F}}^2} \right) \\ &= \frac{1}{\pi} \int_0^{\frac{\pi}{2}} \exp\left(-\frac{\varphi \|\mathbf{H}_c \Psi\|_{\mathrm{F}}^2}{2 \sin^2 \theta} \right) d\theta \end{aligned} \tag{3.2}$$

where $\Psi = (\mathbf{x}_{\ell_t, s_t} - \mathbf{x}_{\ell, s})$, and from [171, 172], the alternative integral expression of the Q–

function is,

$$Q(x) = \frac{1}{\pi} \int_0^{\frac{\pi}{2}} \exp\left(\frac{x^2}{2\sin^2\theta}\right) d\theta \tag{3.3}$$

Taking the expectation of (3.2),

$$\mathrm{E}_{\mathbf{H}}\left\{\Pr_{\text{error}}\right\} = \frac{1}{\pi} \int_0^{\frac{\pi}{2}} \Phi\left(-\frac{\varphi}{2\sin^2\theta}\right) d\theta \tag{3.4}$$

where $\Phi(\cdot)$ is the moment-generation function (MGF) of the random variable $\|\mathbf{H}_c\Psi\|^2$ and $\varphi = 1/\left(2\sigma_n^2\right)$.

From [173], the argument of the MGF in (3.4) can be written as,

$$\begin{aligned} \|\mathbf{H}_c\Psi\|^2 &= \mathrm{tr}\left(\mathbf{H}_c\Psi\Psi^H\mathbf{H}_c^H\right) \\ &= \mathrm{vec}\left(\mathbf{H}_c^H\right)^H \left(\mathbf{I}_{N_r} \otimes \Psi\Psi^H\right) \mathrm{vec}\left(\mathbf{H}_c^H\right) \\ &= \mathrm{vec}\left(\mathbf{H}^H\right)^H \mathbf{R}_s^{\frac{H}{2}} \left(\mathbf{I}_{N_r} \otimes \Psi\Psi^H\right) \mathbf{R}_s^{\frac{1}{2}} \mathrm{vec}\left(\mathbf{H}^H\right) \end{aligned} \tag{3.5}$$

where $\mathrm{tr}(\cdot)$ is the trace function, $\mathbf{I}_n$ is an $n \times n$ identity matrix, and $(\cdot)^H$ denotes the Hermitian.

From [174], for an identical and independently distributed (i.i.d.) complex Gaussian vector $\mathbf{v}$ with mean $\tilde{\mathbf{v}}$, and any Hermitian matrix $\mathbf{Q}$, the MGF of $\mathbf{f} = \mathbf{v}^H\mathbf{Q}\mathbf{v}$ is,

$$\Phi(s) = \frac{\exp\left(s\tilde{\mathbf{v}}^H\mathbf{Q}\left(\mathbf{I} - s\mathbf{L}_{\mathbf{v}}\mathbf{Q}\right)^{-1}\tilde{\mathbf{v}}\right)}{\mathbf{I} - s\mathbf{L}_{\mathbf{v}}\mathbf{Q}} \tag{3.6}$$

where $\tilde{(\cdot)}$ denotes the mean, and $\mathbf{L}_{\mathbf{v}}$ is the covariance matrix of $\mathbf{v}$.

Hence, from (3.5) and (3.6), the MGF in (3.4) is,

$$\Phi(s) = \frac{\exp\left(s\mathrm{vec}\left(\tilde{\mathbf{H}}^H\right)^H \Lambda\left(\mathbf{I}_{N_rN_t} - s\mathbf{L}_{\mathbf{H}}\Lambda\right)^{-1} \mathrm{vec}\left(\tilde{\mathbf{H}}^H\right)\right)}{\left|\mathbf{I} - s\mathbf{L}_{\mathbf{H}}\Lambda\right|} \tag{3.7}$$

where, $\mathbf{L}_{\mathbf{H}}$ is the covariance matrix of $\mathbf{H}$, and,

$$\begin{aligned} \Lambda &= \mathbf{R}_s^{\frac{H}{2}} \left(\mathbf{I}_{N_r} \otimes \Psi\Psi^H\right) \mathbf{R}_s^{\frac{1}{2}} = \left(\mathbf{I}_{N_r} \otimes \Psi\Psi^H\right) \mathbf{R}_s \\ &= \left(\mathbf{I}_{N_r} \otimes \Psi\Psi^H\right) \left(\mathbf{R}_{\text{Rx}} \otimes \mathbf{R}_{\text{Tx}}\right) = \mathbf{R}_{\text{Rx}} \otimes \left(\Psi\Psi^H\mathbf{R}_{\text{Tx}}\right) \end{aligned} \tag{3.8}$$

From (3.2),(3.7), and using the Chernoff bound,

$$\begin{aligned} \mathrm{E}_{\mathbf{H}}\left\{\Pr_{\text{error}}\right\} &= \frac{1}{\pi}\int_0^{\frac{\pi}{2}} \frac{\exp\left(-\frac{\varphi}{2\sin^2\theta}\mathrm{vec}\left(\tilde{\mathbf{H}}^H\right)^H \Lambda\left(\mathbf{I}+\frac{\varphi}{2\sin^2\theta}\mathbf{L}_{\mathbf{H}}\Lambda\right)^{-1}\mathrm{vec}\left(\tilde{\mathbf{H}}^H\right)\right)}{\left|\mathbf{I}+\frac{\varphi}{2\sin^2\theta}\mathbf{L}_{\mathbf{H}}\Lambda\right|} d\theta \\ &\leq \frac{1}{2\pi}\frac{\exp\left(-\frac{\varphi}{2}\mathrm{vec}\left(\tilde{\mathbf{H}}^H\right)^H \Lambda\left(\mathbf{I}+\frac{\varphi}{2}\mathbf{L}_{\mathbf{H}}\Lambda\right)^{-1}\mathrm{vec}\left(\tilde{\mathbf{H}}^H\right)\right)}{\left|\mathbf{I}+\frac{\varphi}{2}\mathbf{L}_{\mathbf{H}}\Lambda\right|} \end{aligned} \tag{3.9}$$

The mean matrix $\tilde{\mathbf{H}}$ and the covariance matrix $\mathbf{L}_{\mathbf{H}}$ depends on the type of channel, where for,

1. Rayleigh Fading

$$\tilde{\mathbf{H}} = \mathbf{0}_{N_r\times N_t} \tag{3.10}$$
$$\mathbf{L}_{\mathbf{H}} = \mathbf{I}_{N_rN_t} \tag{3.11}$$

2. Rician Fading

$$\tilde{\mathbf{H}} = \sqrt{\frac{K}{1+K}}\times\mathbf{1}_{N_r\times N_t} \tag{3.12}$$
$$\mathbf{L}_{\mathbf{H}} = \frac{1}{1+K}\times\mathbf{I}_{N_rN_t} \tag{3.13}$$

   where $\mathbf{1}_{N_r\times N_t}$ is an $N_r\times N_t$ all ones matrix.

3. Nakagami–m Fading

$$\tilde{\mathbf{H}} = \frac{\Gamma\left((m/2)+1/2\right)}{\Gamma(m/2)\sqrt{m/2}}e^{j\frac{\pi}{4}}\times\mathbf{1}_{N_r\times N_t} \tag{3.14}$$
$$\mathbf{L}_{\mathbf{H}} = 1-\frac{2}{m}\left(\frac{\Gamma\left((m/2)+1/2\right)}{\Gamma(m/2)}\right)^2\times\mathbf{I}_{N_rN_t} \tag{3.15}$$

In Section 3.4, the bound in (3.9) is shown to be a tight upper bound for SM.

3.3 Complexity Analysis

In this section, the receiver complexity for SM–ML is compared to the complexity of SMX–ML, for the same search space size, *i.e.* the same spectral efficiency. Note, the spectral efficiency of SM is $\eta_{\text{SM}} = \log_2 N_t M$, and the spectral efficiency for SMX is $\eta_{\text{SMX}} = N_t \log_2 M$. The complexity is computed as the number of real multiplicative operations $(\times, \div)$ needed by each algorithm [175].

- SM–ML: The computational complexity of the SM–ML receiver in (2.16) is equal to

$$\mathcal{C}_{\text{SM–ML}} = 8 N_r 2^{\eta}_{\text{SM}} \tag{3.16}$$

  where the ML detector searches through the whole transmit and receive search spaces. Note, evaluating the Euclidean distance $\left(|y_r - h_{\ell,r} s|^2\right)$ requires two complex multiplications, where each complex multiplication requires four real multiplications.

- SMX–ML: The computational complexity of SMX–ML is equal to,

$$\mathcal{C}_{\text{SMX–ML}} = 4\left(N_t + 1\right) N_r 2^{\eta}_{\text{SMX}} \tag{3.17}$$

  Note, in (2.13), $\left(|\mathbf{y} - \mathbf{H}\mathbf{x}|^2\right)$ requires $(N_t + 1)$ complex multiplications.

From (3.16) and (3.17), the reduction of SM–ML receiver complexity relative to the complexity of the SMX–ML decoder for the same spectral efficiency, *i.e.* , $\eta_{\text{SM}} = \eta_{\text{SMX}}$, is given by,

$$\mathcal{C}_{\text{rel}} = 100 \times \left(1 - \frac{2}{N_t + 1}\right) \tag{3.18}$$

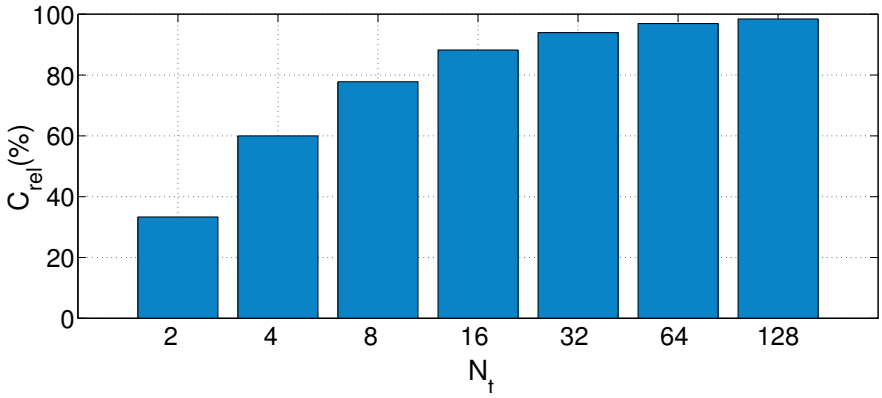

Figure 3.1: *The reduction of SM–ML receiver complexity relative to the complexity of SMX–ML*

From (3.16), the complexity of SM does not depend on the number of transmit antennas, and it is equal to the complexity of single–input multiple–ouput (SIMO) systems. However, the complexity of SMX increases linearly with the number of transmit antennas. This can be seen in Fig. 3.1 where the relative complexity for $N_t = [2, 4, 8, \ldots, 128]$ is shown. The reduction in complexity offered by SM increases with the increase in the number of transmit antennas. *e.g.* for $N_t = 4$, SM offers a 60% reduction in complexity, and as the number of transmit antennas increase the reduction increases. For $N_t = 128$, SM offers 98% reduction in complexity.

3.4 Results

In the following, Monte Carlo simulation results for the ABER performance of SM for at least 10^6 channel realisation are shown and compared with with the derived analytical bound. Furthermore, the ABER performance of SM is compared with the ABER performance of SMX.

3.4.1 Analytical performance of SM

The ABER simulation results for SM over correlated and uncorrelated, Rayleigh channels, Rician channels with $K = 5$ dB, and Nakagami–m channels with $m = 2, 4$, are depicted in Figs. 3.2-3.9 and, compared with analytical results obtained from the bound in Section 3.2, for $\eta = 8$, $N_t = 8, 32, 128$ and $N_r = 4$. The correlation decay coefficients are chosen to model moderate correlation, with $\beta = 0.7$ at the transmitter side and $\beta = 0.6$ at the receiver side. Analytical and simulation results demonstrate close match for wide and pragmatic range of SNR values and for different channel conditions, which validates the derived analysis in this chapter.

Comparing Rayleigh fading results, Fig. 3.2 and Fig. 3.3, with Rician fading results, Fig. 3.4 and Fig. 3.5, clearly highlight the negative impact of the existence of line of sight (LoS) component. The presence of LoS component increases the correlation between different channel paths and degrades the performance of SM system. Performance degradation of about $3 \sim 4$ dB can be noticed in the figures. As well, similar degradation can be noticed for correlated SM system. For instance, the performance of different configurations in Fig. 3.3 degrades by about 2 dB as compared to the results in Fig. 3.2.

ABER results of SM system with uncorrelated and correlated Nakagami–m channel are depicted in Figs. 3.6-3.9. Again, SM performance degrades in Nakagami–m channel as compared

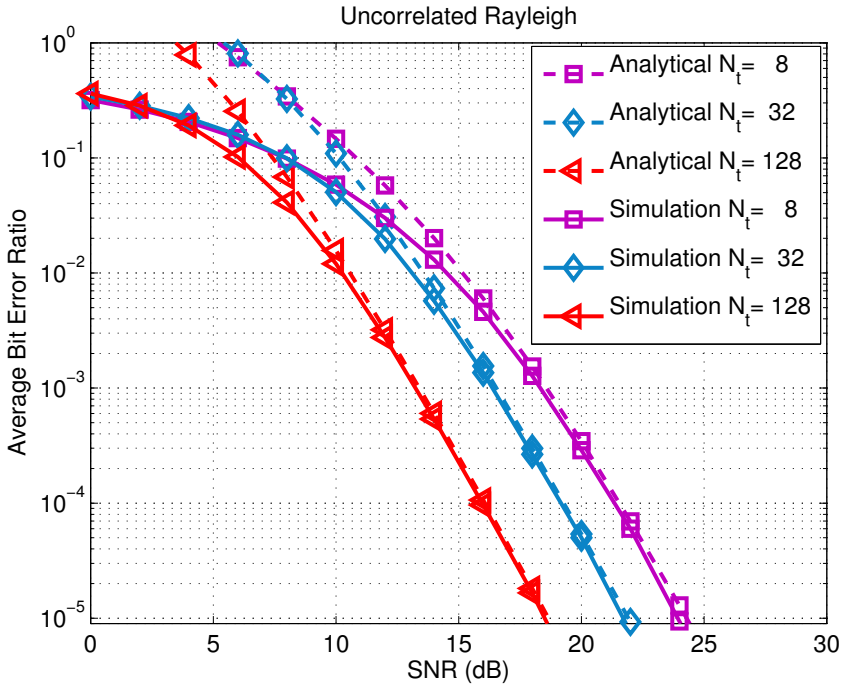

Figure 3.2: *ABER versus SNR for SM over uncorrelated Rayleigh channels, where* $\eta = 8$ *and* $N_r = 4$*. (Dashed line) analytical upper bound, (solid line) simulation.*

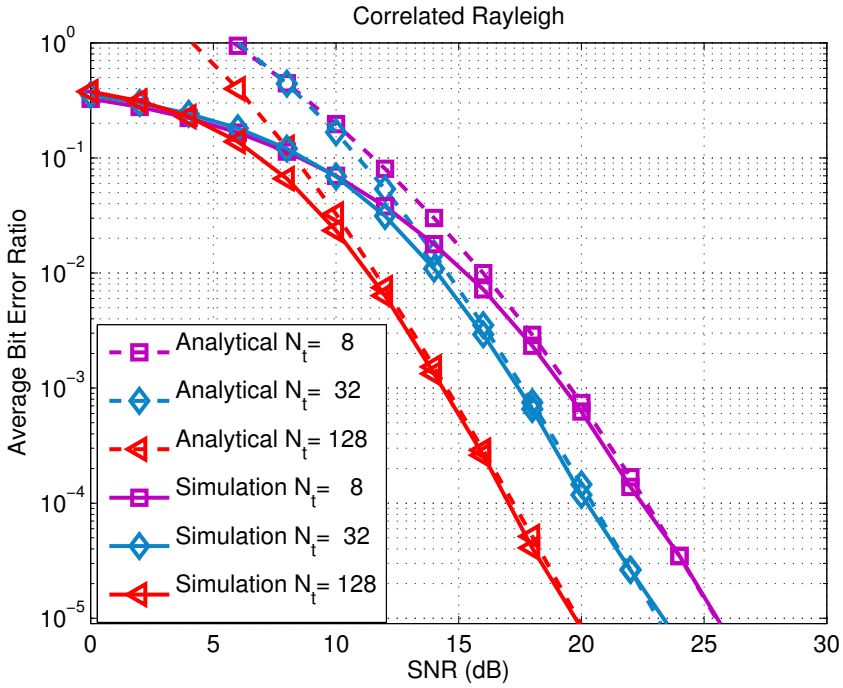

Figure 3.3: *ABER versus SNR for SM over correlated Rayleigh channels, where* $\eta = 8$ *and* $N_r = 4$*. (Dashed line) analytical upper bound, (solid line) simulation.*

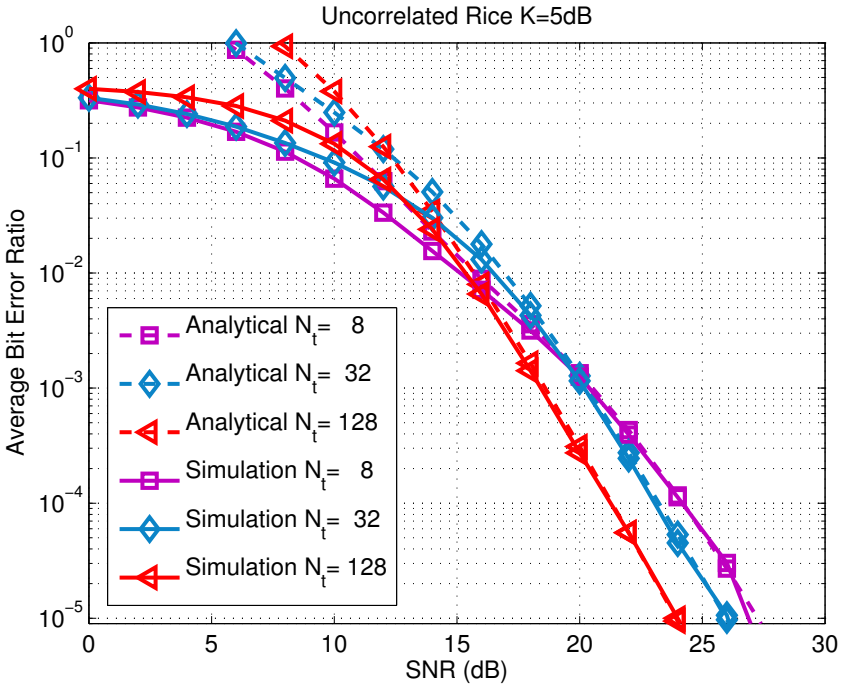

Figure 3.4: *ABER versus SNR for SM over uncorrelated Rician channels with $K = 5$ dB, where $\eta = 8$ and $N_r = 4$. (Dashed line) analytical upper bound, (solid line) simulation.*

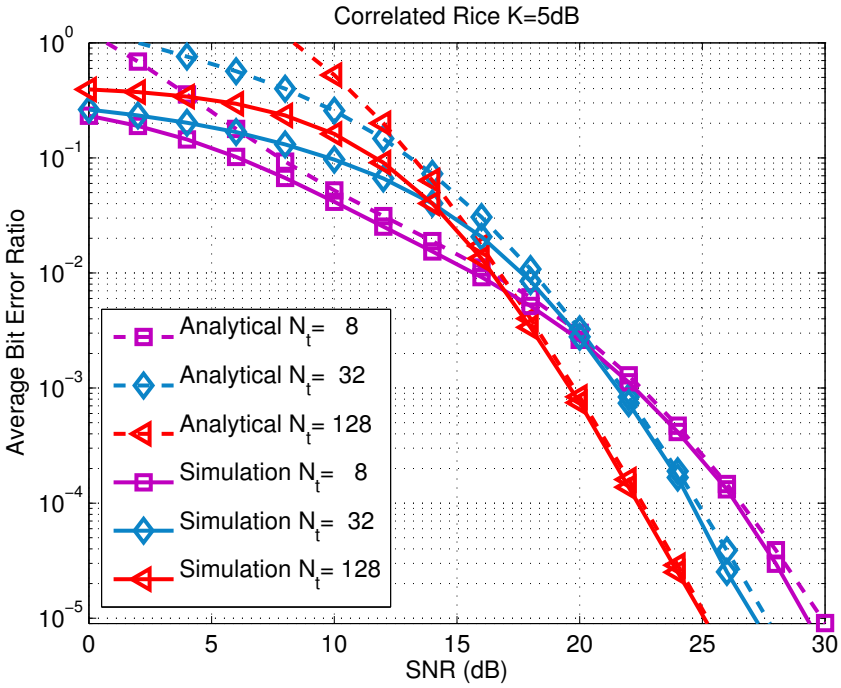

Figure 3.5: *ABER versus SNR for SM over correlated Rician channels wit $K = 5$ dB, where $\eta = 8$ and $N_r = 4$. (Dashed line) analytical upper bound, (solid line) simulation.*

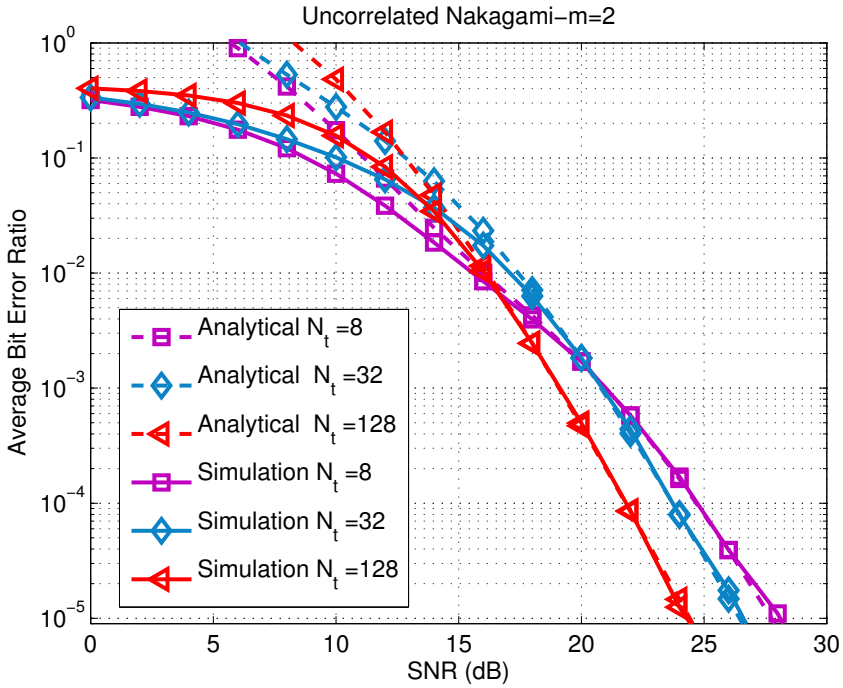

Figure 3.6: *ABER versus SNR for SM over uncorrelated Nakagami–m channels with $m = 2$, where $\eta = 8$ and $N_r = 4$. (Dashed line) analytical upper bound, (solid line) simulation.*

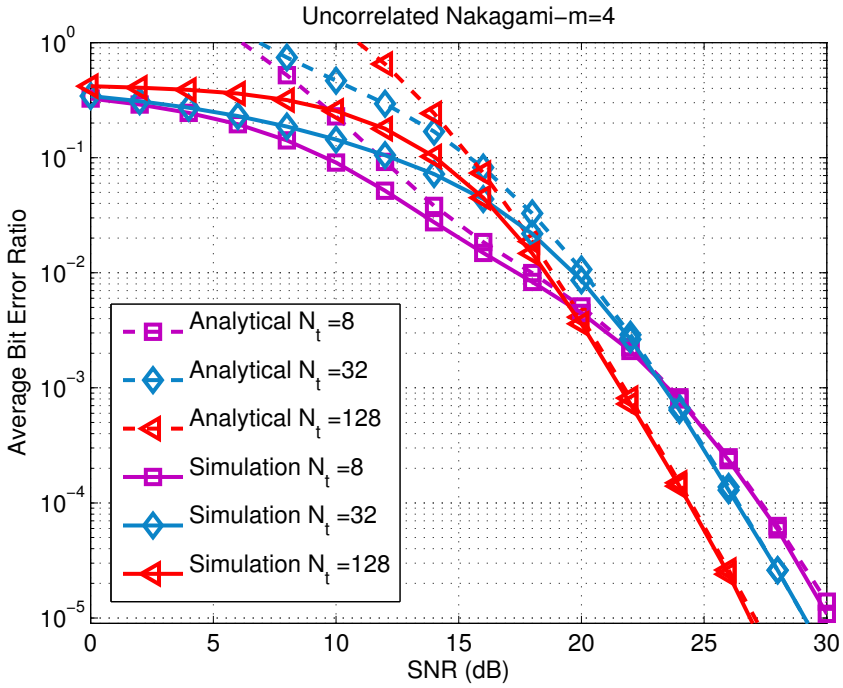

Figure 3.7: *ABER versus SNR for SM over uncorrelated Nakagami–m channels with $m = 4$, where $\eta = 8$ and $N_r = 4$. (Dashed line) analytical upper bound, (solid line) simulation.*

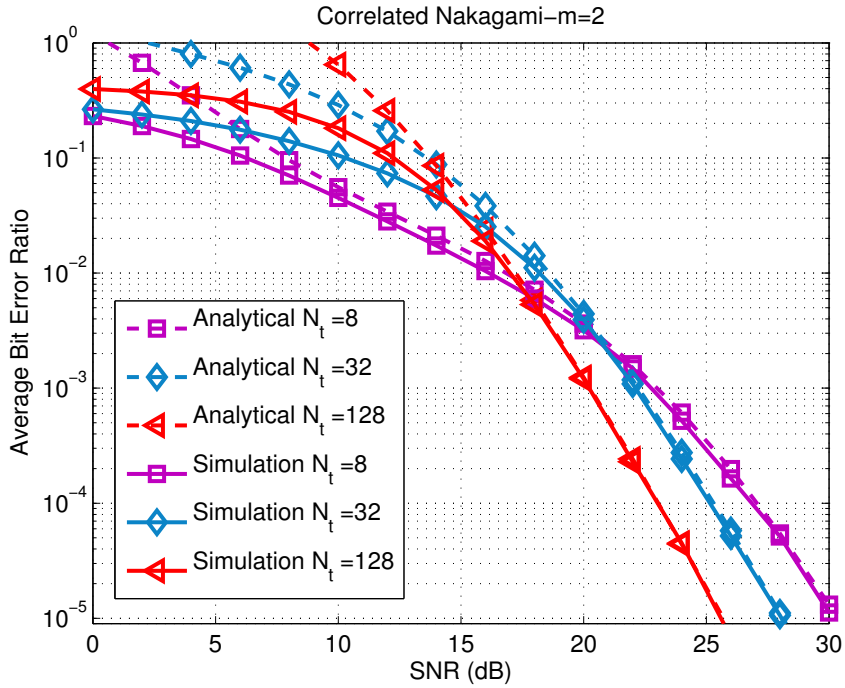

Figure 3.8: *ABER versus SNR for SM over correlated Nakagami–m channels with $m = 2$, where $\eta = 8$ and $N_r = 4$. (Dashed line) analytical upper bound, (solid line) simulation.*

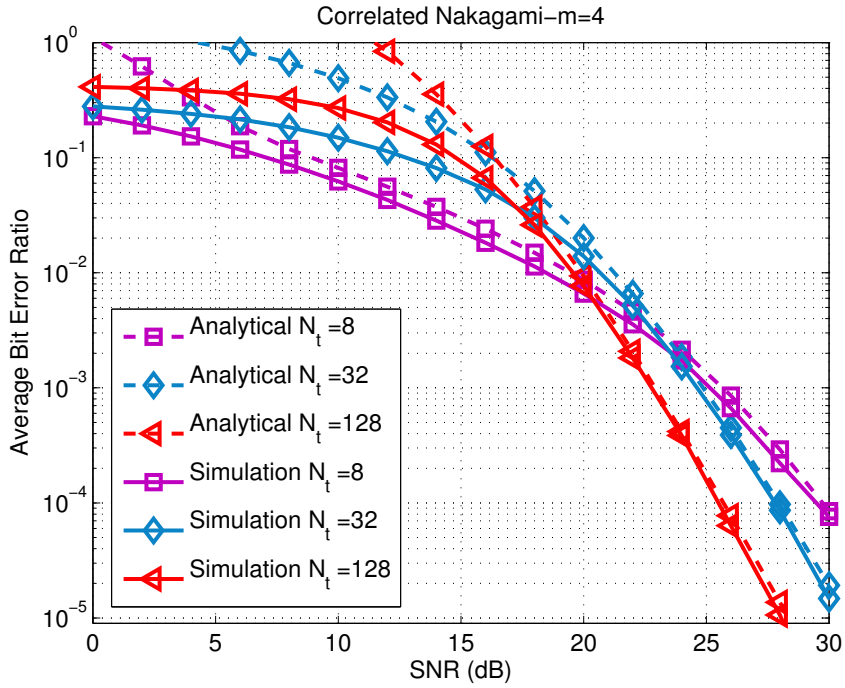

Figure 3.9: *ABER versus SNR for SM over correlated Nakagami–m channels with $m = 4$, where $\eta = 8$ and $N_r = 4$. (Dashed line) analytical upper bound, (solid line) simulation.*

to Rayleigh channel. For instance, 6 dB degradation can be noticed in Fig. 3.6 for $m = 2$ and about 8.5 dB performance degradation is noticed for $m = 4$ as shown in Fig. 3.7. Performance degradation in Nakagami–m channel can be attributed to the fact that the spatial correlation between different channel paths increases with increasing the value of m. In fact, as $m \to \infty$, the Nakagami–m fading channel converges to a nonfading additive white Gaussian noise (AWGN) channel and separating different channel paths would be impossible. This is a very interesting observation that contradicts the already reported results in [20], where it is shown that SM performance enhances as m increases.

3.4.2 Comparison in the ABER performance of SM and SMX

Figs. 3.10 - 3.17 compare the ABER performance of SM with $N_t = 8, 32, 128$ and SMX with $N_t = 2, 8$, over uncorrelated and correlated, Rayleigh, Rice, and Nakagami-m fading channels with similar parameters as discussed above.

3.4.2.1 Rayleigh Fading

In Fig. 3.10 and Fig. 3.11 the ABER results for SM and SMX over correlated and uncorrelated Rayleigh channels are shown. It can be observed that the ABER performance depends on the the number of transmit antennas used and, consequently, the constellation size. The smaller the constellation size, the better the performance. Another observation is that SM and SMX offer nearly the same performance when using the same constellation size. Moreover, comparing the uncorrelated case with the correlated case, SM is more robust to channel correlation, where for the uncorrelated case SM with $N_t = 128$ offers 1 dB better performance than SMX with $N_t = 8$. However, for the correlated case SM offers 2 dB better performance.

3.4.2.2 Rician Fading

Performance comparison between SM and SMX over correlated and uncorrelated Rician channels are shown in Fig. 3.12 and Fig. 3.13. For the uncorrelated case, SM with $N_t = 128$ performs almost the same as SMX with $N_t = 8$, as both systems are using same signal constellation size. However, for the correlated case SM performs better by 1.3 dB when compared to SMX. Also, SM with $N_t = 32$ performs almost the same as SMX with $N_t = 2$ for the uncorrelated case, but for the correlated case SM performs better than SMX by about 2.3 dB.

3.4.2.3 Nakagami–m Fading

Fig. 3.12 and Fig. 3.13 shows the ABER results for SM and SMX over correlated and uncorrelated Nakagami–m channels with $m = 2, 4$. For the uncorrelated case, SM with $N_t = 128$ and $N_t = 32$ performs the same as SMX with $N_t = 8$ and $N_t = 2$ respectively. However, for the correlated case SM performs better than SMX for both $m = 2$ and $m = 4$. For $m = 2$ and $m = 4$ SM with $N_t = 2$ and $N_t = 8$ performs 1.25 dB and 2.5 dB better than SMX with $N_t = 2$ and $N_t = 8$, respectively.

□

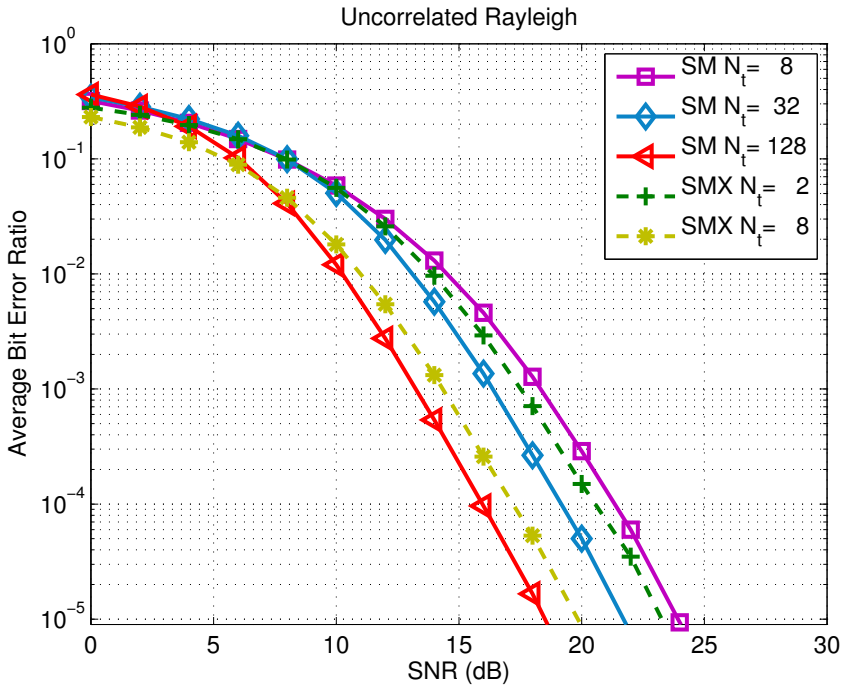

Figure 3.10: *ABER versus SNR for SM and SMX over uncorrelated Rayleigh channels, where $\eta = 8$ and $N_r = 4$. (Dashed line) SMX, (solid line) SM.*

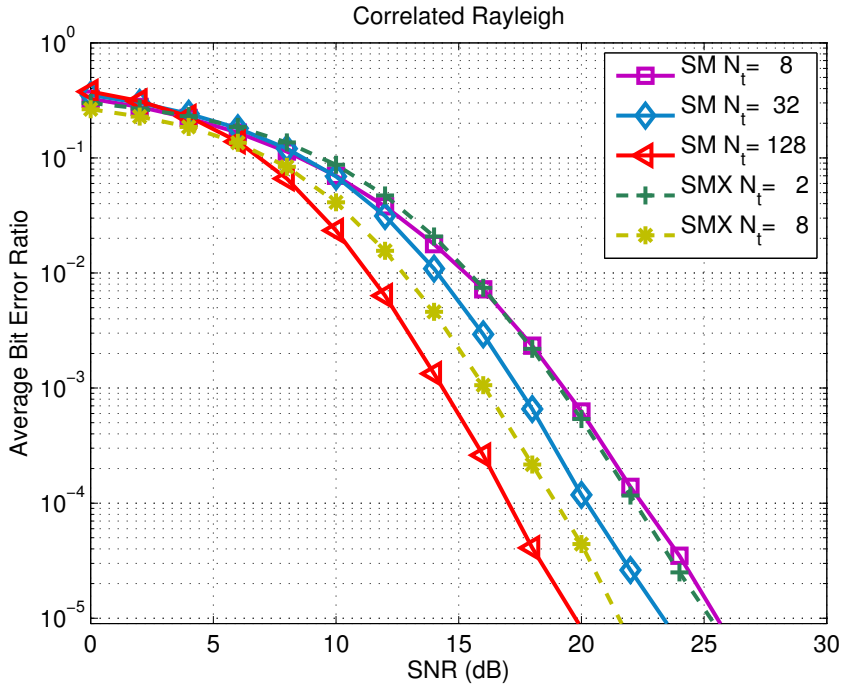

Figure 3.11: *ABER versus SNR for SM and SMX over correlated Rayleigh channels, where* $\eta = 8$ *and* $N_r = 4$*. (Dashed line) SMX, (solid line) SM.*

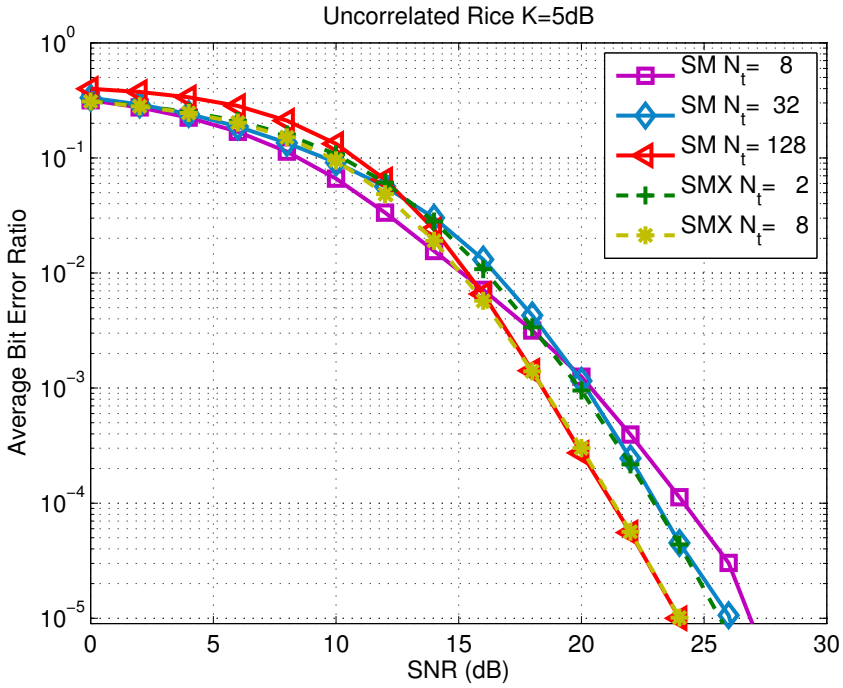

Figure 3.12: *ABER versus SNR for SM and SMX over uncorrelated Rician channels with* $K = 5$ *dB, where* $\eta = 8$ *and* $N_r = 4$*. (Dashed line) SMX, (solid line) SM.*

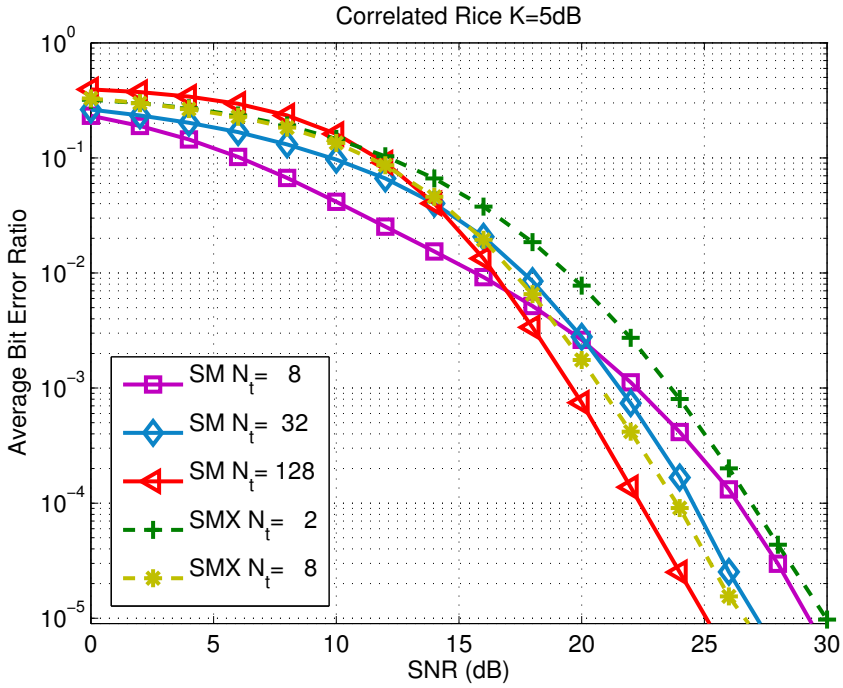

Figure 3.13: *ABER versus SNR for SM and SMX over correlated Rician channels with $K = 5$ dB, where $\eta = 8$ and $N_r = 4$. (Dashed line) SMX, (solid line) SM.*

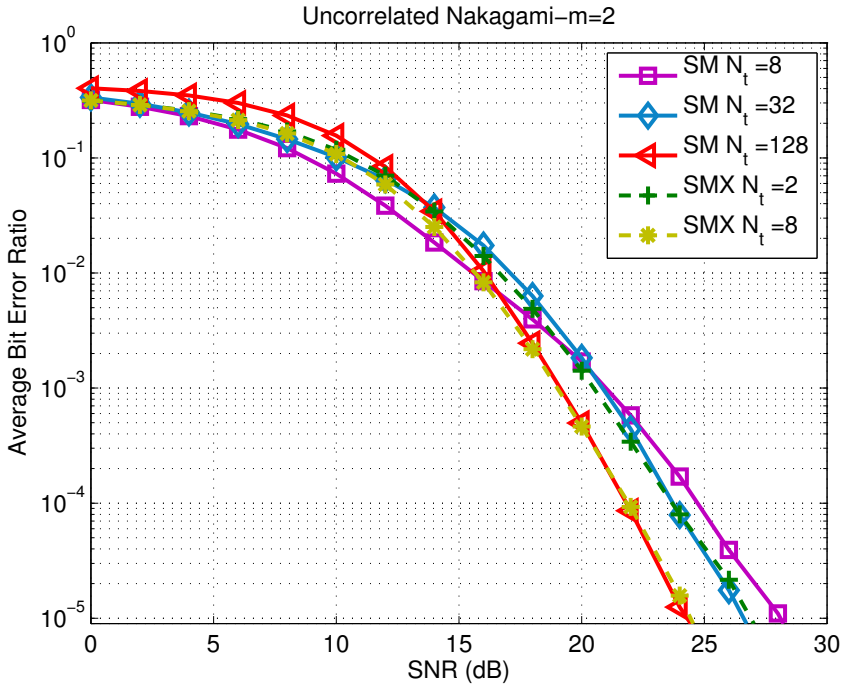

Figure 3.14: *ABER versus SNR for SM and SMX over uncorrelated Nakagami–m channels with $m = 2$, where $\eta = 8$ and $N_r = 4$. (Dashed line) SMX, (solid line) SM.*

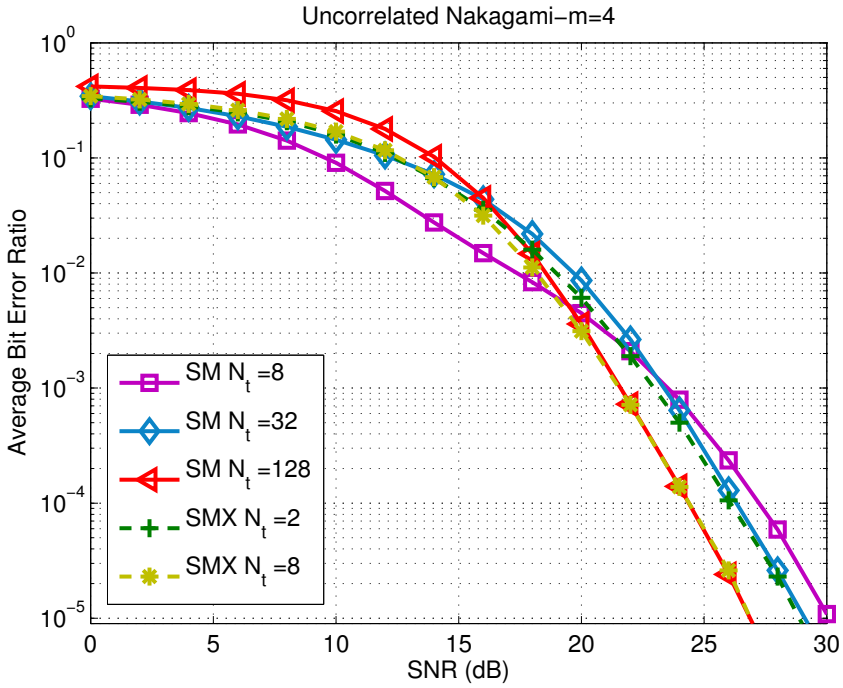

Figure 3.15: *ABER versus SNR for SM and SMX over uncorrelated Nakagami–m channels with $m = 4$, where $\eta = 8$ and $N_r = 4$. (Dashed line) SMX, (solid line) SM.*

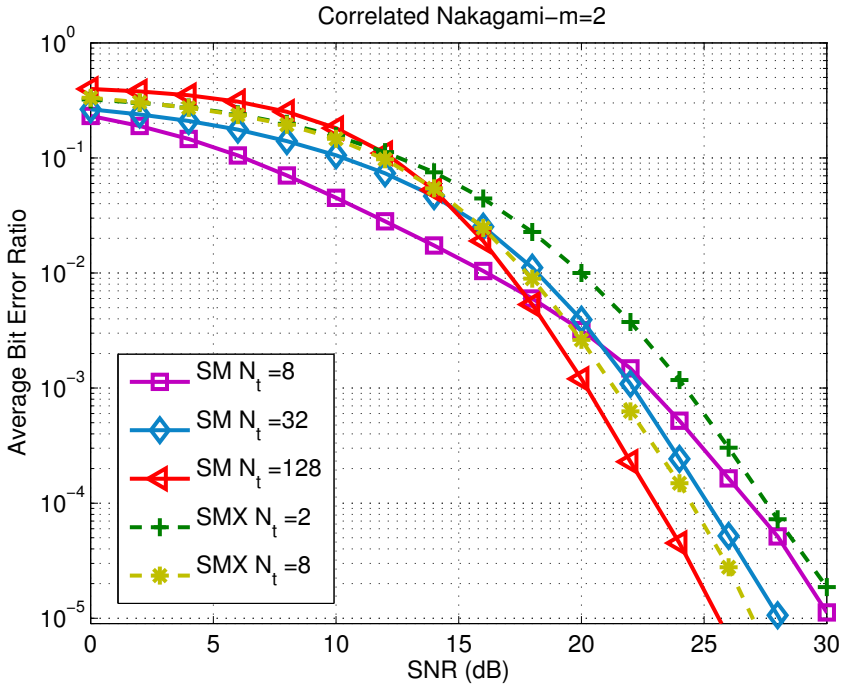

Figure 3.16: *ABER versus SNR for SM and SMX over correlated Nakagami–m channels with $m = 2$, where $\eta = 8$ and $N_r = 4$. (Dashed line) SMX, (solid line) SM.*

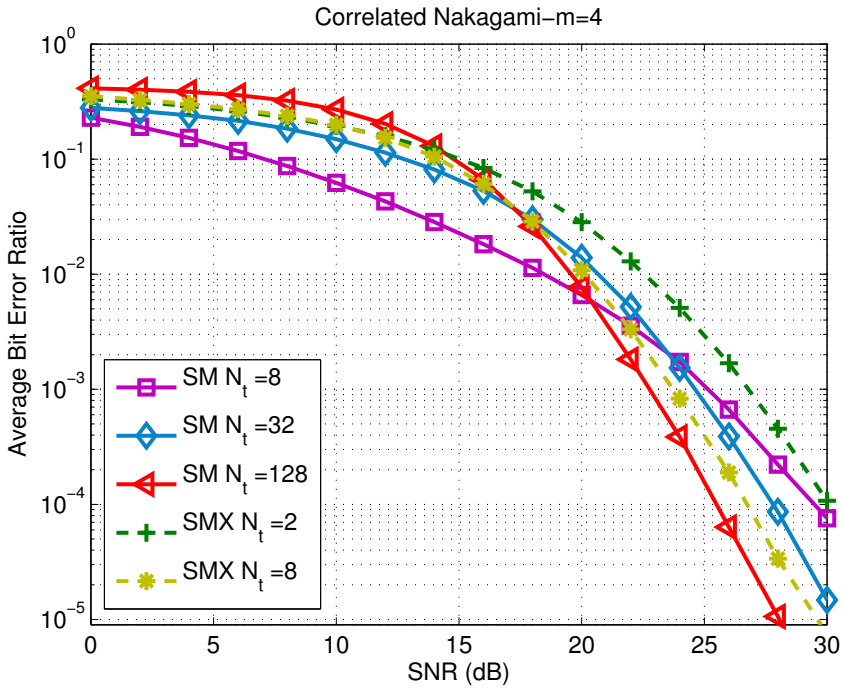

Figure 3.17: *ABER versus SNR for SM and SMX over correlated Nakagami–m channels with $m = 4$, where $\eta = 8$ and $N_r = 4$. (Dashed line) SMX, (solid line) SM.*

3.5 Summary

In this chapter, a novel, simple and accurate analytical upper bound to compute the ABER for SM over Rayleigh, Rician and Nakagami–m fading channels has been proposed. The upper bound allows the calculation of the ABER of SM in correlated and uncorrelated channels, and for small and large scale multiple–input multiple–output (MIMO) with any digital modulation scheme. The performance of SM is also compared with the performance of SMX, where it is shown that SM offers nearly the same or slightly better performance than SMX.

To sum up, SM exhibits i) an ABER performance that improves with the increase of the number transmit antennas, and ii) a reduction in complexity that increases up to 98% when compared to SMX, while the complexity is independent of the number of available transmit antenna elements.

Chapter 4
Generalised Sphere Decoding

In this chapter, sphere decoder (SD) algorithms for spatial modulation (SM) are developed to reduce the computational complexity of maximum–likelihood (ML) detectors. Two SDs specifically designed for SM are proposed and analysed in terms of average bit error ratio (ABER) and computational complexity. Using Monte Carlo simulations and mathematical analysis, it is shown that by carefully choosing the initial radius the proposed SD algorithms offer the same ABER as ML detection, with a significant reduction of the computational complexity. A tight closed form bound for the ABER performance of SM–SD is derived, along with an algorithm for choosing the initial radius which provides optimum performance. Also, it is shown that none of the proposed SDs is always superior to the others, but the best SD to use depends on the target spectral efficiency. Finally, the performance of SM–SDs are compared to spatial multiplexing (SMX), applying ML decoder and applying SD. It is shown that for the same spectral efficiency, SM–SD offers up to 84% reduction in complexity compared to SMX–SD, with up to 1 dB better ABER performance than SMX–ML decoder.

4.1 Introduction

In spite of the low–complexity implementation of spatial modulation (SM), there is still potential for further complexity reduction, by using the sphere decoder (SD) principle. However, existing SD algorithms in the literature do not consider the basic and fundamental principle of SM, that at any given time, only one antenna is active. Therefore, they cannot be applied to SM, and two modified SD algorithms based on the tree search structure that are tailored to SM are proposed. The first SD will be called receiver–centric SD (Rx-SD). The Rx–SD aims at reducing the complexity by combining the received signals from each antenna at the receiver, as long as the Euclidean distance from the received point is less than a given radius. This SD–based detector is especially suitable when the number of receive–antennas is large. It reduces the size of the search space related to the multiple antennas at the receiver (this search space is denoted as "receive search space"). It will be shown later that there is no loss in either the diversity order or the coding gain, *i.e.* the average bit error ratio (ABER) is very close to that of the maximum–likelihood (ML) detector. However, its main limitation is that it does not reduce the search space related to the number of possible transmitted points (this search space is denoted as "transmit search space"). This prevents the detector from achieving a significant reduction in computational complexity when high data rate is required, *i.e.* , when the number of antennas is large.

The second SD, which will be called Transmit–centric (Tx–SD) aims at reducing the transmit search space, by limiting the number of possible antenna and constellation combinations searched over [36]. The Tx–SD algorithm avoids an exhaustive search by examining only those points that lie inside a sphere with a given radius. However, it is limited to the non–underdetermined multiple–input multiple–output (MIMO) setup $(N_t \leq N_r)$, where N_t and N_r are the number of transit and receiver antennas respectively. In [34, 35], it is shown that Tx–SD in [36] still can be used for the case of $(2N_r - 1) \geq N_t > N_r$, where it is referred to as E–Tx–SD. Moreover, in [34, 35] a detector for the case of $N_t > N_r$ referred to as G–Tx–SD is proposed. By using the division algorithm the G–Tx–SD technique: 1) Divides the set of possible antennas into a number of subsets. 2) Performs E–Tx–SD over each subset. 3) Takes the minimum solution of all the sets. However, in this chapter a simple solution is proposed, where as it will be shown later, all what is needed is to set a constant ε to 0 for $N_t \leq N_r$ and $\varepsilon = \sigma_n^2$ for $N_t > N_r$, where σ_n^2 is the noise variance. In [34, 35], the normalised expected number of nodes visited by the Tx–SD algorithm is used to compare its complexity with the complexity of the SM–ML. This does not take into account the pre–computations needed by

the Tx–SD algorithm. In this chapter, when comparing the complexity of Tx–SD with the complexity of SM–ML and Rx–SD, the pre–computations needed by the Tx–SD are taken into account. Because of those pre–computations, the Tx–SD is not always the best solution, where in some cases it is even more complex than SM–ML. Finally, the performance of both SDs is closely tied to the choice of the initial radius. The chosen radius should be large enough so that the sphere contains the solution. On the one hand, the larger the radius is, the longer the search takes, which increases the complexity. On the other hand, a small radius may cause the algorithm to fail in finding any point inside the sphere.

In this chapter, a careful study of the performance of these two detectors is provided, along with an accurate comparison of their computational complexity. Numerical results show that the proposed solutions provide a substantial reduction in computational complexity with respect to SM–ML decoder, and no loss in the ABER performance. The closed form expression for the ABER performance of SM–SD is derived and shown that the initial radius can be chosen such that SM–SD gives an optimum performance. Furthermore, it is shown that Rx–SD is less complex than Tx–SD for lower spectral efficiencies, while Tx–SD is the best solution for higher spectral efficiencies. Finally, using numerical results it is shown that SM with SD offers a significant reduction and nearly the same performance when compared to spatial multiplexing (SMX) with ML decoder or SD.

The reminder of this chapter is organised as follows. In Section 4.2, the new spatial modulation receiver–centric SD (SM–Rx) and spatial modulation transmit–centric SD (SM–Tx) receivers are described. In Section 4.3, an accurate analysis of the computational complexity of both SM–Rx and SM–Tx is performed. In Section 4.4, the analytical ABER performance for SM–SDs is derived along with the initial radius selection method. Numerical results are presented in Section 4.5, and the chapter is concluded in Section 4.6. Note, the operating principle of SM is explained in 2.4.1, the channel model is introduced in 2.2.3.3, and the SM–ML decoder is described in 2.4.2.

4.2 Sphere Decoders for SM

In this section two SDs tailored for SM are introduced, Rx–SD and Tx–SD. Rx–SD aims at reducing the number of summations over N_r required by the ML receiver in (2.16). Tx–SD aims at reducing the number of points (ℓ, s) the ML receiver searches over.

First, for ease of derivation, the real–valued equivalent of the complex–valued model in (2.16) following [176] is introduced,

$$\begin{aligned} \bar{\mathbf{y}} &= \bar{\mathbf{H}}\bar{\mathbf{x}}_{\ell_t,s_t} + \bar{\mathbf{n}} \\ &= \bar{\mathbf{h}}_{\ell_t}\bar{\mathbf{s}}_t + \bar{\mathbf{n}} \end{aligned} \tag{4.1}$$

where,

$$\bar{\mathbf{y}} = \left[\mathrm{Re}\left\{\mathbf{y}^T\right\}, \mathrm{Im}\left\{\mathbf{y}^T\right\}\right]^T \tag{4.2}$$

$$\bar{\mathbf{H}} = \begin{bmatrix} \mathrm{Re}\{\mathbf{H}\} & \mathrm{Im}\{\mathbf{H}\} \\ -\mathrm{Im}\{\mathbf{H}\} & \mathrm{Re}\{\mathbf{H}\} \end{bmatrix} \tag{4.3}$$

$$\bar{\mathbf{x}}_{\ell_t,s_t} = \left[\mathrm{Re}\left\{\mathbf{x}^T_{\ell_t,s_t}\right\}, \mathrm{Im}\left\{\mathbf{x}^T_{\ell_t,s_t}\right\}\right]^T \tag{4.4}$$

$$\bar{\mathbf{n}} = \left[\mathrm{Re}\left\{\mathbf{n}^T\right\}, \mathrm{Im}\left\{\mathbf{n}^T\right\}\right]^T \tag{4.5}$$

$$\bar{\mathbf{h}}_\ell = \left[\bar{\mathbf{H}}_\ell, \bar{\mathbf{H}}_{\ell+N_t}\right] \tag{4.6}$$

$$\bar{\mathbf{s}} = \begin{bmatrix} \mathrm{Re}\{s\} \\ \mathrm{Im}\{s\} \end{bmatrix} \tag{4.7}$$

where $\mathrm{Re}\{\cdot\}$ and $\mathrm{Im}\{\cdot\}$ denote real and imaginary parts respectively, and $\bar{\mathbf{H}}_\ell$ is the ℓ–th column of $\bar{\mathbf{H}}$.

4.2.1 Rx–SD Detector

The Rx–SD is a reduced–complexity and close–to–optimum ABER–achieving decoder, which aims at reducing the receive search space. The detector can formally be written as follows:

$$\left[\hat{\ell}_t^{(\mathrm{Rx-SD})}, \hat{s}_t^{(\mathrm{Rx-SD})}\right] = \underset{\substack{\ell\in\{1,2,\ldots N_t\} \\ s\in\{s_1,s_2,\ldots s_M\}}}{\arg\min} \left\{ \sum_{r=1}^{\tilde{N}_r(\ell,s)} \left|\bar{y}_r - \bar{\mathbf{h}}_{r,\ell}\bar{\mathbf{s}}\right|^2 \right\} \tag{4.8}$$

where $\bar{\mathbf{h}}_{r,\ell}$ is the r–th element of $\bar{\mathbf{h}}_\ell$, and,

$$\tilde{N}_r\left(\ell, s\right) = \max_{n\in\{1,2,\ldots 2N_r\}} \left\{ n \left| \sum_{r=1}^{n} \left|y_r - h_{r,\ell} s\right|^2 \leq R^2 \right. \right\}. \tag{4.9}$$

The idea behind Rx–SD is that it keeps combining the received signals as long as the Euclidean distance in (4.8) is less or equal to the radius R. Whenever a point is found to be inside the sphere, the radius, R, is updated with the Euclidean distance of that point. The point with the minimum Euclidean distance and $\tilde{N}_r\left(\cdot,\cdot\right) = 2N_r$ is considered to be the solution.

4.2.2 Tx–SD Detector

The conventional SD is designed for SMX, where all antennas are active at each time instance [10, 140, 141, 142]. However, in SM only one antenna is active at a time. Therefore, a modified SD algorithm tailored for SM, named Tx–SD, is presented. More specifically, similar to conventional SDs, the Tx–SD scheme reduces the number of points (ℓ, s) for $\ell \in \{1, 2, \ldots N_t\}$ and $s \in \{s_1, s_2, \ldots s_M\}$ to be searched through in (2.16), *i.e.*, the transmit search space, by computing the Euclidean distances only for those points that lie inside a sphere with radius R and are centred around the received signal. However, unlike conventional SDs, in our scheme the set of points inside the sphere are much simpler to compute, as there is only a single active antenna in SM. This section, shows how to compute the set of points.

The Cholesky factorisation of the $(2N_t \times 2N_t)$ positive definite matrix $\bar{\mathbf{G}} = \bar{\mathbf{H}}^T\bar{\mathbf{H}} + \varepsilon\bar{\mathbf{I}}_{N_t}$ is $\bar{\mathbf{G}} = \bar{\mathbf{D}}^T\bar{\mathbf{D}}$, where

$$\varepsilon = \begin{cases} \sigma_n^2 & N_t > N_r \\ 0 & N_t \leq N_r \end{cases} \tag{4.10}$$

Then the Tx–SD can be formally written as follow,

$$\left[\hat{\ell}_t^{(\mathrm{Tx-SD})}, \hat{s}_t^{(\mathrm{Tx-SD})}\right] = \underset{(\ell,s)\in\Theta_R}{\arg\min} \left\{ \left\| \bar{\mathbf{z}} - \bar{\mathbf{D}}\bar{\mathbf{x}}_{\ell,s} \right\|_{\mathrm{F}}^2 \right\} \tag{4.11}$$

where Θ_R is the subset of points (ℓ, s) for $\ell \in \{1, 2, \ldots N_t\}$ and $s \in \{s_1, s_2, \ldots s_M\}$ in the transmit search space that lie inside a sphere with radius R and centred around the received signal $\bar{\mathbf{z}}$, $\bar{\mathbf{z}} = \bar{\mathbf{D}}\bar{\rho}$ and $\bar{\rho} = \bar{\mathbf{G}}^{-1}\bar{\mathbf{H}}^T\bar{\mathbf{y}}$.

Unlike Rx–SD, Tx–SD reduces the computational complexity of the ML receiver by reducing the transmit search space, which is done by the efficient computation of the subset Θ_R. After some algebraic manipulations as shown in Appendix A. The subset of points Θ_R lie in the intervals:

$$\frac{-R_i + \bar{z}_{\ell+N_t}}{\bar{D}_{(\ell+N_t,\ell+N_t)}} \leq \mathrm{Im}\{s\} \leq \frac{R_i + \bar{z}_{\ell+N_t}}{\bar{D}_{(\ell+N_t,\ell+N_t)}} \tag{4.12}$$

$$\frac{-R' + \bar{z}_{\ell|\ell+N_t}}{\bar{D}_{\ell,\ell}} \leq \mathrm{Re}\{s\} \leq \frac{R' + \bar{z}_{\ell|\ell+N_t}}{\bar{D}_{\ell,\ell}} \tag{4.13}$$

where

$$\bar{z}_{a|b} = \bar{z}_a - \bar{D}_{(a,b)}\mathrm{Im}\{s\} \tag{4.14}$$

$$R'^2 = R^2 - \sum_{\nu=N_t+1}^{2N_t} \bar{z}^2_{\nu|\ell+N_t} \tag{4.15}$$

Note, every time a point is found inside the sphere, the radius R is updated with the Euclidean distance of that point,

$$\begin{aligned} R^2_{i+1} &= \left\|\bar{\mathbf{z}} - \bar{\mathbf{D}}\bar{\mathbf{x}}_{\ell,s}\right\|^2_{\mathrm{F}} \\ &= (R_i^2 - R'^2) + \sum_{\nu=1}^{N_t} \left(z_\nu - D_{(\nu,\ell)}\mathrm{Re}\{s\} - D_{(\nu,\ell+N_t)}\mathrm{Im}\{s\}\right)^2 \end{aligned} \tag{4.16}$$

Moreover, (4.13) needs to be computed only for those points that lie inside the interval in (4.12), for the reason that (4.13) depends implicitly on (4.12).

Because of the unique properties of SM the intervals in (4.12) and (4.13) needs to be calculated only once for each possible transmit point, unlike conventional SDs where the intervals have to be calculate N_t times for each transmit point. Furthermore, note that SM–Tx works for both underdetermined MIMO setup with $N_t > N_r$, and overdetermined MIMO setup with $N_t \leq N_r$.

As opposed to the Rx–SD scheme, the Tx–SD scheme uses some pre–computations to estimate the points that lie inside the sphere of radius R. These additional computations are carefully taken into account in the analysis of the computational complexity of the Tx–SD scheme and its comparison with the ML–optimum detector in section 4.3.

4.3 Computational Complexity of Rx–SD and Tx–SD

In this section, the computational complexity of SM–ML, Rx–SD and Tx–SD is analysed. The complexity is here computed as the number of real multiplications and divisions operations needed by each algorithm [175].

4.3.1 SM–ML

The computational complexity of the SM–ML receiver in (2.16), yields,

$$\mathcal{C}_{\text{SM–ML}} = 8N_r 2^{\eta} \tag{4.17}$$

as the ML detector searches through the whole transmit and receive search spaces. Note, evaluating the Euclidean distance $\left(|y_r - h_{\ell,r}s|^2\right)$ requires 8 real multiplications.

The computational complexity of the SMX–ML receiver in (2.13) results in,

$$\mathcal{C}_{\text{SMX–ML}} = 4\left(N_t + 1\right) N_r 2^{\eta} \tag{4.18}$$

Note, $\left(|\mathbf{y} - \mathbf{H}\mathbf{x}|^2\right)$ in (2.13) requires $(N_t + 1)$ complex multiplications.

From (4.17) and (4.18), the complexity of SM does not depend on the number of transmit antennas, and it is equal to the complexity of single–input multiple–ouput (SIMO) systems. However, the complexity of SMX increases linearly with the number of transmit antennas.

The reduction of SM–ML receiver complexity relative to the complexity of the SMX–ML decoder for the same spectral efficiency is given by,

$$\mathcal{C}_{\text{rel}}^{\text{ML}} = 100 \times \left(1 - \frac{2}{N_t + 1}\right) \tag{4.19}$$

From (4.19), the reduction in complexity offered by SM increases with the increase in the number of transmit antennas. For example for $N_t = 4$, SM offers a 60% reduction in complexity compared to SMX, and as the number of transmit antennas increase the reduction increases.

4.3.2 Rx–SD

The complexity of the Rx–SD receiver is given by:

$$\mathcal{C}_{\mathrm{Rx-SD}} = 3\sum_{\ell=1}^{N_t}\sum_{s=1}^{M}\tilde{N}_r\left(\ell, s\right) \tag{4.20}$$

It is easy to show that $\mathcal{C}_{\mathrm{Rx-SD}}$ lies in the interval $3 \times 2^{\eta} \leq \mathcal{C}_{\mathrm{Rx-SD}} \leq 6N_r 2^{\eta}$, where the lower bound corresponds to the scenario where $\tilde{N}_r\left(\ell, s\right) = 1$, and the upper bound corresponds to the scenario where $\tilde{N}_r\left(\ell, s\right) = 2N_r$ for $\ell \in \{1, 2, \ldots N_t\}$ and $s \in \{s_1, s_2, \ldots s_M\}$. An interesting observation is that Rx–SD offers a reduction in complexity even for the case of $N_r = 1$, where the complexity lies in the interval $3 \times 2^{\eta} \leq \mathcal{C}_{\mathrm{Rx-SD}} \leq 6 \times 2^{\eta}$. Note, the Rx–SD solution requires no pre–computations with respect to the ML–optimum detector. In fact, $\tilde{N}_r\left(\ell, s\right)$ for $\ell \in \{1, 2, \ldots N_t\}$ and $s \in \{s_1, s_2, \ldots s_M\}$ in (4.9) are implicitly computed when solving the detection problem in (4.8).

4.3.3 Tx–SD

The computational complexity of Tx–SD can be upper–bounded by,

$$\mathcal{C}_{\mathrm{Tx-SD}} \leq \mathcal{C}_{\Theta_R} + 3N_t\bar{\bar{\Theta}}_R \tag{4.21}$$

where $\bar{\bar{a}}$ denotes the cardinality of a, and $\mathcal{C}_{\Theta_R}$ is the complexity of finding the points in the subset Θ_R,

$$\mathcal{C}_{\Theta_R} = \mathcal{C}_{\text{Pre-Comp}} + \mathcal{C}_{\text{Interval}} \tag{4.22}$$

where,

1. $\mathcal{C}_{\text{Pre-Comp}}$ is the number of operations needed to compute the Cholesky decomposition. Calculating the upper triangular matrix $\bar{\mathbf{D}}$ using Cholesky decomposition has the complexity [175],

$$\mathcal{C}_{\mathrm{CH}} = 4N_t^3/3 \tag{4.23}$$

Calculation of $\bar{\mathbf{G}}$, $\bar{\rho}$ and $\bar{\mathbf{z}}$ can be easily shown that it requires $2N_rN_t(2N_t+1)$, $2N_t(2N_t+2N_r+1)$ and $N_t(2N_t+1)$ real operations respectively, where back–substitution algorithm was used for calculating $\bar{\rho}$ [175]. Hence,

$$\mathcal{C}_{\text{Pre-Comp}} = \mathcal{C}_{\mathrm{CH}} + N_t(4N_rN_t + 6N_r + 6N_t + 3) \tag{4.24}$$

2. $\mathcal{C}_{\text{Interval}}$ is the number of operations need to compute the intervals in (4.12),(4.13),

$$\mathcal{C}_{\text{interval}} = 2N_t + (2N_t + 3)N_{(4.13)} \tag{4.25}$$

where,

- For (4.12): $2N_t$ real divisions are needed.
- For (4.13): $(2N_t + 3)\, N_{(4.13)}$ real multiplication are needed, where $(2N_t + 3)$ is the number of real computations need to compute (4.13), and $N_{(4.13)}$ is the number of times (4.13) is computed, which is calculated by simulations. Note that: i) the interval in (4.13) depends on the antenna index ℓ and only the imaginary part of the symbol s, ii) some symbols share the same imaginary part. Therefore, (4.13) is only calculated for those points (ℓ, s) which lie in the interval in (4.12) and does not have the same ℓ and $\text{Im}\{s\}$ as a previously calculated point.

4.4 Error Probability of SM–SDs and Initial Radius Selection Method

In this section, an analytical upper bound for the ABER performance of SM–SD is derived. Moreover, this section shows that SM–SD offers a near optimum performance. The ABER for SM–SD is estimated using the union bound [110], which is as follows,

$$\underset{\text{SM–SD}}{\text{ABER}} \leq \sum_{\ell_t, s_t} \sum_{\ell, s} \frac{N\left(\bar{\mathbf{x}}_{\ell_t, s_t}, \bar{\mathbf{x}}_{\ell, s}\right)}{\eta} \frac{\text{E}_{\mathbf{H}}\left\{\text{Pr}_{e,\text{SM–SD}}\right\}}{2^{\eta}} \tag{4.26}$$

where $N\left(\bar{\mathbf{x}}_{\ell_t, s_t}, \bar{\mathbf{x}}_{\ell, s}\right)$ is the number of bits in error between $\bar{\mathbf{x}}_{\ell_t, s_t}$ and $\bar{\mathbf{x}}_{\ell, s}$, and,

$$\underset{e,\text{SM–SD}}{\text{Pr}} = \text{Pr}\left(\left(\tilde{\ell}_{\text{SM–SD}}, \tilde{s}_{\text{SM–SD}}\right) \neq (\ell_t, s_t)\right) \tag{4.27}$$

is the pairwise error probability of deciding on the point $\left(\tilde{\ell}_{\text{SM–SD}}, \tilde{s}_{\text{SM–SD}}\right)$ given that the point (ℓ_t, s_t) is transmitted.

The probability of error $\text{Pr}_{e,\text{SM–SD}}$ can be thought of as two mutually exclusive events depending on whether the transmitted point (ℓ_t, s_t) is inside the sphere. In other words, the probability of error for SM–SD can be separated in two parts, as shown in [177]:

- $\Pr\left((\tilde{\ell}_{\text{SM–ML}}, \tilde{s}_{\text{SM–ML}}) \neq (\ell_t, s_t)\right)$: The probability of deciding on the incorrect transmitted symbol and/or used antenna combination, given that the transmitted point (ℓ_t, s_t) is inside the sphere.

- $\Pr\left((\ell_t, s_t) \notin \Theta_R\right)$: The probability that the transmitted point (ℓ_t, s_t) is outside the set of points Θ_R considered by the SD algorithm.

Therefore, the probability of error for SM–SD can be written as,

$$\Pr_{e,\text{SM–SD}} \leq \left(\Pr\left((\tilde{\ell}_{\text{SM–ML}}, \tilde{s}_{\text{SM–ML}}) \neq (\ell_t, s_t)\right) + \Pr\left((\ell_t, s_t) \notin \Theta_R\right)\right) \tag{4.28}$$

However, the probability of error for the ML decoder is,

$$\Pr_{e,\text{SM–ML}} \leq \Pr\left((\tilde{\ell}, \tilde{s}) \neq (\ell_t, s_t)\right) \tag{4.29}$$

Thus, SM–SD will have a near optimum performance when,

$$\Pr\left((\ell_t, s_t) \notin \Theta_R\right) << \Pr\left((\tilde{\ell}, \tilde{s}) \neq (\ell_t, s_t)\right) \tag{4.30}$$

The probability of *not* having the transmitted point (ℓ_t, s_t) inside Θ_R can be written as,

$$\begin{aligned}
\Pr\left((\ell_t, s_t) \notin \Theta_R\right) &= \Pr\left(\sum_{r=1}^{2N_r} \left|\bar{y}_r - \bar{\mathbf{h}}_{\ell_t,r}\bar{\mathbf{s}}_t\right|^2 > R^2\right) \\
&= \Pr\left(\kappa > \left(\frac{R}{\sigma_n/\sqrt{2}}\right)^2\right) \\
&= 1 - \frac{\gamma\left(N_r, \left(\frac{R}{\sigma_n}\right)^2\right)}{\Gamma(N_r)}
\end{aligned} \tag{4.31}$$

where,

$$\kappa = \sum_{r=1}^{2N_r} \left|\frac{\bar{n}_r}{\sigma_n/2}\right|^2 \tag{4.32}$$

is a central chi-squared random variable with $2N_r$ degree of freedom, and a cumulative distribution function (CDF) equal to [110],

$$F_\kappa(a,b) = \frac{\gamma(b/2, a/2)}{\Gamma(b/2)} \tag{4.33}$$

where $\gamma(c,d)$ is the lower incomplete gamma function given by,

$$\gamma(c,d) = \int_0^d t^{c-1} e^{-t} dt \tag{4.34}$$

and $\Gamma(c)$ is the gamma function given by,

$$\Gamma(c) = \int_0^\infty t^{c-1} e^{-t} dt \tag{4.35}$$

The initial sphere radius considered in SM–SD is a function of the noise variance as given in [178],

$$R^2 = 2\varrho N_r \sigma_n^2 \tag{4.36}$$

where ϱ is a constant chosen to satisfy (4.30). In this chapter, this is done by assuming $\Pr\left((\ell_t, s_t) \notin \Theta_R\right) = 10^{-6}$ and back solving (4.31). For $N_r = 1, 2, 4$, $\varrho = 13.8, 8.3, 5.3$ respectively.

From all above, $\Pr_{e,\text{SM–SD}}$ can be formulated as,

$$\begin{aligned} \Pr_{e,\text{SM–SD}} &= \Pr\left(\left\|\bar{\mathbf{y}} - \bar{\mathbf{h}}_\ell \bar{\mathbf{s}}\right\|^2 > \left\|\bar{\mathbf{y}} - \bar{\mathbf{h}}_{\ell_t} \bar{\mathbf{s}}_t\right\|^2\right) \\ &= \Pr\left(\xi > \left\|\bar{\mathbf{h}}_{\ell_t} \bar{\mathbf{s}}_t - \bar{\mathbf{h}}_\ell \bar{\mathbf{s}}\right\|\right) \end{aligned} \tag{4.37}$$

where,

$$\xi = 2\text{Re}\left\{\left(\bar{\mathbf{h}}_{\ell_t} \bar{\mathbf{s}}_t - \bar{\mathbf{h}}_\ell \bar{\mathbf{s}}\right)^T \bar{\mathbf{n}}\right\} \sim \mathcal{N}\left(0, 2\sigma_n^2 \left(\left\|\bar{\mathbf{h}}_{\ell_t} \bar{\mathbf{s}}_t - \bar{\mathbf{h}}_\ell \bar{\mathbf{s}}\right\|\right)\right) \tag{4.38}$$

Then,

$$\Pr_{e,\text{SM–SD}} = Q\left(\sqrt{\frac{\left\|\bar{\mathbf{h}}_{\ell_t} \bar{\mathbf{s}}_t - \bar{\mathbf{h}}_\ell \bar{\mathbf{s}}\right\|^2}{2\sigma_n^2}}\right) \tag{4.39}$$

where $Q(x) = (1/\sqrt{2\pi}) \int_x^{+\infty} e^{-t^2/2} dt$.

In the case of Rayleigh fading, the closed form solution for $\mathrm{E}_{\mathbf{H}}\{\mathrm{Pr}_{e,\text{SM–SD}}\}$ in (4.26) can be derived by employing the solution from [179, eq. (62)]. Note that the argument within (4.39) can be represented as the summation of $2N_r$ squared Gaussian random variables, with zero mean and variance equal to 1. This means that the argument in the Q–function can be described by a central chi–squared distribution with $2N_r$ degrees of freedom. The result for $\mathrm{E}_{\mathbf{H}}\{\mathrm{Pr}_{e,\text{SM–SD}}\}$ is given as,

$$\mathrm{E}_{\mathbf{H}}\left\{\underset{e,\text{SM–SD}}{\mathrm{Pr}}\right\} = \left[\zeta\left(\frac{\sigma_s^2}{4\sigma_n^2}\right)\right]^{N_r}\sum_{r=0}^{N_r-1}\binom{N_r-1+r}{r}\left[1-\zeta\left(\frac{\sigma_s^2}{4\sigma_n^2}\right)\right]^{r} \tag{4.40}$$

where $\sigma_s^2 = \|\bar{\mathbf{x}}_{\ell_t,s_t} - \bar{\mathbf{x}}_{\ell,s}\|_{\mathrm{F}}^2$ and,

$$\zeta(c) = \frac{1}{2}\left(1-\sqrt{\frac{c}{1+c}}\right) \tag{4.41}$$

Plugging (4.40) into (4.26) gives a closed form upper bound for the ABER of SM–SD. Next section shows that (4.26) gives a tight upper bound for the ABER of SM–SD, and that SM–SD offers a near optimum performance.

4.5 Results

In the following, Monte Carlo simulation results for at least 10^6 Rayleigh fading channel realisations are shown to compare the performance and computational complexity of large scale MIMO, SM–ML, SM–SD and SMX–SD.

4.5.1 Analytical performance of SM–SD

Figs. 4.1-4.2 show ABER simulation results for SM–ML, Rx–SD and Tx–SD compared with the analytical bound derived in section 4.4, where $\eta = 6, 8$ and $N_r = 4$. From the figures it can be seen that both Tx–SD and Rx–SD offer a near optimum performance, where the results overlap with the results of the SM–ML optimum receiver. Furthermore, Figs. 4.1-4.2 the figure validates the analytical bound as for BER $< 10^{-2}$ all graphs closely match the analytical curve. Note, it is will–known that the union bound is loose for low SNR [110].

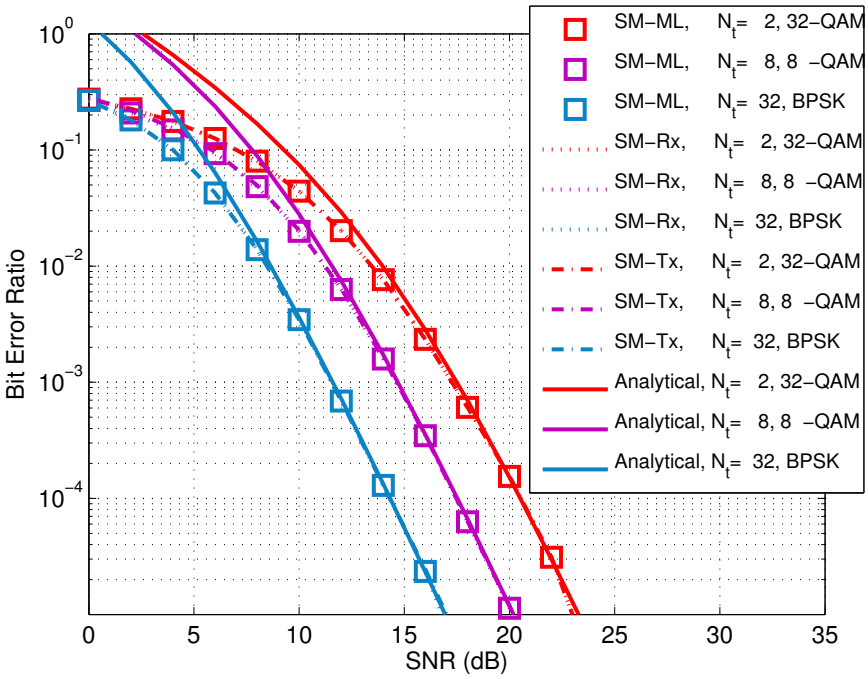

Figure 4.1: *ABER against SNR.* $\eta = 6$*, and* $N_r = 4$*.*

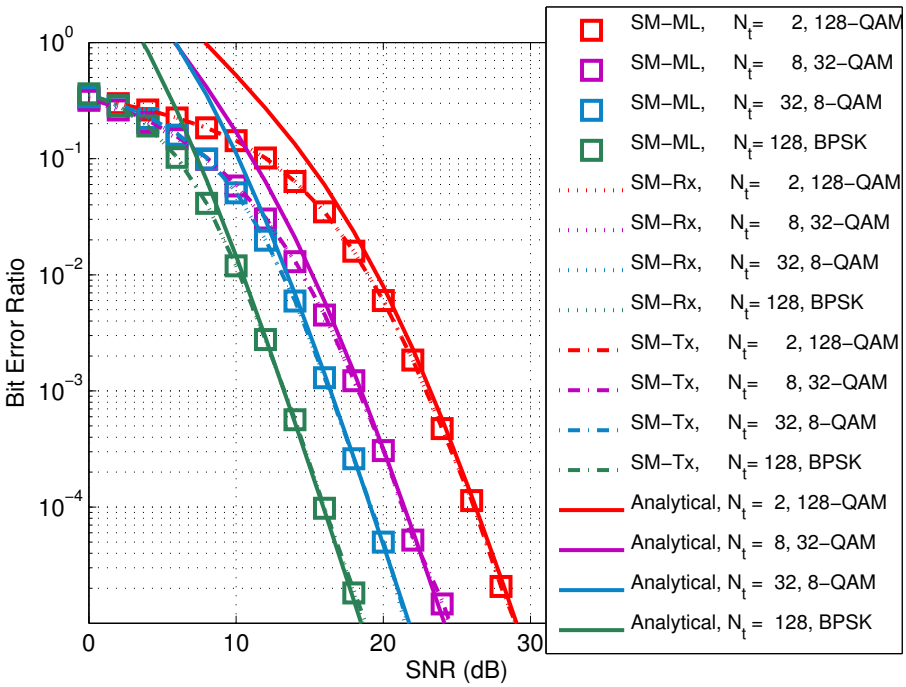

Figure 4.2: *ABER against SNR.* $\eta = 8$*, and* $N_r = 4$*.*

4.5.2 Comparison of the ABER performance of SM and SMX

Figs. 4.3 and 4.4 depict the ABER comparison between all possible combinations of SM and SMX for $\eta = 6$ and $N_r = 2, 4$. In Fig. 4.3, we can observe that the ABER performance depends on the number of transmit antennas used and, consequently, the constellation size. The smaller the constellation size, the better the performance. Another observation that can be made is that SM and SMX offer nearly the same performance when using the same constellation size. However, in Fig. 4.4, where the number of receive antennas is increased, it can be noticed that SM performs better than SMX. In particular, binary phase shift keying (BPSK)–SM provides 1 dB better performance than BPSK–SMX. Also 8–quadrature amplitude modulation (QAM) SM offers a slightly better performance (~ 0.5 dB) than 8-QAM SMX.

In Figs. 4.5 and 4.6, the ABER comparisons for $\eta = 8$ and $N_r = 2, 4$ are shown. In Fig. 4.5, SM and SMX offers almost similar performance for the same constellation size. However, from Fig. 4.6 SM offers a better performance when the number of receive antennas increases.

In summary, SM offers a better or nearly the same ABER as SMX, where the ABER of both systems depends on the size of the constellation diagram and the number of receive antennas. Note, the ABER performance of SM can be improved by increasing the number of receive antennas.

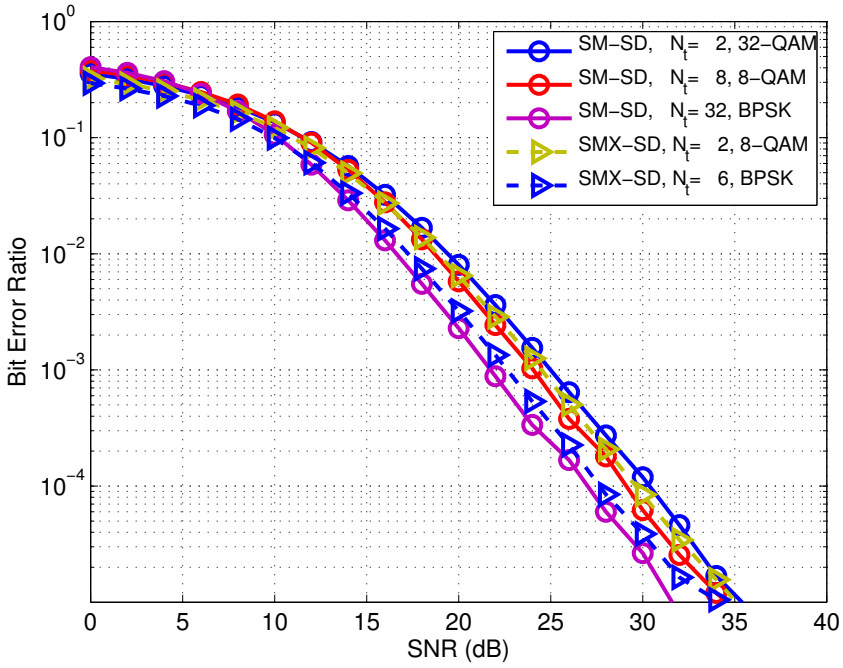

Figure 4.3: *ABER against SNR.* $\eta = 6$*, and* $N_r = 2$*.*

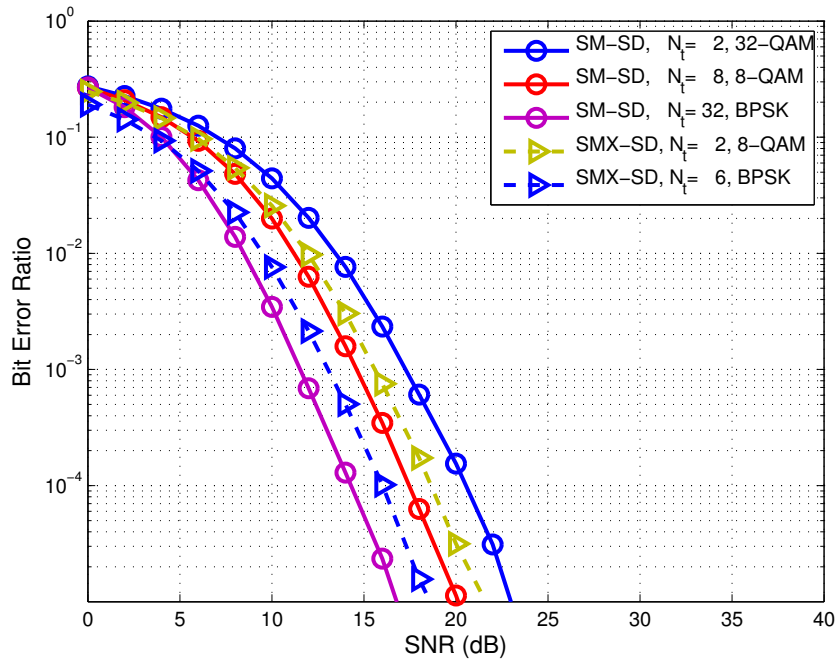

Figure 4.4: *ABER against SNR.* $\eta = 6$*, and* $N_r = 4$*.*

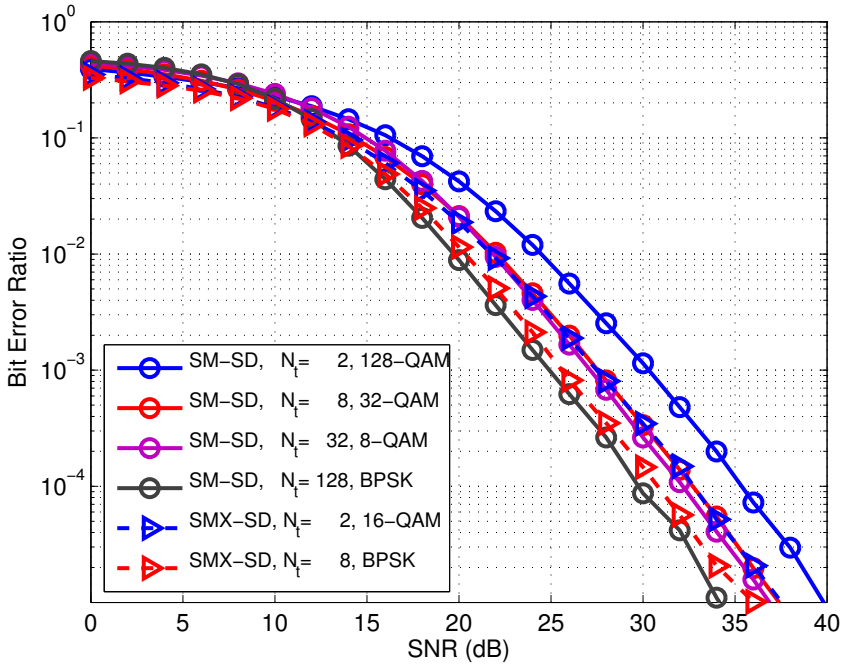

Figure 4.5: *ABER against SNR.* $\eta = 8$*, and* $N_r = 2$*.*

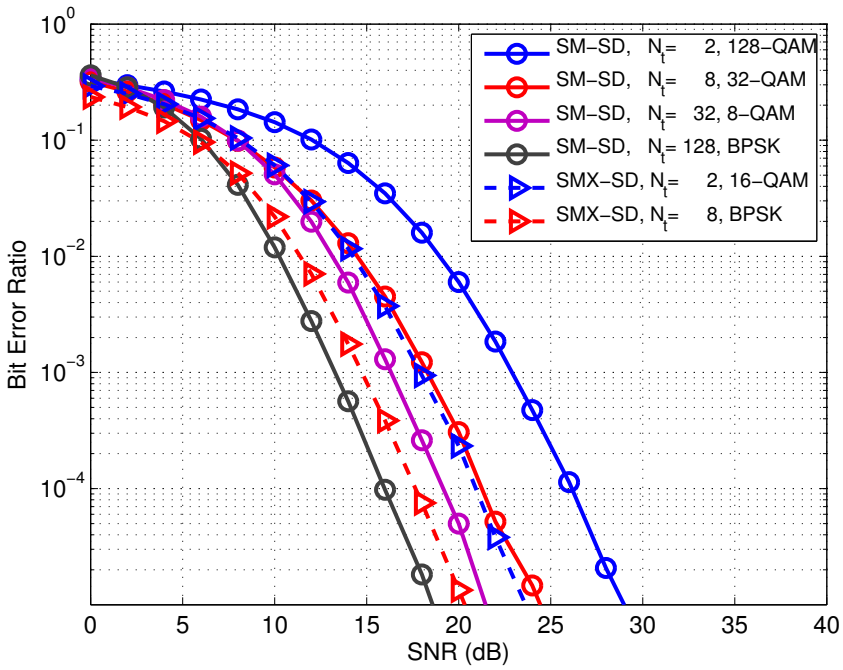

Figure 4.6: *ABER against SNR.* $\eta = 8$*, and* $N_r = 4$*.*

4.5.3 Complexity Analysis

In Figs. 4.7-4.10, the computational complexity of Rx–SD and Tx–SD provided in (4.20) and (4.21) respectively is compared with the complexity of SMX–SD, where the initial radius is chosen according to (4.36). In particular, the figures show the relative computational complexity of the SDs with respect to the ML–optimum detector, *i.e* $\mathcal{C}_{\text{rel}}\,(\%) = 100 \times (\mathcal{C}_{\text{SD}}/\mathcal{C}_{\text{ML}})$. Note, for SM the SD with the lowest complexity is chosen.

In Figs. 4.7 and 4.8, the relative complexities for $\eta = 6$ and $N_r = 2, 4$ are shown. Fig. 4.7, shows that for large constellation size the lowest relative complexity is offered by Tx–SD $N_t = 2$. The relative computational complexity ranges between 40% for low signal to noise ratio (SNR) and 16% for high SNR. However, for lower constellation size Rx–SD provides the lowest relative complexity, which is between 56% for low SNR and 26% for high SNR. As Rx–SD reduces the receive search space, the reduction in complexity offered by Rx–SD does not depend on the number of transmit antennas. Therefore, only Rx–SD with $N_t = 4, 32$ are shown, where both scenarios offer nearly the same relative computational complexity. Finally, from Fig. 4.7 it can be seen that SMX–SD, $N_t = 2$ and $N_t = 3$ are less complex than SM–ML

with a relative complexity (48%) and $79\% - 82\%$ respectively. However, comparing SM–SD to SMX–SD $N_t = 2$, for 32–QAM SM–SD is 32% less complex than SMX–SD, and for BPSK SM–SD is 22% less complex than SMX–SD. In Fig. 4.8, it can be seen that for large constellation size Tx–SD is still the best choice with a relative complexity that ranges between $22\% - 12\%$, which is 15% less than SMX–SD, $N_t = 2$. For smaller constellation size Rx–SD is the best choice with relative complexity that ranges between $(55\% - 14\%))$, offering a (23%) extra reduction in complexity when compared to SMX–SD, $N_t = 2$. Note, i) SMX–SD, $N_t = 6$ is not shown in the figure, because this scenario has a complexity higher than the complexity of SM–ML, ii) the complexity of SMX–SD, $N_t = 3$ increased with the increase of SNR, for the reason that, in the under-determined case ε depends on the SNR (4.10).

The relative complexity for $\eta = 8$ and $N_r = 2, 4$ is shown in Fig. 4.9 and 4.10. Since Tx–SD reduces the transmit search space, the reduction in complexity increased by more than 10% with the increase in the spectral efficiency and consequently the constellation size. In Fig. 4.9 for high constellation size Tx–SD, $N_t = 2$ is the best choice with a relative complexity that reaches 4% for high SNR, and in Fig. 4.10 for high constellation size Tx–SD, $N_t = 2$ and $N_t = 4$ are the best choice with a relative complexity that reaches 3% and 10% respectively. On the other hand, Rx–SD reduces the receive search space, therefore, it still offers nearly the same relative complexity. However, the complexity reduces with the increase of N_r, where Rx–SD, $N_r = 4$ is $\sim 10\%$ less complex than Rx–SD $N_r = 2$. Finally, from both figures it can be seen that although SM–ML is much less complex than SMX–ML, SMX–SD is less complex than SM–ML. For that reason, SM–SD has to be developed, where SM–SD is $\sim 20\%$ less complex than SMX–SD for $N_r = 2$, and $\sim 10\%$ less complex than SMX–SD for $N_r = 4$. Note, the complexity of both SM–Tx and SMX–SD decreases with the increase of N_r, because for the case of $N_r < N_t$, the less under-determined the system, the fewer pre–computations are needed.

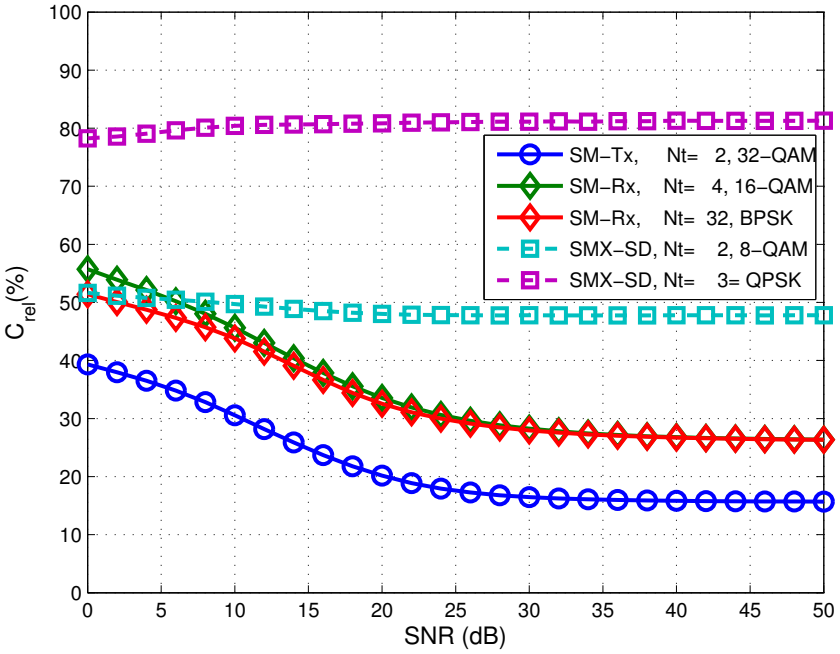

Figure 4.7: *Computational complexity against SNR.* $\eta = 6$*, and* $N_r = 2$*.*

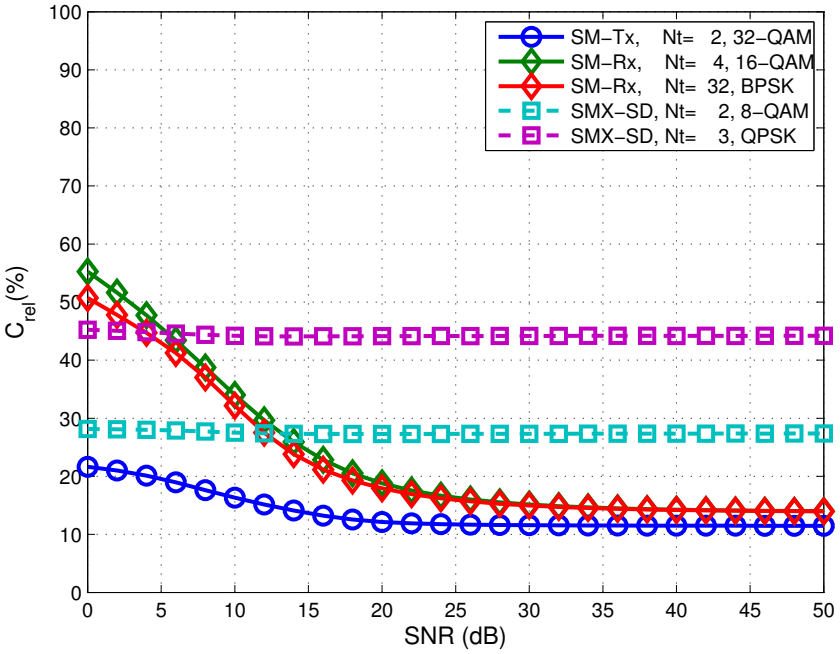

Figure 4.8: *Computational complexity against SNR.* $\eta = 6$*, and* $N_r = 4$*.*

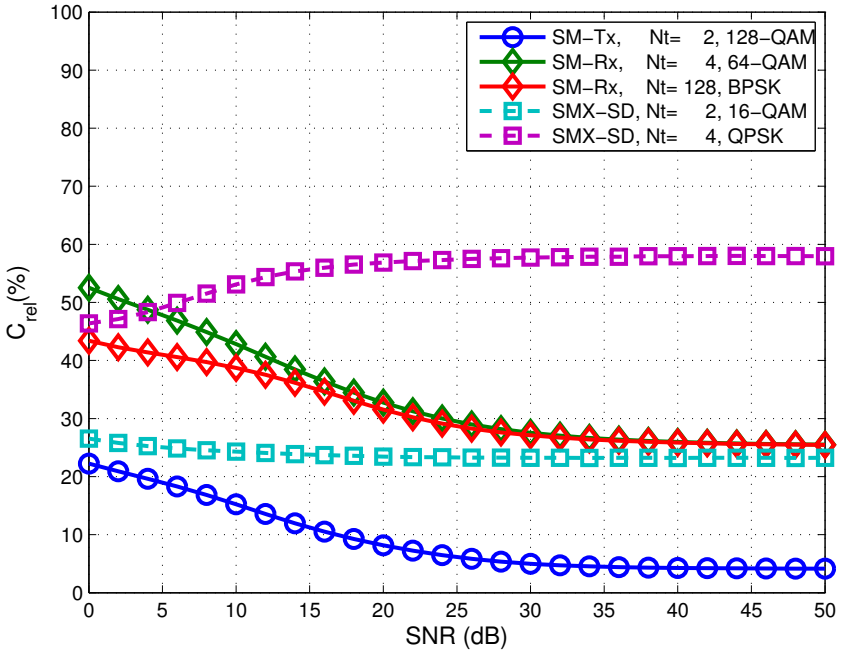

Figure 4.9: *Computational complexity against SNR.* $\eta = 8$*, and* $N_r = 2$*.*

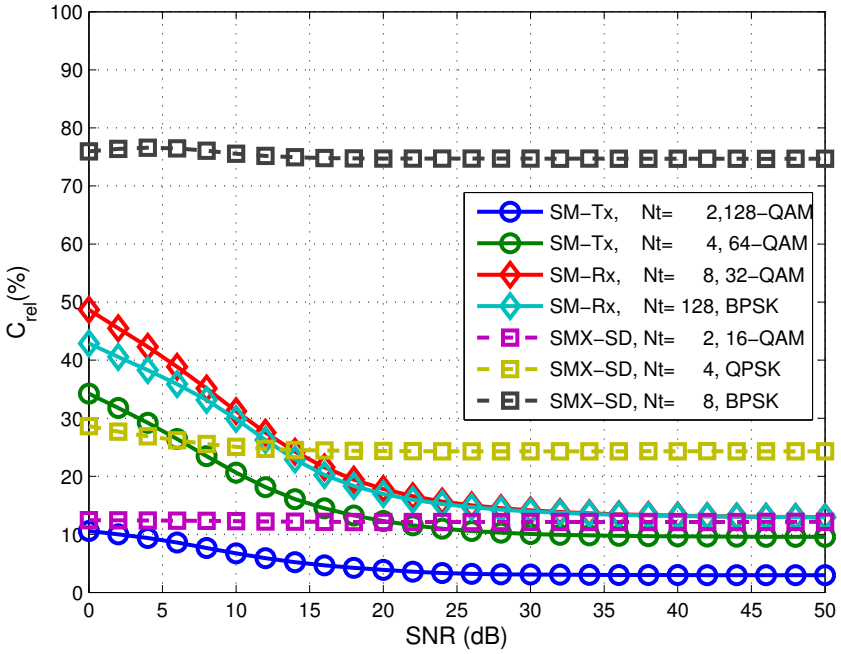

Figure 4.10: *Computational complexity against SNR.* $\eta = 8$*, and* $N_r = 4$*.*

4.6 Summary

This chapter introduced and analysed the performance/complexity trade–off of two SDs designed specifically for SM. Tx–SD which reduces the transmit search space, and Rx–SD which reduces the receive search space. The proposed SDs provide a substantial reduction in the computational complexity while retaining the same ABER as the ML–optimum detector. The closed–form analytical performance of SM in identical and independently distributed (i.i.d.) Rayleigh flat–fading channels has been derived, and analytical and simulation results were shown to closely agree. Furthermore, numerical results have highlighted that no SD is superior to the others, and that the best solution to use depends on the particular MIMO setup, and the SNR at the receiver. In general, Rx–SD is the best choice for lower spectral efficiencies, and Tx–SD is the best option for higher spectral efficiencies. Finally, simulation results showed that SM using SD offers a significant reduction in computational complexity and nearly the same ABER performance as SMX using ML decoder or SD.

In summary, SM–SD offers i) computational complexity and power consumption that does not depend on the number of transmit antennas, ii) ABER performance that improves with the increase of the number transmit antennas, and iii) significant reduction in computational complexity compared to SMX.

Chapter 5
Generalised Spatial Modulation with Variable Number of Active Antennas

In this chapter, a generalised techniques for spatial modulation (SM) are presented. Generalised spatial modulation (GNSM) and variable generalised spatial modulation (VGSM) overcome the constraint in the number of transmit antennas needed by SM in a novel fashion. In GNSM and VGSM, a block of information bits is mapped to a constellation symbol and a spatial symbol. The spatial symbol is a combination of transmit antennas activated at each instance to transmit the constellation symbol. While in GNSM the number of active antennas is constant, however, for VGSM the number of active antennas varies. This is unlike SM where single transmit antenna is activated at each instance. Hence, GNSM and VGSM increase the overall spectral efficiency by base-two logarithm of the number of antenna combinations, thus reducing the number of transmit antennas needed. Three receivers to determine the full information bits by detecting the antenna combination and the transmitted symbol are proposed. The first receiver is based on the maximum–likelihood (ML) principle, and the last two receivers are based on the sphere decoder (SD) principle. The performance of GNSM and VGSM is analysed in this chapter, and a tight bound on the average bit error ratio (ABER) performance over, correlated and uncorrelated, Rayleigh and Rician channels is derived. Finally, the performance of GNSM and VGSM is validated through Monte Carlo simulations and compared to the performance of SM and spatial multiplexing (SMX), where it is shown that the proposed schemes, GNSM and VGSM use much smaller number of antennas than SM, have significantly lower computational complexity than SMX, and need only one radio frequency (RF) chain, while having a small penalty in the ABER performance. Therefore, the proposed schemes are good candidates for low hardware, and computational complexity multiple–input multiple–output (MIMO) solutions.

5.1 Introduction

The logarithmic increase in spectral efficiency offered by spatial modulation (SM) and the requirement that the number of antennas must be a power of two would require large number of antennas. Fractional bit encoding spatial modulation (FBE–SM) in [37], was proposed to overcome this limitation by using the theory of modulus conversion. By doing so, an arbitrary number of transmit antennas can be used. However, FBE–SM suffers from error propagation.

Motivated by that, two new multiple–input multiple–output (MIMO) modulation systems, generalised spatial modulation (GNSM) and variable generalised spatial modulation (VGSM), are proposed to over come the limitation in the number of transmit antennas. In GNSM and VGSM the same symbol is transmitted simultaneously from more than than one transmit antenna. Hence, more than one antenna is active and transmits the same symbol at a time. GNSM is first proposed in [38] and in [39], where in [38], GNSM with maximum–likelihood (ML)–optimum receiver is proposed, and in [39], GNSM with maximal ratio combining (MRC) sub–optimal receiver is proposed. In GNSM the number of active antennas is constant. However, in VGSM the number of active antennas varies from only one active antenna at a time to all antennas being active and transmitting the same symbol. As a result, the number of transmit antennas required by GNSM and VGSM to achieve a certain spectral efficiency and a constellation size is reduced. For example, for $\eta = 4$ and binary phase shift keying (BPSK) modulations, GNSM and VGSM reduces the number of transmit antennas needed by SM, by 37% and 50% respectively. The mapping procedure for GNSM and VGSM after grouping the incoming data sequence in groups of η bits, can be summarised in two points: 1) The first η_ℓ bits determine which antenna combination to activate. 2) The last η_s bits are modulated and transmitted through the active antennas.

Transmitting the same data symbol from the active antennas, retains the key advantages of SM:

- The complete avoidance of inter–channel interference (ICI) at the receiver, where all active antennas transmit the same symbol.
- The low computational complexity, which is equal to the complexity of single–input multiple–ouput (SIMO) systems.
- Only one radio frequency (RF) chain is needed, as all active antennas transmit the same symbol.

At the receiver three decoders are proposed. The first one is the ML–optimum receiver. The other two sphere decoders (SDs) are Tx–SD and Rx–SD proposed for SM where in this chapter they are extended to be used for GNSM and VGSM.

In this chapter, a careful study of the performance of both systems, GNSM and VGSM, using the three proposed detectors, along with an accurate comparison of their computational complexity is provided. Moreover, a tight closed form expression for the average bit error ratio (ABER) performance of GNSM and VGSM, over correlated and uncorrelated, Rayleigh and Rician fading channels is derived. Results show that the proposed schemes, VGSM and GNSM, use much smaller number of antennas than SM and have significantly lower computational complexity than spatial multiplexing (SMX), while having a small penalty in the ABER performance. More specifically, VGSM and GNSM, reduces the number of transmit antennas by up to 93%, when compared to SM. Furthermore, VGSM and GNSM, reduce the computational complexity by at least $(40\%$ when compared to SMX, while having an ABER penalty between $1.5 - 4$ dB. Therefore, proposed schemes are good candidates for low hardware and computational complexity MIMO solutions.

The reminder of this chapter is organised as follows. In Section 5.2 and Section 5.3, the system models for GNSM and VGSM are summarised. In Section 5.4, the three receivers, ML, Tx–SD, and Rx–SD, are described. An accurate analysis of the computational complexity of, ML, Tx–SD, and Rx–SD, is performed in Section 5.5. The analytical ABER performance for GNSM and VGSM is derived along with the initial radius selection method in Section 5.6. Finally, numerical results are presented in Section 5.7, and the chapter is concluded in Section 5.8. Note, the channel model is introduced in 2.2.3.3.

5.2 Generalised Spatial Modulation

Unlike SM in GNSM more than one transmit antenna is active and sending the same complex symbol at a time. Hence, a set of antenna combinations can be formed, and used as spatial constellation points. The number of possible antenna combinations is $\binom{N_t}{N_u}$, where N_t is the number of transmit antennas, N_u is the number of active antennas at each instance, and $\binom{\cdot}{\cdot}$ denotes the binomial operation. However, the number of antenna combinations that can be considered for transmission must be a power of two. Therefore, only $\varrho_{\text{GNSM}} = 2^{\eta_\ell}$ combinations, can be used, where $\eta_\ell = \lfloor \log_2 \binom{N_t}{N_u} \rfloor$, and $\lfloor \cdot \rfloor$ is the floor operation.

Grouped Bits	Antenna Combination (Υ^{GNSM})
000	(1,2)
001	(1,3)
010	(1,4)
011	(1,5)
100	(2,3)
101	(2,4)
110	(2,5)
111	(3,4)

Table 5.1: *GNSM Mapping Table for $N_t = 5$ and $N_u = 2$, where $(\cdot, \cdot)$ indicates the indexes of the active antennas*

The GNSM mapper divides the incoming bit stream into blocks of $\eta = \eta_\ell + \eta_s$ bits, where η is the spectral efficiency and $\eta_s = \log_2(M)$ where M is the size of the constellation diagram. 1) The first η_ℓ bits are used to select which antennas to activate. In this chapter, the transmit–antennas which are active for transmission are denoted by Υ_t^{GNSM}, with $\Upsilon_t^{\text{GNSM}} \in \{\Upsilon_1^{\text{GNSM}}, \Upsilon_2^{\text{GNSM}}, \ldots, \Upsilon_{\varrho_{\text{GNSM}}}^{\text{GNSM}}\}$. 2) The last η_s bits are used to choose a symbol in the signal–constellation diagram. Without loss of generality, quadrature amplitude modulation (QAM) is considered in this chapter. The transmitted complex symbol is denoted by s_t, with $s_t \in \{s_1, s_2, \ldots, s_M\}$.

In general, the maximum number of bits that can be transmitted using GNSM is given by,

$$\eta_{\text{GNSM}} = \eta_\ell + \eta_s = \left\lfloor \log_2 \binom{N_t}{N_u} \right\rfloor + \log_2 M \tag{5.1}$$

An example of the possible antennas combinations for the case of $N_t = 5$ and $N_u = 2$ is shown in Table 5.1. Note, the antenna combinations $(3, 4), (4, 5)$ are not used, that is because the number of possible antenna combinations is $\binom{5}{2} = 10$. However, only $\varrho_{\text{GNSM}} = 2^{\lfloor \log_2(10) \rfloor} = 8$ can be used. Therefore, only the first eight antenna combinations are used. Now let $\mathbf{g} = \begin{bmatrix} 1 & 0 & 0 & 1 \end{bmatrix}$ be the incoming data sequence. Then, from Table 5.1, the first $\eta_\ell = 3$ bits, $\mathbf{g}_\ell = \begin{bmatrix} 1 & 0 & 0 \end{bmatrix}$, give the antenna combination $\Upsilon_5^{\text{GNSM}} = (2, 3)$ to be used, and the last $\eta_s = 1$ bit, $\mathbf{g}_s = \begin{bmatrix} 1 \end{bmatrix}$, is modulated using BPSK modulation to $s_t = +1$. Hence, the transmitted vector is $\mathbf{x}_{\ell_t, s_t} = \begin{bmatrix} 0 & \frac{+1}{\sqrt{2}} & \frac{+1}{\sqrt{2}} & 0 & 0 \end{bmatrix}^T$. Note, the symbol is divided by the $\sqrt{N_u}$ so that $\mathrm{E}[|x|^2] = 1$.

If SM is to be used instead of GNSM, for the same modulation order and spectral efficiency, the number of antennas must be increased to eight, *i.e.*, GNSM offered about $\sim 37.5\%$ reduction in N_t when compared to SM. Note, the spectral efficiency for SM is $\eta_{\text{SM}} = \log_2(N_t) + \eta_s$.

5.3 Variable Generalised Spatial Modulation

Even though GNSM offers a large reduction in the number of transmit antennas when compared to SM, there is still possibility for further reductions. In this section VGSM is proposed, where the number of active antennas varies from only one active transmit antenna to all antennas being active, and transmitting the same symbol. In this way, the number of possible antenna combinations increases to,

$$\varrho'_{\text{VGSM}} = \sum_{n=1}^{N_t} \binom{N_t}{n} = 2^{N_t} - 1 \tag{5.2}$$

However, as the number of combinations must be a power of two, only $\varrho_{\text{VGSM}} = 2^{\eta_\ell}$ can be used, where,

$$\eta_\ell = \lfloor \log_2 \left(2^{N_t} - 1\right) \rfloor = N_t - 1 \tag{5.3}$$

Therefore, the spectral efficiency of VGSM is,

$$\eta_{\text{VGSM}} = \eta_s + \eta_\ell = \eta_s + N_t - 1 \tag{5.4}$$

Comparing the number of transmit antennas needed by VGSM to the number of transmit antennas needed by SM, for $\eta = 4$ bit and BPSK modulation, it can be seen that VGSM offers 50% reduction in the number of transmit antennas, which is an extra 12.5% reduction in comparison to the reduction offered by GNSM, and VGSM only needs four transmit antennas. Now, comparing the spectral efficiency of VGSM with the spectral efficiency of SMX, where the spectral efficiency for SMX is $\eta_{\text{SMX}} = \eta_s N_t$, it can be seen that the spectral efficiency of VGSM does not increase linearly as the spectral efficiency of SMX. This means that VGSM needs a larger number of transmit antennas/larger constellation size to have the same spectral efficiency as SMX. However, because in VGSM the active antennas transmit the same symbol, the computational complexity of VGSM, as it is going to be shown later, does not depend on the number of transmit antennas. Unlike SMX where the computational complexity increases linearly with the number of transmit antennas. The computational complexity of VGSM is the same as the computational complexity of SIMO systems.

An example of the possible antenna combinations that can be used for VGSM with $N_t = 4$ is shown in Table 5.2. It can be seen from the table that depending on the incoming bits, in some cases, for example $\mathbf{g}_\ell = \begin{bmatrix} 0 & 1 & 0 \end{bmatrix}$, only one transmit antenna, the third antenna, is

Grouped Bits	Antenna Combination (Υ^{VGSM})
000	(1)
001	(2)
010	(3)
011	(4)
100	(1,2)
101	(1,3)
110	(1,4)
111	(2,3)

Table 5.2: *VGSM Mapping Table for $N_t = 4$, where $(\cdot, \cdot)$ indicates the indexes of the active antennas*

active. And in other case, for example $\mathbf{g}_\ell = \begin{bmatrix} 1 & 0 & 1 \end{bmatrix}$, two transmit antennas, first and third antenna, are active and transmitting the same symbol.

As in GNSM, the mapping procedure for VGSM, after grouping the incoming data sequence in groups of η_{VGSM} bits, can be summarised in two points,

- The first η_ℓ bits are used to find which antenna combination to be used.
- The last η_s bits are modulated using M–QAM modulation, and transmitted from all the active antennas.

5.4 Maximum Likelihood Receiver and Sphere Decoder

In this section two low complexity receivers designed for GNSM and VGSM are introduced. The first receiver is ML–optimum detector, and the second receiver is based on the SD idea, which avoids an exhaustive search by examining only those points that lie inside a sphere with radius R. First, the real–valued equivalent of the complex–valued model in (2.1) following [176] is introduced,

$$\bar{\mathbf{y}} = \bar{\mathbf{H}}_c \bar{\mathbf{x}}_{\ell_t, s_t} + \bar{\mathbf{n}} = \bar{\mathbf{h}}_c^{\ell_t} \bar{\mathbf{s}}_t + \bar{\mathbf{n}} \tag{5.5}$$

where denoting $\mathrm{Re}\{\cdot\}$ and $\mathrm{Im}\{\cdot\}$ the real and imaginary parts respectively, and,

$$\bar{\mathbf{y}} = \left[\mathrm{Re}\left\{\mathbf{y}^T\right\}, \mathrm{Im}\left\{\mathbf{y}^T\right\}\right]^T \tag{5.6}$$

$$\bar{\mathbf{H}}_c = \begin{bmatrix} \mathrm{Re}\{\mathbf{H}_c\} & \mathrm{Im}\{\mathbf{H}_c\} \\ -\mathrm{Im}\{\mathbf{H}_c\} & \mathrm{Re}\{\mathbf{H}_c\} \end{bmatrix} \tag{5.7}$$

$$\bar{\mathbf{x}}_{\ell_t,s_t} = \left[\mathrm{Re}\left\{\mathbf{x}^T_{\ell_t,s_t}\right\}, \mathrm{Im}\left\{\mathbf{x}^T_{\ell_t,s_t}\right\}\right]^T \tag{5.8}$$

$$\bar{\mathbf{n}} = \left[\mathrm{Re}\left\{\mathbf{n}^T\right\}, \mathrm{Im}\left\{\mathbf{n}^T\right\}\right]^T \tag{5.9}$$

$$\bar{\mathbf{h}}^{\ell}_c = \left[\sum_{n\in\Upsilon_\ell} \bar{\mathbf{h}}_n, \sum_{n\in\Upsilon_\ell} \bar{\mathbf{h}}_{n+N_t}\right] \tag{5.10}$$

$$\bar{\mathbf{s}} = \begin{bmatrix} \mathrm{Re}\{s\} \\ \mathrm{Im}\{s\} \end{bmatrix} \tag{5.11}$$

where $\bar{\mathbf{h}}_\mathbf{i}$ is the i–th column of $\bar{\mathbf{H}}_\mathbf{c}$.

5.4.1 ML–Optimum Detector

The ML–optimum receiver for MIMO systems can be written as,

$$\hat{\mathbf{x}}^{(\mathrm{ML})}_t = \underset{\mathbf{x}\in\mathcal{Q}^\eta}{\arg\min} \left\{ \left\| \bar{\mathbf{y}} - \bar{\mathbf{H}}_c \bar{\mathbf{x}} \right\|^2_{\mathrm{F}} \right\} \tag{5.12}$$

where $\mathcal{Q}^\eta$ is a 2^η space containing all possible $(N_t \times 1)$ transmitted vectors, $\|\cdot\|_{\mathrm{F}}$ is the Frobenius norm, and $\hat{\cdot}$ denotes the estimated spatial and constellation symbols. In GNSM and VGSM all active antennas transmit the same symbol. Therefore, (5.12) can be simplified to,

$$\begin{aligned} \left[\hat{\ell}^{(\mathrm{ML})}_t, \hat{s}^{(\mathrm{ML})}_t\right] &= F \underset{\substack{s\in M\text{–QAM} \\ \ell\in\{1,2,\ldots,\varrho\}}}{\arg\min} \left\{ \left\| \bar{\mathbf{y}} - \bar{\mathbf{h}}^{\ell}_c \bar{\mathbf{s}} \right\|^2_{\mathrm{F}} \right\} \\ &= \underset{\substack{s\in M\text{–QAM} \\ \ell\in\{1,2,\ldots,\varrho\}}}{\arg\min} \left\{ \sum_{r=1}^{2N_r} \left| \bar{y}_r - \bar{\mathbf{h}}^{\ell}_{c,r} \bar{\mathbf{s}} \right|^2 \right\} \end{aligned} \tag{5.13}$$

where $\bar{y}_r$ is the r–th entry of $\bar{\mathbf{y}}$, and $\bar{\mathbf{h}}^{\ell}_{c,r}$ is the r–th row of $\bar{\mathbf{h}}^{\ell}_c$.

5.4.2 Sphere Decoding

Two SDs are presented here, Rx–SD and Tx–SD. Rx–SD aims at reducing the number of summations over N_r done by the ML receiver in (5.13). Tx–SD aims at reducing the number of points (ℓ, s) the ML receiver searches over.

5.4.2.1 Rx–SD Detector

The Rx–SD is a reduced–complexity and close–to–optimal ABER–achieving decoder, which aims at reducing the receive search space. The detector can formally be written as follows:

$$\left[\hat{\ell}_t^{(\mathrm{Rx-SD})}, \hat{s}_t^{(\mathrm{Rx-SD})}\right] = \underset{\substack{s\in M\text{–QAM} \\ \ell\in\{1,2,\ldots,\varrho\}}}{\arg\min} \left\{ \sum_{r=1}^{\tilde{N}_r(\ell,s)} \left| \bar{y}_r - \bar{\mathbf{h}}_{c,r}^{\ell} \bar{\mathbf{s}} \right|^2 \right\} \tag{5.14}$$

where,

$$\tilde{N}_r\left(\ell, s\right) = \max_{n\in\{1,2,\ldots 2N_r\}} \left\{ n \left| \sum_{r=1}^{n} \left| \bar{y}_r - \bar{\mathbf{h}}_{c,r}^{\ell} \bar{\mathbf{s}} \right|^2 \leq R^2 \right\}. \tag{5.15}$$

The algorithm executes the following steps: 1) It keeps combining the received signals as long as the Euclidean distance in (5.14) is less or equal to the radius R. 2) Whenever a point is found to be inside the sphere, the radius, R, is updated with the Euclidean distance of that point. 3) The point with the minimum Euclidean distance and $\tilde{N}_r\left(\cdot,\cdot\right) = 2N_r$ is considered to be the solution.

5.4.2.2 Tx–SD Detector

SD in literature is designed for SMX, where all antennas are active and transmitting different symbols [10, 140, 141, 142], or for SM, where only one antenna is active [180]. However, in GNSM and VGSM more than one antenna can be active and transmitting the same symbol. Therefore, a modified SD that reduces the transmit search space, designed for GNSM and VGSM is presented. The transmit search space is reduced by computing the Euclidean distances only for those points, $(\ell, s) \in (\Upsilon, M\text{–QAM})$, which lie inside a sphere with radius R and are centred around the received signal.

Let Cholesky factorisation of the $(2N_t \times 2N_t)$ positive definite matrix $\bar{\mathbf{G}} = \bar{\mathbf{H}}^T\bar{\mathbf{H}} + \varepsilon\bar{\mathbf{I}}_{N_t}$ be $\bar{\mathbf{G}} = \bar{\mathbf{D}}^T\bar{\mathbf{D}}$, where

$$\varepsilon = \begin{cases} \sigma_n^2 & N_t > N_r \\ 0 & N_t \leq N_r \end{cases} \tag{5.16}$$

Then the Tx–SD can be formally written as follow,

$$\begin{aligned}\left[\hat{\ell}_t^{(\mathrm{Tx-SD})}, \hat{s}_t^{(\mathrm{Tx-SD})}\right] &= \underset{(\ell,s)\in\Theta_R}{\arg\min}\left\{\left\|\bar{\mathbf{z}} - \bar{\mathbf{D}}\bar{\mathbf{x}}_{\ell,s}\right\|_{\mathrm{F}}^2\right\} \\ &= \underset{(\ell,s)\in\Theta_R}{\arg\min}\left\{\left\|\bar{\mathbf{z}} - \left[\sum_{n\in\Upsilon_\ell}\bar{\mathbf{d}}_n, \sum_{n\in\Upsilon_\ell}\bar{\mathbf{d}}_{n+N_t}\right]\bar{\mathbf{s}}\right\|_{\mathrm{F}}^2\right\} \quad (5.17)\end{aligned}$$

where Θ_R is the subset of points (ℓ, s) for $\ell \in \{1, 2, \ldots, \varrho\}$ and $s \in M$–QAM in the transmit search space which lie inside a sphere with radius R and are centred around the received signal $\bar{\mathbf{z}}$, $\bar{\mathbf{z}} = \bar{\mathbf{D}}\bar{\rho}$, $\bar{\rho} = \bar{\mathbf{G}}^{-1}\bar{\mathbf{H}}^T\bar{\mathbf{y}}$, and $\bar{\mathbf{d}}_n$ is the n–th column of $\bar{\mathbf{D}}$.

After some algebraic manipulations on (5.17), the subset of points Θ_R lie in the intervals:

$$\frac{-R_i + \bar{z}_{\Upsilon_\ell^1+N_t}}{\sum_{n\in\Upsilon_\ell}\bar{D}_{(\Upsilon_\ell^1+N_t,n+N_t)}} \leq \mathrm{Im}\{s\} \leq \frac{R_i + \bar{z}_{\Upsilon_\ell^1+N_t}}{\sum_{n\in\Upsilon_\ell}\bar{D}_{(\Upsilon_\ell^1+N_t,n+N_t)}} \quad (5.18)$$

$$\frac{-R' + \bar{z}_{\Upsilon_\ell^1|\ell}}{\sum_{n\in\Upsilon_\ell}\bar{D}_{\Upsilon_\ell^1,n}} \leq \mathrm{Re}\{s\} \leq \frac{R' + \bar{z}_{\Upsilon_\ell^1|\ell}}{\sum_{n\in\Upsilon_\ell}\bar{D}_{\Upsilon_\ell^1,n}} \quad (5.19)$$

where Υ_ℓ^1 is the index of the first antenna in the antenna combination Υ_ℓ, and,

$$\bar{z}_{a|b} = \bar{z}_a - \sum_{n\in\Upsilon_b}\bar{D}_{(a,n+N_t)}\mathrm{Im}\{s\} \quad (5.20)$$

$$R'^2 = R^2 - \sum_{n_t=N_t+1}^{2N_t}\bar{z}_{n_t|\ell}^2 \quad (5.21)$$

Note, every time a point is found inside the sphere, the radius R is updated with the Euclidean distance of that point,

$$\begin{aligned}R_{i+1}^2 &= \left\|\bar{\mathbf{z}} - \left[\sum_{n\in\Upsilon_\ell}\bar{\mathbf{d}}_n, \sum_{n\in\Upsilon_\ell}\bar{\mathbf{d}}_{n+N_t}\right]\bar{\mathbf{s}}\right\|_{\mathrm{F}}^2 \\ &= (R_i^2 - R'^2) + \sum_{\nu=1}^{N_t}\left(z_\nu - \sum_{n\in\Upsilon_\ell}D_{(\nu,n)}\mathrm{Re}\{s\} - \sum_{n\in\Upsilon_\ell}D_{(\nu,n+N_t)}\mathrm{Im}\{s\}\right)^2 \quad (5.22)\end{aligned}$$

Furthermore, Tx–SD works for both under-determined MIMO setup with $N_t > N_r$, and non-under-determined MIMO setup with $N_t \leq N_r$.

5.5 Computational Complexity of Rx–SD and Tx–SD

In this section, the computational complexity of SM–ML, Rx–SD and Tx–SD is analysed. The complexity is here computed as the number of real multiplicative operations $(\times, \div)$ needed by each algorithm [175].

5.5.1 ML–Optimum Detector

The computational complexity of GNSM–ML and VGSM–ML receiver in (5.13), is equal to,

$$\mathcal{C}_{\text{ML}} = 6N_r 2^{\eta} \tag{5.23}$$

as the ML detector searches through the whole transmit and receive search spaces. Note, evaluating the Euclidean distance $\left(\left|\bar{y}_r - \bar{\mathbf{h}}_r^{\ell}\bar{\mathbf{s}}\right|^2\right)$ requires 6 real multiplications.

The computational complexity of SMX–ML receiver in (5.12) is equal to

$$\mathcal{C}_{\text{SMX–ML}} = 4\left(N_t + 1\right) N_r 2^{\eta} \tag{5.24}$$

Note, in (5.12) $\left(\left|\mathbf{y} - \mathbf{H}\mathbf{x}\right|^2\right)$ requires $(N_t + 1)$ complex multiplications.

From (5.23), the complexity of GNSM and VGSM does not depend on the number of transmit antennas, and it is equal to the complexity of SIMO systems. However, the complexity of SMX increases linearly with the number of transmit antennas, as shown in (5.24).

The reduction of GNSM and VGSM –ML receiver complexity relative to the complexity of the SMX–ML decoder for the same spectral efficiency is given by,

$$\mathcal{C}_{\text{rel}}^{\text{ML}} = 100 \times \left(1 - \frac{3}{2(N_t + 1)}\right) \tag{5.25}$$

The reduction in complexity offered by GNSM and VGSM increases with the increase in the number of transmit antennas. For example for $N_t = 8$, GNSM and VGSM both offer a 83.33% reduction in complexity, and as the number of transmit antennas increase the reduction increases.

5.5.2 Rx–SD

The complexity of the Rx–SD receiver is given by:

$$\mathcal{C}_{\text{Rx–SD}} = 3\sum_{\ell=1}^{\varrho}\sum_{s=1}^{M}\tilde{N}_r\left(\ell, s\right) \tag{5.26}$$

Note that the Rx–SD solution has no pre–computations with respect to the ML–optimum detector. In fact, $\tilde{N}_r\left(\ell, s\right)$ for $\ell \in \{1, 2, \ldots \varrho\}$ and $s \in M$–QAM in (5.15) are implicitly computed when solving the hypothesis–detection problem in (5.14).

5.5.3 Tx–SD

The computational complexity of Tx–SD can be upper–bounded by,

$$\mathcal{C}_{\text{Tx–SD}} \leq \mathcal{C}_{\Theta_R} + 3N_t\bar{\bar{\Theta}}_R \tag{5.27}$$

where $\bar{\bar{a}}$ denotes the cardinality of a, and $\mathcal{C}_{\Theta_R}$ is the complexity of finding the points in the subset Θ_R,

$$\mathcal{C}_{\Theta_R} = \mathcal{C}_{\text{Pre-Comp}} + \mathcal{C}_{\text{Interval}} \tag{5.28}$$

where,

$$\mathcal{C}_{\text{Pre-Comp}} = \mathcal{C}_{\text{CH}} + N_t(4N_rN_t + 6N_r + 6N_t + 3) \tag{5.29}$$

$$\mathcal{C}_{\text{interval}} = 2N_t + (2N_t + 3)N_{(5.19)} \tag{5.30}$$

where $\mathcal{C}_{\text{CH}} = 4N_t^3/3$ is the number of operations needed to compute the Cholesky decomposition [175], and $N_{(5.19)}$ is the number of times (5.19) is computed.

Note, from Chapter 4, and (5.23), (5.26) and (5.27), the complexity of GNSM and VGSM receivers is equal to the complexity of SM ML and SD receivers.

5.6 Analytical Analysis for GNSM and VGSM

5.6.1 Average Bit Error Rate Performance

The ABER for ML–GNSM and ML–VGSM systems can be approximated by using the union bound [110], which can be expressed as follows,

$$\text{ABER} \leq \frac{1}{2^{\eta}} \sum_{\ell_t, s_t} \sum_{\ell, s} \frac{N\left(\mathbf{x}_{\ell_t, s_t}, \mathbf{x}_{\ell, s}\right)}{\eta} \mathrm{E}_{\mathbf{H}} \left\{ \Pr_{\text{error}} \right\} \tag{5.31}$$

where $N\left(\mathbf{x}_{\ell_t, s_t}, \mathbf{x}_{\ell, s}\right)$ is the number of bits in error between $\mathbf{x}_{\ell_t, s_t}$ and $\mathbf{x}_{\ell, s}$, $\mathrm{E}_{\mathbf{H}}\{\cdot\}$ is the expectation across the channel $\mathbf{H}$, and $\Pr_{\text{error}}$ is the conditional pairwise error probability (PEP) of deciding on $\mathbf{x}_{\ell, s}$ given that $\mathbf{x}_{\ell_t, s_t}$ is transmitted,

$$\begin{aligned} \Pr_{\text{error}} &= \Pr\left(\left\| \mathbf{y} - \mathbf{H}_c \mathbf{x}_{\ell_t, s_t} \right\|^2 > \left\| \mathbf{y} - \mathbf{H}_c \mathbf{x}_{\ell, s} \right\|^2 \middle| \mathbf{H} \right) \\ &= Q\left(\sqrt{\frac{\left\| \mathbf{H}_c \Psi \right\|^2}{2\sigma_n^2}} \right) = \frac{1}{\pi} \int_0^{\frac{\pi}{2}} \exp\left(-\frac{\left\| \mathbf{H}_c \Psi \right\|^2}{4\sigma_n^2 \sin^2 \theta} \right) d\theta \end{aligned} \tag{5.32}$$

where $\Psi = \left(\mathbf{x}_{\ell_t, s_t} - \mathbf{x}_{\ell, s}\right)$, and from [171, 172], the alternative integral expression of the Q-function is,

$$Q(x) = \frac{1}{\pi} \int_0^{\frac{\pi}{2}} \exp\left(\frac{x^2}{2\sin^2 \theta} \right) d\theta \tag{5.33}$$

Taking the expectation of (5.32),

$$\mathrm{E}_{\mathbf{H}} \left\{ \Pr_{\text{error}} \right\} = \frac{1}{\pi} \int_0^{\frac{\pi}{2}} \Phi\left(-\frac{1}{4\sigma_n^2 \sin^2 \theta} \right) d\theta \tag{5.34}$$

where $\Phi\left(\cdot\right)$ is the moment-generation function (MGF) of the random variable $\left\| \mathbf{H}\Psi \right\|^2$.

From [173], the argument of the MGF in (5.34) can be written as,

$$\left\| \mathbf{H}_c \Psi \right\|^2 = \text{vec}\left(\mathbf{H}^H \right)^H \mathbf{R}_s^{\frac{H}{2}} \left(\mathbf{I}_{N_r} \otimes \Psi\Psi^H \right) \mathbf{R}_s^{\frac{1}{2}} \text{vec}\left(\mathbf{H}^H \right) \tag{5.35}$$

where $\mathbf{I}_n$ is an $n \times n$ identity matrix, and $\left(\cdot\right)^H$ denotes the Hermitian.

From [174], for an identical and independently distributed (i.i.d.) complex Gaussian vector $\mathbf{v}$ with mean $\tilde{\mathbf{v}}$, and any Hermetian matrix $\mathbf{Q}$, the MGF of $\mathbf{f} = \mathbf{v}^H\mathbf{Q}\mathbf{v}$ is,

$$\Phi(s) = \frac{\exp\left(s\tilde{\mathbf{v}}^H\mathbf{Q}\left(\mathbf{I} - s\mathbf{L}_\mathbf{v}\mathbf{Q}\right)^{-1}\tilde{\mathbf{v}}\right)}{|\mathbf{I} - s\mathbf{L}_\mathbf{v}\mathbf{Q}|} \tag{5.36}$$

where $\tilde{(\cdot)}$ denotes the mean, and $\mathbf{L}_\mathbf{v}$ is the covariance matrix of $\mathbf{v}$. Hence, from (5.35) and (5.36), the MGF in (5.34) is,

$$\Phi\left(s\right) = \frac{\exp\left(s \times \text{vec}\left(\tilde{\mathbf{H}}^H\right)^H \Lambda\left(\mathbf{I}_{N_rN_t} - s\mathbf{L}_\mathbf{H}\Lambda\right)^{-1}\text{vec}\left(\tilde{\mathbf{H}}^H\right)\right)}{|\mathbf{I} - s\mathbf{L}_\mathbf{H}\Lambda|} \tag{5.37}$$

where $(\cdot)^H$ denotes the Hermitian, $\mathbf{L}_\mathbf{H}$ is the covariance matrix of $\mathbf{H}$, and,

$$\Lambda = \mathbf{R}_s^{\frac{H}{2}}\left(\mathbf{I}_{N_r} \otimes \Psi\Psi^H\right)\mathbf{R}_s^{\frac{1}{2}} = \mathbf{R}_{\text{Rx}} \otimes \left(\Psi\Psi^H\mathbf{R}_{\text{Tx}}\right) \tag{5.38}$$

From (5.32),(5.37), and using the Chernoff bound,

$$\begin{aligned}
\text{E}_\mathbf{H}\left\{\Pr_{\text{error}}\right\} &= \frac{1}{\pi}\int_0^{\frac{\pi}{2}} \frac{\exp\left(-\frac{1}{4\sigma_n^2\sin^2\theta}\text{vec}\left(\tilde{\mathbf{H}}^H\right)^H\Lambda\left(\mathbf{I}_{N_rN_t} + \frac{1}{4\sigma_n^2\sin^2\theta}\mathbf{L}_\mathbf{H}\Lambda\right)^{-1}\text{vec}\left(\tilde{\mathbf{H}}^H\right)\right)}{\left|\mathbf{I}_{N_rN_t} + \frac{1}{4\sigma_n^2\sin^2\theta}\mathbf{L}_\mathbf{H}\Lambda\right|} d\theta \\
&\leq \frac{1}{2\pi}\frac{\exp\left(-\frac{1}{4\sigma_n^2}\text{vec}\left(\tilde{\mathbf{H}}^H\right)^H\Lambda\left(\mathbf{I}_{N_rN_t} + \frac{1}{4\sigma_n^2}\mathbf{L}_\mathbf{H}\Lambda\right)^{-1}\text{vec}\left(\tilde{\mathbf{H}}^H\right)\right)}{\left|\mathbf{I}_{N_rN_t} + \frac{1}{4\sigma_n^2}\mathbf{L}_\mathbf{H}\Lambda\right|}
\end{aligned} \tag{5.39}$$

The mean matrix $\tilde{\mathbf{H}}$ and the covariance matrix $\mathbf{L}_\mathbf{H}$ depends on the type of channel, where for,

1. Rayleigh Fading

$$\tilde{\mathbf{H}} = \mathbf{0}_{N_r \times N_t} \tag{5.40}$$

$$\mathbf{L}_\mathbf{H} = \mathbf{I}_{N_rN_t} \tag{5.41}$$

2. Rician Fading

$$\tilde{\mathbf{H}} = \sqrt{\frac{K}{1+K}} \times \mathbf{1}_{N_r \times N_t} \tag{5.42}$$

$$\mathbf{L}_\mathbf{H} = \sqrt{\frac{1}{1+K}} \times \mathbf{I}_{N_rN_t} \tag{5.43}$$

where $\mathbf{1}_{N_r \times N_t}$ is an $N_r \times N_t$ all ones matrix.

In Section 5.7, the bound is shown to be a tight upper bound for GNSM and VGSM.

5.6.2 Initial Radius Selection Method for Rx–SD and Tx–SD

From [177], the probability of error for SD can be written as,

$$\underset{e,\text{SD}}{\text{Pr}} \leq \left(\underset{e,\text{ML}}{\text{Pr}} + \Pr\left((\ell_t, s_t) \notin \Theta_R\right) \right) \tag{5.44}$$

where $\Pr\left((\ell_t, s_t) \notin \Theta_R\right)$ is the probability of the transmitted point (ℓ_t, s_t) being outside the set of points Θ_R considered by SD.

Therefore, SD will have a near optimum performance when,

$$\Pr\left((\ell_t, s_t) \notin \Theta_R\right) << \underset{e,\text{ML}}{\text{Pr}} \tag{5.45}$$

The probability of *not* having the transmitted point (ℓ_t, s_t) inside Θ_R can be written as,

$$\begin{aligned} \Pr\left((\ell_t, s_t) \notin \Theta_R\right) &= \Pr\left(\sum_{r=1}^{2N_r} \left| \bar{y}_r - \bar{\mathbf{h}}_{c,r}^{\ell_t} \bar{\mathbf{s}}_t \right|^2 > R^2 \right) \\ &= \Pr\left(\kappa > \left(\frac{R}{\sigma_n/\sqrt{2}} \right)^2 \right) = 1 - \frac{\gamma\left(N_r, \left(\frac{R}{\sigma_n} \right)^2 \right)}{\Gamma(N_r)} \end{aligned} \tag{5.46}$$

where $\kappa = \sum_{r=1}^{2N_r} \left| \frac{\bar{n}_r}{\sigma_n/2} \right|^2$ is a central chi-squared random variable with $2N_r$ degree of freedom, and a cumulative distribution function (CDF) equal to [110],

$$F_\kappa(a, b) = \frac{\gamma(b/2, a/2)}{\Gamma(b/2)} \tag{5.47}$$

where $\gamma(c, d)$ is the lower incomplete gamma function, and $\Gamma(c)$ is the gamma function,

$$\gamma(c, d) = \int_0^d t^{c-1} e^{-t} dt \quad (5.48) \qquad \Gamma(c) = \int_0^\infty t^{c-1} e^{-t} dt \quad (5.49)$$

Note, $\bar{n}_r$ is the r–th element of the noise vector $\bar{\mathbf{n}}$.

The initial sphere radius considered in this chapter is a function of the noise variance as given in [178],

$$R^2 = 2\varrho N_r \sigma_n^2 \tag{5.50}$$

where ϱ is a constant chosen to satisfy (5.45). This done assuming $\Pr\left((\ell_t, s_t) \notin \Theta_R\right) = 10^{-6}$ and back solving (5.46) to obtain ϱ. For $N_r = 1, 2, 4$, $\varrho = 13.8, 8.3, 5.3$ respectively.

5.7 Results

In the following, Monte Carlo simulation results for at least 10^6 channel realisations are shown to compare the ABER performance and the computational complexity of VGSM, GNSM, SM and SMX.

5.7.1 Analytical Performance of GNSM and VGSM

Figs. 5.1 - 5.4 show the ABER simulation results for GNSM and VGSM using ML, Rx–SD and Tx–SD over correlated and uncorrelated, Rayleigh and Rician channels, compared with the analytical bound derived in Sec. 5.6. Note, $\eta = 8$, $N_r = 4$, for GNSM $N_t = 12$ and $N_u = 3$, for VGSM $N_t = 8$, and BPSK modulation is used.

The figures shows that both Rx–SD and Tx–SD offer a near optimum performance, where they directly overlap with results attained from the ML–optimum receiver. Furthermore, the figures validate the derived analytical bound as for ABER $< 10^{-2}$ all detection techniques produce results that follow closely the analytical curves. Another observation is that for non–line of sight (NLoS) channels there is only 1 dB difference between the performance of GNSM and VGSM. However, for line of sight (LoS) channels VGSM performs the same as GNSM.

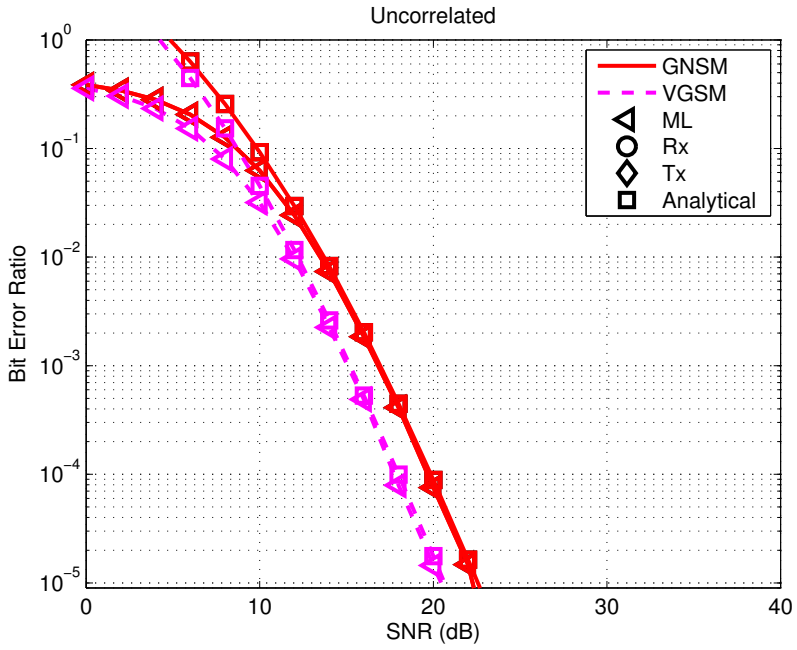

Figure 5.1: *ABER against SNR for GNSM and VGSM over a Rayleigh channel, where $\eta = 8$, $N_r = 4$, for GNSM $N_t = 12$ and $N_u = 3$, for VGSM $N_t = 8$, and BPSK modulation is used.*

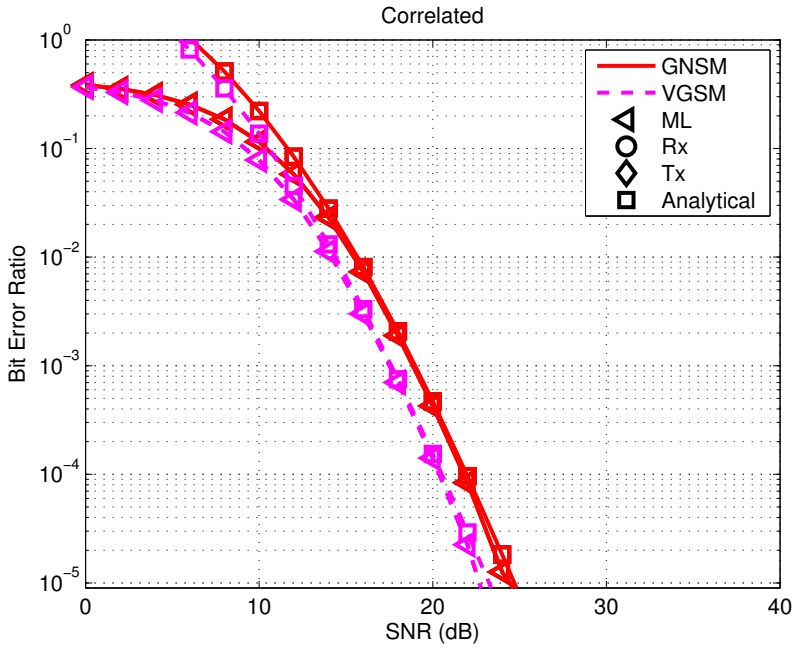

Figure 5.2: *ABER against SNR for GNSM and VGSM over a Rayleigh channel, where* $\eta = 8$*,* $N_r = 4$*, for GNSM* $N_t = 12$ *and* $N_u = 3$*, for VGSM* $N_t = 8$*, and BPSK modulation is used.*

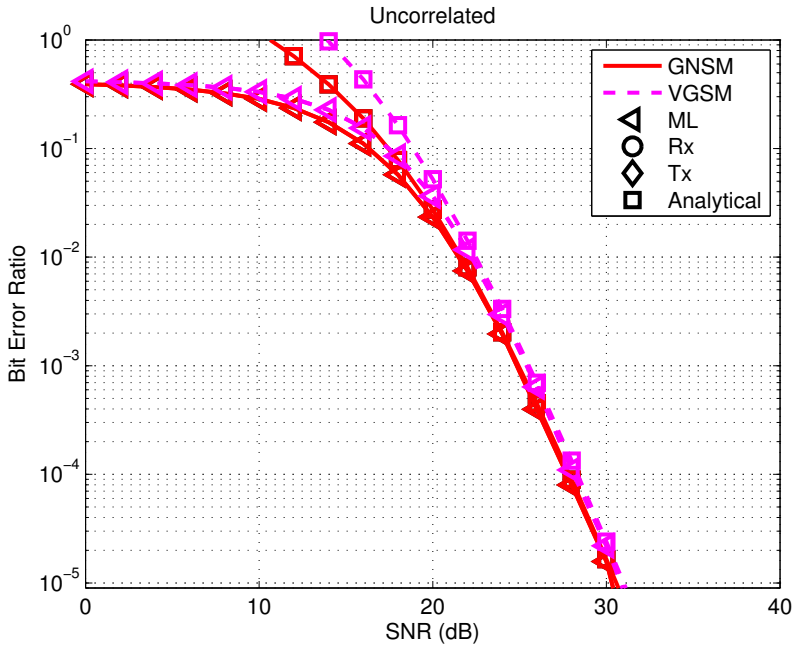

Figure 5.3: *ABER against SNR for GNSM and VGSM over a Rician channel, where* $\eta = 8$*,* $N_r = 4$*, for GNSM* $N_t = 12$ *and* $N_u = 3$*, for VGSM* $N_t = 8$*, and BPSK modulation is used.*

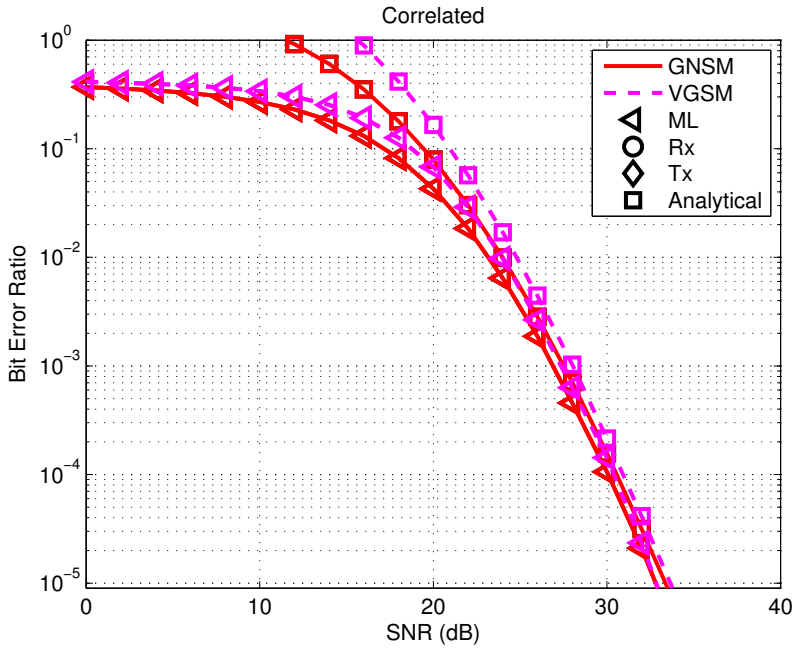

Figure 5.4: *ABER against SNR for GNSM and VGSM over a Rician channel, where* $\eta = 8$*,* $N_r = 4$*, for GNSM* $N_t = 12$ *and* $N_u = 3$*, for VGSM* $N_t = 8$*, and BPSK modulation is used.*

5.7.2 ABER Performance Comparison

Figs. 5.5 - 5.8, show a comparison of the ABER performance between GNSM with $N_t = 12$ and $N_u = 3$, VGSM with $N_t = 8$, SM with $N_t = 128$, SMX with $N_t = 8$, using BPSK modulation, over uncorrelated and correlated, Rayleigh channels and Rician channels with $K = 10$ dB, for $\eta = 8$ and $N_r = 4$. The correlation decay coefficients are chosen to model moderate correlation, with $\beta_t = 0.7$ at the transmitter size and $\beta_r = 0.6$ at the receiver side.

Comparing Figs. 5.5 and 5.6, with Figs. 5.7 and 5.8, it can be seen that GNSM and VGSM perform better with Rayleigh channels, because in the case of NLoS channels it is easier to distinguish the active antennas at the transmitter. However, in the presence of a strong line-of–sight component, the performance of GNSM and VGSM degrades as it is more difficult to distinguish the active antennas. For Rayleigh channels in Figs. 5.5 and 5.6, it can be seen that for both cases, correlated and uncorrelated channels, VGSM and GNSM perform ~ 4 dB and ~ 3 dB worse than SM respectively. However, VGSM and GNSM need only $N_t = 8$ and $N_t = 12$, while SM needs $N_t = 128$. Now, comparing VGSM and GNSM to SMX, on the one hand, VGSM and GNSM perform ~ 2.5 dB and ~ 1.5 dB worse then SMX. On the other hand, from (5.25) the complexity of VGSM and GNSM is 83.33% less than the complexity of SMX as it does not depend on the number of transmit antennas.

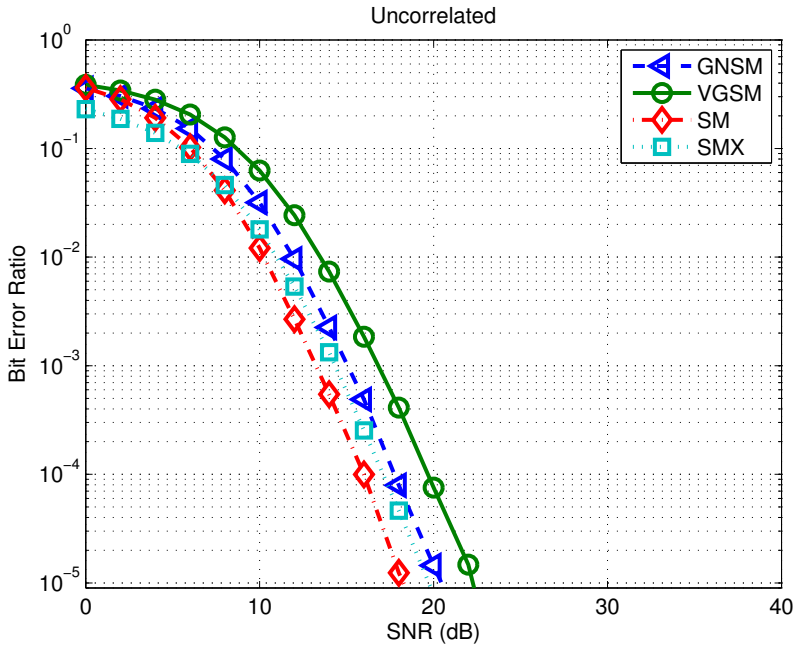

Figure 5.5: *ABER against SNR for GNSM, VGSM, SM and SMX over a Rayleigh channel, where* $\eta = 8$*,* $N_r = 4$*, for GNSM* $N_t = 12$ *and* $N_u = 3$*, for VGSM* $N_t = 8$*, for SM* $N_t = 128$*, for SMX* $N_t = 8$*, using BPSK modulation.*

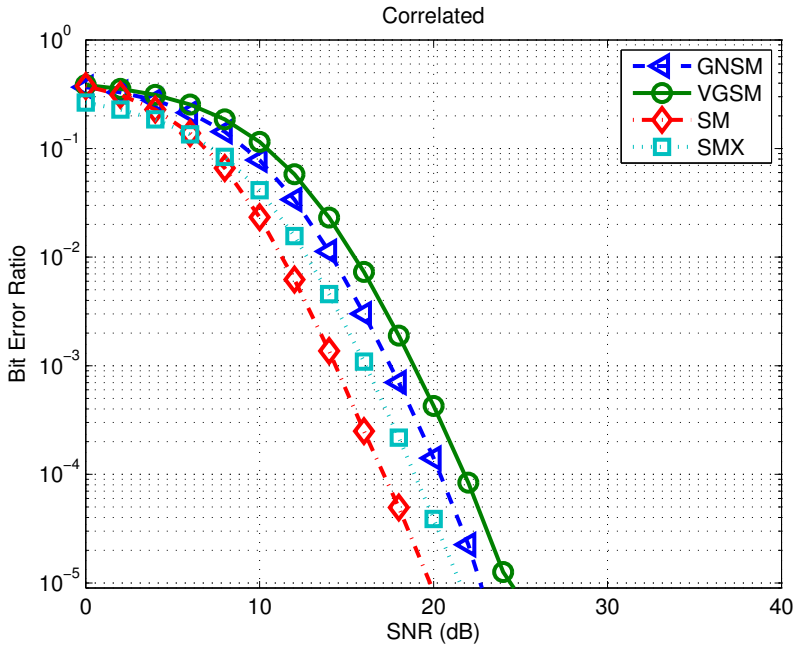

Figure 5.6: *ABER against SNR for GNSM, VGSM, SM and SMX over a Rayleigh channel, where* $\eta = 8$*,* $N_r = 4$*, for GNSM* $N_t = 12$ *and* $N_u = 3$*, for VGSM* $N_t = 8$*, for SM* $N_t = 128$*, for SMX* $N_t = 8$*, using BPSK modulation.*

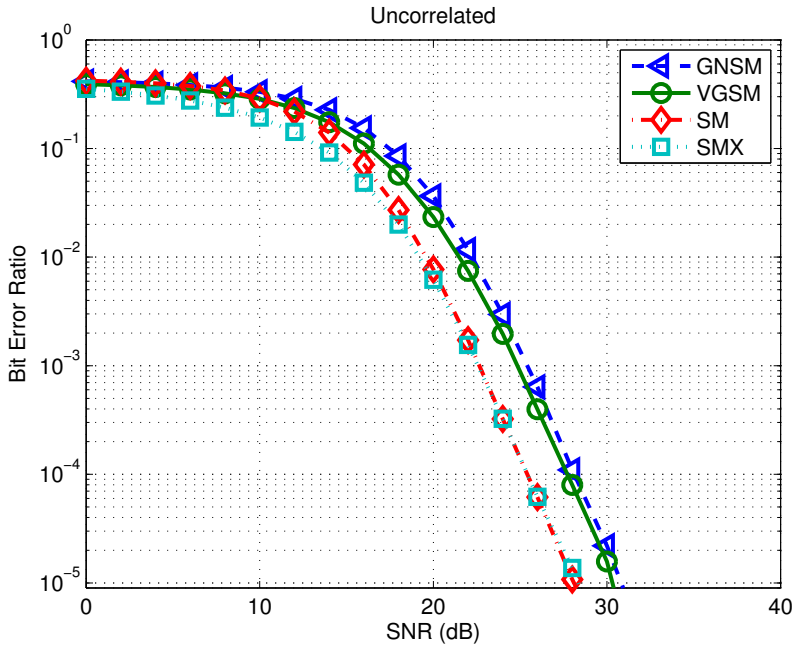

Figure 5.7: *ABER against SNR for GNSM, VGSM, SM and SMX over a Rician channel, where* $\eta = 8$, $N_r = 4$, *for GNSM* $N_t = 12$ *and* $N_u = 3$, *for VGSM* $N_t = 8$, *for SM* $N_t = 128$, *for SMX* $N_t = 8$, *using BPSK modulation.*

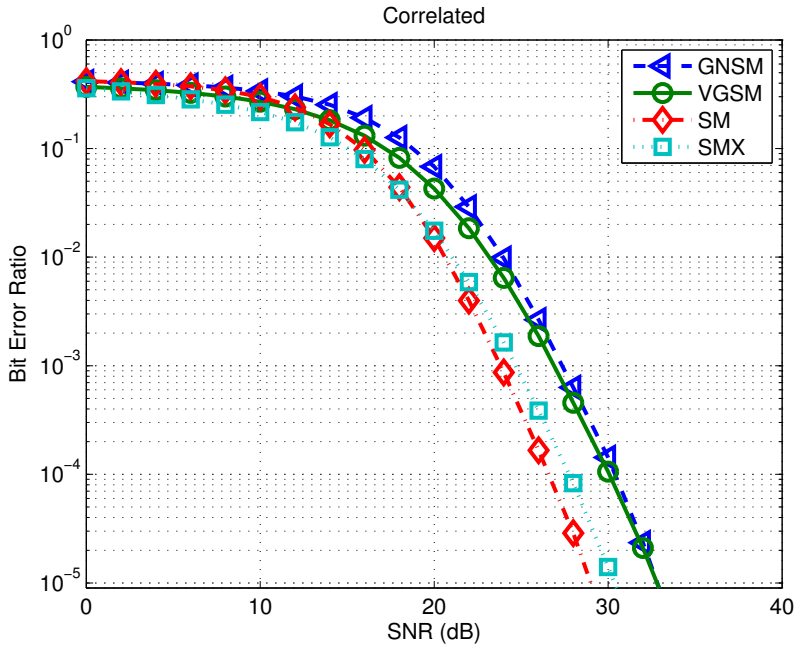

Figure 5.8: *ABER against SNR for GNSM, VGSM, SM and SMX over a Rician channel, where* $\eta = 8$, $N_r = 4$, *for GNSM* $N_t = 12$ *and* $N_u = 3$, *for VGSM* $N_t = 8$, *for SM* $N_t = 128$, *for SMX* $N_t = 8$, *using BPSK modulation.*

In summary, VGSM and GNSM does not offer the same performance as SM or SMX as the Euclidean distances between the different spatial and constellation symbols are smaller. However, it offers an acceptable performance, with a much smaller number of transmit antennas compared to SM, up to (93.75%) and (90.625%) reduction in the number of antennas by VGSM and GNSM respectively. Furthermore, a much lower complexity compared to SMX, where up to (83.33%) reduction in complexity is offered.

5.7.3 Computational Complexity Comparison between Tx–SD and Rx–SD

Fig. 5.9 shows the computational complexity of VGSM–SD for $\eta = 6, 8, 10, 12$, $N_t = 6$ and $N_r = 4$, where BPSK, 8–QAM, 32–QAM, and 128–QAM is used. The initial radius is chosen according to (5.50). Note, in order to keep the results clear and to highlight the main points, the Tx–SD and Rx–SD algorithms, with the lowest complexity are shown. In particular, the figure shows the relative computational complexity of the SDs with respect to the SIMO ML–optimum detector, *i.e* $\mathcal{C}_{\text{rel}}\,(\%) = 100 \times (\mathcal{C}_{\text{SD}}/\mathcal{C}_{\text{ML}})$.

Tx–SD reduces the transmit search space, more specifically it reduces the search over the possible constellation points used for each antenna combination, this offers a large reduction in transmit search space. However, Tx–SD requires some pre–computations, and the reduction in complexity has to be large enough to compensate for these pre–computations. Therefore, the Tx–SD reduces the complexity of the ML–optimum receiver only for large constellation diagrams. For small constellation diagrams, Rx–SD is the best choice, as it does not require any pre–computations. Fig. 5.9 summarises this investigation, where for large constellation diagrams, 32–QAM and 128-QAM, Tx–SD was chosen, as the reduction in the transmit search space is large enough to compensate for the pre–computations. However, for small constellation diagrams, BPSK and 8–QAM, Rx–SD was the best choice. Finally, comparing BPSK Rx–SD with 8–QAM Rx–SD, it can be seen that they both offer the same reduction, even though the latter is using four times bigger constellation digram. That is because the Rx–SD reduces the receive search space, and therefore does not depend on the size of the constellation diagram used.

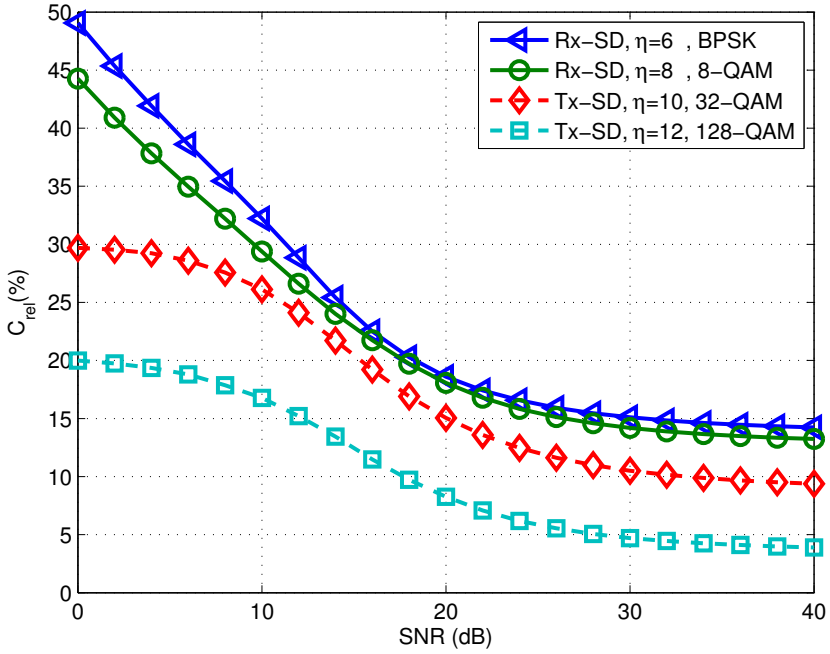

Figure 5.9: *Computational complexity against SNR, for uncorrelated Rayleigh channels, where* $N_r = 4$.

5.7.4 Computational Complexity Comparison between GNSM, VGSM, SM and SMX

In Figs. 5.10-5.13, the computational complexity of GNSM–SD with $N_t = 12$ and $N_u = 3$, and VGSM–SD with $N_t = 8$ is compared with the complexity of SM–SD with $N_t = 128$ and SMX–SD with $N_t = 8$, over uncorrelated and correlated, Rayleigh and Rician channels, for $\eta = 8$, $N_r = 4$, and BPSK modulation. Note, for GNSM, VGSM, and SM the SD, (Rx–SD, Tx–SD), with the lowest complexity is chosen.

In all figures it can be seen that GNSM–SD and VGSM–SD offer a relative complexity as low as SM, where it is in the range between 43% for low signal to noise ratio (SNR) and 13% for high SNR. Moreover, GNSM–SD and VGSM–SD is at least 30% less complex than SMX–SD. Another point to notice is that, the reduction in complexity offered by GNSM–SD and VGSM–SD is the same for correlated and uncorrelated, Rayleigh and Rician channels, *i.e.* the performance of GNSM–SD and VGSM–SD does *not* depend on the channel, unlike SMX–SD where the reduction in complexity is not the same for correlated and uncorrelated channels. For uncorrelated Rayleigh channels SMX–SD offers a relative complexity that is about 75%,

for correlated Rayleigh channels SMX–SD offers 86%. However, for Rician correlated and uncorrelated channels SMX–SD has a relative complexity that is higher than 100%.

In summary, GNSM–SD and VGSM–SD reduce the number of transmit antennas needed by SM while attaining the same reduction in computational complexity, which is significantly less than the complexity of SMX–SD.

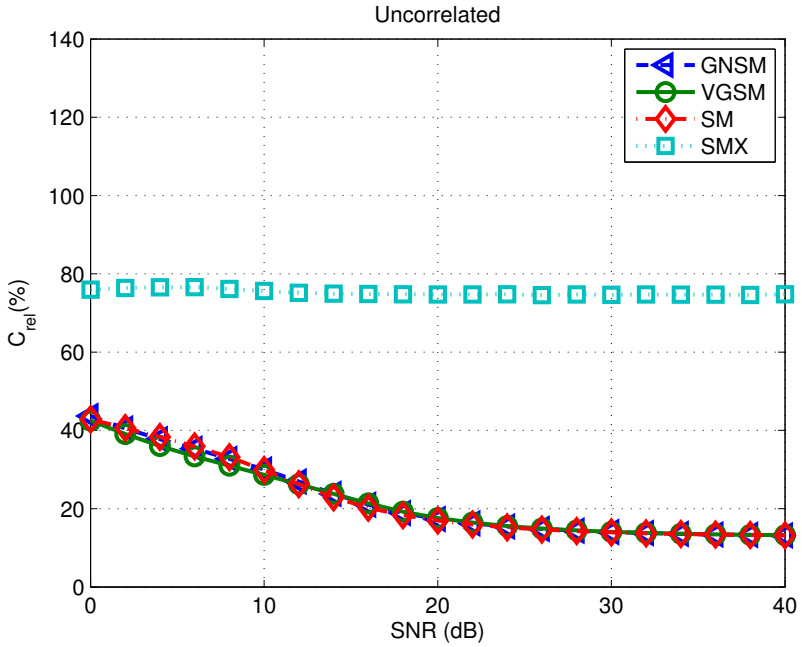

Figure 5.10: *Computational complexity against SNR, for Rayleigh channels, where* $\eta = 8$*,* $N_r = 4$*, for GNSM* $N_t = 12$ *and* $N_u = 3$*, for VGSM* $N_t = 8$*, for SM* $N_t = 128$*, for SMX* $N_t = 8$*, using BPSK modulation.*

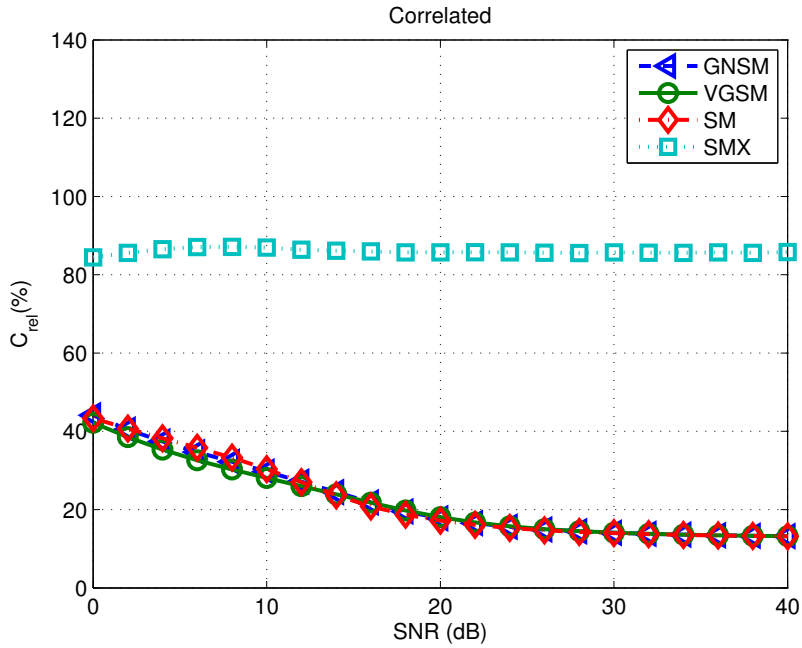

Figure 5.11: *Computational complexity against SNR, for Rayleigh channels, where* $\eta = 8$*,* $N_r = 4$*, for GNSM* $N_t = 12$ *and* $N_u = 3$*, for VGSM* $N_t = 8$*, for SM* $N_t = 128$*, for SMX* $N_t = 8$*, using BPSK modulation.*

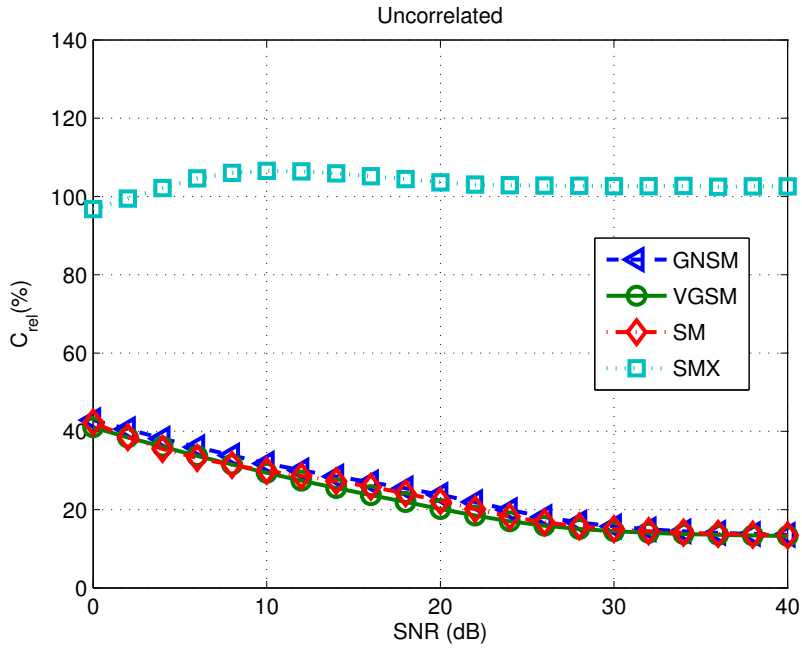

Figure 5.12: *Computational complexity against SNR, for Rician channels, where* $\eta = 8$*,* $N_r = 4$*, for GNSM* $N_t = 12$ *and* $N_u = 3$*, for VGSM* $N_t = 8$*, for SM* $N_t = 128$*, for SMX* $N_t = 8$*, using BPSK modulation.*

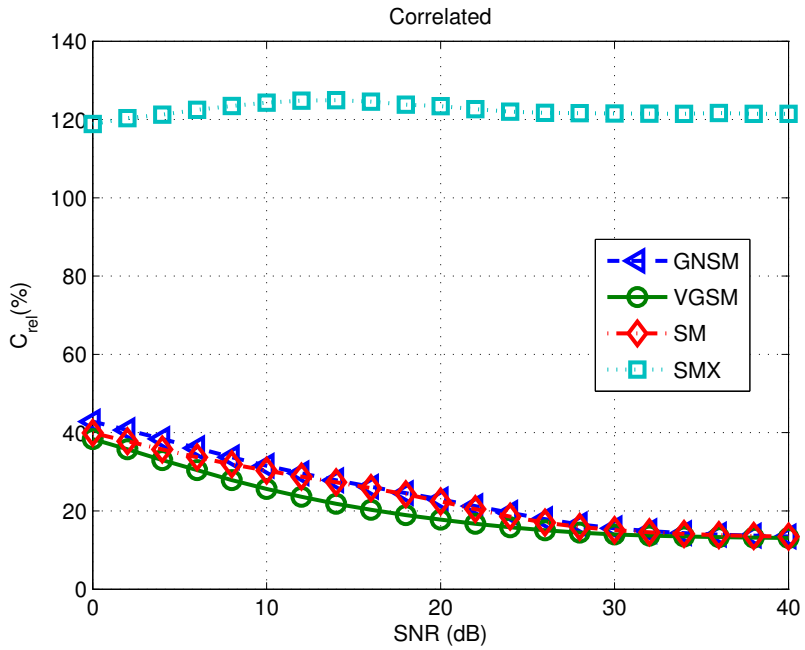

Figure 5.13: *Computational complexity against SNR, for Rician channels, where* $\eta = 8$*,* $N_r = 4$*, for GNSM* $N_t = 12$ *and* $N_u = 3$*, for VGSM* $N_t = 8$*, for SM* $N_t = 128$*, for SMX* $N_t = 8$*, using BPSK modulation.*

5.8 Summary

In this chapter, the idea of SM was generalised by sending the same symbol from more than one transmit antenna at a time. Hence, the basic idea of SM is no longer limited to a power of two number of transmit antennas and an arbitrary number of transmit antennas can be used. Furthermore, three receivers were proposed. The first receiver is based on the ML principle, and the last two receivers, Tx–SD and Rx–SD, are based on the SD principle. Also a tight closed form expression for the ABER performance of GNSM and VGSM, over correlated and uncorrelated, Rayleigh and Rician fading channels was provided. Results show that the proposed schemes, VGSM and GNSM, use much smaller number of antennas than SM and have significantly lower computational complexity and number of RF chains than SMX, while having a small penalty in the ABER performance. Overall, GNSM and VGSM are good candidates for smaller number of transmit antennas and low computational complexity MIMO solutions.

Chapter 6
Performance of Spatial Modulation using Measured Real-World Channels

6.1 Introduction

In this chapter, for the first time real–world channel measurements are used to analyse the performance of spatial modulation (SM). An analysis of the average bit error ratio (ABER) of SM using measured urban correlated and uncorrelated Rayleigh fading channels is provided. The channel measurements which are taken from an outdoor urban multiple–input multiple–output (MIMO) measurement campaign were provided by Dr. William Thompson and Prof. Mark Beach, university of Bristol, as part of the beyond fourth generation (4G), UK–China bridges project. Moreover, performance results using simulated Rayleigh fading channels are provided and compared with the analytical bound for the ABER of SM, and the ABER results using the measured urban channels. It is shown that the results using the measured urban channels validate the derived analytical bound and the ABER results using the simulated channels. The ABER of SM is compared with the performance of spatial multiplexing (SMX) using the measured urban channels for small and large scale MIMO. It is shown that SM offers nearly the same or a slightly better performance than SMX for small scale MIMO. However, SM offers large reduction in ABER for large scale MIMO.

The remainder of this chapter is organised as follows. In Section 6.2, the channel measurements are introduced. In Section 6.3, an analytical bound for SM over correlated and uncorrelated Rayleigh channels is derived. The results are presented in Section 6.4, and the chapter is concluded in Section 6.5. Note, the operating principle of SM is explained in 2.4.1, the channel model is introduced in 2.2.3.3, and the SM–maximum–likelihood (ML) decoder is described in 2.4.2.

6.2 Channel Measurement and Model

The channel measurements used within this chapter were acquired within the Mobile VCE MIMO elective [181]. MIMO channel measurements were taken around the centre of Bristol in the United Kingdom, using a MEDAV RUSK channel sounder, a 4×4 antenna configuration, with 20 MHz bandwidth centred at 2 GHz. The transmitter consisted of a pair of dual polarised ($\pm 45^{\circ}$) Racal Xp651772 antennas [182] separated by 2 m, positioned atop a building, providing elevated coverage of the central business and commercial districts of Bristol city. At the receiver two different receiver devices are used, both equipped with four antennas [183, 184].

The two receiver devices are a reference headset and a laptop. The reference antenna design is based on 4-dipoles mounted on a cycle helmet, thus avoiding any shadowing by the user. The laptop is equipped with 4 PIFA elements, both devices are detailed in [181]. Fifty–eight

measurement locations were chosen around the city. At each location the user walked, holding the laptop in front of them and the reference device on their head, in a straight line roughly 6 m long, until 4096 channel snapshots have been recorded. A second measurement is then taken with the user walking a second path perpendicular to the first. As the measurement speed is significantly faster than the coherence time of the channel, the measurements are averaged in groups of four to reduce measurement noise.

One set of measurement results with the laptop and reference device, and a second set of only the reference device measurements taken at the same locations, but on different days, is also included in the measurement data for analysis. This provides a total of 348 different measurement sets, each containing 1024 snapshots of a 4×4 MIMO channel, with 128 frequency bins spanning the 20 MHz bandwidth. As the simulations are carried out using flat fading channels, a single frequency bin centred around 2 GHz, is chosen from each measurement snapshot to create the narrowband channel.

6.2.1 Small Scale MIMO

For small scale MIMO, Rayleigh fading channels were distinguished using the Chi-squared goodness of fit test, with a significance level of 1%, where of the 348 measurements, only 20 measurements fulfilled this requirement. Fig. 6.1 shows the probability distribution function (PDF) for the envelop of one of the chosen channel measurements, and compare it with the PDF for a Rayleigh distribution. It can be seen from Fig. 6.1 that the distribution of the channel envelop is not exactly a Rayleigh distribution, however, it closely follow a Rayleigh distribution. For each measurement the transmit and receive correlation matrices are estimated, then the decay of the correlation, based on the antenna indices, is fitted to an exponential decay model [137], Two channels with the lowest mean square error between the exponential decay in (2.12) and the actual correlation matrices were chosen for the two correlated channel results. Both of the chosen channels are from measurements taken using the laptop device, and the measured decay coefficients for the transmitter and receiver are 0.5 and 0.8 for the first channel and 0.7 and 0.4 for the second channel respectively.

For the uncorrelated channels, the two channels with the lowest average correlation coefficient between their MIMO channels are chosen. One is from the laptop measurements, and the other from the reference headset device measurements. Selecting the channels in this manner may not provide completely uncorrelated channels, as there may still be a small correlation between the channels. However, this manner of selection will provide the channel measurements that experienced the lowest spatial correlations.

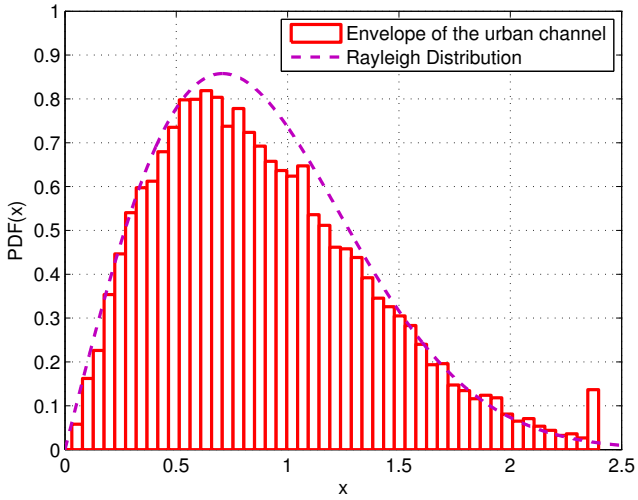

Figure 6.1: *The PDF for the envelope of the urban channel measurements compared with the PDF for the Rayleigh distibution.*

6.2.2 Large Scale MIMO

The original measurements were taken using 4×4 system. However, a larger virtual MIMO systems can be created by exploiting the measurements. In particular, the following steps are taken in order to create the large scale channel array:

1. Channel measurements from the reference device are used to exclude the body shadowing effects.
2. The original channels are reversed, such that the mobile station becomes the transmitting device. The reason for that is that the transmitters of the original channel measurements are fixed on top of a building, while the receiver device moved.
3. The first channel from each snapshot of the walking measurements, was chosen to form each of the virtual array transmitters, resulting in a virtual array with 1024 elements.
4. To reduce the correlation between adjacent channels, every fourth element of this array was chosen, forming a maximum array size of 256 antennas. These are equally spaced along a path of about 6 m in length.
5. The locations with good fitting to Rayleigh fading distributions were first chosen, and then those that showed the lowest variation in their Rayleigh fading statistics between each virtual spatial channel were selected. This is done to avoid the scenario where the user experienced significant channel shadowing along part of the walking measurement, as this would introduce a significant power imbalance in the virtual MIMO channel.

The Rayleigh fading mean statistic of the normalised constructed virtual MIMO channel has an average of 0.70, and a variance of 0.16.

6.3 Analytical Modelling of SM–ABER over Correlated and Uncorrelated Channels

The ABER for SM system can be approximated by using the union bound [110], which can be expressed as follows,

$$\underset{\text{SM}}{\text{ABER}} \leq \sum_{\ell_t,s_t} \sum_{\ell,s} \frac{N\left(\mathbf{x}_{\ell_t,s_t}, \mathbf{x}_{\ell,s}\right)}{\eta} \frac{\mathrm{E}_{\mathbf{H}}\left\{\Pr\left(\mathbf{x}_{\ell,s} \neq \mathbf{x}_{\ell_t,s_t}\right)\right\}}{2^{\eta}} \tag{6.1}$$

where $N\left(\mathbf{x}_{\ell_t,s_t}, \mathbf{x}_{\ell,s}\right)$ is the number of bits in error between $\mathbf{x}_{\ell_t,s_t}$ and $\mathbf{x}_{\ell,s}$, $\mathrm{E}_{\mathbf{H}}\{\cdot\}$ is the expectation across the channel $\mathbf{H}$ and $\Pr\left(\mathbf{x}_{\ell,s} \neq \mathbf{x}_{\ell_t,s_t}\right)$ is the conditional pairwise error probability (PEP) of deciding on $\mathbf{x}_{\ell,s}$ given that $\mathbf{x}_{\ell_t,s_t}$ is transmitted,

$$\begin{aligned}
\Pr\left(\mathbf{x}_{\ell,s} \neq \mathbf{x}_{\ell_t,s_t}\right) &= \Pr\left(\left\|\mathbf{y} - \mathbf{H}_c\mathbf{x}_{\ell_t,s_t}\right\|^2 > \left\|\mathbf{y} - \mathbf{H}_c\mathbf{x}_{\ell,s}\right\|^2 \middle| \mathbf{H}\right) \\
&= Q\left(\sqrt{\frac{\left\|\mathbf{H}_c\Psi\right\|^2}{2\sigma_n^2}}\right) \\
&= \frac{1}{\pi}\int_0^{\frac{\pi}{2}} \exp\left(-\frac{\left\|\mathbf{H}_c\Psi\right\|^2}{4\sigma_n^2\sin^2\theta}\right) d\theta
\end{aligned} \tag{6.2}$$

where $\Psi = \left(\mathbf{x}_{\ell_t,s_t} - \mathbf{x}_{\ell,s}\right)$, from [171,172] the alternative integral expression of the Q-function is,

$$Q(x) = \frac{1}{\pi}\int_0^{\frac{\pi}{2}} \exp\left(\frac{x^2}{2\sin^2\theta}\right) d\theta. \tag{6.3}$$

Taking the expectation of (6.2),

$$\mathrm{E}_{\mathbf{H}}\left\{\Pr\left(\mathbf{x}_{\ell,s} \neq \mathbf{x}_{\ell_t,s_t}\right)\right\} = \frac{1}{\pi}\int_0^{\frac{\pi}{2}} \Phi\left(-\frac{1}{4\sigma_n^2\sin^2\theta}\right) d\theta \tag{6.4}$$

where $\Phi\left(\cdot\right)$ is the moment-generation function (MGF) of the random variable $\left\|\mathbf{H}_c\Psi\right\|^2$.

From [173], and noting that in SM only one antenna is active at a time, the MGF in (6.4) for quasi–static fading with spatial correlation is equal to,

$$\Phi\left(s\right) = \prod_{j=1}^{N_r}\left(1 - s\lambda_j\mu\right)^{-1} \tag{6.5}$$

where λ_j are the eigenvalues of $\mathbf{R}_{\text{Rx}}$ and $\mu = |s_t|^2 + |s|^2 - 2\text{Re}\{s_t s^*\}\mathbf{R}_{\text{Tx}}(\ell_t, \ell)$.

Substituting (6.5) and (6.4) in (6.1) and using the Chernoff bound, the ABER for SM over correlated Rayleigh channels is,

$$\underset{\text{SM}}{\text{ABER}} \leq \frac{1}{2\pi} \sum_{\ell_t, s_t} \sum_{\ell, s} \prod_{j=1}^{N_r} \frac{N\left(\mathbf{x}_{\ell_t, s_t}, \mathbf{x}_{\ell, s}\right)}{\eta} \frac{1}{2^{\eta}} \left(1 + \frac{\lambda_j \mu}{4\sigma_n^2}\right)^{-1} \tag{6.6}$$

For the case of uncorrelated Rayleigh channels, the ABER for SM is,

$$\underset{\text{SM}}{\text{ABER}} \leq \frac{1}{2\pi} \sum_{\ell_t, s_t} \sum_{\ell, s} \frac{N\left(\mathbf{x}_{\ell_t, s_t}, \mathbf{x}_{\ell, s}\right)}{\eta} \frac{1}{2^{\eta}} \left(1 + \frac{|\Psi|^2}{4\sigma_n^2}\right)^{-N_r} \tag{6.7}$$

Section 6.4, shows that the two bounds; for uncorrelated and correlated Rayleigh channels, i) are tight upper bounds for SM, and ii) they validate the experimental results.

6.4 Results

In the following, Monte Carlo simulation results for the ABER performance of SM using the measured urban channels and simulated Rayleigh channels are compared with the derived analytical bound. Note, each channel of the measured urban channels contains 1024 snapshots. Furthermore, the performance of SM using the measured urban channel are compared with the performance of SMX over the same channels for small and large scale MIMO.

6.4.1 Validation of SM analytical ABER performance using experimental results

Fig. 6.2 and Fig. 6.3 show the ABER performance of SM using the measured urban channels (solid line) and using simulated Rayleigh channels (red dashed line). The results are compared with the derived analytical bound (blue dotted line), for $\eta = 4$ and $N_t = N_r = 4$. Both figures show that the results using the measured urban channels validate the results and conclusions from the previous chapters. Fig. 6.2 shows the ABER for uncorrelated channels and Fig. 6.3 shows the ABER for correlated channels. As can be seen from the figures, the experimental results closely match the simulation and analytical curves for ABER $< 10^{-2}$. In Fig. 6.2, SM offers the same performance for both chosen channels, where both channels are uncorrelated. However, in Fig. 6.3, there is a slight difference in the performance, since the two chosen correlated channels have different correlation matrices. Moreover, comparing the results for uncorrelated channels in Fig. 6.2 with those correlated channels in Fig. 6.3, SM performs better when the channels are uncorrelated, as it is easier to distinguish the different channel paths.

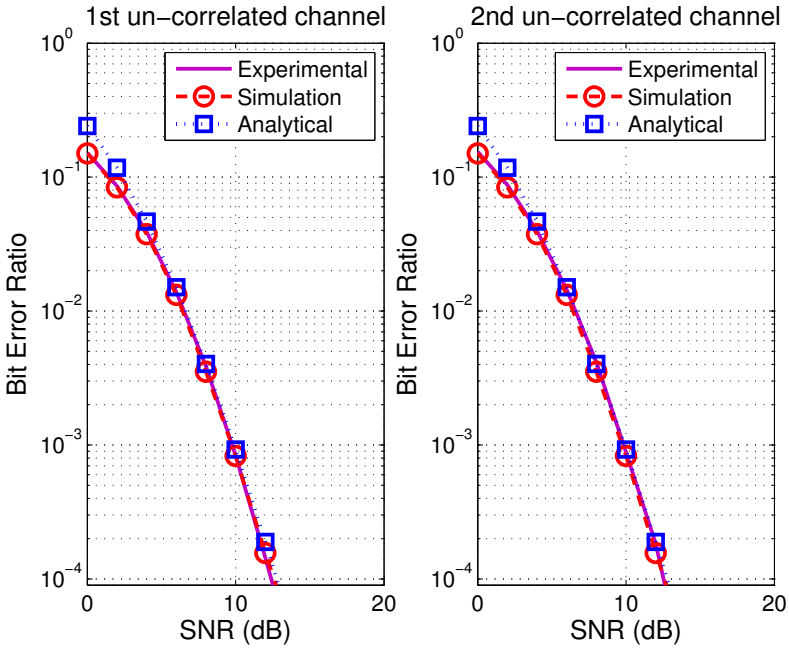

Figure 6.2: *ABER versus SNR for SM over an uncorrelated channel.* $\eta = 4$, $N_t = 4$ *and* $N_r = 4$.

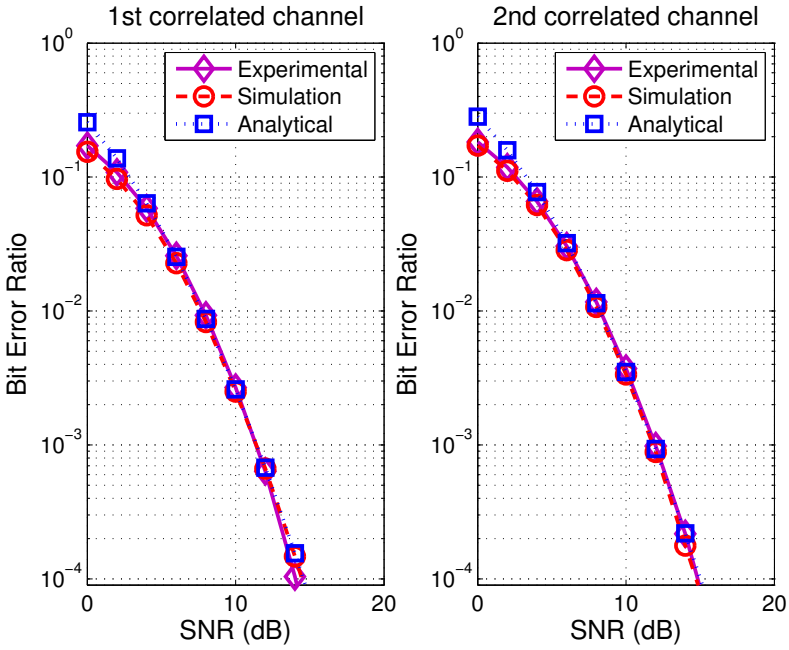

Figure 6.3: *ABER versus SNR for SM over a correlated channel.* $\eta = 4$, $N_t = 4$ *and* $N_r = 4$.

6.4.2 Comparison in the ABER performance of SM and SMX

6.4.2.1 Small Scale MIMO

Figs. 6.4 and 6.5 compare the ABER between SM (solid line) and SMX (dashed line) using the measured urban channels for $\eta = 4$ and $N_t = N_r = 4$. Once more the results using the measured urban channels validates the conclusions made in the previous chapters, where SM offers almost the same as or slightly better performance than SMX. Note, in Fig. 6.4, the performance of both systems does not change for both channels since the channels are uncorrelated. However, as shown in Fig. 6.5, this is not the case for the correlated channels, where the performance is different due to the different correlation coefficients.

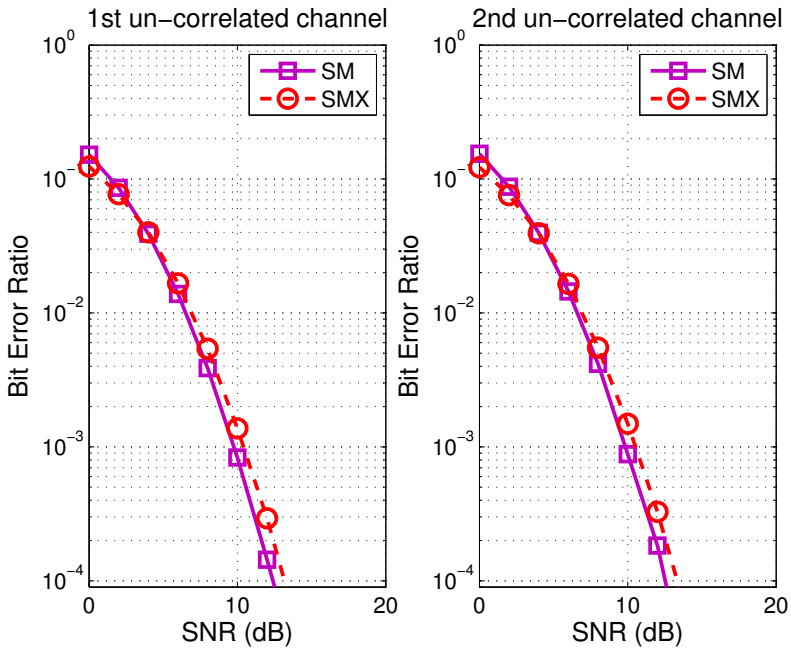

Figure 6.4: *ABER versus SNR for SM and SMX over an uncorrelated channel.* $\eta = 4$, $N_t = 4$ *and* $N_r = 4$.

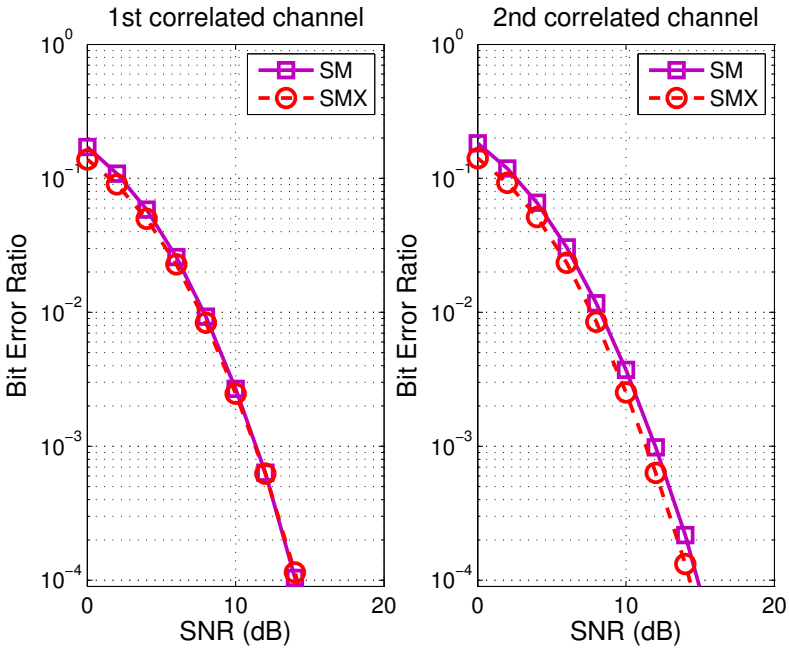

Figure 6.5: *ABER versus SNR for SM and SMX over a correlated channel.* $\eta = 4$*,* $N_t = 4$ *and* $N_r = 4$*.*

6.4.2.2 Large Scale MIMO

Fig. 6.6 compares the ABER between SM (solid line) and SMX (dashed line) using the virtual large scale MIMO channel created using the measured urban channels as explained in Sec.6.2.2, where $\eta = 8$, $N_r = 4$. For $\eta = 8$ the maximum number of transmit antennas that SMX can use is $N_t = 8$, where $\eta_{\text{SM}} = N_t \log_2(M)$. However, for SM one bit can be transmitted using the constellation symbol and seven bit using the spatial symbol, *i.e.* , for $\eta = 8$ SM can use up to $N_t = 2^7 = 128$ transmit antennas, making it possible to exploit large scale MIMO. Note that for SM it holds that: $\eta_{\text{SM}} = \log_2(N_t) + \log_2(M)$.

Finally, in Fig. 6.6, it can be seen that SM with $N_t = 128$ and $N_t = 64$ offers 6 dB and 4 dB better performance than SMX with $N_t = 8$ and $N_t = 4$ respectively. Note that the constellation size is the same for both SM with $N_t = 128$ and SMX with $N_t = 8$, as is for SM with $N_t = 64$ and SMX with $N_t = 4$. As the constellation size of the signal symbol is increased, the ABER of SM and SMX increases, *i.e.*, moving to $N_t = 16$ for SM it can be seen that SM offers only a 1 dB performance increase relative to SMX with $N_t = 2$. Note, the number of bits sent per transmission for both SM and SMX for all the scenarios is equal, and $\eta = 8$.

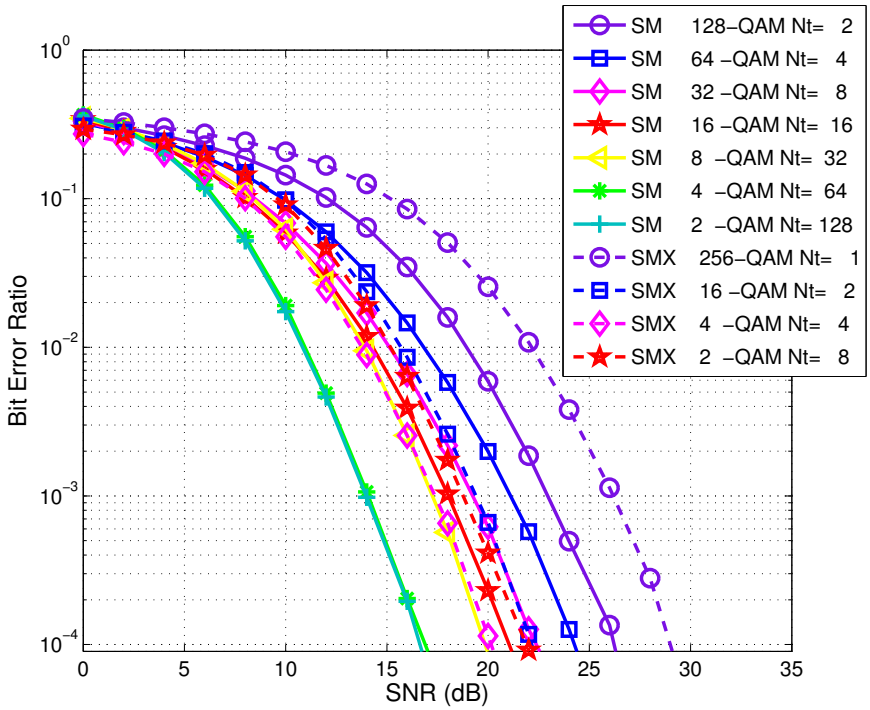

Figure 6.6: *ABER versus SNR for SM and SMX over real measured channels.* $\eta = 8$ *and* $N_r = 4$.

6.5 Summary

In this chapter, performance analysis of SM using urban Rayleigh channel measurements for both correlated and uncorrelated scenarios has been carried out. An analytical bound has been derived and performance results using simulated channels have been provided. An important observation is that experimental results confirm the analytical bound as well as computer simulations of the system. The performance of SM has been compared with the performance of SMX using the same urban channels. It has been demonstrated that for small scale MIMO, SM offers similar or slightly better ABER performance. However, for large scale MIMO, SM exhibits a significant enhancement in the ABER performance at no increase in complexity.

Chapter 7
Performance of Spatial Modulation in an Experimental World System

In this chapter the performance of spatial modulation (SM) and spatial multiplexing (SMX) is characterised with an experimental testbed. Two National Instruments (NI)–PXIe devices are used for the system testing, one for the transmitter and one for the receiver. The digital signal processing that formats the information data in preparation for transmission is described along with the digital signal processing that recovers the information data. In addition, the hardware limitations of the system are also analysed. The average bit error ratio (ABER) of the system is validated through both theoretical analysis and simulation results for SM and SMX under line of sight (LoS) channel conditions.

7.1 Introduction

In this chapter, the average bit error ratio (ABER) performance of spatial modulation (SM) is analysed in a practical testbed and compared with that for spatial multiplexing (SMX). In particular, the National Instruments (NI)–PXIe–1075 chassis is used at the transmitter and receiver. The design of the testbed hardware and the software used are explained in detail along with the transmission chain. The effects of the entire transmission chain on the system performance are examined. The basic elements of the transmission link are the transmit radio frequency (RF) chain, the wireless channel, and the receive RF chain. In addition to the effects of the wireless channel on the phase and amplitude of the signal, the impact of the power imbalances (PIs) on the system performance in the transmitter and receiver RF chains is discussed. Furthermore, an analytical upper bound for the ABER performance of SM over non–line of sight (NLoS) channels with PI is derived, and compared to the experimental and computer simulation results. The experimental results validate the analytical bound as well as the attained computer simulations. Finally the performance of SM is compared with the theoretical and experimental results of SMX. As part of the beyond fourth generation (4G), UK-China bridges project, the digital signal processing algorithms were developed jointly with Dr. Read Mesleh and Dr. Nikola Serafimovski, along with the collection of the measurement results. Furthermore, the data used to obtain the channel statistics was collected by Dr. Pat Chambers.

The remainder of this chapter is organised as follows. The system set-up, equipment and digital signal processing are presented in Section 7.2. The equipment constraints are then considered in Section 7.3 while the analytical modelling is discussed in Section 7.4. The performance of SM is then characterised in the experimental and simulation environments in Section 7.5, where it is compared with the theoretical and experimental results of a SMX system. Finally, the chapter is summarised in Section 7.6.

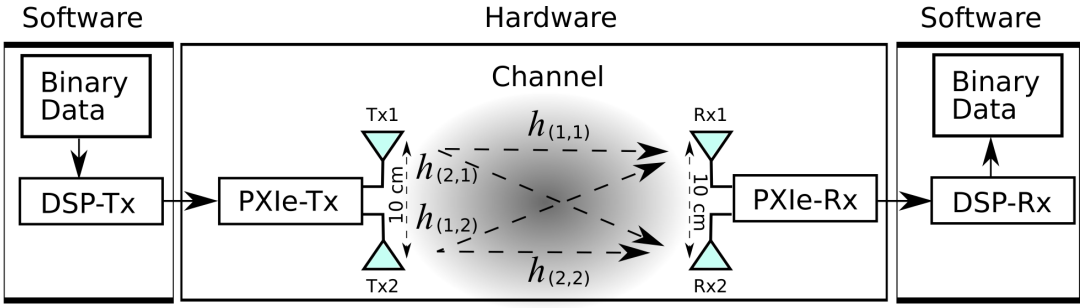

Figure 7.1: *Block sequence of the main steps in the experiment, from the generation of the binary data to its recovery.*

7.2 Testbed Set–up and System Model

The testbed set–up and transmission chain can be separated into software and hardware parts, as shown in Fig. 7.1. The hardware consists of the NI–PXIe chassis at the transmitter (PXIe–Tx) and the NI–PXIe chassis at the receiver (PXIe–Rx), each equipped with the relevant NI modules. The software consists of the digital signal processing at the transmitter (DSP–Tx) and the digital signal processing at the receiver (DSP–Rx).

The binary data to be broadcast is first processed by DSP–Tx, before being transmitted through the fading channel by PXIe–Tx. The channel coefficient on the link between transmit antenna n_t, and receive antenna n_r, is denoted by $h_{(n_r,n_t)}$. Note that the number of antennas at the transmitter and the receiver are denoted by N_t and N_r, respectively. At the receiver, PXIe–Rx records the RF signal and passes it through to DSP–Rx for processing, where the original data stream is recovered.

7.2.1 Testbed Hardware

The NI–PXIe–1075 chassis is equipped with a 1.8 GHz Intel–i7 processor with 4 GB RAM and are shown in Fig. 7.2.

The system has two transmit antennas and two receive antennas. Each antenna at the transmitter and receiver contains two quarter–wave dipoles, and one half–wave dipole placed in the middle. All three dipoles are vertically polarised. In addition, each antenna has a peak gain of 7 dBi in the azimuth plane, with an omnidirectional radiation pattern.

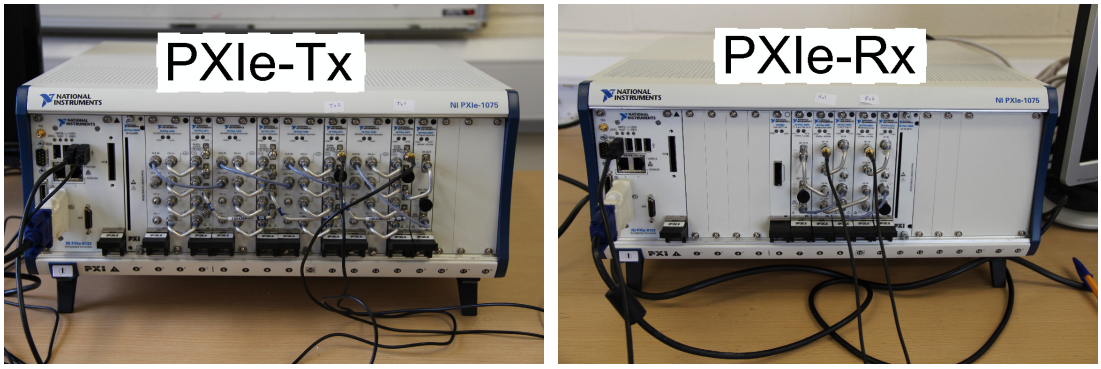

(a) PXIe–Tx (b) PXIe–Rx

Figure 7.2: *NI–PXIe–1075 chassis with the relevant on–board modules at the transmitter (PXIe–Tx), and at the receiver (PXIe–Rx).*

7.2.1.1 Transmitter hardware (PXIe–Tx)

The following NI–PXIe modules are used at the transmitter,

- NI-PXIe-5450 16-Bit I/Q Signal Generator (SG–16bit),
- NI-PXIe-5652 RF Signal Generator with a 500 kHz to 6.6 GHz frequency range (SG–RF),
- NI-PXIe-5611 intermediate frequency (IF) to carrier RF up–converter (up–converter).

The PXIe–Tx has an operational frequency range of 85 MHz to 6.6 GHz and can facilitate a bandwidth of 100 MHz at a maximum transmission power of 5 dBm.

At the transmitter, the SG–16bit performs a linear mapping of the signed 16-bit range to the output power and polarisation, *i.e.* , peak voltage amplitude is assigned to any value in the transmission vector equal to 2^{15} with a linear scale of the voltage amplitude down to zero. The output from SG–16bit is fed into the SG–RF, which is connected to the up–converter. The up–converter outputs the analogue waveform corresponding to the data resulting from DSP–Tx at a carrier frequency of 2.3 GHz. This completes a single RF chain. The transmission of the RF signal is synchronised by using a reference signal at 10 MHz.

7.2.1.2 Receiver hardware (PXIe–Rx)

The following NI–PXIe modules are used at the receiver,

- NI-PXIe-5652 used as an on-board reference clock (SG–RF),
- NI-PXIe-5622 16-Bit Digitiser (16-Bit Digitiser),
- NI-PXIe-5601 RF down–converter (down–converter).

The PXIe–Rx can operate in a frequency range of 10 MHz to 6.6 GHz and can facilitate an operational bandwidth of 50 MHz. For more details about the specifications of each model the interested reader can refer to [185].

At the receiver, the down–converter is used to detect the analogue RF signal from the antennas. The signal is then sent to the 16-Bit Digitiser. The 16-Bit Digitiser applies a bandpass filter with

a real flat bandwidth equal to $B_f = (0.4 \times f_s)$, where f_s is the sampling rate [185]. The sampling rate in the experiment is 10 Ms/s which results in a real flat bandwidth of 4 MHz. This may result in frequency-selective fading, however, it is not considered since equalisation is not required for the detection of SM signals. This is because: i) there are no multi–tap delays in the experimental setup, and ii) maximum–likelihood (ML) detection is used to decode the receiver signal for SM, and full channel state information (CSI) at the receiver is assumed [17]. Furthermore, the 16–Bit Digitiser is synchronised with the SG–RF on-board reference clock and writes the received binary files. The PXIe–Rx has two RF chains and the sequence described above defines a single RF chain. The simultaneous recording of the two signals coming from Tx1 and Tx2 is enabled by the use of the multiple processing cores and the multiple NI-PXIe modules. Finally, the recorded files are then processed by DSP–Rx.

7.2.2 Testbed Software

Matlab is used to facilitate the digital signal processing required at the transmitter and receiver, DSP–Tx and DSP–Rx, respectively. DSP–Tx serves to process the incoming information data and generate files that can be transmitted by PXIe–Tx. DSP–Rx serves to process the data received by PXIe–Rx and recover the original binary data stream. Fig. 7.3 outlines the processing algorithms at the DSP–Tx and the DSP–Rx.

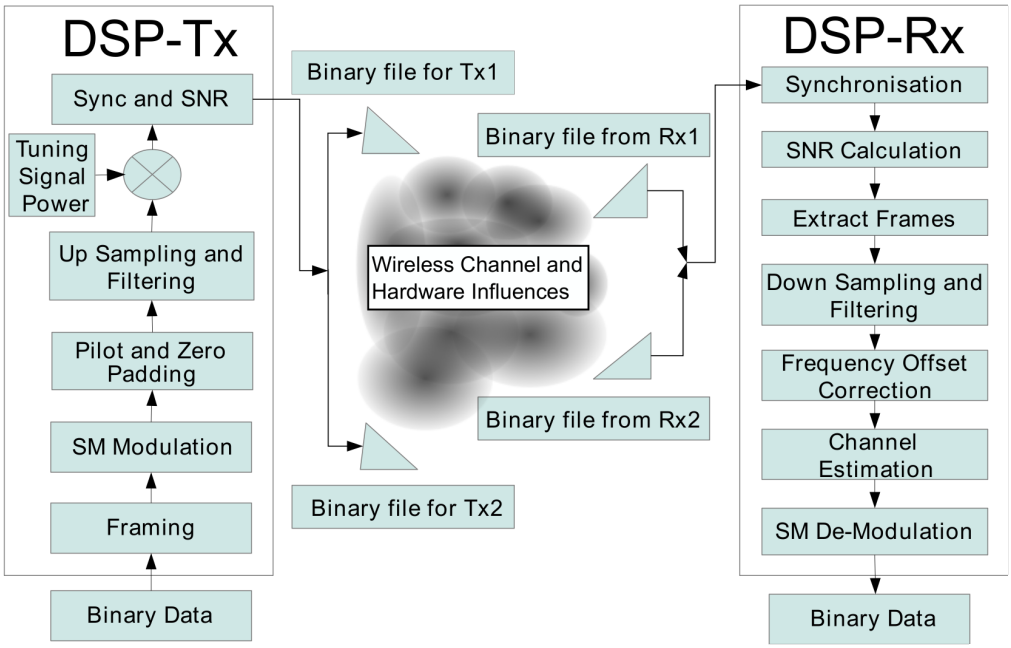

Figure 7.3: *A step-by-step layout of the binary data encoder (DSP–Tx) and decoder (DSP–Rx) processes.*

7.2.2.1 DSP–Tx

The DSP–Tx process takes the incoming binary information data and performs the following,

1.1 **Framing**: The incoming data is split into frames consisting of 100 symbols per frame.

1.2 **Modulation**:The data in each frame is modulated using SM or SMX:

- **SM**: The bit stream is divided into blocks containing $\eta = \log_2(N_t M)$ bits each, where η is the spectral efficiency, and M is the signal constellation size. The following mapping rule is then used [16]:
  (a) The first $\log_2(N_t)$ bits determine which transmit antenna is active, *i.e.* , they determine the spatial constellation point of SM. In this chapter, the transmit antenna broadcasting is denoted by ℓ_t with $\ell_t \in \{1, 2, \ldots, N_t\}$.
  (b) The second $\log_2(M)$ bits are used to choose a symbol in the signal–constellation diagram. Without loss of generality, quadrature amplitude modulation (QAM) is considered. The actual complex symbol emitted by the transmit antenna ℓ_t is denoted by s_t, with $s_t \in \{s_1, s_2, \ldots, s_M\}$.

  By following the above steps, the $N_t \times 1$ dimensional transmit vector is:

$$\mathbf{x}_{\ell_t, s_t} = \left[\mathbf{0}_{1\times(\ell_t-1)}, s_t, \mathbf{0}_{1\times(N_t-\ell_t)}\right]^T, \tag{7.1}$$

  where $[\cdot]^T$ denotes the transpose operation, and $\mathbf{0}_{p\times q}$ is a $p \times q$ all–zero matrix.
- **SMX**: In this case, the bit stream is divided into blocks of $N_t \log_2(M)$ bits, then, according to [2]:
  (a) Each $\log_2(M)$ bits are separately modulated using M–QAM modulation.
  (b) The modulated symbols are then transmitted simultaneously from the N_t transmit antennas.

1.3 **Pilot and Zero Padding**: The least squares (LS) channel estimation algorithm with local orthogonal pilot sequences is used to estimate the channel [186]. Two pilot signals are added for each frame, one at the start of the frame, and one at the end. Each pilot signal contains ten pilot sequences, where the orthogonal pilot sequence for the n_t–th transmit antenna is defined as,

$$\Theta_{n_t}(\ell) = \exp\left(2\pi j \frac{n_t \ell}{\bar{\bar{\Theta}}}\right) \tag{7.2}$$

where $\Theta_{n_t}(\ell)$ is the ℓ–th element of the pilot sequence Θ_{n_t} transmitted from antenna n_t, $\bar{\bar{a}}$ is the cardinality of a, and $j = \sqrt{-1}$ is the imaginary unit. In this work, the length of each

pilot sequence is $\bar{\bar{\Theta}} = 10$. To avoid inter–frame interference (IFI), an all zero sequence of 50 zero valued symbols is added to both the start and the end of the frame. Furthermore, a sequence of constant valued symbols is added to enable frequency offset (FO) estimation at the receiver. The length of the FO estimation sequence is 1000 symbols.

1.4 **Up Sampling and Filtering**: To maximise the signal to noise ratio (SNR) and reduce inter-symbol interference (ISI), up–sampling and matched filtering (pulse shaping) are used [187]. Each frame is up–sampled with an up-sampling ratio of 4, and then passed through a root raised cosine (RRC)-finite impulse response (FIR) filter with 40 taps and a roll–off factor of 0.75. The long tap–delay and the large roll–off factor are necessary to ensure that the power is focused in a short time and ensure that only a single RF chain is active when using SM.

1.5 **Tuning Signal Power**: To obtain the ABER, the SNR is varied by changing the power of the transmitted signal. This is done by multiplying each transmission vector with a "Tuning Signal Power" factor to obtain the desired transmit power.

1.6 **Synchronisation and SNR**: Several preamble–autocorrelation based methods for frame synchronisation were tested [188, 189, 190]. However, despite the introduction of an interpolation filter at the receiver and due to the channel attenuations, the estimated start of the signal was typically in error by one or two samples. This meant that sample synchronisation could not be achieved consistently, resulting in off-by-one errors. Therefore, as a temporary measure, peak detection is used for synchronisation. In particular, a sequence of 20 symbols with maximum power, separated by 50 zero valued symbols between each, are added to the start of the transmitted signal. The large power difference between the maximum power peaks and the power of the "Data section" symbols is reasonable since the instantaneous channel power may fluctuate by as much as 20 dB due to fast fading [191, 192]. The power difference between the synchronisation section and the remaining sections is set to be larger than the maximum channel variation, so that a successful peak detection is guaranteed. If this is not the case, no peak may be detected at the receiver and all further decoding would be erroneous.

To facilitate SNR calculations at the receiver, two sequences of power and no power are added after the synchronisation pulses of the transmitted signal, indicated by "SNR section" in Fig. 7.4. Each sequence contains 5 blocks of 50000 symbols and 50000 zeros. The first sequence is transmitted from the first antenna while the second antenna is off. The second sequence is transmitted from the second antenna while the first antenna is off.

After the DSP–Tx process is completed, the transmit vector symbols are converted to I16 format and are recorded to a binary file. This binary file is then loaded and broadcasted by PXIe–Tx.

Fig. 7.4 shows the absolute value representation of the processed incoming data that is passed to the first transmit antenna (Tx1) and Fig. 7.5 shows the absolute value representation of each frame. Note that the "Data section" is a series of concatenated frames. In Fig. 7.5, it can be seen that each frame contains $26,100$ samples. Therefore, the period of each frame is $T_{\text{Frame}} = 26100/f_s = 2.6\,\text{ms}$, which is much less than the coherence time of the channel given that, typically, the coherence time for a stationary indoor environment is approximately $7\,\text{ms}$, [192, and references therein]. Hence, the channel estimation at the receiver is valid for the frame duration.

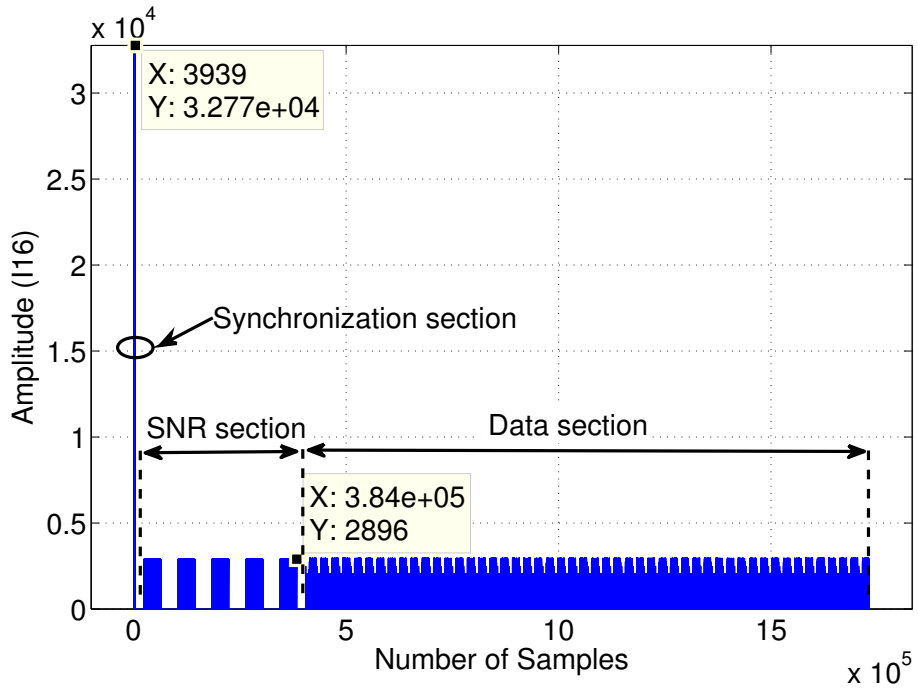

Figure 7.4: *The absolute value representation of the transmission vector being sent to* Tx1. *The synchronisation, SNR estimation and Data sections are shown. The value of the peak must equal* 2^{15} *since the 16 bit–Digitiser operates using an* I16 *format before tuning the signal power of the data. The highest value in the SNR section is the same as the highest value in the information data section. There is approximately a* $21.1\,\text{dB}$ *difference between the peak power in the synchronisation section and the peak power in the SNR estimation and data sections. This is apparent when looking at the two data points shown in the figure.*

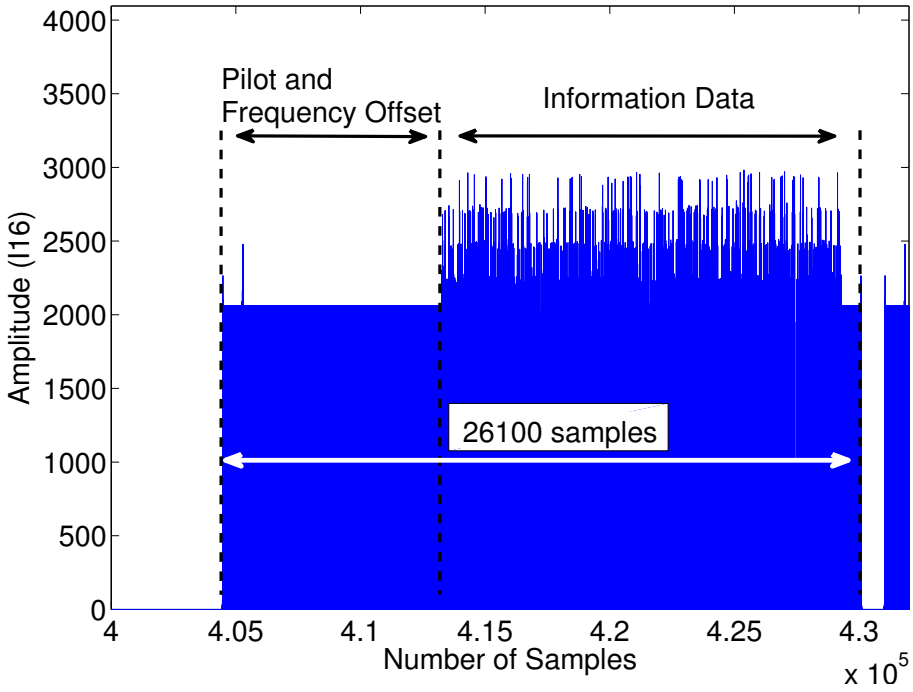

Figure 7.5: *The absolute value representation of a single frame from the vector being transmitted by* Tx1 *in the* I16 *data format which is a signed* 15 *bit representation of an integer number. Each frame is composed of the pilot and FO estimation along with the information data section. Each frame has at most* $26,100$ *samples.*

7.2.2.2 DSP–Rx

The data received by the PXIe–Rx is processed by DSP–Rx to recover the original data stream. To accomplish this, the following steps are required:

2.1 **Synchronisation**: This is achieved by searching for the peaks with a value above a certain threshold in the received signal. The threshold is set as 70% of the highest value in the received vector. This threshold level accounts for the natural voltage variations in the system, *i.e.* , the difference between peak voltage and root-mean-square voltage. If the number of peaks found is less than 20, then the received vector is discarded from further calculations.

2.2 **SNR Calculation**: The SNR is defined as,

$$\text{SNR} = \frac{\text{E}\left[\|\mathbf{Hx}\|_{\text{F}}^2\right]}{\sigma_n^2} \tag{7.3}$$

where $\mathbf{H}$ is the $N_r \times N_t$ channel matrix, $\mathbf{x}$ is the $N_t \times 1$ transmitted vector, $\text{E}[\cdot]$ is the expectation operator, σ_n is the noise variance, and $\|\cdot\|_{\text{F}}$ is the Forbenius norm.

Assuming that the noise at the receiver is additive white Gaussian noise (AWGN), the received signal for the duration of the SNR sequence can be written as follows:

$$\mathbf{y} = \mathbf{h}_{n_t} s_t + \mathbf{n} \tag{7.4}$$

where $\mathbf{y}$ is the $N_r \times 1$ received vector, $\mathbf{h}_{n_t}$ is n_t column of the channel matrix $\mathbf{H}$, $\mathbf{n}$ is the $N_r \times 1$ AWGN vector with σ_n^2 variance and μ_n mean, and s_t is the transmitted symbol from the n_t antenna. As mentioned in Section 7.2.2.1, only a single transmit antennas is active when broadcasting the SNR sequence and s_t is either equal to the maximum value in the "Data section" $x_{\max}$ or zero, as shown in Fig. 7.4. Hence, the received signal in (7.4) can be re–written as,

$$\mathbf{y} = \begin{cases} \mathbf{h}_{n_t} x_{\max} + \mathbf{n}, & s_t = x_{\max} \\ \mathbf{n}, & s_t = 0 \end{cases} \tag{7.5}$$

Proceeding from (7.5),

$$\mathrm{E}\left[\|\mathbf{H}\mathbf{x}\|_{\mathrm{F}}^2\right] = \mathrm{E}\left[\|\mathbf{y} - \mathbf{n}\|_{\mathrm{F}}^2\right] \tag{7.6}$$

$$\sigma_n^2 = \mathrm{E}\left[\|\mathbf{n}\|_{\mathrm{F}}^2\right] - \mathrm{E}\left[\|\mathbf{n}\|_{\mathrm{F}}\right]^2 \tag{7.7}$$

where $[\cdot]^H$ is the hermitian operation. As discussed in Section 7.2.2.1, each SNR sequence contains $50,000$ symbols and $50,000$ zero valued symbols. Since the noise in the system represents an ergodic processed, the ensemble average in (7.6) can be replaced with time averaging,

$$\mathrm{E}\left[\|\mathbf{H}\mathbf{x}\|_{\mathrm{F}}^2\right] = \sum_{i=1}^{50000} \left(\|\mathbf{y}_i - \mathbf{n}_i\|_{\mathrm{F}}^2\right) \tag{7.8}$$

$$\sigma_n^2 = \sum_{i=1}^{50000} \|\mathbf{n}_i\|_{\mathrm{F}}^2 - \left[\sum_{i=1}^{50000} \|\mathbf{n}_i\|_{\mathrm{F}}\right]^2 \tag{7.9}$$

where $\mathbf{y}_i$ and $\mathbf{n}_i$ are the i–th received vector. To get a more accurate estimation, the SNR is calculated for the 5 transmitted SNR sequences received at both antennas and then averaged again over those measurements.

2.3 **Extract Frames**: After finding the start of the transmission and calculating the SNR, DSP–Rx performs a serial to parallel conversion to separate the received frames.

2.4 **Down Sampling and Filtering**: To complete the matched filter described in Section 7.2.2.1, each frame is down–sampled by a factor of 4 and passed through an RRC–FIR filter.

2.5 **Frequency Offset (FO) Correction**: The DSP–Rx estimates the FO for each frame by,

$$\Delta_f = \frac{\angle x_{1000} - \angle x_1}{2\pi \times 1000} \tag{7.10}$$

where $\angle x_{1000}, \angle x_1$ are the angles of the first and the last sample of the FO sequence transmitted by the DSP–Tx where the FO sequence has exactly 1000 symbols. These angle values are obtained by correcting the radian phase angles in a vector by adding multiples of $\pm 2\pi$ as required. This enables a better estimate of the phase offset. Assuming a linear phase rotation, the FO can be estimated by (7.10). The FO for each frame is then corrected by,

$$\widehat{y}_i = y_i \times e^{-j2\pi\Delta_f i} \tag{7.11}$$

where $\widehat{y}_i, y_i$ is the i–th element of the corrected and the uncorrected received frame, respectively.

2.6 **Channel Estimation**: The channel estimation is done by using the LS channel estimation algorithm proposed in [186], where for each frame the channel is estimated by,

$$\widehat{\mathbf{H}}_{\text{LS}} = \frac{1}{N_\Theta} \Theta^H \mathbf{H}_r \tag{7.12}$$

where $\mathbf{H}_r$ is the received pilot sequence. To enable a more accurate evaluation of the system, the channel is estimated and averaged over 10 pilot sequences. Furthermore, two channels are estimated per frame, the first channel estimate is used for the first half of the data symbols in the frame, and the second is used for the second half of the data symbols in the frame.

2.7 **Demodulation**: The ML optimum receiver for multiple–input multiple–output (MIMO) systems is used, which can be written as,

$$\hat{\mathbf{x}}_t^{(\text{ML})} = \underset{\mathbf{x} \in \mathcal{Q}}{\arg\min} \left\{ \|\mathbf{y} - \mathbf{H}\mathbf{x}\|_{\text{F}}^2 \right\} \tag{7.13}$$

where $\mathcal{Q}$ contains every possible $(N_t \times 1)$ transmit vector, and $\hat{\cdot}$ denotes the estimated transmission vector.

Finally, the recovered binary data along with the estimated SNR are used to obtain the ABER performance of SM.

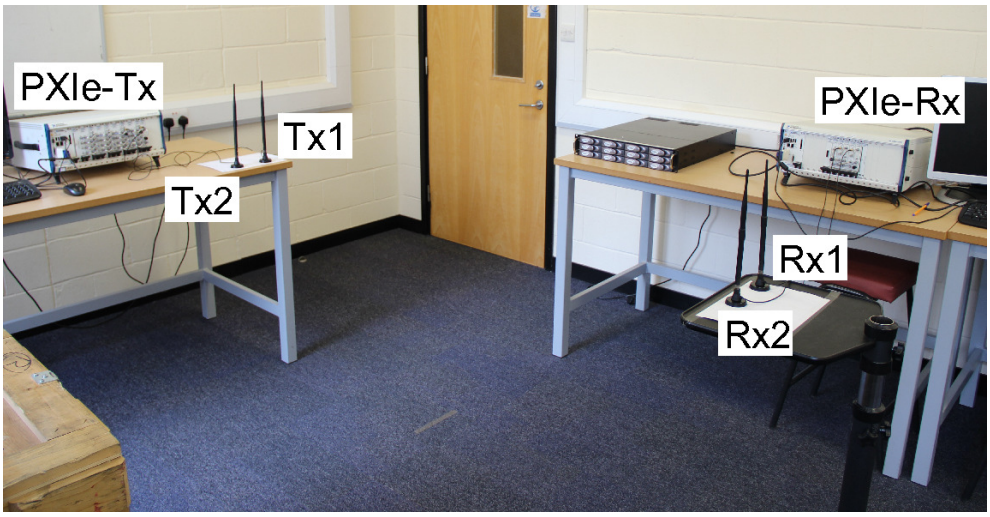

Figure 7.6: *Experimental setup in the laboratory.*

7.2.3 Propagation Environment (Channel)

The physical layout of the experimental set-up is shown in Fig. 7.6 and the relative antenna spacing is provided in Fig. 7.7. In particular, the two transmit and two receive antennas are identical and are placed directly across from each other. As such, the channel between the transmitter and receiver has a strong line of sight (LoS) component. Therefore, the transmitter to receiver channel is defined as a Rician fading channel with a large K-factor due to the distance between the transmit and receive antennas where K is the ratio of the coherent power component, usually the LoS, to the non-coherent power components, usually NLoS. In addition, the omnidirectional transmit antennas broadcast on a frequency of 2.3 GHz at 10 Ms/s.

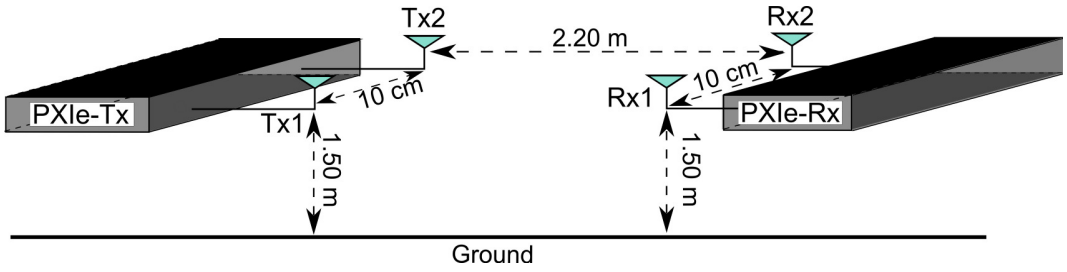

Figure 7.7: *Physical experimental layout: A pair of receive and a pair of transmit antennas are set* $2.2\,\mathrm{m}$ *apart from each other with a direct line of sight. Each pair of antennas is* $1.5\,\mathrm{m}$ *from the ground and there is a* $10\,\mathrm{cm}$ *spacing between the antennas in either pair corresponding to* 0.77 *times the wavelength at* 2.3 GHz*. All antennas are omnidirectional.*

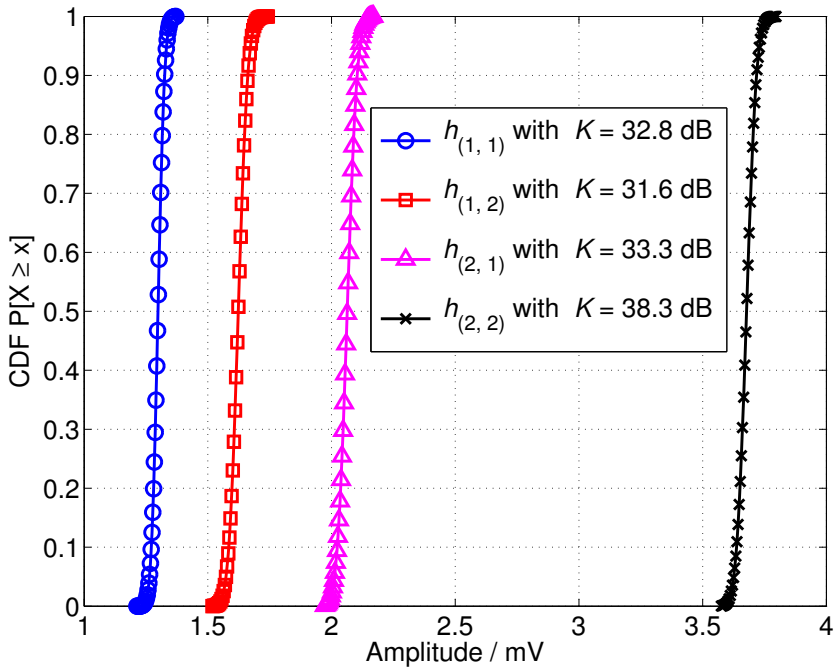

Figure 7.8: *CDF for each of the fast fading coefficients, $h_{(r,n_t)}$, of the four channels in the experiment. Each is defined by a Rician distribution with a unique K-factor. The markers denote the measurement points while the lines denote the best fit approximation. Note that the wireless channel mean values fall in the range of* 1.3 mV *to* 3.6 mV.

Channel measurements were collected to verify that the channel environment followed a Rician distribution. To achieve this, the transmitter broadcasts pulses at 10 Ms/s on a carrier frequency of 2.3 GHz at 4 dBm peak power. Each pulse includes a FO estimation section and a total of 10^5 pulse samples were collected. A best fit approximation is then calculated for the collected data. In particular, a maximum likelihood estimation is fitted to the collected data. A Chi-squared goodness-of-fit test is then performed to ascertain that the distribution resulting from the maximum likelihood estimation fits at least 95% of the data. The empirical cumulative distribution function (CDF) for each link of the resultant channels are presented in Fig. 7.8. The CDFs show that the channel does indeed follow a Rician distribution with a K factor that ranges between $31 - 38$ dB. The different K-factors on the links between the transmit and receive antennas may be explained by the room geometry, the antenna positioning and the overall propagation environment. However, note that each of the CDFs has a different mean, which will be discussed in the next section.

7.3 Equipment Constraints

Fig. 7.7 shows the physical layout of the experiment. Note that the 10 cm inter–antenna separation used here is sufficient to guarantee very low, if any, spatial correlation when broadcasting at 2.3 GHz with a 2.2 m separation between the transmitter and receiver [193].

The physical environment through which the signal passes, starting from the SG–RF at the transmitter, until it reaches the 16–Bit Digitisers at the receiver, suffers from connector losses, differences in the RF chains, different phase responses, attenuations and similar. To study and model the effects of the hardware imperfections on the signal power:

- An RF coaxial cable with a 10 dB attenuation is connected between each transmit and receive antenna.
- A pulse is transmitted at 10 Ms/s on a carrier frequency of 2.3 GHz at -10 dBm peak power. Each pulse includes a FO estimation section and a total of 10^5 pulse samples were collected.
- The CDF for each of the fading coefficients is calculated and is shown in Fig. 7.9.

In an ideal environment, the means of the CDFs in Fig. 7.9 should be equal. However, imperfections in the hardware result in different means for each transmit to receiver antenna pair, as can be seen in Fig. 7.9. The differences between the channels can be modeled as a PI between the various link pairs in the channel matrix $\mathbf{H}$. Therefore, the channel coefficients are redefined as,

$$h^{\text{PI}}_{(n_r,n_t)} = \sqrt{\alpha_{(n_r,n_t)}} \times h_{(n_r,n_t)} \tag{7.14}$$

where $\alpha_{(r,n_t)}$ is the channel attenuation coefficient from receive antenna n_r to transmit antenna n_t.

To locate the source of the discrepancy between the different channel attenuations, *i.e.* , determine if the NI modules or the NI chassis is the source, the RF chains at the receiver were swapped around and the channels were estimated in configuration (I) and configuration (II). Fig. 7.9(a) shows the channel CDFs for configuration (I) while Fig. 7.9(b) shows the channel CDFs for configuration (II).

Taking $h_{(1,1)}$ as a reference, the channel attenuation coefficients for configuration (I) are,

$$\alpha_{(1,1)} = 0\,\mathrm{dB}, \qquad \alpha_{(2,1)} = 0.25\,\mathrm{dB}, \qquad \alpha_{(1,2)} = 0.88\,\mathrm{dB}, \qquad \alpha_{(2,2)} = 1.1\,\mathrm{dB}, \quad (7.15)$$

while the channel attenuation coefficients for configuration (II) are,

$$\alpha_{(1,1)} = 0\,\mathrm{dB}, \qquad \alpha_{(2,1)} = 0.29\,\mathrm{dB}, \qquad \alpha_{(1,2)} = 1.13\,\mathrm{dB}, \qquad \alpha_{(2,2)} = 1.17\,\mathrm{dB}. \quad (7.16)$$

Comparing Fig. 7.9(a) and Fig. 7.9(b), and the attenuations in (7.15) to that in (7.16) shows that they are very similar, and that the swapping of the RF chains has a minimal impact on the estimated mean of each channel attenuation. Thus, it can be assumed that the NI modules that compose the receive RF chains are the source of the hardware imperfections, and consequently lead to the differences in the means of the estimated CDFs. Unfortunately, due to the warranty restrictions on the hardware, we are unable to specify the exact components responsible for the observed effects. Nonetheless, to account for these imperfections, the channel attenuation coefficients in (7.15) and (7.16) are taken into consideration by deriving an analytical model in Section 7.4. The accuracy of the derived analytical bound using the channel attenuation coefficients in (7.15) and (7.16) is demonstrated in Section 7.5 by comparing it to empirical results.

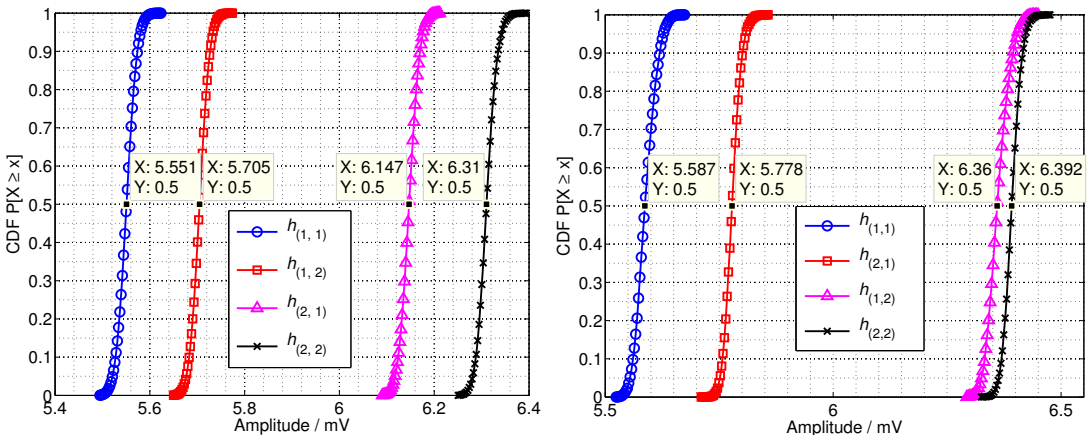

(a) Configuration (I) of the receive RF chains.

(b) Configuration (II) of the receive RF chains.

Figure 7.9: *CDF for each of the fast fading coefficients, $h_{(r,n_t)}$, of the four channels in the experiment. Each is defined by a Rician distribution with a unique K-factor. The markers denote the measurement points while the lines denote the best fit approximation. Despite using a coaxial cable with a* $10\,\mathrm{dB}$ *attenuation to connect the RF chains, each channel exhibits a unique mean.*

7.4 Analytical Modeling

An analytical model for the ABER performance of the experimental system is developed by considering the system model presented in Section 7.2 and the system constraints in Section 7.3. The performance of SM and SMX over a single link in a noise-limited scenario is characterised by,

$$\mathrm{ABER} \leq \frac{1}{2^{\eta}} \sum_{\ell_t, s_t} \sum_{\ell, s} \frac{N\left(\mathbf{x}_t, \mathbf{x}\right)}{\eta} \mathrm{E}_{\mathbf{H}} \left\{ \Pr_{\text{error}} \right\} \tag{7.17}$$

where $N\left(\mathbf{x}_t, \mathbf{x}\right)$ is the number of bits in error between the transmitted vector $\mathbf{x}_t$ where the symbol s_t is sent from the antenna ℓ_t and $\mathbf{x}$ where the symbol s is transmitted from the antenna ℓ, $\mathrm{E}_{\mathbf{H}}\{\cdot\}$ is the expectation across the channel $\mathbf{H}$, and $\Pr_{\text{error}}$ is the conditional pairwise error probability (PEP) of deciding on $\mathbf{x}$ given that $\mathbf{x}_t$ is transmitted,

$$\begin{aligned} \Pr_{\text{error}} &= \Pr\left(\left\| \mathbf{y} - \mathbf{H}\mathbf{x}_t \right\|_{\mathrm{F}}^2 > \left\| \mathbf{y} - \mathbf{H}\mathbf{x} \right\|_{\mathrm{F}}^2 \middle| \mathbf{H} \right) \\ &= Q\left(\sqrt{\varphi \left\| \mathbf{H}\left(\mathbf{x}_t - \mathbf{x}\right) \right\|_{\mathrm{F}}^2} \right) \end{aligned} \tag{7.18}$$

where $\varphi = 1/(2\sigma_n^2)$, and $Q(\omega) = \frac{1}{\sqrt{2\pi}} \int_{\omega}^{\infty} \exp\left(-\frac{t^2}{2}\right) \mathrm{dt}$ is the Q-function. As Fig. 7.7 indicates, the transmit and receive antennas in the experiment experience a very strong LoS environment. Accordingly, the channel between each transmit to receive antenna pair is characterised by Rician fading. A generic Rician channel is defined as

$$h_{(r,n_t)} = \sqrt{\frac{K}{1+K}} + \sqrt{\frac{1}{1+K}} h'_{(r,n_t)}, \tag{7.19}$$

where $h'_{(r,n_t)} \sim \mathcal{CN}(0,1)$ is a complex normal, circular symmetric random variable with zero mean and unit variance. $n_t \in \{1,2\}$, $r \in \{1,2\}$ are the index of the transmit and receive antenna respectively.

To account for the hardware imperfections that result from the power imbalances, the fast fading channel coefficients are redefined according to (7.14) and (7.15). Section 7.5 validates the derived analytical bound by comparing it to experimental and simulation results.

7.5 Experimental Results and Numerical Analysis

The simulation, analytical and experimental results for the ABER performance of SM in a LoS channel are illustrated in Fig. 7.10, where a stream of 10^5 information bits is sent per transmission to obtain the experimental results, and the presented SNR along the x–axis is equivalent to the SNR on $h_{1,1}$. The results validate the theoretical work done in the field [20]. As the experimental results approximate the performance of the simulation results with PIs and both the simulation, and experimental results, are closely approximated by the derived upper bound at a low ABER.

The large error between the experimental, simulation and analytical curves at high ABER is the results of incorrect frequency offset estimation, timing recovery errors synchronisation problems, and poor channel estimation. However, as the SNR increases, frequency offset estimation, timing recovery and channel estimation improve, resulting in a lower ABER as shown in Fig. 7.10. Quantifying those imperfections is deemed important and requires channel modelling and interference measurement. However, addressing these effects is beyond the scope of this work and will be subject of future works.

SM performs best when the channel between each transmit and receive antenna is unique, *i.e.* , the larger the Euclidean distance between two received vectors is, the better the ABER performance of SM. The channel uniqueness can be the result of a rich scattering environment, or as in this experiment the channel uniqueness is the result of PIs caused by hardware tolerances. This is demonstrated in Fig. 7.10, where the performance of SM in a Rician environment is largely enhanced by introducing PIs between the transmit and receive paths. Please note that the PIs between the links are always obtained relative to the channel with the greatest attenuation, *i.e.* , the values of the PI factors in (7.15) and (7.16) are always positive.

Furthermore, PIs between the transmitting antennas are shown to offer improved performance in terms of the ABER when only the spatial constellation of SM is used, *i.e.* , when space shift keying (SSK) is the underlying modulation technique. In particular, an optimised power allocation for a various number of transmit antennas is addressed in [155], where the authors show that there is an optimal power allocation between the transmitting antennas which can serve to increases the Euclidean distance between the channel signatures and improve the ABER performance of SM. Indeed, SM has also been successfully applied to an AWGN optical wireless channel where it is shown that PIs greatly improve the ABER performance [168].

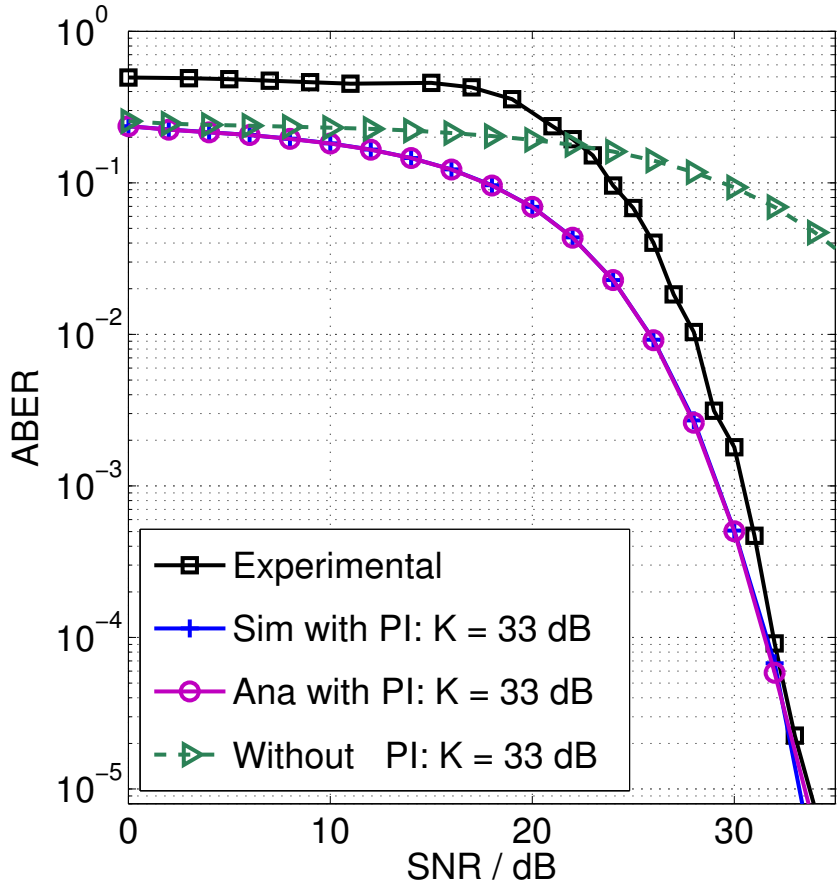

Figure 7.10: *ABER for SM in an experimental set-up with* 2 *transmit antennas,* 2 *receive antennas and a spectral efficiency of* $2\,\mathrm{bits/s/Hz}$*. The SNR is set as measured on* $h_{(1,1)}$ *with* $\alpha_{(1,1)} = 0\,\mathrm{dB}$*. The solid black line with square markers denotes the experimental results. The green diamond markers denote simulation results with no PI between the links while the green dashed line is the analytical prediction. The remaining curves denote the simulation* (Sim) *and analytical* (Ana) *results.*

The simulation, analytical and experimental results for the ABER performance of SMX in a LoS channel are illustrated in Fig. 7.11. In particular, the experimental results closely follow the performance of the simulation results with PIs and both the simulation, and experimental results, are closely approximated by the derived upper bound at low ABER when the hardware imperfections are taken into account. This result serves to validate theoretical work done in the field. The results in Fig. 7.11 demonstrate that the SMX system, like the SM system, also benefits from the PIs in the hardware. The SMX system exhibits approximately a $3\,\mathrm{dB}$ coding gain when compared to SM at an ABER of 10^{-4}. The coding gain of SMX relative to SM is expected when there are few transmit antennas. The Euclidean distance between the transmit vectors, and therefore the variance in (7.18), in SMX is larger than in SM. However, the aim of this chapter is to show that empirical results validate the simulation and analytical work done

in the field, which can be seen in both Fig. 7.10 and Fig. 7.11. Unfortunately, due to the limited number of transmitter and receiver RF chains available, there are no experimental results for systems with a larger number of transmit or receive antennas where SM is shown to perform better than SMX. These empirical results will be the focus of future research. Nonetheless, the accuracy of the theoretical and simulation results of SMX and SM with a large number of transmit and receive antennas can be extrapolated from the presented results.

This work demonstrates that the hardware tolerances of practical communication systems are beneficial for the ABER performance of both SM and SMX. This behaviour along with the requirement for a single RF chain, make SM a viable candidate for future wireless networks.

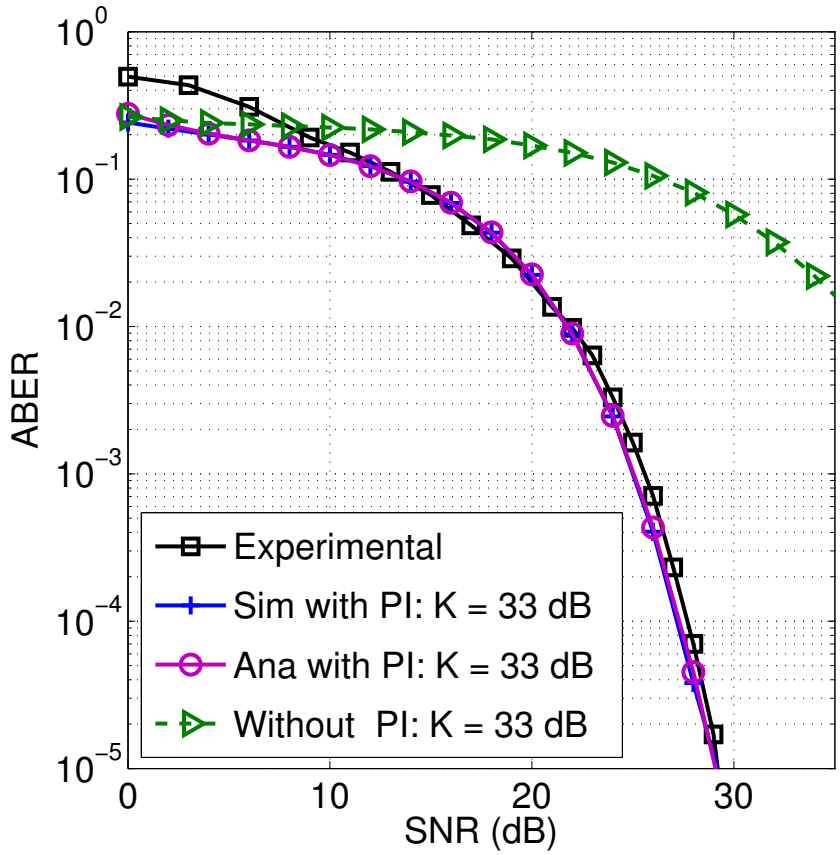

Figure 7.11: *ABER for SMX in an experimental set-up with* 2 *transmit antennas,* 2 *receive antennas and a spectral efficiency of* $2\,\mathrm{bits/s/Hz}$*. The SNR is set as measured on* $h_{(1,1)}$ *with* $\alpha_{(1,1)} = 0\,\mathrm{dB}$*. The solid black line with square markers denotes the experimental results. The green diamond markers denote simulation results with no PI between the links while the green dashed line is the analytical prediction. The remaining curves denote the simulation* (Sim) *and analytical* (Ana) *results.*

7.6 Summary

For the first time ever, the ABER performance of SM and SMX has been validated using a practical testbed, in particular NI kits were used. The design of the testbed, hardware and software, were explained in detail along with the transmission chain. Moreover, the channel conditions were described and the ABER performance for SM and SMX over LoS channels was obtained. The ABER results were compared to both simulation and analytical results, and shown that a Rician channel with different PIs closely described the behaviour of SM and SMX in this particular physical environment. Furthermore, the PIs caused by the hardware imperfections were analysed and studied. The induced power imbalances resulted in significant coding gains for the practical systems compared to the theoretical results without PIs. To this extent, SM and SMX performed as expected relative to the theoretical work when the power imbalances were introduced in the analytical model. The experimental results validated the SM principle, and the performance gains exhibited by SM in the practical implementation as a result of the hardware tolerances made SM a viable candidate for future wireless networks.

Chapter 8
Conclusions, Limitations and Future work

8.1 Summary and Conclusions

In Chapter 3, an analytical bound for the average bit error ratio (ABER) of spatial modulation (SM) over Rayleigh, Rician and Nakagami–m fading channels is proposed. The bound is an easy to calculate closed form upper bound for the ABER of SM, which can be used for correlated and uncorrelated channels, small and large scale multiple–input multiple–output (MIMO), and for any modulation scheme. The performance of SM is also compared with the performance of spatial multiplexing (SMX), where it is shown that SM offers nearly the same or slightly better performance than SMX.

Chapter 4 introduced and analysed the performance/complexity trade–off of two sphere decoders (SDs) designed specifically for SM. The proposed SDs provide a substantial reduction of the computational complexity while retaining the same ABER as the maximum–likelihood (ML)–optimum detector. The closed–form analytical upper bound for the ABER of SM–SD in identical and independently distributed (i.i.d.) Rayleigh flat–fading channels has been derived, and analytical and simulation results were shown to closely agree. Furthermore, numerical results have highlighted that no SD is superior to the others, and that the best solution to use depends on the MIMO setup, and the signal to noise ratio (SNR) at the receiver. In general, Rx–SD is the best choice for lower spectral efficiencies, and Tx–SD is the best option for higher spectral efficiencies. Finally, simulation results showed that SM using SD offers a significant reduction in computational complexity, up to 97% reduction in computational complexity, and nearly the same ABER performance as SMX using ML decoder or SD.

In Chapter 5, the idea of SM was generalised by sending the same symbol from more than one transmit antenna at a time, and two new MIMO systems, variable generalised spatial modulation (VGSM) and generalised spatial modulation (GNSM), were proposed. Note, the basic idea of SM is no longer limited to a power of two number of transmit antenna and an arbitrary number of transmit antennas can be used. Moreover, three receivers were proposed. The first receiver is based on ML principle, and the last two receivers, Tx–SD and Rx–SD, are based on the SM–SD principle presented in Chapter 4. Furthermore, a tight closed form upper bound for the ABER of GNSM and VGSM, over correlated and uncorrelated Rayleigh and Rician fading channels was provided. Finally, results showed that the proposed schemes, VGSM and GNSM, use much fewer antennas than SM, and have significantly lower computational complexity than SMX, while having a small penalty in the ABER performance. Thus, GNSM and VGSM are good candidates for low number of transmit antennas and low computational complexity MIMO solutions.

In Chapter 6, performance analysis of SM using urban Rayleigh channel measurements for both correlated and uncorrelated scenarios has been carried out. An analytical bound was derived and performance results using simulated channels have been provided. An important observation is that experimental results confirm the analytical bound as well as computer simulations of the system. The performance of SM is compared with the performance of SMX using the same urban channels. It was demonstrated that for small scale MIMO, SM offers similar or slightly better ABER performance. However, for large scale MIMO, SM exhibits a significant enhancement in the ABER performance compared to SMX at no increase in complexity.

Finally in Chapter 7, the ABER performance of SM and SMX has been validated using a practical testbed, in particular National Instruments (NI) kits were used. The design of the testbed, hardware and software, were explained in detail along with the transmission chain. Moreover, the channel conditions were described and the ABER performance for SM and SMX over line of sight (LoS) channels was obtained. The ABER results were compared to both simulation and analytical results, and shown that a Rician channel with different power imbalance (PI) closely described the behaviour of SM and SMX in this particular physical environment. Furthermore, the PIs caused by the hardware imperfections were analysed and studied. The induced power imbalances resulted in significant coding gains for the practical systems compared to the theoretical results without PIs. To this extent, the experimental results validated the analytical bound as well as the computer simulations.

The contributions of the thesis can be summarised as follows:

- A tight closed form analytical upper bound for the ABER performance of SM over correlated and uncorrelated, Rayleigh, Rician, and Nakagami–m channels, small and large scale MIMO, and for any modulation scheme, has been derived. For Rayligh channels, the bound was validated using experimental results carried out over urban channels.

- The ABER performance of SM was compared to the ABER performance of SMX over small and large scale MIMO, different modulation schemes, correlated and uncorrelated, Rayleigh, Rician, and Nakagami–m channels. Furthermore, for Rayleigh channels urban measured channels were also use, and for Rician channels an experimental system was used to validate the developed theories. For small scale MIMO, SM offers similar or slightly better ABER performance than SMX. However, for large scale MIMO, SM exhibits a significant enhancement in the ABER performance.

- The complexity of SM using a ML decoder was calculated and compared to the complexity of SMX using a ML decoder. It was shown that SM–ML offers a large reduction in complexity when compared to SMX–ML, where the complexity of SM–ML does not depend on the number of transmit antennas. Moreover, the complexity of SM was further reduced by the use of SD principle. Two SDs were proposed, Tx–SD and Rx–SD, and shown that no SD is superior to the other, and that the best solution to use depends on the MIMO setup and the SNR at the receiver. Furthermore, the complexity of SM–SDs was compared with SMX–SD and was shown that SM–SD offers up to 97% reduction in computational complexity.

- Two MIMO systems, VGSM and GNSM, were proposed to overcome the limitation in the number of antennas in SM. This was carried out by sending the same symbol from more than one transmit antenna at a time. Furthermore, three receivers were proposed. The first receiver is based on ML principle, and the last two receivers, Tx–SD and Rx–SD, are based on the SM–SD principle.

From all above, SM is an ideal candidate for low complexity, large scale MIMO.

8.2 Limitations and Future Works

SM has been studied extensively in the academic community. This thesis has explored some of the advantages that SM offers and proposed solutions to overcome some of its limitations. However, there is still scope for extensive academic research into the advantages, possible uses and possible constraints of spatial modulation. Various issues in the area present a wide scope for further academic investigation, for example:

- The performance of spatial modulation over urban channels and practical systems is a field that offers a wide scope for further academic exploration. It has been explored for the first time in a thesis, but only for Rayleigh in the case of Urban channels, and 2×2 binary phase shift keying (BPSK) systems with Rician channels for practical systems. This should be extended to different constellations sizes, small and large scale MIMO and different channels, as it is an important step toward developing SM to be introduced to future mobile communication standards.

- The switching between the different antennas is an area which has yet to be explored academically. Academic investigation of this area would provide extremely useful and relevant information for the future development of SM to be used for high data rate practical systems.
- The possible effect of channel imperfections and channel estimation errors on spatial modulation is also a pertinent issue in the field. Academic investigation of this field would also provide valuable information and data to further the development of spatial modulation.

Appendix A
Proof of the intervals (4.12)**,** (4.13)

Proof:

1. First (4.11) can be thought of as an inequality,

$$R^2 \geq \left\{ \|\bar{\mathbf{y}} - \bar{\mathbf{H}}\bar{\mathbf{x}}_{\ell,s}\|_{\mathrm{F}}^2 \right\} \tag{A.1}$$

Add $\epsilon\bar{\mathbf{x}}_{\ell,s}^T\bar{\mathbf{x}}_{\ell,s}$ to both sides of (A.1),

$$\begin{aligned} R^2 + \epsilon\bar{\mathbf{x}}_{\ell,s}^T\bar{\mathbf{x}}_{\ell,s} &\geq \left\{ \|\bar{\mathbf{y}} - \bar{\mathbf{H}}\bar{\mathbf{x}}_{\ell,s}\|_{\mathrm{F}}^2 + \epsilon\bar{\mathbf{x}}_{\ell,s}^T\bar{\mathbf{x}}_{\ell,s} \right\} && \text{(A.2)} \\ &\geq \left\{ \bar{\mathbf{y}}^T\bar{\mathbf{y}} - \bar{\mathbf{y}}^T\bar{\mathbf{H}}\bar{\mathbf{x}}_{\ell,s} + \bar{\mathbf{x}}_{\ell,s}^T\bar{\mathbf{H}}^T\bar{\mathbf{y}} + \bar{\mathbf{x}}_{\ell,s}^T\bar{\mathbf{G}}\bar{\mathbf{x}}_{\ell,s} \right\} && \text{(A.3)} \end{aligned}$$

where $\bar{\mathbf{G}} = \bar{\mathbf{H}}^T\bar{\mathbf{H}} + \epsilon\bar{\mathbf{I}}_{N_t}$ is a $(2N_t \times 2N_t)$ positive definite matrix, with a Cholesky factorisation defined as $\bar{\mathbf{G}} = \bar{\mathbf{D}}^T\bar{\mathbf{D}}$, where $\bar{\mathbf{D}}$ is a $(2N_t \times 2N_t)$ upper triangular matrix. Now by defining $\bar{\rho} = \bar{\mathbf{G}}^{-1}\bar{\mathbf{H}}^T\bar{\mathbf{y}}$ a $(2N_t \times 1)$ vector, and adding $\bar{\rho}\bar{\mathbf{D}^T}\mathbf{D}\bar{\rho}$ to the both side of (A.3), it can be re–written as,

$$\begin{aligned} R_\epsilon^2 &\geq \left\{ \|\bar{\mathbf{z}} - \bar{\mathbf{D}}\bar{\mathbf{x}}_{\ell,s}\|_{\mathrm{F}}^2 \right\} \\ &\geq \sum_{i=1}^{2N_t} \left(\bar{z}_i - \sum_{j=i}^{2N_t} \bar{D}_{i,j}\bar{x}_{\ell,s}\left(j\right) \right)^2 && \text{(A.4)} \end{aligned}$$

where, $\bar{\mathbf{z}} = \bar{\mathbf{D}}\bar{\rho}$ and,

$$\begin{aligned} R_\epsilon^2 &= R^2 + \epsilon\bar{\mathbf{x}}_{\ell,s}^T\bar{\mathbf{x}}_{\ell,s} + \bar{\mathbf{y}}^T\bar{\mathbf{H}}\bar{\rho} - \bar{\mathbf{y}}^T\bar{\mathbf{y}} && \text{(A.5)} \\ \epsilon &= \begin{cases} \sigma_n^2 & N_t > N_r \\ 0 & N_t \leq N_r \end{cases} && \text{(A.6)} \end{aligned}$$

For simplicity $R_\epsilon^2 = R^2$ is assumed.

2. Second, note that a necessary condition that the points of the transmit search space need to satisfy to belong to the subset Θ_R is (for all $i = 1, 2, \ldots, 2N_t$):

$$R^2 \geq \left(\bar{z}_i - \sum_{j=i}^{2N_t} \bar{D}_{i,j} \bar{x}_{\ell,s}\left(j\right) \right)^2 \tag{A.7}$$

which is a condition similar to conventional SD algorithms [140].

3. Takeing into account that in SM only a single antenna is active at any time instance. In the equivalent real–valued signal model in (4.4), this is equivalent to having only two, out of $2N_t$, non–zero entries in the signal vectors $\bar{\mathbf{x}}_{\ell_t,s_t}$ and $\bar{\mathbf{x}}_{\ell,s}$, respectively. By taking this remark into account, it follows that: a) if $i = N_t + 1, N_t + 2, \ldots, 2N_t$, then only the imaginary part of $\bar{\mathbf{x}}_{\ell,s}$ plays a role in (A.7), and, thus, only one entry $\bar{\mathbf{x}}_{\ell,s}(\ell + N_t)$ can be non–zero; and b) if $i = 1, 2, \ldots, N_t$, then both real and imaginary parts of $\bar{\mathbf{x}}_{\ell,s}$ play a role in (A.7), and, thus, only two entries $\bar{\mathbf{x}}_{\ell,s}(\ell), \bar{\mathbf{x}}_{\ell,s}(\ell + N_t)$ can be non–zero. The considerations in a) and b) lead to the intervals in (4.12) and (4.13), respectively, which are directly obtained by solving the inequality in (A.7).

4. Last, every time a point is found inside the sphere, the radius R, is updated with the Euclidean distance of that point, thus,

$$\begin{aligned} R^2_{\text{new}} &= \left\{ \|\bar{\mathbf{z}} - \bar{\mathbf{D}}\bar{\mathbf{x}}_{\ell,s}\|^2_{\text{F}} \right\} \\ &= \sum_{i=N_t+1}^{2N_t} \left(\bar{z}_i - \bar{D}_{(i,\ell+N_t)} \text{Im}\{\text{s}\} \right)^2 + \sum_{i=1}^{N_t} \left(z_i - D_{(i,\ell)} \text{Re}\left\{s\right\} - D_{(i,\ell+N_t)} \text{Im}\left\{s\right\} \right)^2 \\ &= (R^2 - R'^2) + \sum_{i=1}^{N_t} \left(z_i - D_{(i,\ell)} \text{Re}\left\{s\right\} - D_{(i,\ell+N_t)} \text{Im}\left\{s\right\} \right)^2 \end{aligned} \tag{A.8}$$

where R'^2 is defined in (4.15).

□

Appendix B

List of Publications

This appendix contains a list of papers either published, accepted for publication or submitted for publication.

B.1 Published

- **A. Younis**, S. Sinanović, M. Di. Renzo, R. Mesleh, and H. Haas, "Generalised Sphere Decoding for Spatial Modulation", *IEEE Transactions on Communications*, vol. 61, no. 7, pp. 2805–2815, Jul. 2013.

- N. Serafimovski, **A. Younis**, R. Mesleh, P. Chambers, M. Di Renzo, C.-X. Wang, P. M. Grant, M. A. Beach and H. Haas, "Practical Implementation of Spatial Modulation", *IEEE Transactions on Vehicular Technology*, vol. 62, no. 9, pp. 4511–4523, Nov. 2013..

- **A. Younis**, N. Serafimovski, R. Mesleh and H. Haas, "Sphere Decoding for Spatial Modulation", *IEEE International Wireless Communications Symposium (ICC'11 WCS)*, Kyoto, Japan, 5-9 Jun. 2011.

- **A. Younis**, R. Mesleh, H. Haas and P. M. Grant, "Reduced Complexity Sphere Decoder for Spatial Modulation Detection Receivers", *IEEE Globecom 2010 - Wireless Communications Symposium (GC10 - WC)* , Miami, Florida, USA, 6-10 Dec. 2010.

- **A. Younis**, M. Di Renzo, R. Mesleh and H. Haas, "Generalised Spatial Modulation", *Asilomar Conference on Signals, Systems, and Computers*, Pacific Grove, California, 7-10 Nov.2010.

- **A. Younis**, W. Thompson, M. D. Renzo, C.-X Wang, M. A. Beach, H. Haas and P. M. Grant, "Performance of Spatial Modulation using Measured Real-World Channels", *IEEE 78th Vehicular Technology Conference (VTC 2013-Fall)*, Las Vegas, USA, 2-5 Sep. 2013.

- N. Serafimovski, S. Sinanović, **A. Younis**, M. Di Renzo and H. Haas, "2-User Multiple Access Spatial Modulation", *IEEE GLOBECOM Workshops (GC Wkshps)*, pp.343-347, 5-9 Dec. 2011.

B.2 Submitted

- **A. Younis**, S. Sinanović, R. Mesleh, M. Di. Renzo, and H. Haas, "A Complete Framework for Spatial Modulation", *IEEE Transactions on Wireless Communications*, Aug. 2013.

Appendix C
Selected Publications

This appendix contains all published work.

IEEE TRANSACTIONS ON COMMUNICATIONS, VOL. 61, NO. 7, JULY 2013 2805

Generalised Sphere Decoding for Spatial Modulation

Abdelhamid Younis, Sinan Sinanović, Marco Di Renzo, Raed Mesleh, and Harald Haas

***Abstract*—In this paper, Sphere Decoding (SD) algorithms for Spatial Modulation (SM) are developed to reduce the computational complexity of Maximum–Likelihood (ML) detectors. Two SDs specifically designed for SM are proposed and analysed in terms of Bit Error Ratio (BER) and computational complexity. Using Monte Carlo simulations and mathematical analysis, it is shown that by carefully choosing the initial radius the proposed sphere decoder algorithms offer the same BER as ML detection, with a significant reduction in the computational complexity. A tight closed form expression for the BER performance of SM–SD is derived in the paper, along with an algorithm for choosing the initial radius which provides near to optimum performance. Also, it is shown that none of the proposed SDs are always superior to the others, but the best SD to use depends on the target spectral efficiency. The computational complexity trade–off offered by the proposed solutions is studied via analysis and simulation, and is shown to validate our findings. Finally, the performance of SM–SDs are compared to Spatial Multiplexing (SMX) applying ML decoder and applying SD. It is shown that for the same spectral efficiency, SM–SD offers up to 84% reduction in complexity compared to SMX–SD, with up to 1 dB better BER performance than SMX–ML decoder.**

***Index Terms*—Multiple-input-multiple-output (MIMO) systems, spatial modulation (SM), spatial multiplexing (SMX), sphere decoding (SD), large scale MIMO.**

I. Introduction

MULTIPLE–input multiple–output (MIMO) systems offer a significant increase in spectral efficiency in comparison to single antenna systems [1]. An example is Spatial Multiplexing (SMX) [2], which transmits simultaneously over all the transmit antennas. This method achieves a spectral efficiency that increases linearly with the number of transmit antennas. However, these systems cannot cope with the exponential increase of wireless data traffic, and a larger number of transmit antennas (large scale MIMO) should be used [3]. Large scale MIMO studied in [4]–[6], offers higher data rates and better bit error rate (BER) performance.However, this comes at the expense of an increase in:

1) Computational complexity: A SMX maximum likelihood (ML) optimum receiver searches across all possible combinations, and tries to resolve the inter–channel interference (ICI) caused by transmitting from all antennas simultaneously, on the same frequency. Sphere decoder (SD) was proposed to reduce the complexity of the SMX–ML algorithm while retaining a near optimum performance [7], [8]. The SD reduces the complexity of the ML decoder by limiting the number of possible combinations. Only those combinations that lie within a sphere centred at the received signal are considered. However, even though SMX–SD offers a large reduction in complexity compared to SMX–ML, it still has a high complexity which increases with the increase of the number of transmit antennas.
2) Hardware complexity: In SMX the number of radio frequency (RF) chains is equal to the number of transmit antennas. From [9], RF chains are circuits that do not follow Moore's law in progressive improvement. Therefore, increasing the number of transmit antennas and consequently the number of RF chains increases significantly the cost of real system implementation [10].
3) Energy consumption: RF chains contain Power Amplifiers (PAs) which are responsible for 50–80% of the total power consumption in the transmitter [11]. Therefore, increasing the number of RF chains results in a decrease in the energy efficiency [10].

Thus, SMX may not always be feasible and a more energy efficient and low complexity solution should be considered.

Spatial Modulation (SM) is a transmission technology proposed for MIMO wireless systems. It aims to increase the spectral efficiency, (m), of single–antenna systems while avoiding ICI [12]. This is attained through the adoption of a new modulation and coding scheme, which foresees: i) the activation, at each time instance, of a single antenna that transmits a given data symbol (*constellation symbol*), and ii) the exploitation of the spatial position (index) of the active antenna as an additional dimension for data transmission (*spatial symbol*) [13]. Both the *constellation symbol* and the *spatial symbol* depend on the incoming data bits. An overall increase by the base–two logarithm of the number of transmit–antennas of the spectral efficiency is achieved. This limits the number of transmit antennas to be a power of two unless fractional bit encoding SM (FBE–SM) [14], or generalised SM (GSM) [15]

Manuscript received July 29, 2012; revised December 24, 2012. The editor coordinating the review of this paper and approving it for publication was G. Bauch.

This work was presented in part at IEEE GLOBECOM 2010, Miami, USA, and IEEE ICC 2011, Kyoto, Japan.

A. Younis and H. Haas are with The University of Edinburgh, College of Science and Engineering, Institute for Digital Communications, Joint Research Institute for Signal and Image Processing, King's Buildings, Mayfield Road, Edinburgh, EH9 3JL, UK (e-mail: {a.younis, h.haas}@ed.ac.uk).

S. Sinanović is with Glasgow Caledonian University, School of Engineering and Built Environment, George Moore Building, Cowcaddens Road, Glasgow, G4 0BA, UK (e-mail: sinan.sinanovic@gcu.ac.uk).

M. Di Renzo is with the Laboratory of Signals and Systems (L2S), French National Center for Scientific Research (CNRS), École Supérieure d'Électricité (SUPÉLEC), University of Paris–Sud XI (UPS), 3 rue Joliot–Curie, 91192 Gif–sur–Yvette (Paris), France (e-mail: marco.direnzo@lss.supelec.fr).

R. Mesleh is with the Electrical Engineering Department and SNCS research center, University of Tabuk, P.O.Box: 71491 Tabuk, Saudi Arabia (e-mail: rmesleh.sncs@ut.edu.sa).

Digital Object Identifier 10.1109/TCOMM.2013.061013.120547

are used. Activating only one antenna at a time means that only one RF chain is needed, which significantly reduces the hardware complexity of the system [16]. Moreover, as only one RF chain is needed, SM offers a reduction in the energy consumption which scales linearly with the number of transmit antennas [10], [17]. Furthermore, the computational complexity of SM–ML is equal to the complexity of single–input multiple–output (SIMO) systems [18], *i.e.* the complexity of SM–ML depends only on the spectral efficiency and the number of receive antennas, and does not depend on the number of transmit antennas. Recently the potential benefits of SM have been validated not only by simulations but also via experiments [19], [20]. Moreover, in [21] for the first time the performance of SM is analysed using real–world channel measurements. Accordingly, SM appears to be a good candidate for large scale MIMO [22]–[25].

In spite of its low–complexity implementation, there is still potential for further reductions, by limiting the number of possible combinations using the SD principle. However, existing SD algorithms in literature do not consider the basic and fundamental principle of SM, that only one antenna is active at any given time instance. Therefore, two modified SD algorithms based on the tree search structure that are tailored to SM are proposed. The first SD will be called receiver–centric SD (SM–Rx), which was first presented in [26]. The algorithm in [26] combines the received signal from the multiple receive antennas, as long as the Euclidean distance from the received point is less than a given radius. This SD–based detector is especially suitable when the number of receive–antennas is very large. This technique reduces the size of the search space related to the multiple antennas at the receiver (we denote this search space as "receive search space"). It will be shown later that there is no loss in either the diversity order or the coding gain, *i.e.* the BER is very close to that of the ML detector. However, the main limitation is that it does not reduce the search space related to the number of possible transmitted points (we denote this as "transmit search space"). This limitation prevents the detector from achieving a significant reduction in computational complexity when high data rates are required.

The second SD, which is called Transmit–centric (SM–Tx) was first presented in [27]. It aims at reducing the transmit search space by limiting the number of possible spatial and constellation points. The SM–Tx algorithm avoids an exhaustive search by examining only those points that lie inside a sphere with a given radius. However, SM–Tx is limited to the overdetermined MIMO setup ($N_t \leq N_r$), where N_t and N_r are the number of transit and receiver antennas respectively. In [28], [29], it is shown that SM–Tx in [27] can still be used for the case of $(2N_r - 1) \geq N_t > N_r$, where SM–Tx is referred to as enhanced Tx–SD (E–Tx–SD). Moreover, in [28], [29] a detector for the case of $N_t > N_r$ referred to as generalised Tx–SD (G–Tx–SD) is proposed. By using the division algorithm the G–Tx–SD technique: 1) Divides the set of possible antennas to a number of subsets. 2) Performs E–Tx–SD over each subset. 3) Takes the minimum solution of all the sets. However, in this paper we propose a simple solution, in which all that is needed is to set a constant φ to 0 for $N_t \leq N_r$ and $\varphi = \sigma_n^2$ for $N_t > N_r$, where σ_n^2 is the noise variance. In [28], [29], the normalised expected number of nodes visited by the SM–Tx algorithm is used to compare its complexity with the complexity of the SM–ML algorithm. This does not take into account pre–computations needed by SM–Tx. In this paper, when comparing the complexity of SM–Tx with the complexity of SM–ML and SM–Rx, we take into account the pre–computations needed by the SM–Tx. We show that because of those pre–computations, the SM–Tx technique is not always the best solution, where in some cases it is even more complex than SM–ML. The performance of both SDs is closely tied to the choice of the initial radius. The chosen radius should be large enough for the sphere to contain the solution. On the one hand, the larger the radius is, the larger the search space, which increases the complexity. On the other hand, a small radius may cause the algorithm to fail in finding a point inside the sphere.

In this paper, a careful study of the performance of these two detectors is provided, along with an accurate comparison of their computational complexity. Numerical results show that with no loss in the BER performance, the proposed solutions provide a substantial reduction in computational complexity with respect to the SM–ML decoder. We also derive a closed form expression for the BER performance of SM–SD and show that the initial radius can be chosen such that SM–SD gives an optimum performance. Furthermore, it is shown that SM–Rx is less complex than SM–Tx for lower spectral efficiencies, while SM–Tx is the best solution for higher spectral efficiencies. Finally, using numerical results we show that SM–SD offers a significant reduction and nearly the same performance when compared to SMX with ML decoder or SD.

The remainder of this paper is organised as follows: In section II, the system model along with the ML–optimum detector is summarised. In section III, the new SM–Rx and SM–Tx receivers are described. In section IV, an accurate analysis of the computational complexity of both SM–Rx and SM–Tx is performed. In section V, the analytical BER performance for SM–SDs is derived along with the initial radius selection method. Numerical results are presented in section VI, and the paper is concluded in section VII.

II. System Model

A. SM Modulator

In SM, the bit stream emitted by a binary source is divided into blocks containing $m = \log_2(N_t) + \log_2(M)$ bits each, where M is the constellation size. Then the following mapping rule is used [12]:

- The first $\log_2(N_t)$ bits are used to select the antenna which is switched on for data transmission, while the other transmit antennas are kept silent. In this paper, the actual transmit antenna which is active for transmission is denoted by ℓ_t with $\ell_t \in \{1, 2, \ldots, N_t\}$.
- The second $\log_2(M)$ bits are used to choose a symbol in the signal–constellation diagram. Without loss of generality, Quadrature Amplitude Modulation (QAM) is considered. In this paper, the actual complex symbol emitted by the transmit antenna ℓ_t is denoted by s_t, with $s_t \in \{s_1, s_2, \ldots, s_M\}$.

Accordingly, the $N_t \times 1$ transmitted vector is:

$$\mathbf{x}_{\ell_t,s_t} = \left[\mathbf{0}_{1\times(\ell_t-1)}, s_t, \mathbf{0}_{1\times(N_t-\ell_t)}\right]^T, \quad (1)$$

where $[\cdot]^T$ denotes transpose operation, and $\mathbf{0}_{p\times q}$ is a $p \times q$ matrix with all–zero entries. Note, a power constraint on the average energy per transmission of unity is assumed (*i.e.* $E_s = \mathrm{E}[\mathbf{x}^H\mathbf{x}] = 1$), where $\mathrm{E}\{\cdot\}$ is the expectation operator.

From above, the maximum achievable spectral efficiency by SM is,

$$m_{\text{SM}} = \log_2(N_t) + \log_2(M) \quad (2)$$

However, for SMX,

$$m_{\text{SMX}} = N_t \log_2(M) \quad (3)$$

From (2) and (3), we can see that the spectral efficiency of SM does not increase linearly with the number of transmit antennas as SMX does. Therefore, SM needs a larger number of transmit antennas/ larger constellation size to arrive at the same spectral efficiency as SMX. However, because in SM only one antenna is active:

- The computational complexity of SM does not depend on the number of transmit antennas. Unlike SMX where the computational complexity increases linearly with the number of transmit antennas, the computational complexity of SM is the same as the computational complexity of SIMO systems.
- The number of RF chains needed by SM is significantly less than the number of RF chains needed by SMX. In fact, only one RF chain is required for SM.

For these reasons we believe that SM is a strong candidate for large scale MIMO systems, which strongly motivates this work.

B. Channel Model

The modulated vector, $\mathbf{x}_{\ell_t,s_t}$, in (1) is transmitted through a frequency–flat $N_r \times N_t$ MIMO fading channel with transfer function $\mathbf{H}$, where N_r is the number of receive antennas. In this paper, a Rayleigh fading channel model is assumed. Thus, the entries of $\mathbf{H}$ are modelled as complex independent and identically distributed (i.i.d.) entries according to $\mathcal{CN}(0,1)$. Moreover, a perfect channel state information (CSI) at the receiver is assumed, with no CSI at the transmitter.

Thus, the $N_r \times 1$ received vector can be written as follows:

$$\begin{aligned}\mathbf{y} &= \mathbf{H}\mathbf{x}_{\ell_t,s_t} + \mathbf{n} \\ &= \mathbf{h}_{\ell_t} s_t + \mathbf{n} \end{aligned} \quad (4)$$

where $\mathbf{n}$ is the N_r–dimensional Additive White Gaussian Noise (AWGN) with zero–mean and variance σ^2 per dimension at the receiver input, and $\mathbf{h}_\ell$ is the ℓ–th column of $\mathbf{H}$. Note, the signal-to-noise-ratio is $\text{SNR} = E_s/N_o = 1/\sigma_n^2$.

C. ML–Optimum Detector

The ML optimum receiver for MIMO systems can be written as,

$$\hat{\mathbf{x}}_t^{(\text{ML})} = \underset{\mathbf{x}\in\mathcal{Q}^m}{\arg\min} \left\{ \|\mathbf{y} - \mathbf{H}\mathbf{x}\|_{\text{F}}^2 \right\} \quad (5)$$

where $\mathcal{Q}^m$ is a 2^m space containing all possible $(N_t \times 1)$ transmitted vectors, $\|\cdot\|_{\text{F}}$ is the Frobenius norm, and $\hat{\cdot}$ denotes the estimated spatial and constellation symbols.

Note, in SM only one transmit antenna is active at a time. Therefore, the optimal receiver in (5) can be simplified to,

$$\begin{aligned}\left[\hat{\ell}_t^{(\text{ML})}, \hat{s}_t^{(\text{ML})}\right] &= \underset{\substack{\ell\in\{1,2,\ldots N_t\} \\ s\in\{s_1,s_2,\ldots s_M\}}}{\arg\min} \left\{ \|\mathbf{y} - \mathbf{h}_\ell s\|_{\text{F}}^2 \right\} \\ &= \underset{\substack{\ell\in\{1,2,\ldots N_t\} \\ s\in\{s_1,s_2,\ldots s_M\}}}{\arg\min} \left\{ \sum_{r=1}^{N_r} |y_r - h_{\ell,r} s|^2 \right\} \end{aligned} \quad (6)$$

where y_r and $h_{\ell,r}$ are the r–th entries of $\mathbf{y}$ and $\mathbf{h}_\ell$ respectively.

III. Sphere Decoders for SM

In this section we introduce two SDs tailored for SM, SM–Rx and SM–Tx. SM–Rx aims at reducing the number of summations over N_r required by the ML receiver in (6). SM–Tx aims at reducing the number of points (ℓ, s) the ML receiver searches over.

First, for ease of derivation, we introduce the real–valued equivalent of the complex–valued model in (4) following [30],

$$\begin{aligned}\bar{\mathbf{y}} &= \bar{\mathbf{H}}\bar{\mathbf{x}}_{\ell_t,s_t} + \bar{\mathbf{n}} \\ &= \bar{\mathbf{h}}_{\ell_t}\bar{\mathbf{s}}_t + \bar{\mathbf{n}} \end{aligned} \quad (7)$$

where,

$$\bar{\mathbf{y}} = \left[\mathrm{Re}\left\{\mathbf{y}^T\right\}, \mathrm{Im}\left\{\mathbf{y}^T\right\}\right]^T \quad (8)$$

$$\bar{\mathbf{H}} = \begin{bmatrix} \mathrm{Re}\{\mathbf{H}\} & \mathrm{Im}\{\mathbf{H}\} \\ -\mathrm{Im}\{\mathbf{H}\} & \mathrm{Re}\{\mathbf{H}\} \end{bmatrix} \quad (9)$$

$$\bar{\mathbf{x}}_{\ell,s} = \left[\mathrm{Re}\left\{\mathbf{x}_{\ell,s}^T\right\}, \mathrm{Im}\left\{\mathbf{x}_{\ell,s}^T\right\}\right]^T \quad (10)$$

$$\bar{\mathbf{n}} = \left[\mathrm{Re}\left\{\mathbf{n}^T\right\}, \mathrm{Im}\left\{\mathbf{n}^T\right\}\right]^T \quad (11)$$

$$\bar{\mathbf{h}}_\ell = \left[\bar{\mathbf{H}}_\ell, \bar{\mathbf{H}}_{\ell+N_t}\right] \quad (12)$$

$$\bar{\mathbf{s}} = \begin{bmatrix} \mathrm{Re}\{s\} \\ \mathrm{Im}\{s\} \end{bmatrix} \quad (13)$$

where $\mathrm{Re}\{\cdot\}$ and $\mathrm{Im}\{\cdot\}$ denote real and imaginary parts respectively, and $\bar{\mathbf{H}}_\ell$ is the ℓ–th column of $\bar{\mathbf{H}}$.

A. SM–Rx Detector

The SM–Rx is a reduced–complexity and close–to–optimum BER–achieving decoder, which aims at reducing the receive search space. The detector can formally be written as follows:

$$\left[\hat{\ell}_t^{(\text{Rx})}, \hat{s}_t^{(\text{Rx})}\right] = \underset{\substack{\ell\in\{1,2,\ldots N_t\} \\ s\in\{s_1,s_2,\ldots s_M\}}}{\arg\min} \left\{ \sum_{r=1}^{\tilde{N}_r(\ell,s)} \left|\bar{y}_r - \bar{\mathbf{h}}_{\ell,r}\bar{\mathbf{s}}\right|^2 \right\} \quad (14)$$

$$R_{i+1}^2 = \left\|\bar{\mathbf{z}} - \bar{\mathbf{D}}\bar{\mathbf{x}}_{\ell,s}\right\|_{\mathrm{F}}^2 = (R_i^2 - R'^2) + \sum_{\nu=1}^{N_t} \left(z_\nu - D_{(\nu,\ell)}\mathrm{Re}\left\{s\right\} - D_{(\nu,\ell+N_t)}\mathrm{Im}\left\{s\right\}\right)^2 \quad (22)$$

where $\bar{\mathbf{h}}_{\ell,r}$ is the r–th row of $\bar{\mathbf{h}}_\ell$, and,

$$\tilde{N}_r(\ell,s) = \max_{n\in\{1,2,\ldots 2N_r\}} \left\{ n \left| \sum_{r=1}^{n} |y_r - h_{\ell,r}s|^2 \le R^2 \right.\right\} \quad (15)$$

The idea behind SM–Rx is that it keeps combining the received signals as long as the Euclidean distance in (14) is less or equal to the radius R. Whenever a point is found to be inside the sphere, the radius, R, is updated with the Euclidean distance of that point. The point with the minimum Euclidean distance and $\tilde{N}_r(\cdot,\cdot) = 2N_r$ is considered to be the solution.

B. SM–Tx Detector

The conventional SD is designed for SMX, where all antennas are active at each time instance [7], [31]–[33]. However, in SM only one antenna is active at a time. Therefore, a modified SD algorithm tailored for SM, named SM–Tx, is presented. More specifically, similar to conventional SDs, the SM–Tx scheme reduces the number of points (ℓ, s) for $\ell \in \{1, 2, \ldots N_t\}$ and $s \in \{s_1, s_2, \ldots s_M\}$ to be searched through in (6), *i.e.*, the transmit search space, by computing the Euclidean distances only for those points that lie inside a sphere with radius R and are centred around the received signal. However, unlike conventional SDs, in our scheme the set of points inside the sphere are much simpler to compute, as there is only a single active antenna in SM. In this section, we show how to compute the set of points.

The Cholesky factorisation of the $(2N_t \times 2N_t)$ positive definite matrix $\bar{\mathbf{G}} = \bar{\mathbf{H}}^T\bar{\mathbf{H}} + \varphi\bar{\mathbf{I}}_{N_t}$ is $\bar{\mathbf{G}} = \bar{\mathbf{D}}\bar{\mathbf{D}}^T$, where

$$\varphi = \begin{cases} \sigma_n^2 & N_t > N_r \\ 0 & N_t \le N_r \end{cases} \quad (16)$$

Then the SM–Tx can be formally written as follow,

$$\left[\hat{\ell}_t^{(\mathrm{Tx-SD})}, \hat{s}_t^{(\mathrm{Tx-SD})}\right] = \underset{(\ell,s)\in\Theta_R}{\arg\min} \left\{ \left\|\bar{\mathbf{z}} - \bar{\mathbf{D}}\bar{\mathbf{x}}_{\ell,s}\right\|_{\mathrm{F}}^2 \right\} \quad (17)$$

where Θ_R is the subset of points (ℓ, s) for $\ell \in \{1, 2, \ldots N_t\}$ and $s \in \{s_1, s_2, \ldots s_M\}$ in the transmit search space that lie inside a sphere with radius R and centred around the received signal $\bar{\mathbf{z}}$, $\bar{\mathbf{z}} = \bar{\mathbf{D}}\bar{\rho}$ and $\bar{\rho} = \bar{\mathbf{G}}^{-1}\bar{\mathbf{H}}^T\bar{\mathbf{y}}$.

Unlike SM–Rx, SM–Tx reduces the computational complexity of the ML receiver by reducing the transmit search space, which is done by the efficient computation of the subset Θ_R. After some algebraic manipulations as shown in Appendix A, the subset of points Θ_R lie in the intervals:

$$\frac{-R_i + \bar{z}_{\ell+N_t}}{\bar{D}_{(\ell+N_t,\ell+N_t)}} \le \mathrm{Im}\left\{s\right\} \le \frac{R_i + \bar{z}_{\ell+N_t}}{\bar{D}_{(\ell+N_t,\ell+N_t)}} \quad (18)$$

$$\frac{-R' + \bar{z}_{\ell|\ell+N_t}}{\bar{D}_{\ell,\ell}} \le \mathrm{Re}\left\{s\right\} \le \frac{R' + \bar{z}_{\ell|\ell+N_t}}{\bar{D}_{\ell,\ell}} \quad (19)$$

where

$$\bar{z}_{a|b} = \bar{z}_a - \bar{D}_{(a,b)}\mathrm{Im}\left\{s\right\} \quad (20)$$

$$R'^2 = R^2 - \sum_{\nu=N_t+1}^{2N_t} \bar{z}_{\nu|\ell+N_t}^2 \quad (21)$$

Note, every time a point is found inside the sphere, the radius R is updated as shown in (22), with the Euclidean distance of that point. Moreover, (19) needs to be computed only for those points that lie inside the interval in (18), for the reason that (19) depends implicitly on (18).

Because of the unique properties of SM the intervals in (18) and (19) needs to be calculated only once for each possible transmit point, unlike conventional SDs where the intervals have to be calculate N_t times for each transmit point. Furthermore, we note that SM–Tx works for both underdetermined MIMO setup with $N_t > N_r$, and overdetermined MIMO setup with $N_t \le N_r$.

As opposed to the SM–Rx scheme, the SM–Tx scheme uses some pre–computations to estimate the points that lie inside the sphere of radius R. These additional computations are carefully taken into account in the analysis of the computational complexity of the SM–Tx scheme and its comparison with the ML–optimum detector in section IV.

IV. Computational Complexity of SM–Rx and SM–Tx

In this section, we analyse the computational complexity of SM–ML, SM–Rx and SM–Tx. The complexity is computed as the number of real multiplication and division operations needed by each algorithm [34].

A. SM–ML

The computational complexity of SM–ML receiver in (6), yields,

$$\mathcal{C}_{\text{SM–ML}} = 8N_r 2^m, \quad (23)$$

as the ML detector searches through the whole transmit and receive search spaces. Note, evaluating the Euclidean distance $\left(|y_r - h_{\ell,r}s|^2\right)$ requires 8 real multiplications.

The computational complexity of SMX–ML receiver in (5) is equal to

$$\mathcal{C}_{\text{SMX–ML}} = 4\left(N_t + 1\right)N_r 2^m. \quad (24)$$

Note, $\left(|\mathbf{y} - \mathbf{H}\mathbf{x}|^2\right)$ in (5) requires $(N_t + 1)$ complex multiplications.

From (23) and (24), the complexity of SM does not depend on the number of transmit antennas, and it is equal to the complexity of SIMO systems. However, the complexity of SMX increases linearly with the number of transmit antennas.

Thus, the reduction of SM–ML receiver complexity relative to the complexity of the SMX–ML decoder for the same spectral efficiency is given by,

$$\mathcal{C}_{\text{rel}}^{\text{ML}} = 100 \times \left(1 - \frac{2}{N_t + 1}\right). \tag{25}$$

From (25), the reduction in complexity offered by SM increases with the increase in the number of transmit antennas. For example for $N_t = 4$ SM offers a 60% reduction in complexity compared to SMX, and as the number of transmit antennas increases the reduction increases.

B. SM–Rx

The complexity of the SM–Rx receiver is given by:

$$\mathcal{C}_{\text{Rx}-\text{SD}} = 3 \sum_{\ell=1}^{N_t} \sum_{s=1}^{M} \tilde{N}_r\left(\ell, s\right) \tag{26}$$

It is easy to show that $\mathcal{C}_{\text{Rx}-\text{SD}}$ lies in the interval $3 \times 2^m \leq \mathcal{C}_{\text{Rx}-\text{SD}} \leq 6N_r 2^m$, where the lower bound corresponds to the scenario where $\tilde{N}_r\left(\ell, s\right) = 1$, and the upper bound corresponds to the scenario where $\tilde{N}_r\left(\ell, s\right) = 2N_r$ for $\ell \in \{1, 2, \ldots N_t\}$ and $s \in \{s_1, s_2, \ldots s_M\}$. An interesting observation is that SM–Rx offers a reduction in complexity even for the case of $N_r = 1$, where the complexity lies in the interval $3 \times 2^m \leq \mathcal{C}_{\text{Rx}-\text{SD}} \leq 6 \times 2^m$. We note that the SM–Rx solution requires no pre–computations with respect to the ML–optimum detector. In fact, $\tilde{N}_r\left(\ell, s\right)$ for $\ell \in \{1, 2, \ldots N_t\}$ and $s \in \{s_1, s_2, \ldots s_M\}$ in (15) are implicitly computed when solving the detection problem in (14).

C. SM–Tx

The computational complexity of SM–Tx can be upper–bounded by,

$$\mathcal{C}_{\text{Tx}-\text{SD}} \leq \mathcal{C}_{\Theta_R} + 3N_t \text{card}\left\{\Theta_R\right\} \tag{27}$$

where $\text{card}\{\cdot\}$ denotes the cardinality of a set, and $\mathcal{C}_{\Theta_R}$ is the complexity of finding the points in the subset Θ_R,

$$\mathcal{C}_{\Theta_R} = \mathcal{C}_{\text{Pre-Comp}} + \mathcal{C}_{\text{Interval}} \tag{28}$$

where,

1) $\mathcal{C}_{\text{Pre-Comp}}$ is the number of operations needed to compute the Cholesky decomposition. Calculating the upper triangular matrix $\bar{\mathbf{D}}$ using Cholesky decomposition has the complexity [34],

$$\mathcal{C}_{\text{CH}} = 4N_t^3/3 \tag{29}$$

It can be easily shown that the calculation of $\bar{\mathbf{G}}$, $\bar{\rho}$ and $\bar{\mathbf{z}}$ requires $2N_r N_t(2N_t + 1)$, $2N_t(2N_t + 2N_r + 1)$ and $N_t(2N_t + 1)$ real operations respectively, where back–substitution algorithm was used for calculating $\bar{\rho}$ [34].

Hence,

$$\mathcal{C}_{\text{Pre-Comp}} = \mathcal{C}_{\text{CH}} + N_t(4N_r N_t + 6N_r + 6N_t + 3) \tag{30}$$

2) $\mathcal{C}_{\text{Interval}}$ is the number of operations needed to compute the intervals in (18),(19),

$$\mathcal{C}_{\text{interval}} = 2N_t + (2N_t + 3)N_{(19)} \tag{31}$$

where,

- For (18): $2N_t$ real divisions are needed.
- For (19): $(2N_t + 3)\, N_{(19)}$ real multiplications are needed, where $(2N_t + 3)$ is the number of real computations needed to compute (19), and $N_{(19)}$ is the number of times (19) is computed, which is calculated by simulations. Note, i) the interval in (19) depends on the antenna index ℓ and only the imaginary part of the symbol s, ii) some symbols share the same imaginary part. Therefore, (19) is only calculated for those points (ℓ, s) which lie in the interval in (18) and does not have the same ℓ and $\text{Im}\{s\}$ as a previously calculated point.

V. Error Probability of SM–SDs and Initial Radius Selection Method

In this section, we derive an analytical expresion for the BER performance of SM–SD, and we show that SM–SD offers a near optimum performance. The BER for SM–SD is estimated using the union bound [35], which can be expressed as follows,

$$\underset{\text{SM–SD}}{\text{BER}} \leq \sum_{\ell_t, s_t} \sum_{\ell, s} \frac{N\left(\bar{\mathbf{x}}_{\ell_t, s_t}, \bar{\mathbf{x}}_{\ell, s}\right)}{m} \frac{\text{E}_{\mathbf{H}}\left\{\text{Pr}_{e,\text{SM–SD}}\right\}}{2^m} \tag{32}$$

where $N\left(\bar{\mathbf{x}}_{\ell_t, s_t}, \bar{\mathbf{x}}_{\ell, s}\right)$ is the number of bits in error between $\bar{\mathbf{x}}_{\ell_t, s_t}$ and $\bar{\mathbf{x}}_{\ell, s}$, and,

$$\underset{e,\text{SM–SD}}{\text{Pr}} = \text{Pr}\left(\left(\tilde{\ell}_{\text{SM–SD}}, \tilde{s}_{\text{SM–SD}}\right) \neq \left(\ell_t, s_t\right)\right) \tag{33}$$

is the pairwise error probability of deciding on the point $\left(\tilde{\ell}_{\text{SM–SD}}, \tilde{s}_{\text{SM–SD}}\right)$ given that the point (ℓ_t, s_t) is transmitted.

The probability of error $\text{Pr}_{e,\text{SM–SD}}$ can be thought of as two mutually exclusive events depending on whether the transmitted point (ℓ_t, s_t) is inside the sphere. In other words, the probability of error for SM–SD can be separated in two parts, as shown in (34) [36]:

- $\text{Pr}\left((\tilde{\ell}_{\text{SM–ML}}, \tilde{s}_{\text{SM–ML}}) \neq (\ell_t, s_t)\right)$: The probability of deciding on the incorrect transmitted symbol and/or used antenna combination, given that the transmitted point (ℓ_t, s_t) is inside the sphere.
- $\text{Pr}\left((\ell_t, s_t) \notin \Theta_R\right)$: The probability that the transmitted point (ℓ_t, s_t) is outside the set of points Θ_R considered by the SD algorithm.

$$\underset{e,\text{SM–SD}}{\text{Pr}} \leq \left(\text{Pr}\left((\tilde{\ell}_{\text{SM–ML}}, \tilde{s}_{\text{SM–ML}}) \neq (\ell_t, s_t)\right) + \text{Pr}\left((\ell_t, s_t) \notin \Theta_R\right)\right) \tag{34}$$

$$\mathrm{E}_{\mathbf{H}}\left\{\underset{e,\text{SM–SD}}{\Pr}\right\} = \left[\zeta\left(\frac{\sigma_s^2}{4\sigma_n^2}\right)\right]^{N_r}\sum_{r=0}^{N_r-1}\binom{N_r-1+r}{r}\left[1-\zeta\left(\frac{\sigma_s^2}{4\sigma_n^2}\right)\right]^{r} \quad (46)$$

However, the probability of error for the ML decoder is,

$$\underset{e,\text{SM–ML}}{\Pr} \leq \Pr\left((\tilde{\ell},\tilde{s}) \neq (\ell_t, s_t)\right) \quad (35)$$

Thus, SM–SD will have a near optimum performance when,

$$\Pr\left((\ell_t, s_t) \notin \Theta_R\right) << \Pr\left((\tilde{\ell},\tilde{s}) \neq (\ell_t, s_t)\right) \quad (36)$$

The probability of *not* having the transmitted point (ℓ_t, s_t) inside Θ_R can be written as,

$$\begin{aligned}\Pr\left((\ell_t, s_t) \notin \Theta_R\right) &= \Pr\left(\sum_{r=1}^{2N_r}\left|\bar{y}_r - \bar{\mathbf{h}}_{\ell_t,r}\bar{\mathbf{s}}_t\right|^2 > R^2\right)\\ &= \Pr\left(\kappa > \left(\frac{R}{\sigma_n/\sqrt{2}}\right)^2\right)\\ &= 1 - \frac{\gamma\left(N_r, \left(\frac{R}{\sigma_n}\right)^2\right)}{\Gamma(N_r)} \quad (37)\end{aligned}$$

where,

$$\kappa = \sum_{r=1}^{2N_r}\left|\frac{\bar{n}_r}{\sigma_n/2}\right|^2 \quad (38)$$

is a central chi-squared random variable with $2N_r$ degree of freedom having a cumulative distribution function (CDF) equal to [35],

$$F_\kappa(a,b) = \frac{\gamma(b/2, a/2)}{\Gamma(b/2)} \quad (39)$$

where $\gamma(c,d)$ is the lower incomplete gamma function given by,

$$\gamma(c,d) = \int_0^d t^{c-1}e^{-t}dt \quad (40)$$

and $\Gamma(c)$ is the gamma function given by,

$$\Gamma(c) = \int_0^\infty t^{c-1}e^{-t}dt \quad (41)$$

The initial sphere radius considered in SM–SD is a function of the noise variance as given in [37],

$$R^2 = 2\alpha N_r\sigma_n^2 \quad (42)$$

where α is a constant chosen to satisfy (36). This can be done by setting $\Pr\left((\ell_t, s_t) \notin \Theta_R\right) = 10^{-6}$ and back solving (37). For $N_r = 1, 2, 4$, $\alpha = 13.8, 8.3, 5.3$ respectively.

Finally, $\Pr_{e,\text{SM–SD}}$ can be formulated as,

$$\begin{aligned}\underset{e,\text{SM–SD}}{\Pr} &= \Pr\left(\left\|\bar{\mathbf{y}} - \bar{\mathbf{h}}_\ell\bar{\mathbf{s}}\right\|^2 > \left\|\bar{\mathbf{y}} - \bar{\mathbf{h}}_{\ell_t}\bar{\mathbf{s}}_t\right\|^2\right)\\ &= \Pr\left(\xi > \left\|\bar{\mathbf{h}}_{\ell_t}\bar{\mathbf{s}}_t - \bar{\mathbf{h}}_\ell\bar{\mathbf{s}}\right\|\right) \quad (43)\end{aligned}$$

where,

$$\xi = 2\mathrm{Re}\left\{\left(\bar{\mathbf{h}}_{\ell_t}\bar{\mathbf{s}}_t - \bar{\mathbf{h}}_\ell\bar{\mathbf{s}}\right)^T\bar{\mathbf{n}}\right\} \sim \mathcal{N}\left(0, 2\sigma_n^2\left(\left\|\bar{\mathbf{h}}_{\ell_t}\bar{\mathbf{s}}_t - \bar{\mathbf{h}}_\ell\bar{\mathbf{s}}\right\|\right)\right) \quad (44)$$

Thus,

$$\underset{e,\text{SM–SD}}{\Pr} = Q\left(\sqrt{\frac{\left\|\bar{\mathbf{h}}_{\ell_t}\bar{\mathbf{s}}_t - \bar{\mathbf{h}}_\ell\bar{\mathbf{s}}\right\|^2}{2\sigma_n^2}}\right) \quad (45)$$

where $Q(x) = (1/\sqrt{2\pi})\int_x^{+\infty} e^{-t^2/2}dt$.

In the case of Rayleigh fading, we can derive the closed form solution for $\mathrm{E}_{\mathbf{H}}\{\mathrm{Pr}_{e,\text{SM–SD}}\}$ in (32) by employing the solution from [38, eq. (62)]. Note that the argument of the Q-function in (45) can be represented as the summation of $2N_r$ squared Gaussian random variables, with zero mean and variance equal to 1. This means that the argument in the Q–function can be described by a central chi–squared distribution with $2N_r$ degrees of freedom.

The result for $\mathrm{E}_{\mathbf{H}}\{\mathrm{Pr}_{e,\text{SM–SD}}\}$ is as given in (46), where $\sigma_s^2 = \|\bar{\mathbf{x}}_{\ell_t,s_t} - \bar{\mathbf{x}}_{\ell,s}\|_{\mathrm{F}}^2$ and,

$$\zeta(c) = \frac{1}{2}\left(1 - \sqrt{\frac{c}{1+c}}\right) \quad (47)$$

Plugging (46) into (32) gives a closed form expression for the BER of SM–SD. In the next section, we show that (32) gives a tight approximation of the BER of SM–SD, and that SM–SD offers a near optimum performance.

VI. Results

In the following, Monte Carlo simulation results for at least 10^6 Rayleigh fading channel realisations are shown to compare the performance and computational complexity of large scale MIMO, SM–ML, SM–SD and SMX–SD.

A. Analytical performance of SM–SD

Figs. 1-2 show the BER simulation results for SM–ML, SM–Rx and SM–Tx compared with the analytical bound

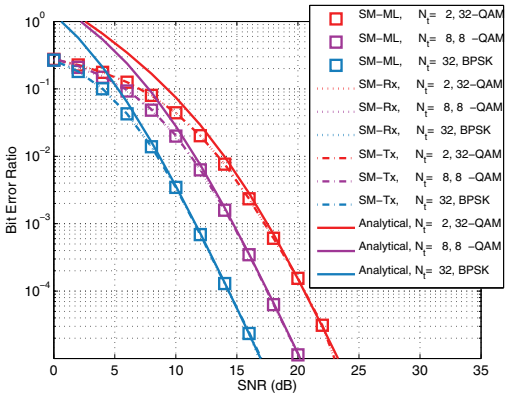

Fig. 1. BER against SNR. $m = 6$, and $N_r = 4$.

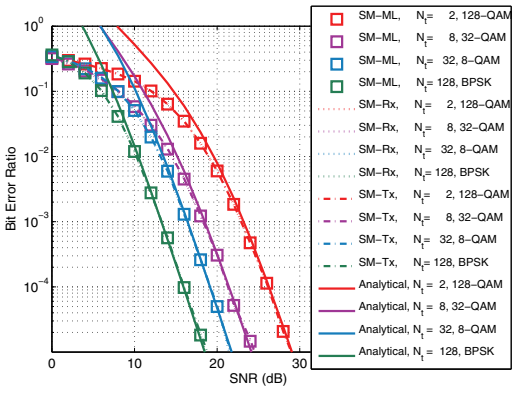

Fig. 2. BER against SNR. $m = 8$, and $N_r = 4$.

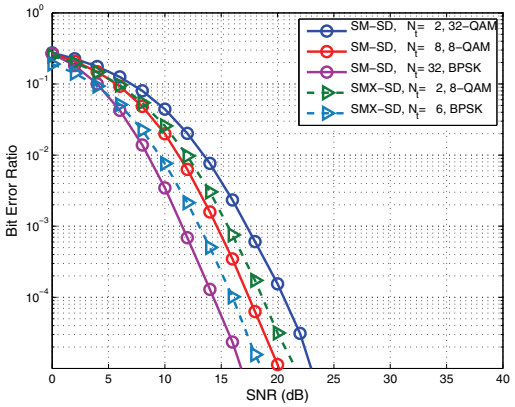

Fig. 4. BER against SNR. $m = 6$, and $N_r = 4$.

derived in section V, where $m = 6, 8$ and $N_r = 4$. From the figures we can see that both SM–Tx and SM–Rx offer a near optimum performance, where the results overlap with SM–ML. Furthermore, Figs. 1-2 validate our analytical bound as for BER $< 10^{-2}$ all graphs closely match the analytical results. Note, it is will–known that the union bound is loose for low SNR [35].

B. Comparison of the BER performance of SM and SMX

Figs. 3 and 4 show a BER comparison between all possible combinations of SM and SMX for $m = 6$ and $N_r = 2, 4$. In Fig. 3, we can observe that the BER performance depends on the the number of transmit antennas used and, consequently, the constellation size. The smaller the constellation size, the better the performance. Another observation that can be made is that SM and SMX offer nearly the same performance when using the same constellation size. In Fig. 4, where the number of receive antennas is increased, we notice that SM performs

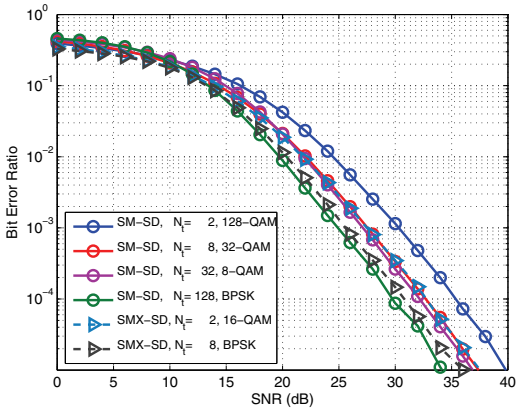

Fig. 5. BER against SNR. $m = 8$, and $N_r = 2$.

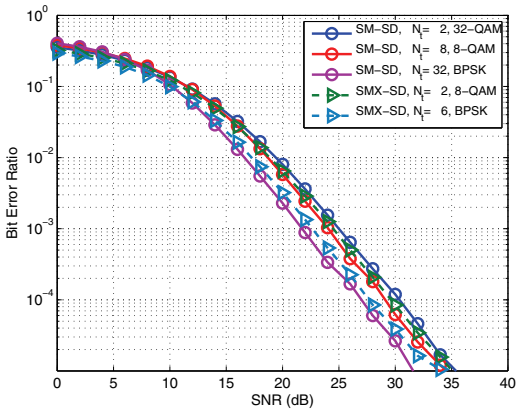

Fig. 3. BER against SNR. $m = 6$, and $N_r = 2$.

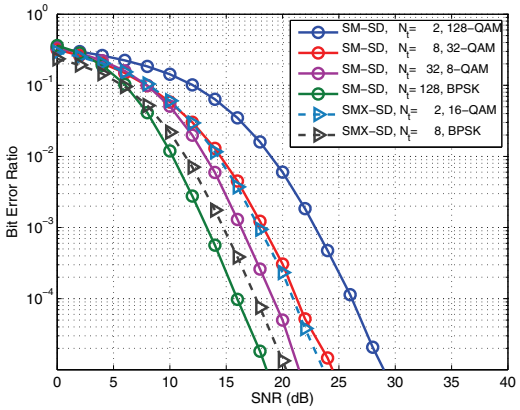

Fig. 6. BER against SNR. $m = 8$, and $N_r = 4$.

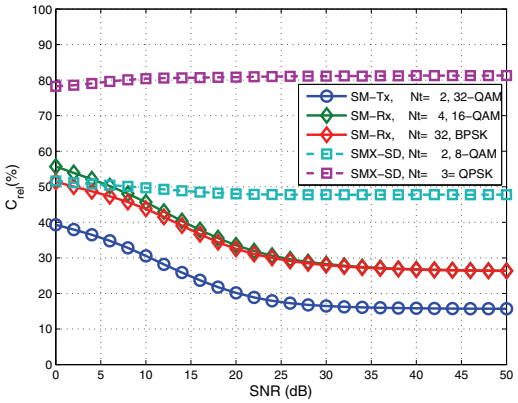

Fig. 7. Computational complexity against SNR. $m = 6$, and $N_r = 2$.

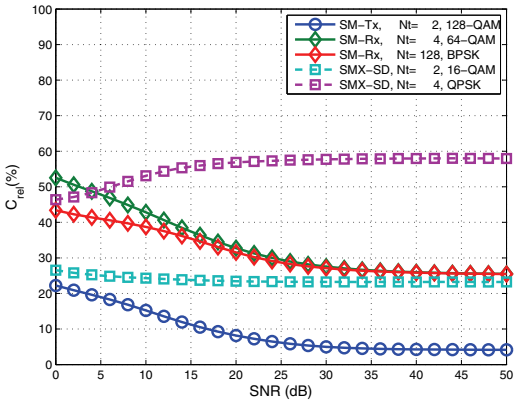

Fig. 9. Computational complexity against SNR. $m = 8$, and $N_r = 2$.

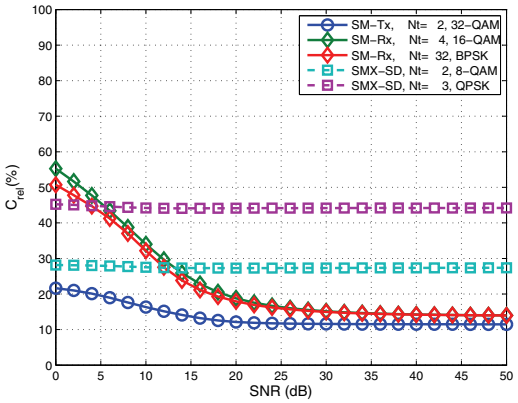

Fig. 8. Computational complexity against SNR. $m = 6$, and $N_r = 4$.

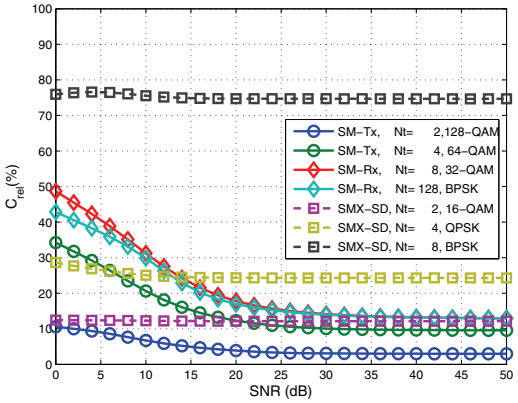

Fig. 10. Computational complexity against SNR. $m = 8$, and $N_r = 4$.

better than SMX. In particular, BPSK–SM provides a 1 dB better performance than BPSK–SMX. Also 8–QAM SM offers a slightly better performance (~ 0.5 dB) than 8-QAM SMX.

In Figs. 5 and 6, the BER comparisons for $m = 8$ and $N_r = 2, 4$ are shown. In Fig. 5, SM and SMX offer similar performance for the same constellation size. However, SM offers a better performance when the number of receive antennas increases as shown in Fig. 6.

In summary, SM offers a similar or better performance than SMX, where the performance of both systems depends on the size of the constellation diagram and the number of receive antennas. We also note that the BER performance of SM can be improved by increasing the number of receive antennas.

C. Complexity Analysis

In Figs. 7-10, the computational complexity of SM–Rx and SM–Tx provided in (26) and (27) respectively is compared with the computational complexity of SMX–SD, where the initial radius is chosen according to (42). In particular, the figures show the relative computational complexity of the SDs with respect to the SM–ML detector, *i.e* $\mathcal{C}_{\text{rel}}(\%) = 100 \times (\mathcal{C}_{\text{SD}}/\mathcal{C}_{\text{ML}})$. Note, for SM the SD with the lowest complexity is chosen.

In Figs. 7 and 8, the relative computational complexities for $m = 6$ and $N_r = 2, 4$ are shown. Fig. 7, shows that for large constellation sizes the lowest relative computational complexity is offered by SM–Tx $N_t = 2$. The relative computational complexity ranges between 40% for low SNR and 16% for high SNR. However, for lower constellation sizes SM–Rx provides the lowest relative computational complexity, which is between 56% for low SNR and 26% for hight SNR. As SM–Rx reduces the receive search space, the reduction in the computational complexity offered by SM–Rx does not depend on the number of transmit antennas. Therefore, only SM–Rx with $N_t = 4, 32$ are shown, where both scenarios offer nearly the same relative computational complexity. Finally, from Fig. 7 we can see that SMX–SD $N_t = 2$ and $N_t = 3$

are less complex than SM–ML with a relative computational complexity 48% and $79\% - 82\%$ respectively. However, comparing SM–SD to SMX–SD $N_t = 2$, for 32–QAM SM–SD is 32% less complex than SMX—SD, and for BPSK SM–SD is 22% less complex than SMX–SD. In Fig. 8, it can be seen that for large constellation sizes SM–Tx is still the best choice with a relative complexity that ranges between 22% for low SNR and 12% for hight SNR, which is 15% less than SMX–SD $N_t = 2$. For smaller constellation sizes SM–Rx is the best choice with relative complexity that ranges between 55% for low SNR and 14% for high SNR, offering a 23% extra reduction in complexity when compared to SMX–SD $N_t = 2$. Note, i) SMX–SD $N_t = 6$ is not shown in the figure, because this scenario has a complexity higher than the complexity of SM–ML, ii) the complexity of SMX–SD $N_t = 3$ increased with the increase of SNR, for the reason that, in the under-determined case φ depends on the SNR (52).

The relative complexity for $m = 8$ and $N_r = 2, 4$ is shown in Fig. 9 and 10. Since SM–Tx reduces the transmit search space, the reduction in complexity increased by more than 10% with the increase in the wordsize and consequently the constellation size. In Fig. 9 for high constellation sizes SM–Tx $N_t = 2$ is the best choice with a relative complexity that reaches 4% for high SNR,. In Fig. 10 for high constellation sizes SM–Tx $N_t = 2$ and $N_t = 4$ are the best choice with a relative complexity that reaches 3% and 10% respectively. On the other hand, SM–Rx reduces the receive search space, therefore, it still offers nearly the same relative complexity. However, the complexity reduces with the increase of N_r, where SM–Rx $N_r = 4$ is $(\sim 10\%)$ less complex than SM–Rx $N_r = 2$. Finally, from both figures it can be seen that although SM–ML is much less complex than SMX–ML, SMX–SD is less complex than SM–ML. For that reason, SM–SD has to be developed, where SM–SD is $(\sim 20\%)$ less complex than SMX–SD for $N_r = 2$, and $(\sim 10\%)$ less complex than SMX–SD for $N_r = 4$. Note, the complexity of both SM–Tx and SMX–SD decreases with the increase of N_r, because for the case of $N_r < N_t$, the less under-determined the system, the fewer pre–computations are needed.

To summarize, two SDs for SM are introduced: SM–Tx which reduces the transmit search space, and SM–Rx which reduces the receive search space. Both detection algorithms are shown to offer a significant reduction in computational complexity while maintaining a near optimum BER performance. For systems with few transmit antennas, SM–Tx is shown to be the better choice. For systems with with a larger number of receive antennas, SM–Rx is shown to be the better candidate in terms of complexity reduction. The decision for the most appropriate SD depends on the particular deployment scenario.

VII. Conclusion

In this paper we have introduced and analysed the performance/complexity trade–off of two SDs designed specifically for SM. The proposed SDs provide a substantial reduction in the computational complexity while retaining the same BER as the ML–optimum detector. The closed–form analytical performance of SM in i.i.d. Rayleigh flat–fading channels has been derived, and analytical and simulation results were shown to closely agree. Furthermore, numerical results have highlighted that no SD is superior to the others, and that the best solution to use depends on the MIMO setup, and the SNR at the receiver. In general, SM–Rx is the best choice for lower spectral efficiencies, and SM–Tx is the best option for higher spectral efficiencies. Finally, simulation results showed that SM using SD offers a significant reduction in computational complexity and nearly the same BER performance as SMX using ML decoder or SD.

Overall, SM–SD offers i) hardware complexity and power consumption that does not depend on the number of transmit antennas, ii) BER performance that increases with the increase of the number of transmit antennas, and iii) a large reduction in computational complexity compared to SMX. Thus, we believe that SM–SD is an ideal candidate for large scale MIMO systems.

Appendix
Proof of the intervals (18), (19)

Proof:

1) First (17) can be thought of as an inequality,

$$R^2 \geq \left\{ \|\bar{\mathbf{y}} - \bar{\mathbf{H}}\bar{\mathbf{x}}_{\ell,s}\|_{\mathrm{F}}^2 \right\} \tag{48}$$

Then add $\varphi \bar{\mathbf{x}}_{\ell,s}^H \bar{\mathbf{x}}_{\ell,s}$ to both sides of (48) to get (49), where $\bar{\mathbf{G}} = \bar{\mathbf{H}}^{\mathbf{H}}\bar{\mathbf{H}} + \varphi \bar{\mathbf{I}}_{\mathbf{N_t}}$ is a $(2N_t \times 2N_t)$ positive definite matrix, with a Cholesky factorisation defined as $\bar{\mathbf{G}} = \bar{\mathbf{D}}^{\mathbf{H}}\bar{\mathbf{D}}$, where $\bar{\mathbf{D}}$ is a $(2N_t \times 2N_t)$ upper triangular matrix.
Now by defining $\bar{\rho} = \bar{\mathbf{G}}^{-1}\bar{\mathbf{H}}^{\mathbf{H}}\bar{\mathbf{y}}$, and adding $\bar{\rho}\mathbf{D}^{\bar{\mathbf{H}}}\mathbf{D}\bar{\rho}$ to both sides of (49), it can be re–written as,

$$\begin{aligned} R_\varphi^2 &\geq \left\{ \|\bar{\mathbf{z}} - \bar{\mathbf{D}}\bar{\mathbf{x}}_{\ell,s}\|_{\mathrm{F}}^2 \right\} \\ &\geq \sum_{i=1}^{2N_t} \left(\bar{z}_i - \sum_{j=i}^{2N_t} \bar{D}_{i,j} \bar{x}_{\ell,s}(j) \right)^2 \end{aligned} \tag{50}$$

where, $\bar{\mathbf{z}} = \bar{\mathbf{D}}\bar{\rho}$ and,

$$R_\varphi^2 = R^2 + \varphi \bar{\mathbf{x}}_{\ell,\mathbf{s}}^{\mathbf{T}} \bar{\mathbf{x}}_{\ell,\mathbf{s}} + \bar{\mathbf{y}}^{\mathbf{T}}\bar{\mathbf{H}}\bar{\rho} - \bar{\mathbf{y}}^{\mathbf{T}}\bar{\mathbf{y}} \tag{51}$$

$$\varphi = \begin{cases} \sigma_n^2 & N_t > N_r \\ 0 & N_t \leq N_r \end{cases} \tag{52}$$

For simplicity, in this paper we assume $R_\varphi^2 = R^2$.

$$\begin{aligned} R^2 + \varphi \bar{\mathbf{x}}_{\ell,s}^H \bar{\mathbf{x}}_{\ell,s} &\geq \left\{ \|\bar{\mathbf{y}} - \bar{\mathbf{H}}\bar{\mathbf{x}}_{\ell,s}\|_{\mathrm{F}}^2 + \varphi \bar{\mathbf{x}}_{\ell,s}^H \bar{\mathbf{x}}_{\ell,s} \right\} \\ &\geq \left\{ \bar{\mathbf{y}}^H\bar{\mathbf{y}} - \bar{\mathbf{y}}^H\bar{\mathbf{H}}\bar{\mathbf{x}}_{\ell,s} + \bar{\mathbf{x}}_{\ell,s}^H\bar{\mathbf{H}}^H\bar{\mathbf{y}} + \bar{\mathbf{x}}_{\ell,s}^H\bar{\mathbf{G}}\bar{\mathbf{x}}_{\ell,s} \right\} \end{aligned} \tag{49}$$

2) Second, we note a necessary condition that the points of the transmit search space need to satisfy to belong to the subset Θ_R is (for all $i = 1, 2, \ldots, 2N_t$):

$$R^2 \geq \left(\bar{z}_i - \sum_{j=i}^{2N_t} \bar{D}_{i,j} \bar{x}_{\ell,s}(j) \right)^2 \quad (53)$$

which is a condition similar to conventional SD algorithms [31].

3) We need to take into account that in SM only a single antenna is active at any time instance. In the equivalent real–valued signal model in (10), this is equivalent to having only two, out of $2N_t$, non–zero entries in the signal vectors $\bar{\mathbf{x}}_{\ell_t,s_t}$ and $\bar{\mathbf{x}}_{\ell,s}$, respectively. By taking this remark into account, it follows that: a) if $i = N_t + 1, N_t + 2, \ldots, 2N_t$, then only the imaginary part of $\bar{\mathbf{x}}_{\ell,s}$ plays a role in (53), and, thus, only one entry $\bar{\mathbf{x}}_{\ell,s}(\ell + N_t)$ can be non–zero; and b) if $i = 1, 2, \ldots, N_t$, then both real and imaginary parts of $\bar{\mathbf{x}}_{\ell,s}$ play a role in (53), and, thus, only two entries $\bar{\mathbf{x}}_{\ell,s}(\ell), \bar{\mathbf{x}}_{\ell,s}(\ell + N_t)$ can be non–zero. The considerations in a) and b) lead to the intervals in (18) and (19), respectively, which are directly obtained by solving the inequality in (53).

□

REFERENCES

[1] E. Telatar, "Capacity of multi-antenna Gaussian channels," *European Trans. Telecommun.*, vol. 10, no. 6, pp. 585–595, Nov./Dec. 1999.

[2] G. J. Foschini, "Layered space-time architecture for wireless communication in a fading environment when using multi-element antennas," *Bell Labs Tech. J.*, vol. 1, no. 2, pp. 41–59, 1996.

[3] J. Hoydis, S. ten Brink, and M. Debbah, "Massive MIMO: how many antennas do we need?" in *Proc. 2011 Allerton Conf. Commun., Control, Comput.*, pp. 545–550.

[4] S. Mohammed, A. Zaki, A. Chockalingam, and B. Rajan, "High-rate space-time coded large-MIMO systems: low-complexity detection and channel estimation," *IEEE J. Sel. Topics Signal Process.*, vol. 3, no. 6, pp. 958–974, Dec. 2009.

[5] B. Cerato and E. Viterbo, "Hardware implementation of a low-complexity detector for large MIMO," in *Proc. 2009 IEEE Int. Symp. Circuits Syst.*, pp. 593–596.

[6] S. Mohammed, A. Chockalingam, and B. Sundar Rajan, "A Low-complexity near-ML performance achieving algorithm for large MIMO detection," in *Proc. 2008 IEEE Int. Symp. Inf. Theory*, pp. 2012–2016.

[7] E. Viterbo and J. Boutros, "A universal lattice code decoder for fading channels," *IEEE Trans. Inf. Theory*, vol. 45, no. 5, pp. 1639–1642, July 1999.

[8] O. Damen, A. Chkeif, and J.-C. Belfiore, "Lattice code decoder for space-time codes," *IEEE Commun. Lett.*, vol. 4, no. 5, pp. 161–163, May 2000.

[9] A. Molisch and M. Win, "MIMO systems with antenna selection," *IEEE Microwave Mag.*, vol. 5, no. 1, pp. 46–56, Mar. 2004.

[10] A. Stavridis, S. Sinanović, M. D. Renzo., H. Haas, and P. Grant, "An energy saving base station employing spatial modulation," in *Proc. 2012 IEEE Int. Workshop Comput. Aided Modeling Design Commun. Links Netw.*, pp. 231–235.

[11] L. Correia, D. Zeller, O. Blume, D. Ferling, A. Kangas, I. Godor, G. Auer, and L. Van Der Perre, "Challenges and enabling technologies for energy aware mobile radio networks," *IEEE Commun. Mag.*, vol. 48, no. 11, pp. 66–72, Nov. 2010.

[12] R. Mesleh, H. Haas, S. Sinanović, C. W. Ahn, and S. Yun, "Spatial modulation," *IEEE Trans. Veh. Technol.*, vol. 57, no. 4, pp. 2228–2241, July 2008.

[13] M. Di Renzo, H. Haas, and P. M. Grant, "Spatial modulation for multiple-antenna wireless systems: A survey," *IEEE Commun. Mag,*, vol. 49, no. 11, pp. 182–191, Nov. 2011.

[14] N. Serafimovski, M. Di Renzo, S. Sinanović, R. Y. Mesleh, and H. Haas, "Fractional bit encoded spatial modulation (FBE–SM)," *IEEE Commun. Lett.*, vol. 14, no. 5, pp. 429–431, May 2010.

[15] A. Younis, N. Serafimovski, R. Mesleh, and H. Haas, "Generalised spatial modulation," in *2010 Asilomar Conf. Signals, Syst., Comput.*.

[16] J. Jeganathan, A. Ghrayeb, L. Szczecinski, and A. Ceron, "Space shift keying modulation for MIMO channels," *IEEE Trans. Wireless Commun.*, vol. 8, no. 7, pp. 3692–3703, July 2009.

[17] A. Stavridis, S. Sinanović, M. D. Renzo, and H. Haas, "A power saving dual-hop architecture based on hybrid spatial modulation," in *Proc. 2012 Asilomar Conf. Signals, Syst. Comput.*, pp. 1366–1370.

[18] J. Jeganathan, A. Ghrayeb, and L. Szczecinski, "Spatial modulation: optimal detection and performance analysis," *IEEE Commun. Lett.*, vol. 12, no. 8, pp. 545–547, 2008.

[19] N. Serafimovski, A. Younis, R. Mesleh, P. Chambers, M. D. Renzo, C.-X. Wang, P. M. Grant, M. A. Beach, and H. Haas, "Practical implementation of spatial modulation," in *IEEE Trans. Veh. Technol.*, to appear. Available: http://arxiv.org/abs/1305.0664

[20] N. Serafimovski, A. Younis, and H. Haas, "Spatial modulation," Oct. 2012. Available: http://youtu.be/cPKIbxrEDho

[21] A. Younis, W. Thompson, M. D. Renzo, C.-X. Wang, M. A. Beach, H. Haas, and P. M. Grant, "Performance of spatial modulation using measured real-world channels," in *Proc. 2013 IEEE Veh. Tech. Conf. – Fall*. Available: http://arxiv.org/abs/1305.3437.

[22] M. Di Renzo and H. Haas, "Bit Error probability of spatial modulation (SM) MIMO over generalized fading channels," *IEEE Trans. Veh. Technol.*, vol. 61, no. 3, pp. 1124–1144, Mar. 2012.

[23] M. Di Renzo and H. Haas, "On transmit-diversity for spatial modulation MIMO: impact of spatial-constellation diagram and shaping filters at the transmitter," in *IEEE Trans. Veh. Technol.*, 2013, to appear. Available: IEEE Xplore Early Access.

[24] M. D. Renzo, D. D. Leonardis, F. Graziosi, and H. Haas, "Space shift keying (SSK) MIMO with practical channel estimates," *IEEE Trans. Commun.*, vol. 60, no. 4, pp. 998–1012, Apr. 2012.

[25] M. Di Renzo and H. Haas, "Bit error probability of space-shift keying MIMO over multiple-access independent fading channels," *IEEE Trans. Veh. Technol.*, vol. 60, no. 8, pp. 3694–3711, Oct. 2011.

[26] A. Younis, R. Mesleh, H. Haas, and P. M. Grant, "Reduced complexity sphere decoder for spatial modulation detection receivers," in *Proc. 2010 IEEE Global Telecommun. Conf.*, pp. 1–5.

[27] A. Younis, M. Di Renzo, R. Mesleh, and H. Haas, "Sphere decoding for spatial modulation," in *Proc. 2011 IEEE Int. Conf. Commun.*, pp. 1–6.

[28] R. Rajashekar and K. V. S. Hari, "Sphere decoding for spatial modulation systems with arbitrary Nt," *CoRR*, vol. abs/1202.5187, 2012.

[29] ——, "Low complexity maximum likelihood detection in spatial modulation systems," *CoRR*, vol. abs/1206.6190, 2012.

[30] H. V. T. Kailath and B. Hassibi, *Space-Time Wireless Systems: From Array Processing to MIMO Communications*, C. P. H. Bolcskei, D. Gesbert and A. J. van der Veen, Eds. Cambridge University Press, 2006.

[31] B. Hassibi and H. Vikalo, "On the sphere-decoding algorithm—I: expected complexity," *IEEE Trans. Signal Process.*, vol. 53, no. 8, pp. 2806–2818, Aug. 2005.

[32] T. Cui and C. Tellambura, "An efficient generalized sphere decoder for rank-deficient MIMO systems," *IEEE Commun. Lett.*, vol. 9, no. 5, pp. 423–425, May 2005.

[33] P. Wang and T. Le-Ngoc, "A low-complexity generalized sphere decoding approach for underdetermined linear communication systems: performance and complexity evaluation," *IEEE Trans. Commun.*, vol. 57, no. 11, pp. 3376–3388, Nov. 2009.

[34] G. H. Golub and C. F. van Loan, *Matrix Computations*. The John Hopkins University Press, 1996.

[35] J. G. Proakis, *Digital Communications*, 4th ed. McGraw–Hill, 2000.

[36] J. Jalden, L. Barbero, B. Ottersten, and J. Thompson, "The error probability of the fixed-complexity sphere decoder," *IEEE Trans. Signal Process.*, vol. 57, no. 7, pp. 2711–2720, July 2009.

[37] X. Xia, H. Hu, and H. Wang, "Reduced initial searching radius for sphere decoder," in *Proc. 2007 IEEE Int. Symp. Personal, Indoor, Mobile Radio Commun.*, pp. 1–4.

[38] M.-S. Alouini and A. Goldsmith, "A unified approach for calculating error rates of linearly modulated signals over generalized fading channels," *IEEE Trans. Commun.*, vol. 47, no. 9, pp. 1324–1334, 1999.

Abdelhamid Younis received a BSc in Electrical and Electronic Engineering with honours in 2007 from the University of Benghazi, Libya and an MSc with distinction in Signal Processing and Communication Engineering in 2009 from the University of Edinburgh, UK. He is currently completing a Ph.D. in Communication Engineering at the Institute of Digital Communications (IDCOM) at the University of Edinburgh where in 2010 he was awarded the Overseas Research Student Award (ORS) in recognition of his work. His main research interests lie in the area of wireless communication and digital signal processing with a particular focus on spatial modulation, MIMO wireless communications, reduced complexity MIMO design and optical wireless communications.

Sinan Sinanović (S'98-M'07) is a lecturer at Glasgow Caledonian University. He has obtained his Ph.D. in electrical and computer engineering from Rice University, Houston, Texas, in 2006. In the same year, he joined Jacobs University Bremen in Germany as a post doctoral fellow. In 2007, he joined the University of Edinburgh in the UK where he has worked as a research fellow in the Institute for Digital Communications. While working with Halliburton Energy Services, he has developed acoustic telemetry receiver which was patented. He has also worked for Texas Instruments on development of ASIC testing. He is a member of the Tau Beta Pi engineering honor society and a member of Eta Kappa Nu electrical engineering honor society. He won an honorable mention at the International Math Olympiad in 1994.

Marco Di Renzo (S'05–AM'07–M'09) was born in L'Aquila, Italy, in 1978. He received the Laurea (cum laude) and the Ph.D. degrees in Electrical and Information Engineering from the Department of Electrical and Information Engineering, University of L'Aquila, Italy, in April 2003 and in January 2007, respectively.

From August 2002 to January 2008, he was with the Center of Excellence for Research DEWS, University of L'Aquila, Italy. From February 2008 to April 2009, he was a Research Associate with the Telecommunications Technological Center of Catalonia (CTTC), Barcelona, Spain. From May 2009 to December 2009, he was an EPSRC Research Fellow with the Institute for Digital Communications (IDCOM), The University of Edinburgh, Edinburgh, United Kingdom (UK).

Since January 2010, he has been a Tenured Researcher ("Chargé de Recherche Titulaire") with the French National Center for Scientific Research (CNRS), as well as a faculty member of the Laboratory of Signals and Systems (L2S), a joint research laboratory of the CNRS, the École Supérieure d'Électricité (SUPÉLEC), and the University of Paris–Sud XI, Paris, France. His main research interests are in the area of wireless communications theory. He is a Principal Investigator of three European–funded research projects (Marie Curie ITN–GREENET, Marie Curie IAPP–WSN4QoL, and Marie Curie ITN–CROSSFIRE).

Dr. Di Renzo is the recipient of the special mention for the outstanding five–year (1997–2003) academic career, University of L'Aquila, Italy; the THALES Communications fellowship for doctoral studies (2003–2006), University of L'Aquila, Italy; the Best Spin–Off Company Award (2004), Abruzzo Region, Italy; the Torres Quevedo award for research on ultra wide band systems and cooperative localization for wireless networks (2008–2009), Ministry of Science and Innovation, Spain; the "Dérogation pour l'Encadrement de Thèse" (2010), University of Paris–Sud XI, France; the 2012 IEEE CAMAD Best Paper Award from the IEEE Communications Society; and the 2012 Exemplary Reviewer Award from the IEEE WIRELESS COMMUNICATIONS LETTERS of the IEEE Communications Society. He currently serves as an Editor of the IEEE COMMUNICATIONS LETTERS.

Raed Mesleh (S'00-M'08-SM'13) Dr Mesleh holds a Ph.D. in Electrical Engineering from Jacobs University in Bremen, Germany and several years of post-doctoral wireless communication and optical wireless communication research experience in Germany. In October 2010, he joined University of Tabuk in Saudi Arabia where he is now an assistant professor and the director of research excellence unit. His main research interests are in spatial modulation, MIMO cooperative wireless communication techniques and optical wireless communication. Dr Mesleh publications received more than 800 citations since 2007. He has published more than 50 publications in top-tier journals and conferences, and he holds seven granted patents. He also serves as on the TPC for academic conferences and is a regular reviewer for most of IEEE/OSA Communication Society's journals and IEEE/OSA Photonics Society's journals.

Professor Harald Haas (S98-A00-M03) holds the Chair of Mobile Communications in the Institute for Digital Communications (IDCOM) at the University of Edinburgh, and he currently is the CTO of a university spin-out company pureVLC Ltd. His main research interests are in interference coordination in wireless networks, spatial modulation and optical wireless communication. Prof. Haas holds 23 patents. He has published more than 60 journal papers including a Science Article and more than 160 peer-reviewed conference papers. Nine of his papers are invited papers. Prof. Haas has co-authored a book entitled *Next Generation Mobile Access Technologies: Implementing TDD* with Cambridge University Press. Since 2007 Prof. Haas has been a Regular High Level Visiting Scientist supported by the Chinese 111-program at Beijing University of Posts and Telecommunications (BUPT). He was an invited speaker at the TED Global conference 2011, and his work on optical wireless communication was listed among the "50 best inventions in 2011" in *Time Magazine*. He recently has been awarded a prestigious Fellowship of the Engineering and Physical Sciences Research Council (EPSRC) in the UK.

IEEE TRANSACTIONS ON VEHICULAR TECHNOLOGY, VOL. 62, NO. 9, NOVEMBER 2013 4511

Practical Implementation of Spatial Modulation

Nikola Serafimovski, Abdelhamid Younis, Raed Mesleh, *Senior Member, IEEE*, P. Chambers, Marco Di Renzo, *Member, IEEE*, Cheng-Xiang Wang, *Senior Member, IEEE*, Peter M. Grant, *Fellow, IEEE*, Mark A. Beach, and Harald Haas, *Member, IEEE*

***Abstract*—In this paper, we seek to characterize the performance of spatial modulation (SM) and spatial multiplexing (SMX) with an experimental testbed. Two National Instruments (NI) PXIe devices are used for the system testing: one for the transmitter and one for the receiver. The digital signal processing (DSP) that formats the information data in preparation for transmission is described, along with the DSP that recovers the information data. In addition, the hardware limitations of the system are also analyzed. The average bit-error ratio (ABER) of the system is validated through both theoretical analysis and simulation results for SM and SMX under the line-of-sight (LoS) channel conditions.**

***Index Terms*—Experimental results, multiple-input multiple-output (MIMO) systems, spatial modulation (SM), spatial multiplexing (SMX), wireless testbed.**

I. Introduction

MULTIPLE-INPUT multiple-output (MIMO) systems offer a significant increase in spectral efficiency in comparison with single-antenna systems [1], [2]. An example is spatial modulation (SM), which increases the spectral efficiency of single-antenna systems while avoiding interchannel interference (ICI) [3]. This is attained, as shown in Fig. 1, through the adoption of a new modulation and coding scheme, which foresees the activation, at each time instance, of a single antenna that transmits a given data symbol (*constellation symbol*) and the exploitation of the spatial position (index) of the active antenna as an additional dimension for data transmission (*spatial symbol*) [4]. Both the *constellation* and *spatial symbols* depend on the incoming data bits. An overall increase by the base-two logarithm of the number of transmit antennas of the spectral efficiency is achieved. This limits the number of transmit antennas to be a power of two, unless fractional-bit-encoded SM [5] or generalized SM (GSM) [6] is used. In particular, in [6], it is shown that the number of spatial symbols does not need to be equal to the number of transmit antennas. For example, if GSM is used, the number of spatial symbols is equal to the number of unique channel signatures between the transmitter and the receiver, where the unique channel signatures can be obtained by activating various combinations of the available transmit antennas. In this paper, however, these unique channel signatures are assumed to be due to the activation of individual transmit antennas.

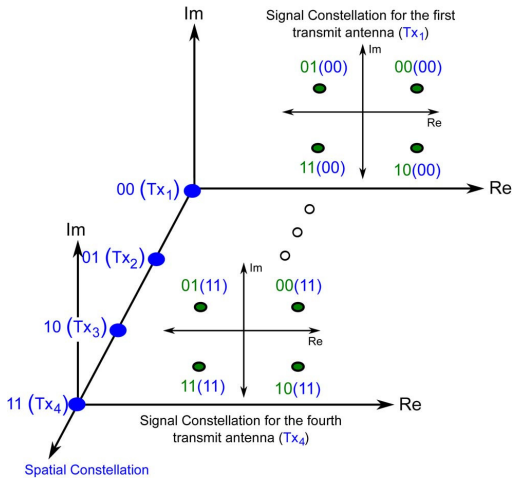

Fig. 1. Unique 3-D constellation diagram for SM. The lower two bits, in the 4-bit word, define the spatial-constellation point, which identifies the active antenna. These are shown in parentheses. The remaining two bits determine the signal-constellation point that is to be transmitted.

Activating only one antenna at a time means that only one radio-frequency (RF) chain is needed, which significantly reduces the hardware complexity of the system [7]. Moreover, the most energy-consuming parts of a base station (BS) are the power amplifiers and the RF chains that are associated with each transmitter [8], where the power requirements of a BS are shown to linearly increase with the number of RF chains that are added [9]. However, as only one RF chain is needed, SM offers a reduction in the energy consumption, which linearly scales with the number of transmit antennas [10], [11]. Furthermore, the computational complexity of the ML detector for SM

Manuscript received October 2, 2012; revised February 18, 2013 and April 24, 2013; accepted May 2, 2013. Date of publication June 6, 2013; date of current version November 6, 2013. This work was supported in part by The University of Edinburgh Initiating Knowledge Transfer Fund, the Engineering and Physical Sciences Research Council Fellowship under Grant EP/K008757/1, by the Research Councils U.K. under Grant EP/G042713/1 [UK–China Science Bridges "R&D on (B)4G Wireless Mobile Communications"], by the European Union under Grant PITNGA2010264759 (GREENET), and by the Key Laboratory of Cognitive Radio and Information Processing, Guilin University of Electronic Technology, Ministry of Education, China, under Grant 2013KF01. The review of this paper was coordinated by Prof. Y. L. Guan.

N. Serafimovski, A. Younis, P. M. Grant, and H. Haas are with The University of Edinburgh, Edinburgh EH9 3JL, U.K. (e-mail: n.serafimovski@ed.ac.uk; a.younis@ed.ac.uk; p.grant@ed.ac.uk; h.haas@ed.ac.uk).

R. Mesleh is with the Department of Electrical Engineering and the Sensor Networks and Cellular Systems Research Center, University of Tabuk, Tabuk, Saudi Arabia (e-mail: rmesleh.sncs@ut.edu.sa).

P. Chambers and C.-X. Wang are with Heriot-Watt University, Edinburgh EH14 4AS, U.K. (e-mail: P.Chambers@hw.ac.uk; Cheng-Xiang.Wang@hw.ac.uk).

M. Di Renzo is with the Laboratoire des Signaux et Systèmes, Unitè Mixte de Recherche 8506, Centre National de la Recherche Scientifique–École Supèrieure d'Électricitè–Universitè Paris-Sud XI, 91192 Gif-sur-Yvette, France (e-mail: marco.direnzo@lss.supelec.fr).

M. A. Beach is with the University of Bristol, Bristol BS8 1UB, U.K. (e-mail: M.A.Beach@bristol.ac.uk).

Color versions of one or more of the figures in this paper are available online at http://ieeexplore.ieee.org.

Digital Object Identifier 10.1109/TVT.2013.2266619

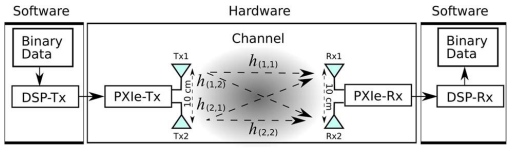

Fig. 2. Block sequence of the main steps in the experiment from the generation of the binary data to its recovery.

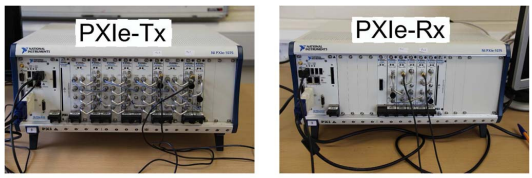

(a) (b)

Fig. 3. NI-PXIe-1075 chassis with the relevant onboard modules at (a) the transmitter (PXIe-Tx) and (b) the receiver (PXIe-Rx).

[SM-maximum likelihood (ML)] is equal to the complexity of single-input multiple-output (SIMO) systems [12], i.e., the complexity of SM-ML depends only on the spectral efficiency and the number of receive antennas and does not depend on the number of transmit antennas. Moreover, in [13]–[15], the complexity of SM is further reduced by using the sphere decoder (SD).

Several papers that seek to understand and improve the performance of SM in various scenarios are available in literature. In [16] and [17], the average bit-error ratio (ABER) performance of SM is improved by introducing trellis coding on the transmitting antennas. The optimal detector is derived with and without channel state information at the receiver in [12], [18], and [19]. The ABER performance is given when considering channel estimation errors in [20]–[22]. The optimal power allocation for the case of two transmit antennas and one receive antenna system is given in closed form in [23], and the ABER performance of SM in correlated fading channels is considered in [24]. In [25] and [26], spectral efficiency and diversity gains are obtained by combining SM with space–time block codes (STBC-SM). Applying SM to relaying systems is also shown to result in significant signal-to-noise-ratio (SNR) gains when compared with noncooperative decode and forward techniques [27]. In [28], the overall power performance of a BS employing SM is studied. More recently, a comprehensive analytical framework to compute the ABER of SM over generalized fading channels has been introduced in [29]. Moreover, in [30], for the first time, the performance of SM is analyzed using real-world channel measurements. The latest research achievements and an outline of some relevant open research issues for SM are reviewed in [31]. All research thus far is strictly theoretical.

In this paper, the ABER performance of SM is analyzed in a practical testbed and compared with that for spatial multiplexing (SMX). In particular, the National Instruments (NI) PXIe-1075 chassis are used at the transmitter and the receiver. The design of the testbed hardware and the software used are explained in detail, along with the transmission chain. The effects of the entire transmission chain on the system performance are examined. The basic elements of the transmission link are the transmit RF chain, the wireless channel, and the receive RF chain. In addition to the effects of the wireless channel on the phase and the amplitude of the signal, the impact on the system performance of the power imbalances (PIs) in the transmitter and receiver RF chains is discussed. Furthermore, an analytical upper bound for the ABER performance of SM over non-line-of-sight (NLoS) channels with PI is derived and compared with the experimental and computer simulation results. The experimental results validate the analytical bound, as well as the attained computer simulations. Finally, the performance of SM is compared with the theoretical and experimental results of SMX.

This paper is organized as follows: The system setup, equipment, and digital signal processing (DSP) are presented in Section II. The equipment constraints are then considered in Section III, while the analytical modeling is discussed in Section IV. In addition, the computational complexity of the SM decoder algorithm is presented in Section V. The performance of SM is then characterized in the experimental and simulation environments in Section VI, where it is compared with the theoretical and experimental results of an SMX system. Finally, this paper is summarized in Section VII.

II. Testbed Setup and System Model

The testbed setup and the transmission chain can be separated into software and hardware parts, as shown in Fig. 2. The hardware consists of the NI-PXIe chassis at the transmitter (PXIe-Tx) and the NI-PXIe chassis at the receiver (PXIe-Rx). The software consists of the DSP at the transmitter (DSP-Tx) and the DSP at the receiver (DSP-Rx).

The binary data to be broadcasted are first processed by the DSP-Tx, before being transmitted through the fading channel by the PXIe-Tx. The channel coefficient on the link between transmit antenna n_t and receive antenna r is denoted by $h_{(r,n_t)}$. Note that the number of antennas at the transmitter and the receiver are denoted by N_t and N_r, respectively. At the receiver, the PXIe-Rx records the RF signal and passes it through to the DSP-Rx for processing, where the original data stream is recovered.

A. Testbed Hardware

The NI-PXIe-1075 chassis are equipped with a 1.8-GHz Intel-i7 processor with 4-GB random access memory and are shown in Fig. 3. The system has two transmit antennas and two receive antennas. Each antenna at the transmitter and the receiver contains two quarter-wave dipoles and one half-wave dipole placed in the middle. All three dipoles are vertically polarized. In addition, each antenna has a peak gain of 7 dBi in the azimuth plane, with an omnidirectional radiation pattern.

1) Transmitter Hardware (PXIe-Tx): The following NI-PXIe modules are used at the transmitter:

I) NI-PXIe-5450 16-bit I/Q Signal Generator (SG-16bit);
II) NI-PXIe-5652 RF Signal Generator with a 500-kHz to 6.6-GHz frequency range (SG-RF);
III) NI-PXIe-5611 intermediate frequency to carrier RF upconverter (upconverter).

The PXIe-Tx has an operational frequency range of 85 MHz to 6.6 GHz and can facilitate a bandwidth of 100 MHz at a maximum transmission power of 5 dBm.

At the transmitter, the SG-16bit performs a linear mapping of the signed 16-bit range to the output power and polarization, i.e., the peak voltage amplitude is assigned to any value in the transmission vector that is equal to 2^{15} with a linear scale of the voltage amplitude down to zero. The output from SG-16bit then goes to SG-RF, which is connected to the upconverter. The upconverter outputs the analog waveform corresponding to the data resulting from DSP-Tx at a carrier frequency of 2.3 GHz. This completes a single RF chain. The transmission of the RF signal by the upconverters is synchronized by using a 10-MHz reference signal.

2) Receiver Hardware (PXIe-Rx): The following NI-PXIe modules are used at the receiver:

I) NI-PXIe-5652 an onboard reference clock (SG-RF);
II) NI-PXIe-5622 16-bit digitizer, which records data samples in an I16 format (16-Bit Digitizer);
III) NI-PXIe-5601 RF downconverter (downconverter).

The PXIe-Rx can operate in a frequency range of 10 MHz to 6.6 GHz and can facilitate an operational bandwidth of 50 MHz. For more details about the specifications of each module, see [32] and [33].

At the receiver, each antenna is associated with a complete RF chain. For each antenna, the downconverter is used to detect the analog RF signal from its dedicated antenna. The signal is then sent to the dedicated 16-Bit Digitizer. The 16-Bit Digitizer applies a bandpass filter with a real flat bandwidth that is equal to $B_f = (0.4 \times f_s)$, where f_s is the sampling rate [32]. The sampling rate in the experiment is 10 Ms/s, which results in a real flat bandwidth of 4 MHz. This may result in frequency-selective fading. Nonetheless, equalization is not required for the detection of SM or SMX signals in this experiment because of the following: 1) There are no multitap delays in the experimental setup due to very small distance between the transmit and receiver antennas. 2) ML detection is used to decode the received signal for both SM and SMX. The use of ML detection is applied to the complete SM symbol, i.e., the spatial and signal symbols are jointly decoded. Finally, after the synchronization of the 16-Bit Digitizer with the onboard reference clock of the SG-RF, the 16-Bit Digitizer writes the received binary files. The simultaneous recording of the two signals coming from Tx1 and Tx2 is facilitated by utilizing multiple processing cores and multiple NI-PXIe modules. The recorded files are then processed according to DSP-Rx in Fig. 4.

B. Testbed Software

MATLAB was used to facilitate the DSP-Tx and the DSP-Rx. The DSP-Tx processes the information data and generates binary files that can be transmitted by the PXIe-Rx. The DSP-Rx processes the received data from the PXIe-Rx and recover the original information data stream. Fig. 4 outlines the processing algorithms at the DSP-Tx and the DSP-Rx.

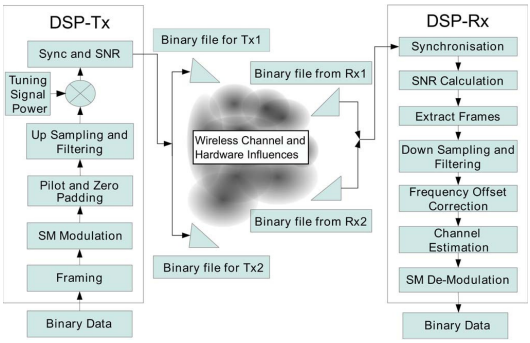

Fig. 4. Step-by-step layout of the binary data encoder (DSP-Tx) and decoder (DSP-Rx) processes.

1) DSP-Tx: The DSP-Tx process takes the incoming binary information data and performs the following.

1.1 **Framing**: The incoming data is split into frames consisting of 100 symbols per frame.

1.2 **Modulation**: The data in each frame is modulated using SM or SMX:

- **SM**: The bit stream is divided into blocks containing $\log_2(N_t\, M)$ bits each, where M is the signal-constellation size. The following mapping rule is then used [4]:
  a) The first $\log_2(N_t)$ bits determine which transmit antenna is active, i.e., they determine the spatial-constellation point of SM. In this paper, the transmit antenna broadcasting is denoted by n_t with $n_t \in \{1, 2, \ldots, N_t\}$.
  b) The second $\log_2(M)$ bits are used to choose a symbol in the signal-constellation diagram. Without loss of generality, quadrature amplitude modulation (QAM) is considered. The actual complex symbol emitted by the transmit antenna n_t is denoted by s_t, with $s_t \in \{s_1, s_2, \ldots, s_M\}$.

  By following the aforementioned steps, the $N_t \times 1$ dimensional transmit vector is

$$\mathbf{x}_{n_t}, s_t = \left[\mathbf{0}_{1\times(n_t-1)}, s_t, \mathbf{0}_{1\times(N_t-n_t)}\right]^T \tag{1}$$

  where $[\cdot]^T$ denotes the transpose operation, and $\mathbf{0}_{p\times q}$ is a $p \times q$ matrix with all-zero entries. Equation (1) is a representation of the transmission vector for SM. Since SM activates only one transmit antenna at any transmission instance, only one transmit antenna can broadcast a symbol, while all others remain silent. To this extent, the transmit vector is composed of all zeros, except for the single symbol s_t, which is broadcasted from antenna n_t. In this manner, SM avoids ICI and allows single-stream ML decoding. In addition, SM is energy efficient since only a single RF chain is active while still providing a multiplexing gain [10].

- **SMX**: In this case, the bit stream is divided into blocks of $N_t \log_2(M)$ bits; then, according to [34], the following mapping rule is used.
  a) Each $\log_2(M)$ bit is separately modulated using M-QAM modulation.
  b) The modulated symbols are then simultaneously transmitted from the N_t transmit antennas.

1.3 **Pilot and zero padding**: The least-square (LS) channel estimation algorithm with local orthogonal pilot sequences is used to estimate the channel [35]. Two pilot signals are added for each frame, one of which at the start of the frame and one at the end. Each pilot signal contains ten pilot sequences, where the orthogonal pilot sequence for the n_tth transmit antenna is defined as

$$\Theta_{n_t}(\ell) = \exp\left(2\pi j \frac{n_t \ell}{N_\Theta}\right) \tag{2}$$

where $\Theta_{n_t}(\ell)$ is the ℓth element of the pilot sequence Θ_{n_t} transmitted from antenna n_t, $j = \sqrt{-1}$ is the imaginary unit, and N_Θ is the cardinality of the pilot sequence. In this paper, the length of each pilot sequence is $N_\Theta = 10$. To avoid interframe interference, an all-zero sequence of 50 zero-valued symbols is added to both the start and the end of the frame. Furthermore, a sequence of constant-valued symbols is added to enable frequency-offset (FO) estimation at the receiver. The length of the FO estimation sequence is 1000 symbols.

1.4 **Upsampling and filtering**: Upsampling and matched filtering (pulse shaping) are used to maximize the SNR and reduce intersymbol interference [36]. Each frame is upsampled with an upsampling ratio of 4 and then passed through a root-raised-cosine (RRC) finite-impulse-response (FIR) filter with 40 taps and a rolloff factor of 0.75. The large rolloff factor is necessary to ensure that the power is focused in a short-time instance to ensure that only a single RF chain is active when using SM.

1.5 **Tuning signal power**: The SNR is varied by changing the power of the transmitted signal to obtain the ABER. This is done by multiplying each transmission vector with a "tuning signal power" factor to obtain the desired transmit power. In particular, the amplitude of the "data section" in the transmission vector is changed by using the "tuning signal power" factor.

1.6 **Synchronization and SNR**: Several preamble-autocorrelation-based methods for frame synchronization were tested [37]–[39]. However, despite the introduction of an interpolation filter at the receiver and due to the channel attenuations, the estimated start of the signal was typically in error by one or two samples. This meant that sample synchronization could not be consistently achieved, resulting in off-by-one errors. The investigation of synchronization techniques is outside the scope of this paper, but to avoid synchronization via a cable, as is often done in similar experimental systems, the peak-detection technique has been applied, which resulted in the desired outcome. We recognize that this technique is suboptimal as it results in power-amplifier saturation and potential signal distortions. Nonetheless, a sequence of 20 symbols with maximum power, each of which is separated by 50 zero-valued symbols, are added to the start of the transmitted signal. The large power difference between the maximum power peaks and the power of the "data section" symbols is reasonable since the instantaneous channel power may fluctuate by as much as 20 dB due to fast fading [40], [41]. The power difference between the synchronization section and the remaining sections is set to be larger than the maximum channel variation. In this manner, successful peak detection is guaranteed. If this is not the case, no peak may be detected at the receiver, and all further decoding would be erroneous. To facilitate SNR calculations at the receiver, two sequences of power and no power are added after the synchronization pulses of the transmitted signal, which are indicated by the "SNR section" in Fig. 5. Each sequence contains five blocks of 50000 symbols and 50000 zeros. The first sequence is transmitted from the first antenna, whereas the second antenna is off. The second sequence is transmitted from the second antenna, whereas the first antenna is off.

After the DSP-Tx process is completed, the transmit vector symbols are converted to I16 format and are recorded to a binary file. This binary file is then broadcast by the PXIe-Tx.

Fig. 5 is an absolute value representation of the processed incoming data that are passed to the first transmit antenna (Tx1), and Fig. 6 shows the absolute value representation of each frame. Note that the "data section" is a series of concatenated frames. In Fig. 6, it is shown that each frame contains 26100 samples. Therefore, the period of each frame is $T_{\text{Frame}} = 26100/f_s = 2.6$ ms. This is much less than the coherence time of the channel given that, typically, the coherence time for a stationary indoor environment is approximately 7 ms (see [41], and references therein). Hence, the channel estimation at the receiver is valid for the frame duration.

2) DSP-Rx: The data that are received by the PXIe-Rx are processed by the DSP-Rx to recover the original data stream. To accomplish this, the following steps are required.

2.1 **Synchronization**: This is achieved by searching for the peaks with a value above a certain threshold in the received signal. The threshold is set as 70% of the highest value in the received vector. This threshold level accounts for the natural voltage variations in the system, i.e., the difference between the peak voltage and the root-mean-square voltage. If the number of peaks found is less than 20, then the received vector is discarded from further calculations.

2.2 **SNR calculation**: The SNR is defined as

$$\text{SNR} = \frac{E\left[\|\mathbf{Hx}\|_F^2\right]}{\sigma_n^2} \tag{3}$$

where $\mathbf{H}$ is the $N_r \times N_t$ channel matrix, $\mathbf{x}$ is the $N_t \times 1$ transmitted vector, $E[\cdot]$ is the expectation operator, and $\|\cdot\|_F$ is the Forbenius norm. Assuming that the noise at the receiver is additive white Gaussian noise (AWGN), the received signal for the duration of the SNR sequence can be written as follows:

$$\mathbf{y} = \mathbf{h}_{n_t} s_t + \mathbf{n} \tag{4}$$

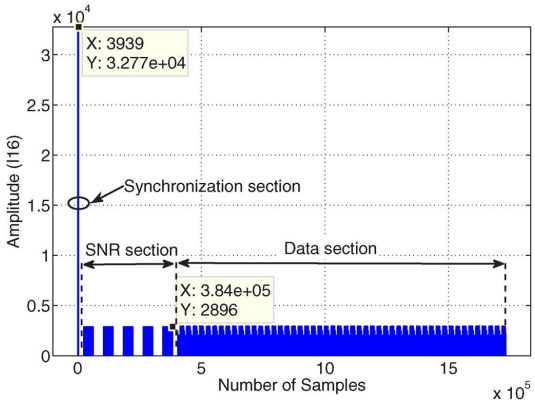

Fig. 5. Absolute value representation of the transmission vector being sent to Tx1. The synchronization, SNR estimation, and data sections are shown. The value of the peak must be equal to 2^{15} since the 16bit-Digitizer operates using an I16 format before tuning the signal power of the data. The highest value in the SNR section is the same as the highest value in the information data section, which in this example, is a value of 2896. The peak value is 2^{15}. There is approximately a 21.1 dB difference between the peak power in the synchronization section and the peak power in the SNR estimation and data sections. This is apparent when looking at the two data points shown in the figure.

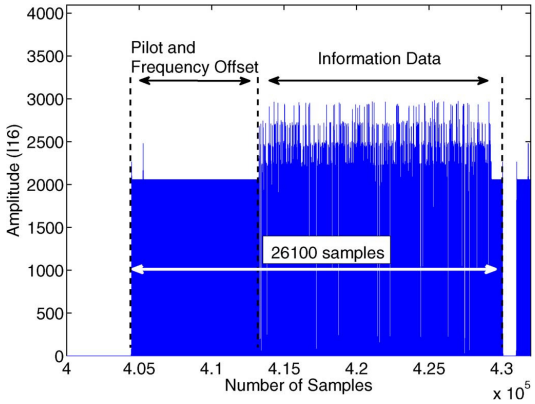

Fig. 6. Absolute value representation of a single frame from the vector being transmitted by Tx1 in the I16 data format, which is a signed 15-bit representation of an integer number.

where $\mathbf{y}$ is the $N_r \times 1$ received vector, $\mathbf{h}_{n_t}$ is the n_t column of the channel matrix $\mathbf{H}$, $\mathbf{n}$ is the $N_r \times 1$ AWGN vector with σ_n^2 variance and μ_n mean, and s_t is the transmitted symbol from the n_t antenna. As mentioned in Section II-B1, only a single transmit antenna is active when broadcasting the SNR sequence, and s_t is either equal to the maximum value in the "data section" $x_{\max}$ or zero, as shown in Fig. 5. Hence, the received signal in (4) can be rewritten as

$$\mathbf{y} = \begin{cases} \mathbf{h}_{n_t} x_{\max} + \mathbf{n}, & s_t = x_{\max} \\ \mathbf{n}, & s_t = 0. \end{cases} \tag{5}$$

Proceeding from (5)

$$E\left[\|\mathbf{Hx}\|_F^2\right] = E\left[\|\mathbf{y} - \mathbf{n}\|_F^2\right] \tag{6}$$

$$\sigma_n^2 = E\left[\|\mathbf{n}\|_F^2\right] - E\left[\|\mathbf{n}\|\right]^2 \tag{7}$$

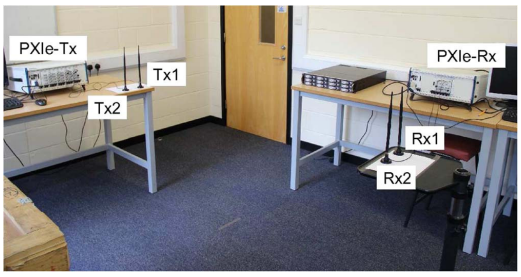

Fig. 7. Experimental setup in the laboratory.

where $[\cdot]^H$ is the Hermitian operation. As discussed in Section II-B1, each SNR sequence contains 50000 symbols and 50000 zero-valued symbols. Since the noise in the system represents an ergodic process, the ensemble average in (6) can be replaced with a time average, i.e.,

$$E\left[\|\mathbf{Hx}\|_F^2\right] = \sum_{i=1}^{50000} \left(\|\mathbf{y}_i\|_F^2 - \|\mathbf{n}_i\|_F^2 - 2\mathbf{y}_i^H \mathbf{n}_i\right) \tag{8}$$

$$\sigma_n^2 = \sum_{i=1}^{50000} \|\mathbf{n}_i\|_F^2 - \left[\sum_{i=1}^{50000} \|\mathbf{n}_i\|_F\right]^2 \tag{9}$$

where $\mathbf{y}_i$ and $\mathbf{n}_i$ are the ith received vector. To get a more accurate estimation, the SNR is calculated for the five transmitted SNR sequences that are received at both antennas and then averaged again over those measurements.

2.3 **Extract frames**: After finding the start of the transmission and calculating the SNR, the DSP-Rx performs a serial-to-parallel conversion to separate the received frames.

2.4 **Downsampling and filtering**: To complete the matched filter that is described in Section II-B1, each frame is downsampled by a factor of 4 and passed through an RRC-FIR filter.

2.5 **FO correction**: The DSP-Rx estimates the FO for each frame by

$$\Delta_f = \frac{\angle x_{1000} - \angle x_1}{2\pi \times 1000} \tag{10}$$

where $\angle x_{1000}, \angle x_1$ are the angles of the first and last samples of the FO sequence transmitted by the DSP-Tx, where the FO sequence has exactly 1000 symbols. These angle values are obtained by correcting the radian phase angles in a vector by adding multiples of $\pm 2\pi$ as required. This enables a better estimate of the phase offset. Assuming a linear phase rotation, the FO can be estimated using (10). The FO for each frame is then corrected by

$$\widetilde{y}_i = y_i \times e^{-j2\pi\Delta_f i} \tag{11}$$

where $\widetilde{y}_i$ and y_i are the ith elements of the corrected and uncorrected received frames, respectively.

2.6 **Channel estimation**: The channel estimation is done by using the LS channel estimation algorithm that is proposed in [35], where, for each frame, the channel is estimated by

$$\widetilde{\mathbf{H}}_{\mathrm{LS}} = \frac{1}{N_\Theta} \Theta^H \mathbf{H}_r \tag{12}$$

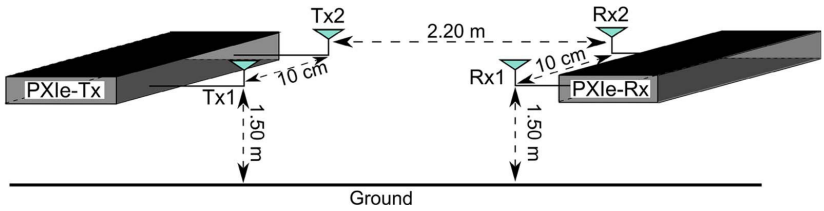

Fig. 8. Physical experimental layout. A pair of receive antennas and a pair of transmit antennas are set 2.2 m apart from each other with a direct LoS. Each pair of antennas is 1.5 m from the ground, and there is a 10-cm spacing between the antennas in either pair corresponding to 0.77 times the wavelength at 2.3 GHz. All antennas are omnidirectional.

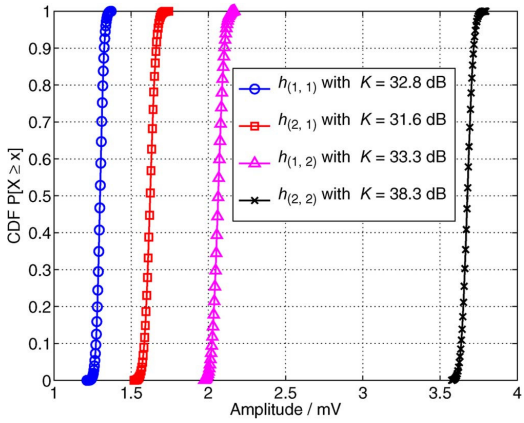

Fig. 9. CDFs for each of the fast-fading coefficients $h_{(r,n_t)}$ of the four channels in the experiment. Each is defined by a Rician distribution with a unique K-factor. (Markers) Measurement points. (Lines) Best-fit approximation. Note that the wireless channel mean values fall in the range of 1.3–3.6 mV.

where $\mathbf{H}_r$ is the received pilot sequence. To enable a more accurate evaluation of the system, the channel is estimated and averaged over ten pilot sequences. Furthermore, two channels are estimated per frame; the first channel estimate is used for the first half of the data symbols in the frame, and the second is used for the second half of the data symbols in the frame.

2.7 **Demodulation**: The ML optimum receiver for MIMO systems is used, which can be written as

$$\hat{\mathbf{x}}_t^{(\mathrm{ML})} = \arg\min_{\mathbf{x}\in\mathcal{Q}} \left\{ \|\mathbf{y} - \mathbf{H}\mathbf{x}\|_F^2 \right\} \tag{13}$$

where $\mathcal{Q}$ contains every possible $(N_t \times 1)$ transmit vector, and $\hat{\cdot}$ denotes the estimated transmission vector. However, since only one transmit antenna is active at a time for a SM system, the optimal receiver in (13) can be simplified to

$$\left[\hat{n}_t^{(\mathrm{ML})}, \hat{s}_t^{(\mathrm{ML})}\right] = \underset{\substack{n_t\in\{1,2,\ldots,N_t\}\\ s\in\{s_1,s_2,\ldots,s_M\}}}{\arg\min} \left\{ \sum_{r=1}^{N_r} \left| y_r - h_{(r,n_t)} s \right|^2 \right\} \tag{14}$$

where y_r is the rth entries of $\mathbf{y}$.

Finally, the recovered binary data, along with the estimated SNR, are used to obtain the ABER performance of both SM and SMX.

C. Propagation Environment (Channel)

The physical layout of the experimental setup is shown in Fig. 7, and the relative antenna spacing is provided in Fig. 8. In particular, the two transmit and two receive antennas are identical and are placed directly across from each other. As such, the channel between the transmitter and the receiver has a strong line-of-sight (LoS) component. Therefore, the channel is assumed to be a Rician fading channel with a large K-factor due to the short distance between the transmit and receive antennas, where K is the ratio of the coherent power component, which is usually the LoS, to the noncoherent power components, which is usually the NLoS. The omnidirectional transmit antennas broadcast on a frequency of 2.3 GHz at 10 Ms/s.

Channel measurements were collected to verify that the channel environment followed a Rician distribution. To achieve this, the transmitter broadcasts pulses at 10 Ms/s on a carrier frequency of 2.3 GHz at 4 dBm peak power. Each pulse includes a FO estimation section, and a total of 10^5 pulse samples are collected. A best-fit approximation is then calculated for the collected data. In particular, a maximum-likelihood estimation is fitted to the collected data. A Chi-squared goodness-of-fit test is then performed to ascertain that the distribution resulting from the maximum-likelihood estimation fits at least 95% of the data. The empirical cumulative density function (CDF) for each link is shown in Fig. 9. The results show that the channel does follow a Rician distribution with a K factor that ranges between 31–38 dB. The different K-factors on the links between the transmit and receive antennas may be explained by the room geometry, the antenna positioning, and the overall propagation environment. However, note that each of the CDFs has a different mean, which will be discussed in the next section.

III. Equipment Constraints

Fig. 8 shows the physical layout of the experiment. Note that the 10-cm interantenna separation that is used here is sufficient to guarantee very low, if any, spatial correlation when broadcasting at 2.3 GHz with a 2.2-m separation between the transmitter and the receiver [42].

The physical environment through which the signal passes, starting from the SG-RF at the transmitter until it reaches the 16-Bit Digitizers at the receiver, suffers from connector losses, differences in the RF chains, different phase responses, attenuations, and similar problems. To study and model the

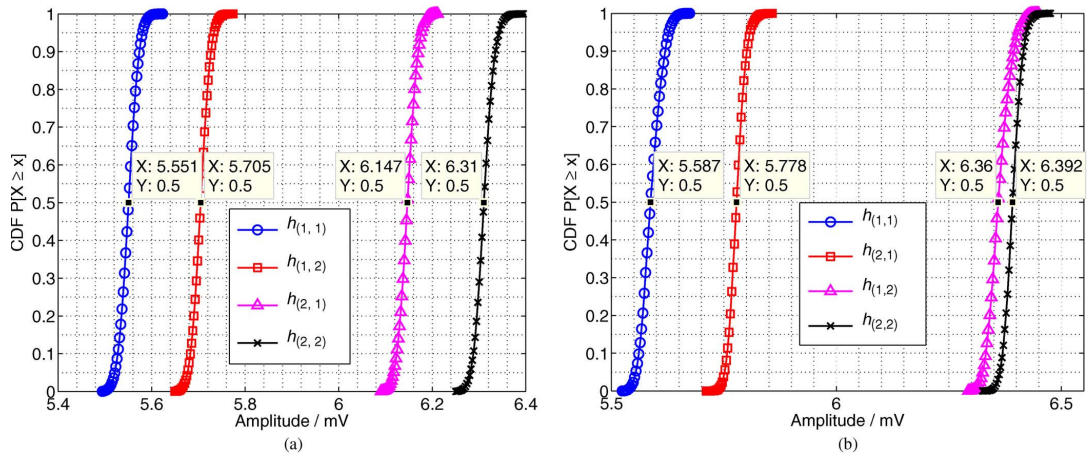

Fig. 10. CDFs for each of the fast-fading coefficients $h_{(r,n_t)}$ of the four channels in the experiment. Each is defined by a Rician distribution with a unique K-factor. (Markers) Measurement points. (Lines) Best-fit approximation. Despite using a coaxial cable with a 10 dB attenuation to connect the RF chains, each channel exhibits a unique mean. Configurations (a) (I) and (b) (II) of the receive RF chains.

effects of the hardware imperfections on the signal power, we have the following.

1) An RF coaxial cable with a 10 dB attenuation is connected between each transmit and receive antenna.
2) A pulse is transmitted at 10 Ms/s on a carrier frequency of 2.3 GHz at -10 dBm peak power. Each pulse includes an FO estimation section, and a total of 10^5 pulse samples were collected.
3) The CDF for each of the fading coefficients is calculated and is shown in Fig. 10.

In an ideal environment, the means of the CDFs in Fig. 10 should be equal. However, imperfections in the hardware result in different means for each transmit-to-receiver antenna pair, as shown in Fig. 10. The differences between the channels can be modeled as a PI between the various link pairs in the channel matrix $\mathbf{H}$. Therefore, the channel coefficients are redefined as

$$h^{\mathrm{PI}}_{(r,n_t)} = \sqrt{\alpha_{(r,n_t)}} \times h_{(r,n_t)} \tag{15}$$

where $\alpha_{(r,n_t)}$ is the channel attenuation coefficient from the receive antenna r to the transmit antenna n_t.

To locate the source of the discrepancy between the different channel attenuations, i.e., determine if the NI modules or the NI chassis are the source, the RF chains at the receiver were swapped around, and the channels were estimated in configurations (I) and (II). To clarify, configuration (I) represents the default modular setup of the testbed, whereas configuration (II) refers to swapping the front-end modules around the transmit chassis. Fig. 10(a) shows the channel CDF for each transmit-to-receive antenna pair in configuration (I), whereas Fig. 10(b) shows the channel CDF for each transmit-to-receive antenna pair in configuration (II). By considering the means of the CDFs in Fig. 10(a) and (b) and taking $h_{(1,1)}$ as a base, the various channel attenuations that result when the receiver is in configuration I or II are given in (16) and (17), shown at the bottom of the page, respectively. Comparing Fig. 10(a) and (b), as well as the attenuations in (16) to those in (17), shows that they are very similar. Indeed, the swapping of the RF chains has a minimal impact on the estimated mean of each channel attenuation. Thus, it can be assumed that the NI modules that compose the receive RF chains are the source of the hardware imperfections and consequently lead to the differences in the means of the estimated CDFs. To account for the hardware imperfections, the channel attenuation coefficients in (16) and (17) are taken into consideration in the derivation of the analytical model in Section IV. The accuracy of the derived analytical bound using the channel attenuation coefficients in the following is demonstrated in Section VI, where it is compared with empirical results.

IV. Analytical Modeling

An analytical model for the ABER performance of the experimental system is developed by considering the system model that is presented in Section II and the system constraints in Section III. The performance of SM and SMX over a single link in a noise-limited scenario is characterized by

$$\mathrm{ABER} \leq \frac{1}{2^m} \sum_{\mathbf{x}_t} \sum_{\mathbf{x}} \frac{N(\mathbf{x}_t, \mathbf{x})}{m} E_{\mathbf{H}} \left\{ \Pr_{\text{error}} \right\} \tag{18}$$

$$\alpha_{(1,1)} = 0 \text{ dB}, \quad \alpha_{(2,1)} = 0.25 \text{ dB}, \quad \alpha_{(1,2)} = 0.88 \text{ dB}, \quad \alpha_{(2,2)} = 1.1 \text{ dB} \tag{16}$$

$$\alpha_{(1,1)} = 0 \text{ dB}, \quad \alpha_{(2,1)} = 0.29 \text{ dB}, \quad \alpha_{(1,2)} = 1.13 \text{ dB}, \quad \alpha_{(2,2)} = 1.17 \text{ dB} \tag{17}$$

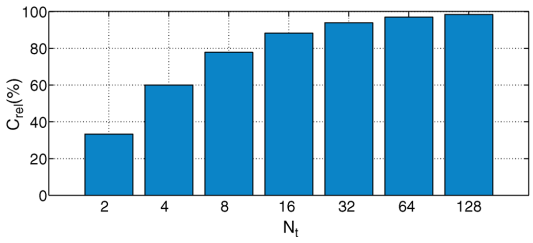

Fig. 11. Relative receiver complexity reduction of the SM-ML receiver versus the SMX-ML receiver.

where $N(\mathbf{x}_t, \mathbf{x})$ is the number of bits in error between the transmitted vector $\mathbf{x}_t$ and $\mathbf{x}$, $E_{\mathbf{H}}\{\cdot\}$ is the expectation across channel $\mathbf{H}$, and $\mathrm{Pr}_{\mathrm{error}}$ is the conditional pairwise error probability of deciding on $\mathbf{x}$ given that $\mathbf{x}_t$ is transmitted [43], i.e.,

$$\begin{aligned}\Pr_{\text{error}} &= \Pr\left(\|\mathbf{y}-\mathbf{H}\mathbf{x}_t\|_F^2 > \|\mathbf{y}-\mathbf{H}\mathbf{x}\|_F^2|\mathbf{H}\right)\\ &= Q\left(\sqrt{\gamma_{\text{ex}}\|\mathbf{H}(\mathbf{x}_t-\mathbf{x})\|_F^2}\right)\end{aligned} \tag{19}$$

where $\gamma_{\text{ex}} = (E_m/2N_0)$ is half of the SNR between the transmitter and the receiver, and $Q(\omega) = (1/\sqrt{2\pi})\int_{\omega}^{\infty}\exp(-(t^2/2))\,\mathrm{dt}$ is the Q-function. As shown in Fig. 8, the transmit and receive antennas in the experiment experience a very strong LoS environment. Accordingly, the channel between each transmit-to-receive antenna pair is characterized by Rician fading. A generic Rician channel is defined as

$$h_{(r,n_t)} = \sqrt{\frac{K}{1+K}} + \sqrt{\frac{1}{1+K}}\widetilde{h}_{(r,n_t)} \tag{20}$$

where $\widetilde{h}_{(r,n_t)} \sim \mathcal{CN}(0,1)$ is a complex normal circular symmetric random variable with zero mean and unit variance. $n_t \in \{1,2\}$ is the index of the transmit antenna, and $r \in \{1,2\}$ is the index of the receive antenna.

To account for the hardware imperfections that result from the PIs, the fast-fading-channel coefficients are redefined according to (15), (16), and (20). Section VI validates the derived analytical bound by comparing it to experimental and simulation results.

V. Complexity Analysis

The computational complexity of SM-ML is compared with that of the ML detector for SMX (SMX-ML). The complexity is computed as the number of real multiplicative operations $(\times, \div)$ needed by each algorithm. The detailed derivation of each expression is considered in [13] and references therein.

- SMX-ML: The computational complexity of the SMX-ML receiver that is outlined in (13) is equal to

$$\mathcal{C}_{\text{SMX}-\text{ML}} = 4(N_t+1)N_r 2^m \tag{21}$$

  where m is the spectral efficiency of the system. Note that $(|\mathbf{y}-\mathbf{H}\mathbf{x}|^2)$ in (13) requires (N_t+1) complex multiplications.

- SM-ML: The computational complexity of the SM-ML receiver that is outlined in (14) is equal to

$$\mathcal{C}_{\text{SM}-\text{ML}} = 8N_r 2^m \tag{22}$$

  where the ML detector searches through the entire transmit and receive search spaces. Note that evaluating the Euclidean distance $(|y_r - h_{(r,n_t)}s_t|^2)$ requires two complex multiplications, where each complex multiplication requires four real multiplications.

Considering (21) and (22), for the same spectral efficiency, the reduction in complexity of the SM-ML receiver relative to that of the SMX-ML receiver is given by

$$\mathcal{C}_{\text{rel}} = 100 \times \left(1 - \frac{2}{N_t+1}\right). \tag{23}$$

On one hand, as shown in (22), the complexity of the SM receiver does not depend on the number of transmit antennas, and it is equal to the complexity of SIMO systems. On the other hand, the complexity of SMX linearly increases with the number of transmit antennas. Therefore, as the number of transmit antennas increases, the relative gain of the SM receiver increases. This is shown in Fig. 11, where the relative complexity for $N_t \in \{2,4,8,\ldots,128\}$ is shown for both systems. In fact, Fig. 11 shows that, for $N_t = 4$, SM offers a 60% reduction in complexity, whereas a 98% reduction in complexity can be seen for $N_t = 128$. The theoretical, simulation, and empirical results for SM and SMX are now discussed.

VI. Experimental Results and Numerical Analysis

A. Measurement Campaign

A stream of 10^5 information bits is sent per transmission to obtain the experimental results. Two transmit antennas are available and binary phase-shift keying is used for the signal constellation. As mentioned in Section II-A2, the real flat bandwidth is 4 MHz. The information data are put in 50 frames with 2000 bits each, as shown in the "data section" in Fig. 5. The channel is estimated at the beginning and the end of every frame, resulting in 100 channel estimations per transmission vector. The experiment is repeated 1000 times for every SNR point. In addition, analytical and simulation ABER curves are shown for SM in a Rician environment with and without the PIs that are given in (16).

B. Results

The simulation, analytical, and experimental results for the ABER performance of SM in an LoS channel are shown in Fig. 12. In particular, the experimental results approximate the performance of the simulation results with PIs, and both the simulation and experimental results are closely approximated by the derived upper bound at a low ABER.

This result serves to validate the theoretical work that is done in the field where the presented SNR along the x-axis is equivalent to the SNR on $h_{(1,1)}$. The large error between the experimental, simulation, and analytical curves at high ABER can be attributed to a number of factors, including incorrect FO estimation, timing recovery errors, synchronization problems,

and poor channel estimation and decoding. Notably, incorrect FO estimation can result in a systematic error that is significantly contributing to the 30% error that are shown at low SNRs in the figure. As the SNR increases, however, FO estimation, timing recovery, and channel estimation improve, leading to a lower ABER, as shown in Fig. 12. Differences between the measured and simulated ABER curves can be attributed to channel imperfections such as channel correlations, mutual coupling, and interference signals from the surrounding environment. Quantifying these imperfections is deemed important and requires channel modeling and interference measurement. However, addressing these effects is beyond the scope of this paper and will be the subject of future works.

SM performs best in a rich scattering environment where the channel between each transmit and receive antenna is unique. In particular, the larger the Euclidean distance between two received vectors is, the better the ABER performance of SM becomes. Conversely, the more similar the channels are, the worse the ABER of SM is. However, the channel uniqueness can be the result of the scattering environment or PIs that are caused by hardware tolerances. The analytical and simulation results in Fig. 12 show the poor performance of SM in a Rician environment with no PI between the various transmitter-to-receiver links. Fig. 12 also shows the analytical and simulation ABERs for SM when PI are introduced. Indeed, the ABER of SM significantly improves when these PIs are introduced, as each channel becomes more separable. This increases the Euclidean distance and improves performance.

If the channels between each transmit antenna to each receive antenna are similar, then the ABER performance of SM degrades. This is seen when looking at the SM system without PIs, which is shown by the dashed green line with triangular markers in Fig. 12. In fact, the ABER of SM can be approximated by separating the error that originates from the estimation of the spatial-constellation symbol and the error that originates from the estimation of the signal-constellation symbol [44]. Therefore, depending on the environment, the main contributor to the overall ABER of a SM system will be the erroneous detection of the spatial or signal constellation.

When PIs are introduced, the Euclidean distance between the channel signatures increases. This decreases the error contribution of the spatial component of SM. Hence, when the SNR is sufficiently high to have near-perfect channel estimation, the error of the system is bounded by the error from the signal component of SM. This separation can be only shown when iterative detection is used, which is proven to be suboptimal [12]. In addition, in [45], it is shown that the error, when only the spatial constellation of SM is used for data transmission, gets worse for an increasing K factor in a Rician environment. This is the opposite of conventional modulation techniques since a larger K factor for SM means a smaller Euclidean distance between the spatial-constellation points, which results in an increased ABER performance. Indeed, it is the Euclidean distance between the different channels that determines the error in the spatial-constellation detection. However, since ML-optimal detection is used at the receiver, separating the error from the spatial and signal symbols is strictly not permitted. Please note that the PIs between the links are always obtained

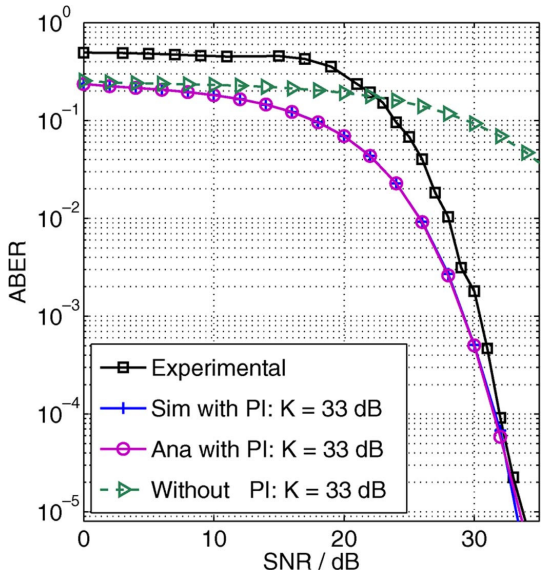

Fig. 12. ABER for SM in an experimental setup with two transmit antennas, two receive antennas, and a spectral efficiency of 2 bits/(s · Hz^{-1}). The SNR is set as measured on $h_{(1,1)}$ with $\alpha_{(1,1)} = 0$ dB. (Solid black line with square markers) Experimental results. (Green diamond markers) Simulation results with no PI between the links. (Green dashed line) Analytical prediction. The remaining curves denote the simulation (Sim) and analytical (Ana) results.

relative to the channel with the greatest attenuation, i.e., the values of the PI factors in (16) and (17) are always positive.

Furthermore, PIs between the transmitting antennas are shown to offer improved performance in terms of the ABER when only the spatial constellation of SM is used, i.e., when space shift keying (SSK) is the underlying modulation technique. In particular, an optimized power allocation for a various number of transmit antennas is addressed in [23], where the authors show that there is optimal power allocation between the transmitting antennas, which can serve to increases the Euclidean distance between the channel signatures and improve the ABER performance of SM. Indeed, SM has been also successfully applied to an AWGN optical wireless channel, where it is shown that PIs greatly improve the ABER performance [46].

The simulation, analytical, and experimental results for the ABER performance of SMX in a LoS channel are shown in Fig. 13. In particular, the experimental results closely follow the performance of the simulation results with PIs, and both the simulation and experimental results are closely approximated by the derived upper bound at low ABER when the hardware imperfections are taken into account. This result serves to validate the theoretical work that is done in the field. The results in Fig. 13 show that the SMX system, like the SM system, also benefits from the PIs in the hardware. The SMX system approximately exhibits a 3 dB coding gain when compared with SM at an ABER of 10^{-4}. This coding gain is also shown at an ABER of 10^{-3} in Fig. 14, where the simulation and analytical results for the ABER performance of SM and SMX are shown when there are no PIs between the links.

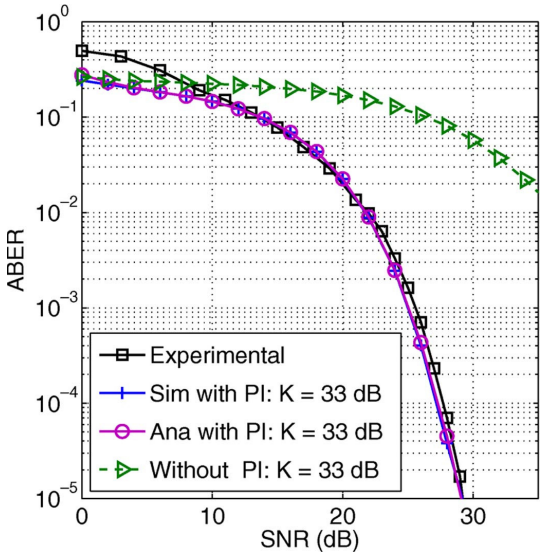

Fig. 13. ABER for SMX in an experimental setup with two transmit antennas, two receive antennas, and a spectral efficiency of 2 bits/(s · Hz^{-1}). The SNR is set as measured on $h_{(1,1)}$ with $\alpha_{(1,1)} = 0$ dB. (Solid black line with square markers) Experimental results. (Green diamond markers) Simulation results with no PI between the links. (Green dashed line) Analytical prediction. The remaining curves denote the simulation (Sim) and analytical (Ana) results.

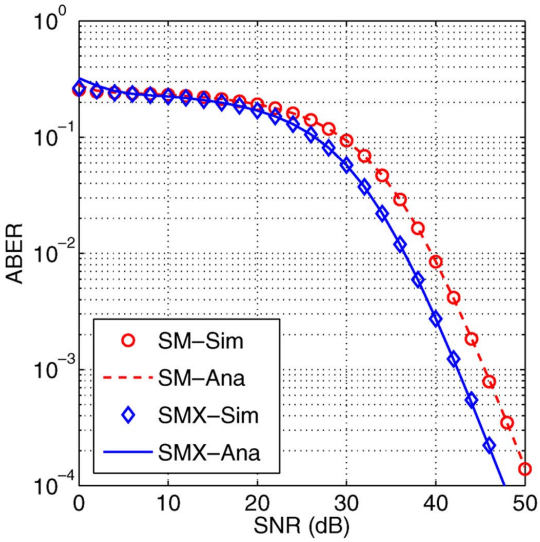

Fig. 14. ABER for SM and SMX in a Rician fading channel where $K = 33$ dB with two transmit antennas, two receive antennas, a spectral efficiency of 2 bits/(s · Hz^{-1}), and no PIs between the channels. (Markers) Simulation (Sim) and (lines) analytical (Ana) results.

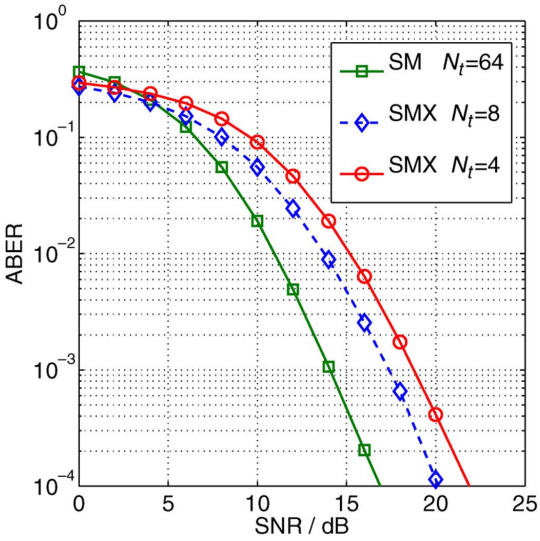

Fig. 15. Simulation results for the ABER for SM and SMX in a Rayleigh fading environment with a spectral efficiency of 8 bits/(s · Hz^{-1}) and no PIs between the channels.

The coding gain of SMX relative to SM is expected when there are few transmit antennas. The Euclidean distance between the transmit vectors and, therefore, the variance in (19) in SMX is larger than in SM. However, the aim of this paper is to show that empirical results validate the simulation and analytical works that are done in the field, which are shown in both Figs. 12 and 13. Unfortunately, due to the limited number of transmitter and receiver RF chains that are available, there are no experimental results for systems with a larger number of transmit or receive antennas where SM is shown to perform better than SMX. These empirical results will be the focus of future research. Nonetheless, the accuracy of the theoretical and simulation results of SMX and SM with a large number of transmit and receive antennas can be extrapolated from the presented results.

Fig. 15 compares the ABER between SM (see solid lines) and SMX (see dashed lines) in a system with a large number of transmit antennas. Each system operates in a Rayleigh fading environment with a spectral efficiency of 8 bits/(s · Hz^{-1}) and four receive antennas. The results demonstrate the coding gains available to a SM system, as compared with SMX when a large number of transmit antennas are available. In particular, SM with $N_t = 64$ offers a coding gain of up to 4 dB with respect to SMX with $N_t = 8$ and a coding gain of 6 dB with respect to SMX with $N_t = 4$. These performance gains stem from the greater Euclidean distance between the transmit vectors for SM. It is important to note that, although SM is simulated as having 64 transmit antennas available, it requires only a single RF chain, whereas SMX requires eight RF chains for the eight transmit antennas. Furthermore, to achieve the ABER performance that is shown in Fig. 15, SM requires 64 unique channels. In this paper, a unique channel is assumed to be available only with the addition of a single transmit antenna. However, the work in [6], [25], and others, look at creating multiple channel signatures without the need for a large number of physical transmit antennas while maintaining a similar ABER performance to the traditional SM scheme.

This paper demonstrates that the hardware tolerances of practical communication systems are beneficial for the ABER performance of both SM and SMX. This behavior, along with the requirement for a single RF chain, makes SM a viable candidate for future wireless networks.

VII. Summary and Conclusion

In this paper, the ABER performance of SM and SMX has been experimentally validated for the first time. In particular, the encoding and decoding processes have been presented. The experimental testbed, equipment, and channel conditions have been described in detail, and the ABERs of SM and SMX have been obtained in a practical testbed environment. In addition, the experimental results have been compared with both simulation and analytical approaches. As a result, it has been shown that a Rician channel with different channel attenuations closely describe the behavior of SM and SMX in the physical environment. Furthermore, it has been demonstrated that the different channel attenuations resulted from various hardware imperfections at the transmitter and receiver RF chains. In fact, the induced PIs resulted in significant coding gains for the practical systems that are relative to the theoretical predictions without such PIs. To this extent, SM and SMX performed as expected, relative to the theoretical work when the PIs have been introduced in the analytical model. This result validated the SM principle. The performance gains exhibited by SM in the practical implementation make SM a viable candidate for future wireless networks and, particularly, for systems with a large number of transmit antennas available.

It is worth noting that this paper may be extended in a number of different ways that would broaden its applicability. Empirical results that demonstrate the performance of SM and SMX with a large number of transmit and receive antennas remain to be obtained. In light of the aforementioned results, the ABER performance of SM and SMX is expected to follow the theoretical models, but these results are essential to validate the ABER performance for both SM and SMX systems. In addition, channel imperfections such as channel correlations and mutual antenna coupling, along with the impact of interfering signals from neighboring transmitters on the same frequency, should be analyzed. Furthermore, obtaining empirical results for the capacity and the energy efficiency of SM are of great interest for future research, particularly since SM is projected to have large energy efficiency gains when compared with other traditional MIMO schemes since it requires only a single RF chain. As a consequence, the quiescent power and circuit power can be kept at low levels. Acquiring the hardware, which would enable the accurate measurement of these aspects, is key. Finally, the implementation of the SM detection algorithm on a DSP or a field-programmable gate array (FPGA) brings with it a number of optimization challenges such as the use of multithreading, pipelining, fixed-point computations, and others. The deployment of SM on an FPGA or a DSP has yet to be demonstrated.

It has been shown that SM is a simple low-cost MIMO technique, which has now demonstrated excellent performance in an LoS wireless channel. Therefore, this paper has shown that SM is a promising practical approach to obtaining the enhanced performance of SMX without introducing high processor complexity and high power consumption that would occur when using other SMX approaches. The aim now is to investigate the performance of SM in a range of experimental channel conditions and further study its potential.

References

[1] E. Telatar, "Capacity of multi-antenna Gaussian channels," *Eur. Trans. Telecommun.*, vol. 10, no. 6, pp. 585–595, Nov./Dec. 1999.

[2] J. Mietzner, R. Schober, L. Lampe, W. H. Gerstacker, and P. A. Höeher, "Multiple-antenna techniques for wireless communications—A comprehensive literature survey," *IEEE Commun. Surveys Tuts.*, vol. 11, no. 2, pp. 87–105, Second Quart., 2009.

[3] R. Mesleh, H. Haas, Y. Lee, and S. Yun, "Interchannel interference avoidance in MIMO transmission by exploiting spatial information," in *Proc. 16th IEEE Int. Symp. PIMRC*, Berlin, Germany, 2005, vol. 1, pp. 141–145.

[4] R. Mesleh, H. Haas, S. Sinanovi, C. W. Ahn, and S. Yun, "Spatial modulation," *IEEE Trans. Veh. Technol.*, vol. 57, no. 4, pp. 2228–2241, Jul. 2008.

[5] N. Serafimovski, M. Di Renzo, S. Sinanovi, R. Y. Mesleh, and H. Haas, "Fractional bit encoded spatial modulation (FBE-SM)," *IEEE Commun. Lett.*, vol. 14, no. 5, pp. 429–431, May 2010.

[6] A. Younis, N. Serafimovski, R. Mesleh, and H. Haas, "Generalised spatial modulation," in *Proc. Asilomar Conf. Signals, Syst. Comput.*, Pacific Grove, CA, USA, Nov. 2010, pp. 1498–1502.

[7] J. Jeganathan, A. Ghrayeb, L. Szczecinski, and A. Ceron, "Space shift keying modulation for MIMO channels," *IEEE Trans. Wireless Commun.*, vol. 8, no. 7, pp. 3692–3703, Jul. 2009.

[8] G. Auer, V. Giannini, C. Desset, I. Godor, P. Skillermark, M. Olsson, M. Imran, D. Sabella, M. Gonzalez, O. Blume, and A. Fehske, "How much energy is needed to run a wireless network?" *IEEE Wireless Commun.*, vol. 18, no. 5, pp. 40–49, Oct. 2011.

[9] C. Desset, B. Debaillie, V. Giannini, A. Fehske, G. Auer, H. Holtkamp, W. Wajda, D. Sabella, F. Richter, M. J. Gonzalez, H. Klessig, I. Godor, M. Olsson, M. A. Imran, A. Ambrosy, and O. Blume, "Flexible power modeling of LTE base stations," in *Proc. IEEE WCNC*, Shanghai, China, Apr. 1–4, 2012, pp. 2858–2862.

[10] A. Stavridis, S. Sinanovi, M. D. Renzo, H. Haas, and P. Grant, "Energy saving base station employing spatial modulation," *Proc. IEEE 17th Int. Workshop CAMAD*, pp. 231–235, Sep. 17–19, 2012.

[11] A. Stavridis, S. Sinanovi, M. D. Renzo, and H. Haas, "A power saving dual-hop architecture based on hybrid spatial modulation," in *Conf. Rec. 46th ASILOMAR*, Nov. 4–7, 2012, pp. 1366–1370.

[12] J. Jeganathan, A. Ghrayeb, and L. Szczecinski, "Spatial modulation: Optimal detection and performance analysis," *IEEE Commun. Lett.*, vol. 12, no. 8, pp. 545–547, Aug. 2008.

[13] A. Younis, S. Sinanovic, M. Di. Renzo, R. Mesleh, and H. Haas, "Generalised sphere decoding for spatial modulation," *IEEE Trans. Commun.*, vol. 61, no. 7, pp. 2805–2815, Jul. 2013.

[14] A. Younis, R. Mesleh, H. Haas, and P. M. Grant, "Reduced complexity sphere decoder for spatial modulation detection receivers," in *Proc. IEEE GLOBECOM*, Miami, FL, USA, Dec. 2010, pp. 1–5.

[15] A. Younis, M. Di Renzo, R. Mesleh, and H. Haas, "Sphere decoding for spatial modulation," in *Proc. IEEE ICC*, Kyoto, Japan, 2011, pp. 1–6.

[16] R. Mesleh, M. Di Renzo, H. Haas, and P. M. Grant, "Trellis coded spatial modulation," *IEEE Trans. Wireless Commun.*, vol. 9, no. 7, pp. 2349–2361, Jul. 2010.

[17] M. Di Renzo and H. Haas, "A general framework for performance analysis of space shift keying (SSK) modulation for MISO correlated Nakagami-m fading channels," *IEEE Trans. Commun.*, vol. 58, no. 9, pp. 2590–2603, Sep. 2010.

[18] S. U. Hwang, S. Jeon, S. Lee, and J. Seo, "Soft-output ML detector for spatial modulation OFDM systems," *IEICE Electron. Exp.*, vol. 6, no. 19, pp. 1426–1431, Oct. 2009.

[19] M. Di Renzo and H. Haas, "Space shift keying (SSK) modulation with partial channel state information: Optimal detector and performance analysis over fading channels," *IEEE Trans. Commun.*, vol. 58, no. 11, pp. 3196–3210, Nov. 2010.

[20] S. S. Ikki and R. Mesleh, "A general framework for performance analysis of space shift keying (SSK) modulation in the presence of Gaussian imperfect estimations," *IEEE Commun. Lett.*, vol. 16, no. 2, pp. 228–230, Feb. 2012.

[21] E. Basar, U. Aygolu, E. Panayirci, and H. V. Poor, "Performance of spatial modulation in the presence of channel estimation errors," *IEEE Commun. Lett.*, vol. 16, no. 2, pp. 176–179, Feb. 2012.

[22] M. D. Renzo, D. D. Leonardis, F. Graziosi, and H. Haas, "Space shift keying (SSK) MIMO with practical channel estimates," *IEEE Trans. Commun.*, vol. 60, no. 4, pp. 998–1012, Apr. 2012.

[23] M. Di Renzo and H. Haas, "Improving the performance of space shift keying (SSK) modulation via opportunistic power allocation," *IEEE Commun. Lett.*, vol. 14, no. 6, pp. 500–502, Jun. 2010.

[24] T. Handte, A. Muller, and J. Speidel, "BER analysis and optimization of generalized spatial modulation in correlated fading channels," in *Proc. IEEE VTC Fall*, Anchorage, AK, USA, Sep. 20–23, 2009, pp. 1–5.

[25] E. Basar, U. Aygolu, E. Panayirci, and V. H. Poor, "Space-time block coded spatial modulation," *IEEE Trans. Commun.*, vol. 59, no. 3, pp. 823–832, Mar. 2011.

[26] M. Di Renzo and H. Haas, "On transmit-diversity for spatial modulation MIMO: Impact of spatial-constellation diagram and shaping filters at the transmitter," *IEEE Trans. Veh. Technol.*, vol. 62, no. 6, pp. 2507–2531, Jul. 2013.

[27] N. Serafimovski, S. Sinanovic, M. Di Renzo, and H. Haas, "Dual-hop spatial modulation (Dh-SM)," in *Proc. IEEE VTC Spring*, Budapest, Hungary, May 15–18, 2011, pp. 1–5.

[28] A. Stavridis, S. Sinanovi, M. D. Renzo, and H. Haas, "Energy evaluation of spatial modulation at a multi-antenna base station," in *Proc. 78th IEEE VTC*, Las Vegas, NV, USA, Sep. 2–5, 2013.

[29] M. Di Renzo and H. Haas, "Bit error probability of spatial modulation (SM) MIMO over generalized fading channels," *IEEE Trans. Veh. Technol.*, vol. 61, no. 3, pp. 1124–1144, Mar. 2012.

[30] A. Younis, W. Thompson, M. D. Renzo, C.-X. Wang, M. A. Beach, H. Haas, and P. M. Grant, "Performance of spatial modulation using measured real-world channels," in *Proc. 78th IEEE VTC*, Las Vegas, NV, USA, Sep. 2–5, 2013.

[31] M. Di Renzo, H. Haas, and P. M. Grant, "Spatial modulation for multiple-antenna wireless systems: A survey," *IEEE Commun. Mag*, vol. 49, no. 12, pp. 182–191, Dec. 2011.

[32] "16-Bit IF Digitizer with Onboard Signal Processing," *NI PXIe-5622 Specifications*, National Instruments, 2011.

[33] P. Chambers, X. Hong, Z. Chen, C.-X. Wang, M. Beach, and H. Haas, "The UC4G wireless MIMO testbed," in *Proc. IEEE GLOBECOM*, Anaheim, CA, USA, Dec. 3–7, 2012, pp. 4368–4373.

[34] G. J. Foschini, "Layered space–time architecture for wireless communication in a fading environment when using multi-element antennas," *Bell Labs Tech. J.*, vol. 1, no. 2, pp. 41–59, 1996.

[35] S. Tiiro, J. Ylioinas, M. Myllyla, and M. Juntti, "Implementation of the least squares channel estimation algorithm for MIMO-OFDM systems," in *Proc. Int. ITG WSA*, Berlin, Germany, 2009.

[36] L. Lo Presti and M. Mondin, "Design of optimal FIR raised-cosine filters," *Electron. Lett.*, vol. 25, no. 7, pp. 467–468, Mar. 1989.

[37] J. L. Massey, "Optimum frame synchronization," *IEEE Trans. Commun.*, vol. 20, no. 2, pp. 115–119, Apr. 1972.

[38] H. Xuefei and C. Jie, "Implementation frame synchronization for MIMO-OFDM system with ZCZ-codes," in *Proc. IEEE Int. Symp. MAPE*, 2005, vol. 1, pp. 241–244.

[39] J.-J. van de Beek, M. Sandell, M. Isaksson, and P. Ola Borjesson, "Low-complex frame synchronization in OFDM systems," in *Proc. IEEE Int. Conf. Universal Pers. Commun.*, Tokyo, Japan, Nov. 6–10, 1995, pp. 982–986.

[40] H. Hashemi, "The indoor radio propagation channel," *Proc. IEEE*, vol. 81, no. 7, pp. 943–968, Jul. 1993.

[41] D. McNamara, M. Beach, and P. Fletcher, "Experimental investigation of the temporal variation of MIMO channels," in *Proc. IEEE 54th VTC Fall*, Atlantic City, NJ, USA, 2001, vol. 2, pp. 1063–1067.

[42] F. Quitin, C. Oestges, F. Horlin, and P. D. Doncker, "Multipolarized MIMO channel characteristics: analytical study and experimental results," *IEEE Trans. Antennas Propag.*, vol. 57, no. 9, pp. 2739–2745, Sep. 2009.

[43] M. D. Renzo and H. Haas, "Performance analysis of spatial modulation," in *Proc. Int. ICST Conf. CHINACOM*, Aug. 2010, pp. 1–7.

[44] M. Di Renzo and H. Haas, "Bit error probability of space modulation over Nakagami-m fading: Asymptotic analysis," *IEEE Commun. Lett.*, vol. 15, no. 10, pp. 1026–1028, Oct. 2011.

[45] M. D. Renzo and H. Haas, "Space shift keying (SSK-) MIMO over correlated Rician fading channels: Performance analysis and a new method for transmit-diversity," *IEEE Trans. Commun.*, vol. 59, no. 1, pp. 116–129, Jan. 2011.

[46] T. Fath, H. Haas, M. Di Renzo, and R. Mesleh, "Spatial modulation applied to optical wireless communications in indoor LOS environments," in *Proc. IEEE GLOBECOM*, Houston, TX, USA, 2011, pp. 1–5.

Nikola Serafimovski received the B.Sc. degree in electrical engineering and computer science and the M.Sc. degree in communications, systems, and electronics from Jacobs University, Bremen, Germany, in 2007 and 2009, respectively, and the Ph.D. degree from The University of Edinburgh, Edinburgh, U.K., where the focus of his research was on multiple-input multiple-output systems and the practical implementation of spatial modulation.

He is currently a Communication Systems Engineer with pureVLC Ltd, Edinburgh, U.K.

Abdelhamid Younis received the B.Sc. degree in electrical and electronic engineering (with honors) in 2007 from the University of Benghazi, Benghazi, Libya, and the M.Sc. degree in signal processing and communication engineering (with distinction) in 2009 from The University of Edinburgh, Edinburgh, U.K., where he is currently working toward the Ph.D. degree in communication engineering in the Institute of Digital Communications.

His main research interests are in the area of wireless communication and digital signal processing with a particular focus on spatial modulation, multiple-input multiple-output (MIMO) wireless communications, reduced complexity MIMO design, and optical wireless communications.

Mr. Younis received the Overseas Research Student Award in 2010 in recognition of his work.

Raed Mesleh (S'00–M'08–SM'13) received the Ph.D. degree in electrical engineering from Jacobs University, Bremen, Germany.

He had several years of postdoctoral wireless-communication and optical-wireless-communication research experience in Germany. Since October 2010, he has been with the University of Tabuk, Tabuk, Saudi Arabia, where he is currently an Assistant Professor and the Director of the research excellence unit. Since 2007, his publications have received more than 800 citations. He has published more than 50 publications in top-tier journals and conferences. He is the holder of seven granted patents. His main research interests are in spatial modulation, multiple-input multiple-output cooperative wireless communication techniques, and optical wireless communication.

Dr. Mesleh serves on the Technical Program Committee for academic conferences and is a regular reviewer for most of the journals of the IEEE/Optical Society of America (OSA) Communication Society and the IEEE/OSA Photonics Society.

P. Chambers received the B.Sc. degree in physics and physics technology and the Ph.D. degree in transmission line and wireless communications from the Dublin Institute of Technology, Dublin, Ireland, in 2002 and 2008, respectively.

From to 2009 to 2010, he worked as a Postdoctoral Researcher with Université Catholique de Louvain, Louvain-la-Neuve, Belgium. Then, he worked as a Research Associate on the U.K.-China Science Bridges: Research and Development on Beyond Fourth-Generation Wireless Mobile Communications (UC4G) Project. From 2010 to 2013, he was with the Defence Science and Technology Laboratory, Heriot-Watt University, Edinburgh, U.K., working on on the development of cognitive radio algorithms. He is currently a Research Associate with the University of Surrey, Surrey, U.K., where he is working on fifth-generation communications standards as part of the Low-Electromagnetic-Field Exposure Network (LexNet) Project Team.

Marco Di Renzo (S'05–AM'07–M'09) was born in L'Aquila, Italy, in 1978. He received the Laurea (*cum laude*) and Ph.D. degrees in electrical and information engineering from the University of L'Aquila, Coppito, Italy, in 2003 and 2007, respectively.

From August 2002 to January 2008, he was with the Center of Excellence for Research "Design Methodologies of Embedded Controllers, Wireless Interconnect and Systems-on-chip (DEWS)," University of L'Aquila. From February 2008 to April 2009, he was a Research Associate with the Telecommunications Technological Center of Catalonia (CTTC), Barcelona, Spain. From May 2009 to December 2009, he was an Engineering and Physical Sciences Research Council Research Fellow with the Institute for Digital Communications, The University of Edinburgh, Edinburgh, U.K. Since January 2010, he has been a Tenured Researcher ("Chargé de Recherche Titulaire") with the French National Center for Scientific Research (CNRS), as well as a Faculty Member with the Laboratory of Signals and Systems, a joint research laboratory of the CNRS, the École Supérieure d' Électricité, and the University of Paris-Sud XI, Paris, France. His main research interests are in the area of wireless communications theory. He is a Principal Investigator of three European-funded research projects (Marie Curie ITN-GREENET, Marie Curie IAPP-WSN4QoL, and Marie Curie ITN-CROSSFIRE).

Dr. Di Renzo received the Special Mention for the Outstanding Five-Year (1997–2003) Academic Career, University of L'Aquila; the Thales Communications fellowship for doctoral studies (2003–2006), University of L'Aquila; the Best Spinoff Company Award (2004), Abruzzo Region, Italy; the Torres Quevedo award for research on ultrawideband systems and cooperative localization for wireless networks (2008–2009), Ministry of Science and Innovation, Spain; the "Dérogation pour l'Encadrement de Thèse" (2010), University of Paris-Sud XI, France; the 2012 IEEE International Workshop on Computer-Aided Modeling Analysis and Design of Communication Links and Networks Best Paper Award from the IEEE Communications Society; and the 2012 Exemplary Reviewer Award from the IEEE WIRELESS COMMUNICATIONS LETTERS of the IEEE Communications Society. He currently serves as an Editor of the IEEE COMMUNICATIONS LETTERS.

Cheng-Xiang Wang (S'01–M'05–SM'08) received the B.Sc. and M.Eng. degrees in communication and information systems from Shandong University, Jinan, China, in 1997 and 2000, respectively, and the Ph.D. degree in wireless communications from Aalborg University, Aalborg, Denmark, in 2004.

Since 2005, he has been with Heriot-Watt University, Edinburgh, U.K., where he was first a Lecturer, then a Reader in 2009, and has been a Professor since 2011. He is also an Honorary Fellow with The University of Edinburgh, U.K., and a Chair/Guest Professor with Shandong University, Huazhong University of Science and Technology, Wuhan, China, and the Southeast University, Nanjing, China. He was a Research Fellow with the University of Agder, Grimstad, Norway, from 2001 to 2005, a Visiting Researcher with Siemens AG-Mobile Phones, Munich, Germany, in 2004, and a Research Assistant with the Technical University of Hamburg-Harburg, Hamburg, Germany, from 2000 to 2001. He has published one book chapter and over 180 papers in refereed journals and conference proceedings. His current research interests include wireless channel modeling and simulation, green communications, cognitive radio networks, vehicular communication networks, large multiple-input multiple-output (MIMO), cooperative MIMO, and Beyond Fourth-Generation wireless communications.

Prof. Wang served or is currently serving as an editor for eight international journals, including the IEEE TRANSACTIONS ON VEHICULAR TECHNOLOGY (2011 to present) and the IEEE TRANSACTIONS ON WIRELESS COMMUNICATIONS (2007–2009). He was the Guest Editor for the IEEE JOURNAL ON SELECTED AREAS IN COMMUNICATIONS, Special Issue on Vehicular Communications and Networks and Special Issue on Spectrum and Energy Efficient Design of Wireless Communication Networks. He served or is serving as a Technical Program Committee (TPC) member, the TPC Chair, and the General Chair for over 70 international conferences. He received the Best Paper Awards from the IEEE Global Communications Conference in 2010, the IEEE International Conference on Communication Technology in 2011, and The 12th International Conference on ITS Telecommunications (ITST 2012). He is a Fellow of the Institution of Engineering and Technology, a Fellow of the Higher Education Academy, and a member of the Engineering and Physical Sciences Research Council Peer-Review College.

Peter M. Grant (M'77–SM'83–F'96) was born in St. Andrews, U.K. He received the B.Sc. degree in electronic engineering from the Heriot-Watt University, Edinburgh, U.K., in 1966, the Ph.D. degree from The University of Edinburgh in 1975, and honorary D.Eng. degrees from the Heriot-Watt University in 2006 and from Napier University, Edinburgh, in 2007.

He worked in radio communications with the Plessey Company. He was then appointed to a research fellowship with The University of Edinburgh, where he was subsequently promoted to a Full Professor of electronic signal processing and a Departmental Chair. From 2002 to 2008, he served as the Head of the School of Engineering and Electronics, Edinburgh. During the academic year 1977–1978, he was a Visiting Professor with the Ginzton Laboratory, Stanford University, Stanford, CA, USA, and from 1985 to 1986, he was a Visiting Staff Member with the Lincoln Laboratory, Massachusetts Institute of Technology, Lexington, MA, USA.

Prof. Grant received the 82nd Faraday Medal from the Institution of Electrical Engineers (IEE) for his work on code-division multiple-access receiver designs and adaptive filters in 2004, the Bulgin premium in 1974 and 1977 and the Lord Mountbatten premium in 1982 from the then Institution of Electronic and Radio Engineers, and both the IEE Marconi and Langham Thompson premia in 1994. From 1980 to 1996, he served as an Honorary Editor of the IEE Proceedings entitled "Vision Image and Signal Processing." He was a member in 1992 and 1996 and the Chair of the 2001 Universities Funding Council research assessment panel for the U.K. Electrical Engineering Departments. He was the Technical Program Chairman for the International Conference on Acoustics, Speech, and Signal Processing in 1989, the Chairman of the European Signal Processing Conference in 1994, and the President of the European Association for Signal Processing (EURASIP) from 2000 to 2002. In 1998, he was appointed by the IEEE Signal Processing Society as a Distinguished Lecturer on digital signal processing for mobile communications. He served as the Director of the Virtual Centre of Excellence In Mobile and Personal Communications Limited from 2007 to 2009. In 2007, he was appointed to be the Eighth Regius Professor of Engineering with The University of Edinburgh. In 2009, he was made an Officer of the Order of the British Empire in the Queen's birthday honors list. He holds fellowships of the Institution of Engineering and Technology, the Royal Academy of Engineering, and the Royal Society of Edinburgh.

Mark A. Beach received the Ph.D. degree from the University of Bristol, Bristol, U.K., in 1987.

He was a Research Assistant from September 1987 to July 1989, a Lecturer from August 1989 to July 1996, a Senior Lecturer from August 1996 to July 1998, a Reader in communication systems from August 1998 to July 2003, the Head of the Department of Electrical and Electronic Engineering from August 2006 to July 2010, and has been a Professor of radio systems engineering since August 2003 with the University of Bristol.

Harald Haas (S'98–A'00–M'03) received the Ph.D. degree from The University of Edinburgh, Edinburgh, U.K., in 2001.

He is the Chair of Mobile Communications with the Institute for Digital Communications, The University of Edinburgh, and he is currently the chief technical officer of a university spinout company pureVLC Ltd. He is the holder of 23 patents. He has published more than 60 journal papers, including a *Science* article and more than 160 peer-reviewed conference papers. Nine of his papers are invited papers. He has coauthored a book entitled *Next Generation Mobile Access Technologies: Implementing TDD* (Cambridge University Press). Since 2007, he has been a Regular High-Level Visiting Scientist supported by the Chinese 111-program with Beijing University of Posts and Telecommunications, Beijing, China. He was an invited speaker at the Technology, Entertainment, Design Global Conference in 2011. His main research interests are in interference coordination in wireless networks, spatial modulation, and optical wireless communication.

Prof. Haas received a prestigious Fellowship of the Engineering and Physical Sciences Research Council, U.K. His work on optical wireless communication was listed among the "50 Best Inventions in 2011" in Time Magazine.

This full text paper was peer reviewed at the direction of IEEE Communications Society subject matter experts for publication in the IEEE ICC 2011 proceedings

Sphere Decoding for Spatial Modulation

Abdelhamid Younis[(1)], Marco Di Renzo[(2)], Raed Mesleh[(3)], and Harald Haas[(1)]
[(1)] *Institute for Digital Communications, Joint Research Institute for Signal and Image Processing*
The University of Edinburgh , Edinburgh EH9 3JL, UK
[(2)] *L2S, UMR 8506 CNRS – SUPELEC – Univ Paris–Sud*
Laboratory of Signals and Systems (L2S), French National Center for Scientific Research (CNRS)
École Supérieure d'Électricité (SUPÉLEC), University of Paris–Sud XI (UPS)
3 rue Joliot–Curie, 91192 Gif–sur–Yvette (Paris), France
[(3)] *University of Tabuk, Electrical Engineering Department,*
P.O.Box: 741, 71491 Tabuk, Saudi Arabia,
E–Mail: {a.younis, h.haas}@ed.ac.uk, marco.direnzo@lss.supelec.fr, raed.mesleh@ieee.org

***Abstract*—In this paper, Sphere Decoding (SD) algorithms for Spatial Modulation (SM) are developed to reduce the computational complexity of Maximum–Likelihood (ML–) optimum detectors, which have a complexity that linearly increases with the product of number of transmit–antenna, receive–antenna, and size of the modulation scheme. Three SDs specifically designed for SM are proposed and analysed in terms of Bit Error Probability (BEP) and computational complexity. By judiciously choosing some key parameters, *e.g.*, the radius of the sphere centered around the received signal, it is shown that the proposed algorithms offer the same BEP as ML–optimum detection, with a significant reduction of the computational complexity. Also, it is shown that none of the proposed SDs is always superior to the others, but the best SD to use depends on the system setup, *i.e.*, the number of transmit–antenna, receive–antenna, and the size of the modulation scheme. The computational complexity trade–off offered by the proposed solutions is studied via analysis and simulation, and numerical results are shown to validate our findings.**

***Index Terms*—Multiple–Input–Multiple–Output (MIMO) Systems, Spatial Modulation (SM), Sphere Decoding (SD).**

I. Introduction

Spatial Modulation (SM) is a recently proposed transmission technology for Multiple–Input–Multiple–Output (MIMO) wireless systems, which has been originally proposed to increase the spectral efficiency of single–antenna systems by avoiding Inter–Channel Interference (ICI) [1]. This is attained through the adoption of a new modulation and coding scheme, which foresees: i) the activation, at each time instance, of a single antenna that transmits a given data symbol (*constellation symbol*), and ii) the exploitation of the spatial position (index) of the active antenna as an additional dimension for data transmission (*spatial symbol*). Both *constellation symbol* and *spatial symbol* depend on the incoming data bits. Thereby, an overall increase, by the base–two logarithm of the number of transmit–antenna, of the spectral efficiency is achieved, while still retaining a complexity comparable to single–antenna systems.

In particular, at the receiver the Maximum Likelihood (ML) optimum decoder is a simple single–stream detector, which performs an exhaustive search over the whole *constellation symbol* and *spatial symbol* space, and whose computational complexity ($\mathcal{C}$) linearly increases with the product of transmit–antenna (N_t), receive–antenna (N_r), and size of the modulation scheme (M), *i.e.*, $\mathcal{C} \propto MN_tN_r$ [2]. Unlike other spatial multiplexing schemes for MIMO systems, such as the V–BLAST (Vertical Bell Laboratories Layered Space–Time) [3], [4], there is a substantial reduction in receiver complexity, as no multi–stream detectors with exponential–growing complexity with N_t are required. In addition to this significant complexity reduction, SM also outperforms many conventional single–antenna and multi–antenna wireless systems [1], [5], thus potentially being an appealing transmission concept for the next generation of wireless systems.

In spite of its low–complexity implementation and superior performance results, there still is potential for further computational complexity reductions, especially when: i) high spectral efficiencies are required (*i.e.*, the product MN_t is large), or ii) high diversity gains and, thus, low error probabilities, are needed (*i.e.*, N_r is large). Furthermore, complexity issues become even more pressing when both MN_t and N_r are large. Motivated by these considerations, some recent research works have focused on developing low–complexity detectors for SM. For example, in [1] and [6] two sub–optimal two–step detectors based on heuristics are proposed. However, in [2] it is shown that the detector in [1] belongs to the family of non–exact methods, and in general it is a few dB worse than the ML–optimum detector. On the other hand, in [7] an exact low–complexity detector for SM has been proposed, which is based on the Sphere Decoding (SD) algorithm [8]. Therein, it is shown that the proposed solution has a computational complexity that is bounded by $8MN_t \leq \mathcal{C} \leq 8MN_tN_r$, and it provides an error performance very close to the ML–optimum detector. This SD–based detector is especially suitable when the number of receive–antenna N_r is very large, as it reduces the size of the search space related to the multiple antennas at the receiver (we denote this search space as "receive search space"). However, it has two main limitations: i) it does not reduce the dimension of the search space due to the number, N_t, of transmit–antenna and the size, M, of the signal modulation diagram (we denote this search space as "transmit search space"), which prevents the detector from achieving a significant reduction in computational complexity when high data rates are required (*i.e.*, when both N_t and M are large), and ii) the detector has the same complexity as the ML–optimum decoder when $N_r = 1$. In general, the reduction

978-1-61284-233-2/11/$26.00 ©2011 IEEE

This full text paper was peer reviewed at the direction of IEEE Communications Society subject matter experts for publication in the IEEE ICC 2011 proceedings

in decoding complexity is not very high when N_r is small, as often happens in the downlink of cellular systems. The detector in [7] is here called Receiver–centric SD (Rx–SD).

Motivated by these considerations, in this paper we move from the results in [7] and propose two new low–complexity detectors for SM, which are based on the SD principle. The first solution aims at reducing the "transmit search space", and, thus, can be seen as a complementary solution to [7]. In particular, as opposed to [7], the proposed decoder is suitable when either N_t or M, or both N_t and M are large. On the other hand, it keeps the "receive search space" the same as the original ML–optimum decoder. This detector is called Transmitter–centric SD (Tx–SD). On the other hand, the second solution combines both Rx–SD and Tx–SD with the aim of reducing the complexity of the ML–optimum receiver in both the receive and transmit search spaces. This detector is called Combined–SD (C–SD). More specifically, the Tx–SD detector is based on a simplified implementation of the conventional SD proposed in [8], which exploits the peculiar property of SM that only a single antenna is active at any time instance. Due to space constraints, in this paper we focus on the so–called non–underdetermined MIMO setup with $N_t \leq N_r$. In the recent period, some efficient SD methods for the underdetermined MIMO setup have been proposed (see, *e.g.*, [9], [10] and references therein). However, the analysis of this setup for SM is postponed to a future research contribution.

In this paper, we provide a careful study of the performance of these three detectors, along with an accurate comparison of their computational complexity. Numerical results show that the proposed solutions provide a substantial reduction in computational complexity with respect to the ML–optimum detector, and no loss in the Bit Error Probability (BEP). Furthermore, it is shown that the Rx–SD is less complex than the C–SD when M is not very large, while the C–SD is the best solution when either M is large or N_r is small.

The reminder of this paper is organised as follows. In Section II, the system model along with the ML–optimum and Rx–SD detectors are summarised. In Section III, the new Tx–SD and C–SD receivers are described. In Section IV, an accurate analysis of the computational complexity of Tx–SD and C–SD is performed. In Section V, some numerical results are shown to compare the proposed receivers. Finally, Section VI concludes the paper.

II. System Model

A. SM Modulator

SM works as follows [1]. The bitstream emitted by a binary source is divided into blocks containing $\log_2(N_t) + \log_2(M)$ bits each, with $\log_2(N_t)$ and $\log_2(M)$ being the number of bits needed to identify the *spatial symbol* and the *constellation symbol*, respectively. Each block is split into two sub–blocks of $\log_2(N_t)$ and $\log_2(M)$ bits each, and the following mapping rule is used:

- The bits in the first sub–block are used to select the antenna that is switched on for data transmission, while all the other transmit–antenna are kept silent. In this paper, the actual transmit–antenna that is active for transmission is denoted by ℓ_t, with $\ell_t \in \{1, 2, \ldots, N_t\}$.
- The bits in the second sub–block are used to choose a symbol in the signal–constellation diagram. Without loss of generality, Quadrature Amplitude Modulation (QAM) is considered. In this paper, the actual complex symbol emitted by the transmit–antenna ℓ_t is denoted by s_t, with $s_t \in \{s_1, s_2, \ldots, s_M\}$.

Accordingly, the $N_t \times 1$ transmitted vector is:

$$\mathbf{x}_{\ell_t, s_t} = \left[\mathbf{0}_{1\times(\ell_t-1)}, s_t, \mathbf{0}_{1\times(N_t-\ell_t)}\right]^T \tag{1}$$

where $[\cdot]^T$ denotes transpose operation, and $\mathbf{0}_{p\times q}$ is a $p \times q$ matrix with all–zero entries.

B. Channel Model

The modulated vector, $\mathbf{x}_{\ell_t, s_t}$, in (1) is transmitted through a frequency–flat $N_r \times N_t$ MIMO fading channel with transfer function $\mathbf{H}$. In this paper, a Rayleigh fading channel model is assumed, and, thus, the entries of $\mathbf{H}$ are modeled as complex independent and identically distributed (i.i.d.) Gaussian random variables with zero–mean and unit–variance. Moreover, a perfect channel state information (CSI) at the receiver is assumed, with no CSI at the transmitter.

Thus, the $N_r \times 1$ received vector can be written as follows:

$$\mathbf{y} = \mathbf{H}\mathbf{x}_{\ell_t, s_t} + \mathbf{n} \tag{2}$$

where $\mathbf{n}$ is the N_r–dimensional Additive White Gaussian Noise (AWGN) with zero–mean and variance σ^2 per dimension at the receiver input.

From (1), (2) simplifies as follows:

$$\mathbf{y} = \mathbf{h}_{\ell_t} s_t + \mathbf{n} \tag{3}$$

where $\mathbf{h}_{\ell_t}$ is the ℓ_t–th column of $\mathbf{H}$.

C. ML–Optimum Detector

The optimum detector based on the ML principle has been derived in [2]:

$$\begin{aligned}\left[\hat{\ell}_t^{(\mathrm{ML})}, \hat{s}_t^{(\mathrm{ML})}\right] &= \underset{\substack{\ell\in\{1,2,\ldots N_t\}\\ s\in\{s_1,s_2,\ldots s_M\}}}{\arg\min} \left\{\|\mathbf{y} - \mathbf{h}_\ell s\|_{\mathrm{F}}^2\right\} \\ &= \underset{\substack{\ell\in\{1,2,\ldots N_t\}\\ s\in\{s_1,s_2,\ldots s_M\}}}{\arg\min} \left\{\sum_{r=1}^{N_r} |y_r - h_{\ell,r} s|^2\right\}\end{aligned} \tag{4}$$

where $\|\cdot\|_{\mathrm{F}}^2$ is the Frobenius norm, $\hat{\cdot}$ identifies the estimated spatial and constellation symbols, and y_r and $h_{\ell,r}$ is the r–th entry of $\mathbf{y}$ and $\mathbf{h}_\ell$, respectively.

The computational complexity of (4), in terms of real multiplications, is equal to:

$$\mathcal{C}_{\mathrm{ML}} = 8MN_tN_r \tag{5}$$

as the ML detector searches through the whole transmit and receive search spaces. Note that evaluating the Euclidean distance $\left(|y_r - h_{\ell,r}s|^2\right)$ requires 8 real multiplications.

This full text paper was peer reviewed at the direction of IEEE Communications Society subject matter experts for publication in the IEEE ICC 2011 proceedings

D. Rx–SD Detector

In [7], a reduced–complexity and close–to–optimal BEP–achieving decoder is proposed, which, as mentioned in Section I, aims at reducing the receive search space. The detector can formally be written as follows:

$$\left[\hat{\ell}_t^{(\mathrm{Rx-SD})}, \hat{s}_t^{(\mathrm{Rx-SD})}\right] = \underset{\substack{\ell\in\{1,2,\dots N_t\}\\ s\in\{s_1,s_2,\dots s_M\}\\ \tilde{N}_r(\ell,s)=N_r}}{\arg\min} \left\{ \sum_{r=1}^{\tilde{N}_r(\ell,s)} |y_r - h_{\ell,r}s|^2 \right\} \tag{6}$$

where $1 \leq \tilde{N}_r(\ell,s) \leq N_r$ is the number of Euclidean distance evaluations $\left(|y_r - h_{\ell,r}s|^2\right)$, that have to be computed by the Rx–SD detector. Note that $\tilde{N}_r(\cdot,\cdot)$ can be different for each point in the transmit search space, *i.e.*, for $\ell \in \{1,2,\dots N_t\}$ and $s \in \{s_1, s_2, \dots s_M\}$.

More specifically, given a sphere with radius R, the receiver computes the set of optimal $\tilde{N}_r(\ell,s)$ for $\ell \in \{1,2,\dots N_t\}$ and $s \in \{s_1, s_2, \dots s_M\}$ as follows:

$$\tilde{N}_r(\ell,s) = \max_{n\in\{1,2,\dots N_r\}} \left\{ n \left| \sum_{r=1}^{n} |y_r - h_{\ell,r}s|^2 \leq R^2 \right. \right\} \tag{7}$$

In other words, for each $\ell \in \{1,2,\dots N_t\}$ and $s \in \{s_1, s_2, \dots s_M\}$, the Rx–SD receiver does not combine, according to the Maximal Ratio Combining (MRC) principle [2], the signals received by all the N_r antennas at the receiver, but it keeps combining the received signals until the Euclidean norm in (6) gives a point that lies inside a sphere of radius R and centered around the received signal itself. However, since the points in the actual search space are only those for which we have $\tilde{N}_r(\cdot,\cdot) = N_r$, it can be shown that there is no loss in either the diversity or the coding gain: the BEP is very close to that of the ML detector in (4).

In [7] the interested reader can find an accurate analysis of the computational complexity of the Rx–SD detector along with an efficient method to choose the radius R, which significantly affects the performance of the algorithm. In this paper, we simply mention that:

- The complexity of the Rx–SD receiver is given by:

$$\mathcal{C}_{\mathrm{Rx-SD}} = 8\sum_{\ell=1}^{N_t}\sum_{s=1}^{M} \tilde{N}_r(\ell,s) \tag{8}$$

  It is easy to show that $\mathcal{C}_{\mathrm{Rx-SD}}$ lies in the interval $8MN_t \leq \mathcal{C}_{\mathrm{Rx-SD}} \leq 8MN_tN_r$, where the lower bound corresponds to the scenario where $\tilde{N}_r(\ell,s) = 1$ for $\ell \in \{1,2,\dots N_t\}$ and $s \in \{s_1, s_2, \dots s_M\}$, and the upper bound corresponds to the scenario where $\tilde{N}_r(\ell,s) = N_r$ for $\ell \in \{1,2,\dots N_t\}$ and $s \in \{s_1, s_2, \dots s_M\}$. In other words, in the best–case scenario Rx–SD has the same complexity as a Multiple–Input–Single–Output (MISO) system, while in the worst-case scenario it has the same complexity as the ML–optimum detector in (4). These results suggest that the larger N_r, the higher the potential gain with respect to the ML–optimum receiver. Let us note that the Rx–SD solution has no pre–computations with respect to the ML–optimum detector. In fact, $\tilde{N}_r(\ell,s)$ for $\ell \in \{1,2,\dots N_t\}$ and $s \in \{s_1, s_2, \dots s_M\}$ in (7) are implicitly computed when solving the hypothesis–detection problem in (6).
- The radius R can be chosen as $R = 2\alpha N_r\sigma^2$, where α is the solution of the equation as follows [8], [7]:

$$\frac{\gamma(N_r, 2\alpha N_r)}{\Gamma(N_r)} = 1 - \varepsilon \tag{9}$$

  and $\gamma(x,a) = \int_0^a \xi^{x-1}\exp(-\xi)\,d\xi$ is the lower incomplete Gamma function, $\Gamma(x) = \int_0^{+\infty} \xi^{x-1}\exp(-\xi)\,d\xi$ is the Gamma function, and ε is an arbitrary small value close to zero, *e.g.*, $\varepsilon = 10^{-6}$.

III. New Low–Complexity Sphere Decoders for SM

As anticipated in Section I, in this section two new SDs for SM are introduced. The first one (Tx–SD), aims at reducing the transmit search space, as opposed to the Rx-SD search space, and the second one (C–SD) combines Rx–SD and Tx–SD decoders in order to reduce both transmit and receive search spaces.

A. Tx–SD Detector

The Tx–SD for SM is a modified version of the well–known SD for MIMO systems [8]. It, however, exploits the peculiar property of SM that only a single antenna is active for transmission. More specifically, similar to conventional SDs, the Tx–SD scheme reduces the number of points (ℓ,s) for $\ell \in \{1,2,\dots N_t\}$ and $s \in \{s_1, s_2, \dots s_M\}$ to be searched through in (4), *i.e.*, the transmit search space, by computing the Euclidean distances only for those points that lie inside a sphere with radius R and centered around the received signal. However, unlike conventional SDs, in our scheme the set of points inside the sphere are much simpler to be computed, as there is only a single active antenna in SM. In this section, using the condition that the point has to lie inside a sphere with radius R, an intervals are computed, while in the next section we provide an estimate of the computational complexity of the proposed detector.

The analytical derivation follows the notations in [8], which here are briefly summarised to make the paper self–contained. First, for ease of analytical derivation, the complex–valued model in (2) is replaced by its real–valued equivalent, as follows [11]:

$$\bar{\mathbf{y}} = \bar{\mathbf{H}}\bar{\mathbf{x}}_{\ell_t,s_t} + \bar{\mathbf{n}} \tag{10}$$

where $\bar{\mathbf{y}}$ is a $2N_r \times 1$ receive vector, $\bar{\mathbf{H}}$ is a $2N_r \times 2N_t$ channel matrix, $\bar{\mathbf{x}}_{\ell_t,s_t}$ is $2N_t \times 1$ transmit vector, and $\bar{\mathbf{n}}$ is a $2N_r \times 1$ noise vector, defined as follows:

$$\bar{\mathbf{y}} = \left[\mathrm{Re}\left\{\mathbf{y}^T\right\}, \mathrm{Im}\left\{\mathbf{y}^T\right\}\right]^T \tag{11}$$

$$\bar{\mathbf{H}} = \begin{bmatrix} \mathrm{Re}\{\mathbf{H}\} & \mathrm{Im}\{\mathbf{H}\} \\ -\mathrm{Im}\{\mathbf{H}\} & \mathrm{Re}\{\mathbf{H}\} \end{bmatrix} \tag{12}$$

$$\bar{\mathbf{x}}_{\ell_t,s_t} = \left[\mathrm{Re}\left\{\mathbf{x}_{\ell_t,s_t}^T\right\}, \mathrm{Im}\left\{\mathbf{x}_{\ell_t,s_t}^T\right\}\right]^T \tag{13}$$

$$\bar{\mathbf{n}} = \left[\mathrm{Re}\left\{\mathbf{n}^T\right\}, \mathrm{Im}\left\{\mathbf{n}^T\right\}\right]^T \tag{14}$$

where $\mathrm{Re}\{\cdot\}$ and $\mathrm{Im}\{\cdot\}$ denote real and imaginary parts respectively.

This full text paper was peer reviewed at the direction of IEEE Communications Society subject matter experts for publication in the IEEE ICC 2011 proceedings

$$\Theta_{\mathrm{R}} = \left\{ (\ell, s) \text{ with } \ell \in \{1, 2, \dots N_t\} \text{ and } s \in \{s_1, s_2, \dots s_M\} | \left\| \bar{\mathbf{y}} - \bar{\mathbf{H}} \bar{\mathbf{x}}_{\ell,s} \right\|_{\mathrm{F}}^2 \leq R^2 \right\}$$
$$= \left\{ (\ell, s) \text{ with } \ell \in \{1, 2, \dots N_t\} \text{ and } s \in \{s_1, s_2, \dots s_M\} | \sum_{i=1}^{2N_t} \left(\bar{z}_i - \sum_{j=i}^{2N_t} \bar{p}_{i,j} \bar{x}_j (\ell, s) \right)^2 \leq R_{\mathrm{Q}}^2 \right\} \quad (17)$$

By performing QR factorisation of the matrix $\bar{\mathbf{H}}$, (10) can be re–written as follows [8]:

$$\bar{\mathbf{y}} = \bar{\mathbf{Q}} \begin{bmatrix} \bar{\mathbf{P}} \\ \mathbf{0}_{(2N_r - 2N_t) \times 2N_t} \end{bmatrix} \bar{\mathbf{x}}_{\ell_t, s_t} + \bar{\mathbf{n}} \quad (15)$$

where $\bar{\mathbf{P}}$ is a $2N_t \times 2N_t$ upper triangular matrix, $\bar{\mathbf{Q}} = \begin{bmatrix} \bar{\mathbf{Q}}_1 & \bar{\mathbf{Q}}_2 \end{bmatrix}$, and $\bar{\mathbf{Q}}_1$, $\bar{\mathbf{Q}}_2$ are $2N_r \times 2N_t$ and $2N_r \times (2N_r - 2N_t)$ matrices, respectively.

The Tx–SD scheme can be formally written as follows:

$$\left[\hat{\ell}_t^{(\mathrm{Tx-SD})}, \hat{s}_t^{(\mathrm{Tx-SD})} \right] = \underset{(\ell,s) \in \Theta_{\mathrm{R}}}{\arg\min} \left\{ \left\| \bar{\mathbf{y}} - \bar{\mathbf{H}} \bar{\mathbf{x}}_{\ell,s} \right\|_{\mathrm{F}}^2 \right\} \quad (16)$$

where Θ_{R} is the subset of points (ℓ, s) for $\ell \in \{1, 2, \dots N_t\}$ and $s \in \{s_1, s_2, \dots s_M\}$ in the transmit search space that lie inside a sphere with radius R and centered around the received signal $\bar{\mathbf{y}}$. The subset Θ_{R} determined as shown in (17) on top of this page, where: i) $\bar{\mathbf{z}} = \mathbf{Q}_1^T \bar{\mathbf{y}}$, ii) $R_{\mathrm{Q}}^2 = R^2 - \left\| \bar{\mathbf{Q}}_2^T \bar{\mathbf{y}} \right\|_{\mathrm{F}}^2$, iii) $\bar{z}_i$ and $\bar{x}_i (\ell, s)$ are the i–th entry of vectors $\bar{\mathbf{z}}$ and $\bar{\mathbf{x}}_{\ell,s}$, respectively, and iv) $\bar{p}_{i,j}$ is the (i, j)–th entry of matrix $\bar{\mathbf{P}}$.

The main reason why the Tx–SD enjoys reduced computational complexity compared to the ML-optimum detector is the efficient computation of the subset Θ_{R}, which should avoid an exhaustive search in the whole transmit search space. As far as SM is concerned, these points can be computed in a very simple way, as summarised in *Lemma 1*.

Lemma 1: The subset of points Θ_{R} in (17) lie in the intervals:

$$\frac{-R_{\mathrm{Q}} + \bar{z}_i}{\bar{p}_{i,i}} \leq \bar{x}_i (\ell, s) \leq \frac{R_{\mathrm{Q}} + \bar{z}_i}{\bar{p}_{i,i}} \quad (18)$$

$$\frac{-R_{\mathrm{Q}} + \bar{z}_{i,i+N_t}}{\bar{p}_{i,i}} \leq \bar{x}_i (\ell, s) \leq \frac{R_{\mathrm{Q}} + \bar{z}_{i,i+N_t}}{\bar{p}_{i,i}} \quad (19)$$

for $i = 2N_t, 2N_t - 1, \dots, N_t + 1$ in (18), $i = N_t, N_t - 1, \dots, 1$ in (19), and we have defined $\bar{z}_{i,i+N_t} = \bar{z}_i - \bar{p}_{i,i+N_t} \bar{x}_{i+N_t} (\ell, s)$.

Proof:

1) First, we note that a necessary condition that the points of the transmit search space need to satisfy in order to belong to the subset Θ_{R} in (17) is (for all $i = 1, 2, \dots, 2N_t$):
$$\left(\bar{z}_i - \sum_{j=i}^{2N_t} \bar{p}_{i,j} \bar{x}_j (\ell, s) \right)^2 \leq R_{\mathrm{Q}}^2 \quad (20)$$
which is a condition similar to conventional SD algorithms [8].
2) Second, we need to take into account that in SM only a single antenna is active at any time instance, *i.e.* there are only two non–zero entries in the signal vectors $\bar{\mathbf{x}}_{\ell_t, s_t}$ and $\bar{\mathbf{x}}_{\ell,s}$ respectively. By taking this remark into account, it follows that: a) if $i = N_t + 1, N_t + 2, \dots, 2N_t$, then only the imaginary part of $\bar{\mathbf{x}}_{\ell,s}$ plays a role in (20), and, thus, only one entry $\bar{x}_j (\ell, s)$ can be non–zero; and b) if $i = 1, 2, \dots, N_t$, then both real and imaginary parts of $\bar{\mathbf{x}}_{\ell,s}$ play a role in (20), and, thus, only two entries $\bar{x}_j (\ell, s)$ can be non–zero. The considerations in a) and b) lead to the intervals in (18) and (19), respectively, which are directly obtained by solving the inequality in (20). □

By comparing the intervals in (18) and (19) with those of a conventional SD [8], we notice that (18) and (19) are much simpler, and this is due to the fact that in SM there is only one active antenna element, while in conventional SDs all the antennas transmit simultaneously. Note that, as (19) depends implicitly on (18), this means that (19) needs to be computed for all the points that lie in the interval in (18).

With respect to the Rx–SD scheme, the Tx–SD scheme requires some pre–computations to estimate the points that lie inside the sphere of radius R. These additional computations are carefully taken into account in the analysis of the computational complexity of the Tx–SD scheme and its comparison with the ML–optimum detector (see Section IV). Furthermore, we note that the radius R in (17) can still be computed from (9).

B. C–SD Detector

In Section II-D and Section III-A, we have seen that Rx–SD and Tx–SD aim at reducing the complexity of the ML–optimum detector by minimising the size of the receive and transmit search spaces, respectively. So, it is natural to combine both of them to further decrease the receiver complexity by reducing the size of both search spaces. The proposed C–SD is a two–step detector that works as follows:

1) First, the Tx–SD algorithm is used to reduce the transmit search space. The subset of points Θ_{R} is computed as shown in (17).
2) Second, the Rx–SD algorithm is used to reduce the receive search space. More specifically, Rx–SD is applied only on the subset of points Θ_{R} computed in the step above.

In formulas, we have:

$$\left[\hat{\ell}_t^{(\mathrm{C-SD})}, \hat{s}_t^{(\mathrm{C-SD})} \right] = \underset{\substack{(\ell,s) \in \Theta_{\mathrm{R}} \\ \tilde{N}_r(\ell,s) = N_r}}{\arg\min} \left\{ \sum_{r=1}^{\tilde{N}_r(\ell,s)} |y_r - h_{\ell,r} s|^2 \right\} \quad (21)$$

where Θ_{R} and $\tilde{N}_r (\ell, s)$ are computed by using (17) and (7), respectively.

This full text paper was peer reviewed at the direction of IEEE Communications Society subject matter experts for publication in the IEEE ICC 2011 proceedings

IV. Analysis of Computational Complexity

In this section, we analyse the computational complexity of Tx–SD and C–SD algorithms by taking into account the pre–computations needed to estimate the points of the reduced search space. In this paper, the complexity is defined as the total number of real multiplications and divisions required. Note, that long multiplication and division have the same computational complexity.

A. Tx–SD

The computational complexity of Tx–SD can be estimated by taking into account that:

1) The QR factorisation in (15), when computed by using the Householder algorithm [12], requires a number of real multiplications equal to:
$$\mathcal{C}_{\mathrm{QR}} = \sum_{k=1}^{N} \left[2f\left(k\right) + f^2\left(k\right) + 2f^3\left(k\right) + 1\right] - N_r^3 \quad (22)$$
where $f\left(k\right) = N_r + 1 - k$ and $N = \min\left\{N_r - 1, N_t\right\}$.
2) The computation of $\bar{\mathbf{z}} = \mathbf{Q}_1^T \bar{\mathbf{y}}$ in (17) needs $4N_tN_r$ real multiplications, *i.e.*, $\mathcal{C}_{\bar{\mathbf{z}}} = 4N_tN_r$.
3) The computation of $\left\|\bar{\mathbf{Q}}_2^T \bar{\mathbf{y}}\right\|_{\mathrm{F}}^2$ in (17) needs $\mathcal{C}_{\left\|\bar{\mathbf{Q}}_2^T \bar{\mathbf{y}}\right\|_{\mathrm{F}}^2} = 2N_r\left(2N_r - 2N_t + 1\right)$ real multiplications, *i.e.*, $\mathcal{C}_{\left\|\bar{\mathbf{Q}}_2^T \bar{\mathbf{y}}\right\|_{\mathrm{F}}^2} = 2N_r\left(2N_r - 2N_t + 1\right)$.
4) The computation of the intervals in (18) and (19) requires: i) $2N_t$ real divisions to compute (18) for N_t antenna indexes; and ii) 1 real multiplication and 2 real divisions for a number of times equal to the total number of points that satisfy (18). In the worst–case scenario, the number of points computed in (18) is equal to the size, M_I, of the imaginary constellation diagram composing the QAM constellation symbol. Accordingly, we have M_IN_t real multiplications and $2M_IN_t$ real divisions, and, thus, the complexity of computing the intervals in (18) and (19) can be upper–bounded by $\mathcal{C}_{\mathrm{interval}} = 2N_t + 3M_IN_t$.

In summary, the analytical complexity resulting from the computation of the points in the subset Θ_{R} can be upper–bounded by:
$$\mathcal{C}_{\Theta_{\mathrm{R}}} \leq \mathcal{C}_{\mathrm{QR}} + \mathcal{C}_{\bar{\mathbf{z}}} + \mathcal{C}_{\left\|\bar{\mathbf{Q}}_2^T \bar{\mathbf{y}}\right\|_{\mathrm{F}}^2} + \mathcal{C}_{\mathrm{interval}} \quad (23)$$

Since (16) requires 8 real multiplications for each computed Euclidean distance, it follows that the computational complexity of the Tx–SD receiver can be upper–bounded as follows:
$$\mathcal{C}_{\mathrm{Tx-SD}} \leq \mathcal{C}_{\Theta_{\mathrm{R}}} + 8N_r \mathrm{card}\left\{\Theta_{\mathrm{R}}\right\} \quad (24)$$
where $\mathrm{card}\left\{\cdot\right\}$ denotes the cardinality, *i.e.*, the number of points, in a set.

B. C–SD

The computational complexity of C–SD follows immediately from (8) and (24), as follows:
$$\mathcal{C}_{\mathrm{C-SD}} \leq \mathcal{C}_{\Theta_{\mathrm{R}}} + 8 \sum_{(\ell,s)\in\Theta_{\mathrm{R}}} \tilde{N}_r\left(\ell, s\right) \quad (25)$$

V. Numerical Results

In this section, Monte Carlo simulation results for at least 10^6 channel realisation are shown to compare the performance and computational complexity of ML–optimum and SD–based receivers. The numerical examples are obtained by assuming the system model in Section II. Furthermore, the radius R is chosen as described in (9) with $\varepsilon = 10^{-6}$.

In Fig. 1, the BEP averaged over Rayleigh fading is shown by considering two different constellation sizes, and $N_t = N_r = 4$. We notice that all the SDs have the same performance, and all of them overlap with the ML–optimum detector. As expected, the performance of SM improves when M decreases.

In Fig. 2, Fig. 3, and Fig. 4, the computational complexity $\mathcal{C}$ is compared using the derivations provided in the sections IV. In particular, the figures show the relative computational complexity of the SDs with respect to the ML–optimum detector, *i.e.*, $C_{\mathrm{rel}}\left(\%\right) = 100 \times \left(C_{\mathrm{ML}} - C_{\mathrm{SD}}\right)/C_{\mathrm{ML}}$. In Fig. 2, we observe that C–SD is always better than Tx–SD, while it is better than Rx–SD only for high SNRs. The reason for this latter result is because of the additional pre–computations required by both C–SD and Tx–SD solutions. As mentioned in Section I, we notice that the Rx–SD scheme is more effective in reducing the complexity when the number of antennas at the receiver is large.

Figures 3 and 4 show an interesting setup where it is clearly highlighted that none of the proposed SDs is superior to the others, and that it depends on the MIMO configuration and the SNR which SD is the best. In particular, in Fig. 3 we notice that when $M = 64$ the best receiver to use is the C–SD, while if we look at Fig. 3 when $M = 8$ and Fig. 4 when $M = 32$ we notice that the Rx–SD detector is optimum. The reason is that in the former case the transmit search space is large enough to compensate for the pre–computations required by Tx–SD and C–SD receivers. On the contrary, in the latter case the transmit search space is not extensive, and, therefore, there is little to be gained in reducing it, and the fixed amount of pre-computations dominate.

Finally, in Fig. 4 when $M = 64$, Rx–SD and C–SD are almost equivalent, as the transmit search space is large and there are many antennas at the receiver creating a large receive search space.

In summary, we can conclude that Rx–SD is the best choice when the number of antennas at the receiver is large, as it can significantly reduce the receiver search space without any pre–computations. On the other hand, C–SD is the best choice when the transmit search space is very large and the number of antennas at the receiver is low. It is interesting to note that the Tx–SD scheme is never the best choice in the investigated system scenarios. Since this latter decoder is most closely related to conventional SDs for MIMO systems, a main contribution of this paper is that it is required to reduce both, the transmit search space as well as the receive search space to arrive at a significant reduction in receiver complexity while maintaining superior bit-error performance.

This full text paper was peer reviewed at the direction of IEEE Communications Society subject matter experts for publication in the IEEE ICC 2011 proceedings

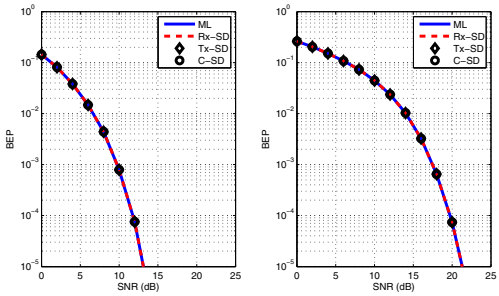

Fig. 1. BEP versus the SNR. $N_t = N_r = 4$, (left) $M = 8$; (right) $M = 64$.

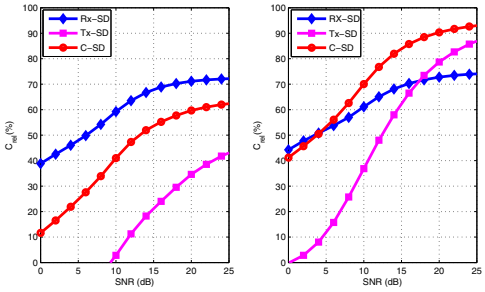

Fig. 3. Computational complexity versus the SNR. $N_t = N_r = 4$, (left) $M = 8$; (right) $M = 64$.

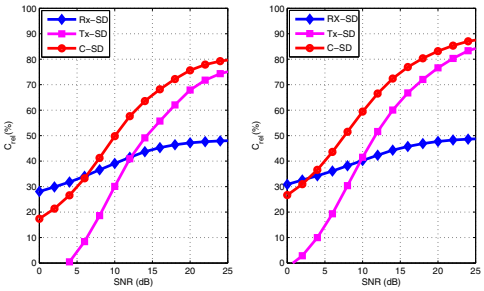

Fig. 2. Computational complexity versus the SNR. $N_t = N_r = 2$, (left) $M = 8$; (right) $M = 16$.

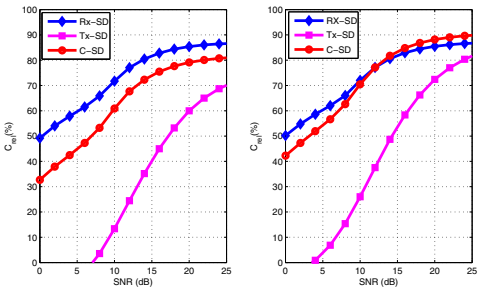

Fig. 4. Computational complexity versus the SNR. $N_t = N_r = 8$, (left) $M = 32$; (right) $M = 64$.

VI. Conclusion

In this paper, we have introduced and analysed the performance/complexity trade–off of three SDs for SM. We have shown that the proposed solutions provide a substantial reduction in the computational complexity while retaining the same BEP as the ML–optimum detector. Numerical results have highlighted that no particular SD is strictly superior to the others, and which SD is optimal, depends on the MIMO configuration employed, *i.e.*, the triplet (N_t, N_r, M) and the SNR at the receiver. Furthermore, Rx–SD is the best choice for large N_r, and C–SD is the best option when either N_r is low or M is large. In general, the results have shown that specially tailored SD can significantly reduce the receiver complexity of SM without deteriorating its BER performance.

Acknowledgement

Prof. Haas acknowledges support from the Scottish Funding Council for his position in the Joint Research Institute in Signal and Image Processing, as part of the Edinburgh Research Partnership in Engineering and Mathematics.

References

[1] R. Mesleh, H. Haas, S. Sinanović, C. W. Ahn, and S. Yun, "Spatial Modulation," *IEEE Trans. Veh. Technol.*, vol. 57, no. 4, pp. 2228 – 2241, July 2008.

[2] J. Jeganathan, A. Ghrayeb, and L. Szczecinski, "Spatial Modulation: Optimal Detection and Performance Analysis," *IEEE Commun. Lett.*, vol. 12, no. 8, pp. 545–547, 2008.

[3] G. J. Foschini, "Layered Space-Time Architecture for Wireless Communication in a Fading Environment when Using Multi-Element Antennas," *Bell Labs Technical Journal*, vol. 1, no. 2, pp. 41–59, 1996.

[4] P. Wolniansky, G. Foschini, G. Golden, and R. Valenzuela, "V-BLAST: an Architecture for Realizing very High Data Rates over the Rich-Scattering Wireless Channel," in *Unino Radio-Scientifique Internationale (URSI) Intern. Symp. on Signals, Systems, and Electronics (ISSSE)*, Sep. 29–Oct. 2, 1998, pp. 295–300.

[5] M. D. Renzo and H. Haas, "Performance Analysis of Spatial Modulation," in *IEEE International Conference on Communication and Networking in China (CHINACOM)*, Beijing, China, Aug. 2010, pp. 1–7, (invited paper).

[6] Y. Yang and B. Jiao, "Information-Guided Channel-Hopping for High Data Rate Wireless Communication," *IEEE Commun. Lett.*, vol. 12, no. 4, pp. 225 –227, Apr. 2008.

[7] A. Younis, R. Mesleh, H. Haas, and P. Grant, "Reduced Complexity Sphere Decoder for Spatial Modulation Detection Receivers," in *2010 IEEE Global Telecommunications Conference GLOBECOM 2010*, Miami, USA, 2010, pp. 1 –5.

[8] B. Hassibi and H. Vikalo, "On the Sphere-Decoding Algorithm I. Expected Complexity," *IEEE Trans. on Signal Process.*, vol. 53, no. 8, pp. 2806–2818, Aug. 2005.

[9] T. Cui and C. Tellambura, "An Efficient Generalized Sphere Decoder for Rank-Deficient MIMO Systems," *IEEE Commun. Lett.*, vol. 9, no. 5, pp. 423 – 425, may. 2005.

[10] P. Wang and T. Le-Ngoc, "A Low-Complexity Generalized Sphere Decoding Approach for Underdetermined Linear Communication Systems: Performance and Complexity Evaluation," *IEEE Trans. on Commun.*, vol. 57, no. 11, pp. 3376 –3388, nov. 2009.

[11] H. V. T. Kailath and B. Hassibi, *Space-Time Wireless Systems: From Array Processing to MIMO Communications*. Cambridge University Press, 2006, ch. MIMO Receive Algorithms.

[12] S. Aubert, F. Nouvel, and A. Nafkha, "Complexity Gain of QR Decomposition Based Sphere Decoder in LTE Receivers," in *IEEE 70th Vehicular Technology Conference Fall (VTC 2009-Fall)*, 2009, pp. 1 –5.

This full text paper was peer reviewed at the direction of IEEE Communications Society subject matter experts for publication in the IEEE Globecom 2010 proceedings.

Reduced Complexity Sphere Decoder for Spatial Modulation Detection Receivers

Abdelhamid Younis*, Raed Mesleh‡, Harald Haas*‡, and Peter M. Grant*
*Institute for Digital Communications, Joint Research Institute for Signal and Image Processing, The University of Edinburgh, Edinburgh EH9 3JL, UK, Email: {a.younis, h.haas & peter.grant}@ed.ac.uk
‡Jacobs University Bremen, School of Engineering and Science, Campus Ring 1, Research 1, 28759 Bremen, Germany, Email: r.mesleh@jacobs-university.de

***Abstract*—In this paper a novel detection algorithm for spatial modulation (SM) based on sphere decoder (SD) tree search idea is proposed. The aim is to reduce the receiver complexity of the existing optimal decoder while maintaining an optimum performance. The algorithm performs a maximum likelihood (ML) search, only over those points that lie inside a sphere, centered at the received signal, of given radius. It is shown with the aid of analytical derivations, that for a SNR (signal-to-noise ratio) between 2 dB and 18 dB at least 45% and up to 85% reduction in the number of complex operations can be achieved with a close to optimal bit-error-ratio (BER) performance.**

***Index Terms*—Spatial modulation, Sphere decoder, MIMO.**

I. Introduction

To cope with the demand for indoor wireless access to bandwidth-intensive applications such as the Internet multimedia streaming applications (Voice over IP (VoIP), streaming video and music, gaming, and network attached storage (NAS)), there is a need for increasing data throughput of current networks [1]. The maximum data rate of most wireless local area networks (WLANs) based on the IEEE 802.11 set of standards (802.11a/b/g) typically ranges from 2 Mbps up to 54 Mbps net bit rate (excluding the physical layer protocol overhead). The IEEE 802.11n amendment is proposed to significantly improve network throughput over previous standards. The increase in the maximum raw physical net bit rate is achieved by introducing the multiple-input multiple-output (MIMO) techniques [1], [2]. A data rate of 600 Mbps can be achieved for four parallel streams at 40 MHz channel bandwidth. However, implementing four parallel streams demands high computational power, which corresponds to long processing time and high power consumption. Therefore, complexity reduction algorithms for spatial multiplexing MIMO systems, such as sphere decoder [3]–[7, and references therein], are proposed to alleviate this problem.

The SD algorithm avoids an exhaustive search by examining only those points that lie inside a sphere with radius C. The performance of the SD algorithm is closely tied to the choice of the initial radius. The chosen radius should be large enough so that the sphere contains the solution. However, the larger the radius is, the longer the search takes, which increases the complexity. On the other hand, a small radius may cause the algorithm to fail finding any point inside the sphere.

In this paper, the SD tree search structure is adopted to reduce the complexity of the optimum ML decoder of SM [8]–[11]. In SM, multiple antennas exist at the transmitter, but only one of them transmits at a time, to avoid interchannel interference (ICI) at the receiver input. The active antenna transmits a symbol from the complex signal constellation diagram. The receiver first determines via an additional *antenna detector* which of the antennas has sent information (digital information is encoded into the antenna constellation). Therefore, there is information transmission at this stage. In a second step, conventional data detection in the complex signal space is carried out. The receiver applies the optimum decoder [11] to estimate the complex symbol and the spatial symbol, and uses the two estimations to retrieve the original data bit sequence. It is shown that the complexity of the optimum receiver increases linearly with the number of transmit antennas. This is unlike other spatial multiplexing MIMO techniques applying ML detection where the complexity increases exponentially with the number of transmit antennas.

The existing SD algorithms in literature can be applied to SM by adding a zero as a constellation point. This, however, does not consider the basic and fundamental principle of SM, that at any giving time, only one antenna is active. Therefore, the complexity of such a system increases exponentially with the number of transmit antennas. In addition, the Euclidean distances between constellation points decrease by considering the zero as a constellation point, which significantly degrades system performance. Thereafter, a modified SD algorithm based on tree search structure that is tailored to SM is presented. It is shown with the aid of analytical derivations, that a reduction of 45% and up to 85% in the number of complex operations can be achieved by using the proposed SM-SD algorithm, while maintaining an almost optimum performance combined with a complexity that increases linearly, and not exponentially, with the number of transmit antennas.

The remainder of this paper is organised as follows: Section II introduces SM system with the optimum ML decoder. In Section III, the proposed SM-SD algorithm for SM is presented. Section IV presents analytical calculations for the complexity of SM-SD and the initial radius selection method. Simulation results are presented in Section V, and the paper is concluded in section VI.

978-1-4244-5638-3/10/$26.00 ©2010 IEEE

This full text paper was peer reviewed at the direction of IEEE Communications Society subject matter experts for publication in the IEEE Globecom 2010 proceedings.

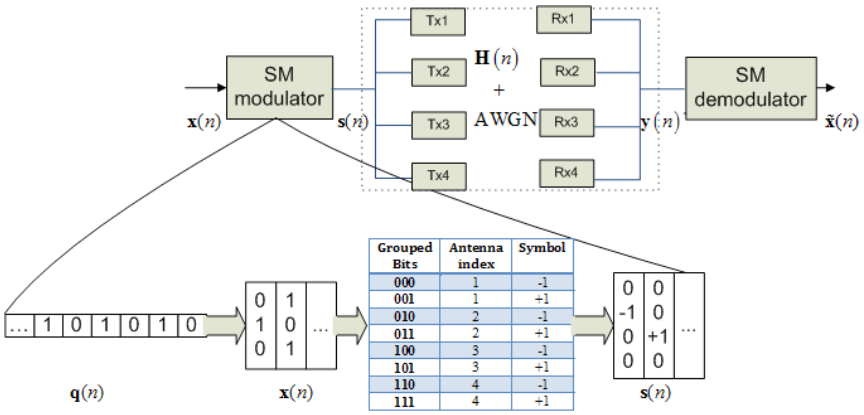

Fig. 1. Spatial modulation system model and the mapping table to antenna indices and BPSK symbols. At each time instance, three bits are transmitted. Two are encoded in the antenna index and one in the BPSK symbol.

II. Spatial Modulation with ML Decoder

The system model of SM with the mapping table to antenna indices and binary phase shift keying (BPSK) symbols is depicted in Fig. 1. A MIMO system consisting of four transmit antennas $N_t = 4$ and four receive antennas $N_r = 4$, for illustration purposes[1], is considered.

In Fig. 1, $\mathbf{q}(n)$ is the incoming binary data to be transmitted over the MIMO channel. In SM, each $m = \log_2(MN_t)$ bits, where M is the QAM constellation size, are transmitted at a particular time instance. The matrix $\mathbf{x}(n)$ is created by grouping each m bits from $\mathbf{q}(n)$ as the column vectors of $\mathbf{x}(n)$. The matrix $\mathbf{x}(n)$ is then mapped to another matrix $\mathbf{s}(n)$ according to the mapping table as shown in Fig. 1. Each column vector in $\mathbf{s}(n)$ contains the data to be transmitted at a particular time instance over the MIMO channel. Since, however, only one element in each column vector of $\mathbf{s}(n)$ is different from zero; only one antenna will be active at a time instance.

For instance, an example is shown in Fig. 1 for two time instances. The incoming data sequence $\mathbf{q}(n) = \begin{bmatrix} 1 & 0 & 1 & 0 & 1 & 0 \end{bmatrix}$ is mapped to

$$\mathbf{s}(n) = \begin{pmatrix} 0 & 0 \\ -1 & 0 \\ 0 & +1 \\ 0 & 0 \\ (n=1) & (n=2) \end{pmatrix}. \tag{1}$$

In the first time instance, the second antenna will be active and transmitting the BPSK symbol $s = -1$. All other antennas at this particular time instance will be off. In the second time instance, all transmit antennas are off except antenna three which will be transmitting the symbol $s = +1$. Hence, an overall increase in spectral efficiency by $\log_2(N_t)$ as compared to single input single output (SISO) system is achieved.

[1] For different number of antennas and different constellation diagrams of SM, the reader is kindly requested to refer to [8] for more details.

The transmitted signal experiences an N_r–dim additive white Gaussian noise (AWGN). The channel is assumed to be flat fading channel with an independent and identically distributed (i.i.d.) entries according to $\mathcal{CN}(0,1)$. The received signal at a specific time instance is given by,

$$\mathbf{y} = \mathbf{H}\mathbf{s} + \mathbf{v} \tag{2}$$

where $\mathbf{H}$ is an $N_r \times N_t$ MIMO channel matrix, and $\mathbf{v}$ is an AWGN vector $\sim \mathcal{CN}(0, \sigma_n^2)$.

At the receiver, the optimum SM decoder is considered to estimate the complex symbol $\tilde{s}$ and the spatial symbol $\tilde{\ell}$ as follows [11]:

$$\left[\tilde{\ell}, \tilde{s}\right] = \underset{\ell,s}{\arg\max}\, p_{\mathbf{y}}\left(\mathbf{y}|\mathbf{s},\mathbf{H}\right) \tag{3}$$

$$= \underset{\ell,s}{\arg\min} \|\mathbf{g}_\ell\|_{\mathbb{F}}^2 - 2\,\mathrm{Re}\left\{\mathbf{y}^H \mathbf{g}_\ell\right\}, \tag{4}$$

where $\mathbf{g}_\ell = \mathbf{h}_\ell s$ is the received vector when transmitting the symbol s from antenna index ℓ where $1 \le \ell \le N_t$ and $s \in \{M\}$, $\mathbf{h}_\ell$ is the channel vector containing the channel path gains from transmit antenna ℓ to all receive antennas, and Re is the real part of a complex number. In addition, $(\cdot)^H$ denotes the Hermitian of a vector or a matrix, $||\cdot||_{\mathbb{F}}$ is the Frobenius norm of a vector/matrix and

$$p_{\mathbf{y}}\left(\mathbf{y}|\mathbf{s},\mathbf{H}\right) = \pi^{-N_t} e^{\left(-\|\mathbf{y}-\mathbf{H}\mathbf{s}\|_{\mathbb{F}}^2\right)}. \tag{5}$$

The evaluation of (4) is computationally expensive as it needs to be evaluated for all possible antennas and modulation symbols. This requires $(4N_r - 1)$ complex operations evaluated $N_t M$ times, *i.e.*,

$$\psi_{\text{opt}} = N_t M(4N_r - 1) \tag{6}$$

From (6) it can be seen, and as stated before, that the receiver complexity increases linearly with the number of transmit antennas.

978-1-4244-5638-3/10/$26.00 ©2010 IEEE

This full text paper was peer reviewed at the direction of IEEE Communications Society subject matter experts for publication in the IEEE Globecom 2010 proceedings.

III. SM WITH SD TREE STRUCTURE

The considered SM-SD algorithm in this paper is a modified version of the SD algorithm presented in [3], by adopting the tree search structure, as shown in Fig. 2. The SM-SD performs a ML search only on paths that lead to points $(\tilde{\ell}, \tilde{s})$ with an error, less than or equal to the sphere radius C. In this paper, the initial radius of the SM-SD algorithm is adjusted according to the noise level assuming the knowledge of the SNR at the receiver side known from previous received data. Then the radius is adapted when a point is found inside the sphere by the Euclidean distance of that point. The initial sphere radius considered in SM-SD is a function of the noise variance as given in [12],

$$C^2 = 2\alpha N_r \sigma_n^2, \tag{7}$$

where σ_n^2 is the noise variance and α is a constant chosen to maximise the probability of having the transmitted point inside the sphere. Depending on the SNR value, a major reduction in the number of calculated paths can be achieved.

The full procedure for SM-SD algorithm is explained in what follows. Let S be a set containing all possible transmit antennas and spatial symbol points, $S = \{(\ell, s) : \ell \in [1, ..., N_t], s \in \{M\}\}$, δ the Euclidean distance error, and φ the depth of the search on each path (ℓ, s). Then, the algorithm can be formulated as follows:

1) for $(\ell, s) \in S$
   a) for $i = 1 : N_r$
      i) $\delta_{(\ell,s)} += |y_i - H_{(i,\ell)} s|^2$
      ii) if $\delta_{(\ell,s)} \geq C^2$ then go to 1
      iii) $\varphi_{(\ell,s)} += 1$
   b) $C^2 = \delta_{(\ell,s)}$
2) $S_\varphi = \arg\limits_{(\ell,s)} (\varphi_{(\ell,s)} = \max(\varphi))$
3) $\left[\tilde{\ell}, \tilde{s}\right] = \arg\limits_{(\ell,s)\in S_\varphi} \min(\delta_{(\ell,s)})$

SM-SD algorithm search the paths leading to each point (ℓ, s) as long as it is still inside the sphere as depicted in Fig. 2. Whenever a point is found to be inside the sphere, the radius, C, is updated with the Euclidean distance of that point. The path with the minimum Euclidean distance is considered to be the solution. A significant advantage of the proposed SM-SD algorithm is that it avoids the problem of having no points inside the sphere, which is a major problem of the conventional SD algorithms. SM-SD algorithm selects the path with the minimum Euclidean distance even if all the points were outside the sphere.

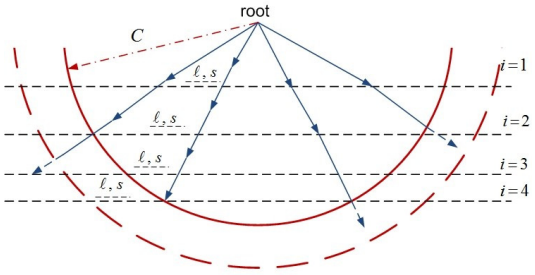

Fig. 2. The Tree Structure and Sphere Constraint for the Sphere Decoder

IV. COMPLEXITY ANALYSIS AND INITIAL RADIUS SELECTION METHOD

The ML receiver for SM, given in (3), can be re-written as,

$$\left[\hat{\ell}_{\mathrm{ml}}, \hat{s}_{\mathrm{ml}}\right] = \arg\min_{\ell,s} \sum_{i=1}^{N_r} |y_i - H_{(i,\ell)} s|^2 \tag{8}$$

let

$$z_i(\ell, s) = y_i - H_{(i,\ell)} s \tag{9}$$

and,

$$y_i = H_{(i,\ell_t)} s_t + v \tag{10}$$

where s_t is the transmitted symbol at a particular time instant from antenna index ℓ_t, and $v \sim \mathcal{CN}(0, \sigma_n^2)$. Then,

$$z_i(\ell, s) = v + H_{(i,\ell_t)} s_t - H_{(i,\ell)} s \tag{11}$$

from (11), the probability density function (PDF) for $z_i(\ell, s)$ is

$$f_{\mathbf{z}}\left(z_i(\ell, s) \middle| s_t, \ell_t, \mathbf{H}, \sigma_n^2\right) = \frac{1}{\sqrt{2\pi\sigma_n^2}} e^{-\frac{\left(z_i(\ell,s) - \mu_i(\ell,s)\right)^2}{2\sigma_n^2}} \tag{12}$$

where $\mu_i(\ell, s)$ is

$$\mu_i(\ell, s) = H_{(i,\ell_t)} s_t - H_{(i,\ell)} s \tag{13}$$

The SM-SD performs a ML search only on paths that lead to points (ℓ, s) with an error, less or equal to C. In other words, the SM-SD algorithm calculates

$$\gamma_k(\ell, s) = \sum_{i=1}^{k} |y_i - H_{(i,\ell)} s|^2 \tag{14}$$

$$= \sum_{i=1}^{k} |z_i(\ell, s)|^2 = \frac{\sigma_n^2}{2} \kappa_k(\ell, s) \tag{15}$$

if $\gamma_k(\ell, s) \leq C^2$, it continues to the next level k, where $k = [1, ..., N_r]$ and

$$\kappa_k(\ell, s) = \sum_{i=1}^{k} \left(\frac{z_i(\ell, s)}{\sigma_n/\sqrt{2}}\right)^2 \tag{16}$$

Hence, the probability of having a point (ℓ, s) at a level k inside the sphere giving a radius C is,

$$p_k(\ell, s, C) = \Pr\left(\gamma_k(\ell, s) \leq C^2 \middle| s_t, \ell_t, \mathbf{H}, \sigma_n^2\right)$$

$$= \Pr\left(\kappa_k(\ell, s) \leq \left(\frac{C}{\sigma_n/\sqrt{2}}\right)^2 \middle| s_t, \ell_t, \mathbf{H}, \sigma_n^2\right) \tag{17}$$

978-1-4244-5638-3/10/$26.00 ©2010 IEEE

This full text paper was peer reviewed at the direction of IEEE Communications Society subject matter experts for publication in the IEEE Globecom 2010 proceedings.

From (16), $\kappa_k(\ell, s)$ is a squared summation of non zero mean normal distributed random variables, with variance equal to one. Thereby, the distribution of the random variable $\kappa_k(\ell, s)$ is a non central chi-squared random variable with $2k$ degree of freedom, and the non-central parameter $\lambda_k(\ell, s)$ equals to [13]

$$\lambda_k(\ell, s) = \frac{\sum_{i=1}^{k} |\mu_i(\ell, s)|^2}{\sigma_n^2/2}. \tag{18}$$

Consequently, the probability of having a point (ℓ, s) at a level k inside the sphere giving a radius C is

$$p_k(\ell, s, C) = F\left(\left(\frac{C}{\sigma_n/\sqrt{2}}\right)^2, 2k, \lambda_k(\ell, s)\right) \tag{19}$$

where $F(B, n, \lambda)$ is the CDF (cumulative distribution function) of the random variable κ. A closed form expression for (19) is not available. However, a solution can be obtained as shown in [13, (2.1-124)] by noting that the degree of freedom is always a multiple of 2. Therefore, (19) can be expressed in terms of the generalised Marcum's Q function as follows,

$$p_k(\ell, s, C) = 1 - Q_k\left(\sqrt{\lambda_k(\ell, s)}, \frac{C}{\sigma_n/\sqrt{2}}\right) \tag{20}$$

From (20), the total number of Euclidean distance equations completed by SM-SD in each path (ℓ, s) is given by,

$$\xi_{\ell,s} = \sum_{k=1}^{N_r} p_k(\ell, s, C) = \sum_{k=1}^{N_r} \left(1 - Q_k\left(\sqrt{\lambda_k(\ell, s)}, \frac{C}{\sigma_n/\sqrt{2}}\right)\right) \tag{21}$$

and the total number of Euclidean distance equations completed by the SM-SD algorithm is

$$\xi = \sum_{\ell=1}^{N_t} \sum_{s \in M\text{-QAM}} \xi_{\ell,s} \tag{22}$$

The derived number of Euclidean distance equations in (22) assumes that, initially, the algorithm knows if the point is inside or outside the sphere. However, this is not true and a correction factor is needed to consider the initial calculated equations. To account for this, the number of Euclidean distance equations is modified as follows,

$$\xi_{\text{SM-SD}} = \begin{cases} \xi + N_t M & \xi \leq N_t M\,(N_r - 1) \\ \xi & \text{otherwise} \end{cases} \tag{23}$$

where $N_t M$ is the initial number of calculated Euclidean distance equations.

The SM-SD updates C whenever a point is found inside the sphere, with the Euclidean distance of that point. Hence, C in (21), is updated as follows,

$$C = \sum_{k=1}^{N_r} |v + \mu_k(\ell, s)|^2 \tag{24}$$

In summary, the calculation for the number of complex operations for the SM-SD algorithm is as follows,

1) for $\ell = 1 : N_r$
   a) for $s \in M$-QAM
      i) calculate $\xi_{\ell,s}$ (21) and $p_{N_r}(\ell, s, C)$ (20)
      ii) if $p_{N_r}(\ell, s) > \varsigma$ then
      $C = \sum_{k=1}^{N_r} |v + \mu_k(\ell, s)|^2$
2) calculate ξ (22)
3) calculate $\xi_{\text{SM-SD}}$ (23)

where by numerical simulations the optimal value for ς is found to be 0.9.

Additionally, (14) needs 3 complex operations, yielding a total number of complex operations equals to,

$$\psi_{\text{SM-SD}} = 3 \times \xi_{\text{SM-SD}} \tag{25}$$

The value of α for the initial radius in (7) is chosen to increase the probability of having the transmitted point (ℓ_t, s_t) inside the sphere. Hence,

$$\begin{aligned} p_{N_r}(\ell_t, s_t, C) &= F\left(\left(\frac{C}{\sigma_n/\sqrt{2}}\right)^2, 2N_r, \lambda_{N_r}(\ell_t, s_t)\right) \\ &= F\left(4\alpha N_r, 2N_r, \lambda_{N_r}(\ell_t, s_t)\right) \\ &= 1 - \varepsilon \end{aligned} \tag{26}$$

The probability $1 - \varepsilon$ is set as a value close to 1. For $\varepsilon = 10^{-6}$ and $N_r = 4, 8$, $\alpha = 3, 2$ respectively.

V. Simulation Results

In the following, Monte Carlo simulation results for at least 10^6 channel realisations are considered to compare the performance of SM with the optimum detection technique and the proposed SM-SD algorithm. In the analysis, two spectral efficiencies are considered, $m = 4, 6$ bits/symbol and $(N_t = N_r = 8)$.

The BER results versus SNR for the two different spectral efficiencies are depicted in Fig. 3. An important observation is that SM-SD algorithm and the optimum detector have an identical performance. That is because the initial radius (C) for SM-SD is chosen so it would give a high probability of having the transmitted point inside the sphere, which is done by choosing α that increases the probability in (26), where in the case of $N_r = 8$ and $\varepsilon = 10^{-6}$, $\alpha = 2$.

The reduction of computational complexity,

$$R = \frac{\psi_{\text{opt}} - \psi_{\text{SM-SD}}}{\psi_{\text{opt}}} \tag{27}$$

is depicted in Fig. 4 and Fig. 5 for the two different spectral efficiencies. A significant reduction of at least 45% and up to 85% is reported. It can be observed that a higher reduction in computational complexity is achieved for high SNR values and/or low modulation orders. At high SNR the sphere radius is small, which leads to lower complexity. The higher complexity reduction for high modulation orders is mainly due to the increase of the number of calculations of the optimal decoder.

978-1-4244-5638-3/10/$26.00 ©2010 IEEE

This full text paper was peer reviewed at the direction of IEEE Communications Society subject matter experts for publication in the IEEE Globecom 2010 proceedings.

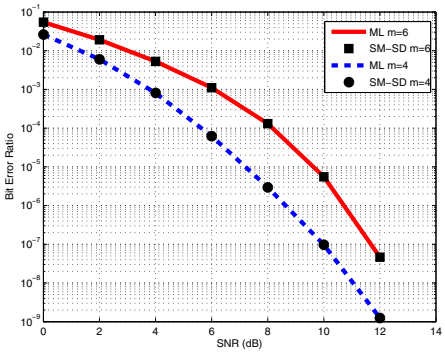

Fig. 3. BER performance versus SNR for $N_t = 8$, $N_r = 8$ and $m = 4, 6$

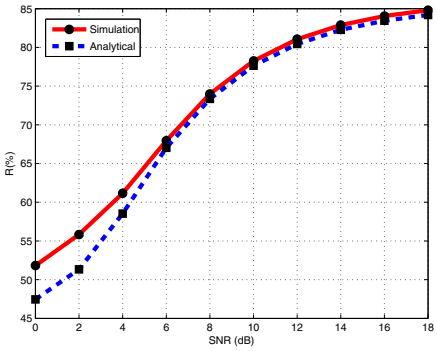

Fig. 4. The percentage of complexity reduction offered by SM-SD versus SNR, for $N_t = 8$, $N_r = 8$ and $m = 4$

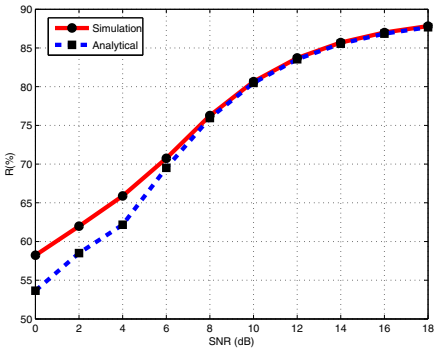

Fig. 5. The percentage of complexity reduction offered by SM-SD versus SNR, for $N_t = 8$, $N_r = 8$ and $m = 6$

VI. Summary and Conclusions

The complexity of the optimum ML detector for SM is significantly reduced using the SD tree search applied in a novel fashion. The existing SD algorithms in literature are computationally more expensive if directly applied to SM and will result in performance degradation. The SM-SD algorithm exploits the fact that only a single antenna is active and performs a ML search only over the points that are inside the sphere of a given radius (depending on the SNR) and centered at the received point. The performance of the proposed detection algorithm is optimum and it yields in excess of 45% reduction in the number of complex operations.

Acknowledgement

Professor Haas acknowledges the Scottish Funding Council support of his position within the Edinburgh Research Partnership in Engineering and Mathematics between the University of Edinburgh and Heriot Watt University.

References

[1] BROADCOM Corporation, "802.11n: Next-Generation Wireless LAN Technology," White paper, BROADCOM Corporation, Tech. Rep., Apr. 2006, retrieved Aug. 4, 2006 http://www.broadcom.com/docs/WLAN/802-11n-WP100-R.pdf.

[2] E. Telatar, "Capacity of Multi-Antenna Gaussian Channels," *European Transaction on Telecommunication*, vol. 10, no. 6, pp. 585–595, Nov. / Dec. 1999.

[3] E. Viterbo and J. Boutros, "A Universal Lattice Code Decoder for Fading Channels," *IEEE Transaction on Information Theory*, vol. 45, no. 5, pp. 1639–1642, Jul. 1999.

[4] B. Hochwald and S. ten Brink, "Achieving Near-Capacity on a Multiple-Antenna Channel," *IEEE Transactions on Communications*, vol. 51, no. 3, pp. 389–399, Mar. 2003.

[5] O. Damen, A. Chkeif, and J.-C. Belfiore, "Lattice Code Decoder for Space-Time Codes," *IEEE Communications Letters*, vol. 4, no. 5, pp. 161–163, May 2000.

[6] A. Burg, M. Borgmann, M. Wenk, M. Zellweger, W. Fichtner, and H. Bolcskei, "VLSI Implementation of MIMO Detection Using the Sphere Decoding Algorithm," *IEEE Journal of Solid-State Circuits*, vol. 40, no. 7, pp. 1566–1577, Jul. 2005.

[7] L. Barbero and J. Thompson, "FPGA Design Considerations in the Implementation of a Fixed-Throughput Sphere Decoder for MIMO Systems," in *Proc. International Conference on Field Programmable Logic and Applications FPL '06*, Madrid, Spain, Aug. 28–30 2006, pp. 1–6.

[8] R. Mesleh, H. Haas, S. Sinanović, C. W. Ahn, and S. Yun, "Spatial Modulation," *IEEE Transactions on Vehicular Technology*, vol. 57, no. 4, pp. 2228 – 2241, Jul. 2008.

[9] R. Mesleh, H. Haas, C. W. Ahn, and S. Yun, "Spatial Modulation – A New Low Complexity Spectral Efficiency Enhancing Technique," in *IEEE International Conference on Communication and Networking in China (CHINACOM)*, Beijing, China, Oct. 25–27, 2006, pp. 1–5.

[10] M. Di Renzo and H. Haas, "A General Framework for Performance Analysis of Spatial Modulation (SM) for MISO Systems over Correlated Nakagami-m Fading Channels," *IEEE Transaction on Communications*, 2010, to appear.

[11] J. Jeganathan, A. Ghrayeb, and L. Szczecinski, "Spatial Modulation: Optimal Detection and Performance Analysis," *IEEE Communication Letters*, vol. 12, no. 8, pp. 545–547, 2008.

[12] X. Xia, H. Hu, and H. Wang, "Reduced Initial Searching Radius for Sphere Decoder," in *Proc. IEEE 18th International Symposium on Personal, Indoor and Mobile Radio Communications PIMRC 2007*, Athens, Greece, Sep. 3–7, 2007, pp. 1–4.

[13] J. G. Proakis, *Digital Communications*, 4th ed., ser. McGraw-Hill Series in Electrical and Computer Engineering, S. W. Director, Ed. McGraw-Hill Higher Education, Dec. 2000.

978-1-4244-5638-3/10/$26.00 ©2010 IEEE

Generalised Spatial Modulation

Abdelhamid Younis*, Nikola Serafimovski*, Raed Mesleh‡ and Harald Haas*‡
*Institute for Digital Communications, Joint Research Institute for Signal and Image Processing, The University of Edinburgh, Edinburgh EH9 3JL, UK, Email: {a.younis & n.serafimovski & h.haas }@ed.ac.uk
‡University of Tabuk, Electrical Engineering Department, P.O.Box: 741, 71491 Tabuk, Saudi Arabia, Email: raed.mesleh@ieee.org

***Abstract*—In this paper, a generalised technique for spatial modulation (SM) is presented. Generalised spatial modulation (GSM) overcomes in a novel fashion the constraint in SM that the number of transmit antennas has to be a power of two. In GSM, a block of information bits is mapped to a constellation symbol and a spatial symbol. The spatial symbol is a combination of transmit antennas activated at each instance. The actual combination of active transmit antennas depends on the random incoming data stream. This is unlike SM where only a single transmit antenna is activated at each instance. GSM increases the overall spectral efficiency by base–two logarithm of the number of antenna combinations. This reduces the number of transmit antennas needed for the same spectral efficiency. The performance of GSM is analysed in this paper, and an upper bound on the bit–error–ratio (BER) performance is derived. In addition, an algorithm to optimise the antenna combination selection is proposed. Finally, the performance of GSM is validated through Monte Carlo simulations. The results are compared with traditional SM. It is shown that for the same spectral efficiency GSM performs nearly the same as SM, but with a significant reduction in the number of transmit antennas.**

***Index Terms*—Spatial modulation, generalised spatial modulation, MIMO.**

I. Introduction

Multiple-input multiple-output (MIMO) systems offer a significant increase in spectral efficiency, in comparison to single antenna systems [1]. An example is the Vertical Bell Labs layered space-time (V-BLAST) architecture [2], where the spectral efficiency increases linearly with the number of transmit antennas. However, transmitting from all antennas at the same time, on the same frequency, causes inter-channel interference (ICI) at the receiver.

Spatial Modulation (SM) is a spatial multiplexing MIMO technique that is proposed in [3] to increase the spectral efficiency and to overcome inter–channel interference (ICI). This is attained by activating only a single transmit antenna at each instance to transmit a certain data symbol, where the active antenna index and the data sent depend on the incoming random data bits. Thereby, an overall increase in the spectral efficiency by base–two logarithm of the number of transmit antennas is achieved. Note that, the number of transmit antennas must be a power of two. A detector that jointly estimates the active antenna index and the sent data symbol is required at the receiver side. The optimal SM decoder is proposed in [4] and SM combined with trellis-coded modulation (TCM) is recently proposed in [5]. Furthermore, space shift keying (SSK) with partial channel state information is presented in [6], and a general framework for performance analysis of SSK for multiple input single output (MISO) systems over correlated Nakagami-m fading channels is shown in [7]. It is shown in [3]–[5] that ICI avoidance results in better BER performance and a significant reduction in detection complexity, as compared to V-BLAST, for instance. However, the logarithmic increase in spectral efficiency and the requirement that the number of antennas must be a power of two would require large number of antennas.

Fractional bit encoded spatial modulation (FBE-SM) is proposed in [8] to overcome the limitation in the number of transmit antennas. FBE-SM is based on the theory of modulus conversion and allows an arbitrary number of transmit antennas. However, the system suffers from error propagation.

An alternative approach to limit the number of transmit antennas is proposed in this paper. Generalised spatial modulation (GSM) activates more than one transmit antenna at a time to simultaneously transmit a data symbol. In GSM the transmitted information is conveyed in the activated combination of transmit antennas and the transmitted symbol from a signal constellation. As a result, the number of transmit antennas required to achieve a certain spectral efficiency is reduced by more than a half in GSM as compared to SM, and generalised space shift keying modulation (GSSK) proposed in [9]. Transmitting the same data symbol from more than one antenna at a time, retains the key advantage of SM, which is the complete avoidance of ICI at the receiver. Moreover, GSM offers spatial diversity gains and increases the reliability of the wireless channel, by providing replicas of the transmitted signal to the receiver [10]. Nonetheless, the activated transmit antennas must be synchronised to avoid inter-symbol interference (ISI). At the receiver, a maximum likelihood (ML) detection algorithm is considered to estimate the activated combination of transmit antennas and the transmitted constellation symbol.

A tight analytical upper bound for the BER performance of GSM is derived in this paper and analytical results are validated through Monte Carlo simulation results. Moreover, GSM performance is shown to be very close to the performance of SM but with major reduction in the required number of transmit antennas.

The remainder of this paper is organised as follows: Section II presents GSM system model and the optimal detection technique. Section III presents the analytical BER derivation for GSM and proposes the selection process for the optimal antenna combinations. The receiver complexity is discussed in

978-1-4244-9721-8/10/$26.00 ©2010 IEEE

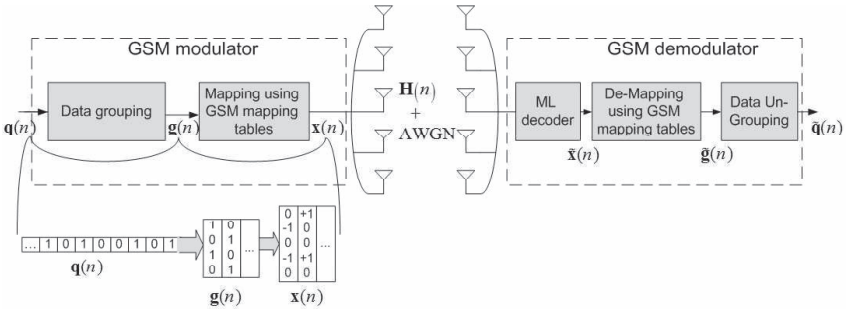

Fig. 1. Generalised spatial modulation system model. At each instance, four bits are transmitted. Three bits are encoded in the indices of the combination of transmit antennas and one bit is conveyed in the signal domain using BPSK modulation.

section IV. Monte Carlo Simulation results are presented in Section V, and the paper is concluded in Section VI.

II. GSM System Model

GSM uses more than one transmit antenna to send the same complex symbol. Hence, a set of antenna combinations can be formed, and used as spatial constellation points. The number of possible antenna combinations is $N_c^{'} = \binom{N_t}{N_u}$, where N_t is the number of transmit antennas and N_u is the number of active antennas at each instance. However, the number of antenna combinations that can be considered for transmission must be a power of two. Therefore, only $N_c = 2^{m_\ell}$ combinations, can be used, where $m_\ell = \lfloor \log_2 \binom{N_t}{N_u} \rfloor$, and $\lfloor \cdot \rfloor$ is the floor operation.

The GSM system model is depicted in Fig. 1 and an example of data mapping and transmission for two instances is also shown. The incoming data bits are mapped to a spatial symbol and a data symbol according to the mapping table shown in Table I. The mapping procedure maps the first m_ℓ bits to the antenna combinations, and the remaining bits (m_s) are modulated using M-QAM modulation, where $M = 2^{m_s}$. In the example, $N_t = 5$ and $N_u = 2$ are assumed. The resultant antenna combinations are listed in Table I. For instance, the data bits to be transmitted at the first instance in Fig. 1 $\mathbf{g}(n) = \begin{bmatrix} 0 & 1 & 0 & 1 \end{bmatrix}$ are mapped to $\mathbf{x}(n) = \begin{bmatrix} +1 & 0 & 0 & +1 & 0 \end{bmatrix}$. Each column vector of $\mathbf{x}(n)$ is transmitted at a specific instance from the existing five transmit antennas where only two antennas are activated at any given time. If SM is used instead with the same modulation order, the number of transmit antennas must be increased to eight to maintain the same spectral efficiency. In general, the number of bits that can be transmitted using GSM is given by,

$$m = m_\ell + m_s = \left\lfloor \log_2 \binom{N_t}{N_u} \right\rfloor + \log_2 M \qquad (1)$$

The GSM modulated signal is transmitted over an $N_r \times N_t$ MIMO Rayleigh flat fading wireless channel, $\mathbf{H}$, and, thus, the entries of $\mathbf{H}$ are modeled as complex independent and identically distributed (i.i.d.) Gaussian random variables with zero–mean and unit–variance, where N_r is the number of receive antennas.

TABLE I
GSM Mapping Table for $N_t = 5$, $N_u = 2$ and BPSK Modulation, where $(\cdot, \cdot)$ indicates the indices of the active antennas

Grouped Bits	Antenna Combination (ℓ)	Symbol (s)
0000	(1,2)	-1
0001	(1,2)	+1
0010	(1,3)	-1
0011	(1,3)	+1
0100	(1,4)	-1
0101	(1,4)	+1
0110	(1,5)	-1
0111	(1,5)	+1
1000	(2,3)	-1
1001	(2,3)	+1
1010	(2,4)	-1
1011	(2,4)	+1
1100	(3,5)	-1
1101	(3,5)	+1
1110	(4,5)	-1
1111	(4,5)	+1

The received signal at any given time is,

$$\mathbf{y} = \mathbf{h}'_\ell s + \mathbf{v} \qquad (2)$$

where $s \in M$-QAM is the transmitted symbol, from the antenna combination $\ell = (\ell_1, \ell_2, \ldots, \ell_{N_u}) \in \Phi$, ℓ_n indicates the index of the n-th antenna in the antenna combination ℓ, and Φ is the set of used antenna combinations. An optimal algorithm for the selection of Φ is proposed in next section. Furthermore the vector $\mathbf{h}'_\ell = \sum_{n=1}^{N_u} \mathbf{h}_{\ell_n}$ contains the summation of the active antennas channel vectors, and $\mathbf{h}_{\ell_n}$ is the channel vector from the active transmit antenna ℓ_n to all receive antennas. $\mathbf{v}$ is an AWGN vector with zero–mean and variance σ_n^2 per dimension at the receiver input.

At the receiver, the spatial symbol and the data symbol are jointly decoded using the ML principle, as follows,

$$\begin{aligned} [\tilde{\ell}, \tilde{s}] &= \arg\max_{\ell,s} p_{\mathbf{y}}(\mathbf{y}|\mathbf{x}, \mathbf{H}) \\ &= \arg\min_{\ell,s} \sum_{i=1}^{N_r} |y_i - h'_{\ell,i} s|^2 \end{aligned} \qquad (3)$$

where,

$$p_{\mathbf{y}}\left(\mathbf{y}|s,\ell,\mathbf{H}\right)=\frac{1}{\left(\pi\sigma_n^2\right)^{N_t}}\exp\left(-\frac{\|\mathbf{y}-\mathbf{h}'_\ell s\|_{\mathrm{F}}^2}{\sigma_n^2}\right) \quad (4)$$

is the probability density function (PDF) of $\mathbf{y}$ conditional on s,ℓ and $\mathbf{H}$, $\|\cdot\|_{\mathrm{F}}^2$ is the Frobenius norm.

III. Analytical derivation and optimal combination selection

A. Analytical BER calculation of GSM

The analytical performance of GSM is estimated using the well-known union bounding technique [11]. The average BER in GSM is,

$$\Pr_{\text{e,bit}}\leq \mathrm{E}_{\mathbf{x}}\left[\sum_{\tilde{\ell},\tilde{s}}\frac{N\left(x_{\ell,s},x_{\tilde{\ell},\tilde{s}}\right)\Pr\left(x_{\ell,s}\rightarrow x_{\tilde{\ell},\tilde{s}}\right)}{2^m}\right] \quad (5)$$

where $x_{\ell,s}$ indicates the symbol s transmitted from the antenna combination ℓ, $N\left(x_{\ell,s},x_{\tilde{\ell},\tilde{s}}\right)$ is the number of bits in error between $x_{\ell,s}$ and $x_{\tilde{\ell},\tilde{s}}$, and $\Pr\left(x_{\ell,s}\rightarrow x_{\tilde{\ell},\tilde{s}}\right)$ denotes the probability of deciding on $x_{\tilde{\ell},\tilde{s}}$ given that $x_{\ell,s}$ is transmitted.

The probability $\Pr\left(x_{\ell,s}\rightarrow x_{\tilde{\ell},\tilde{s}}\right)$ can be computed by using (3) as follows,

$$\Pr\left(x_{\ell,s}\rightarrow x_{\tilde{\ell},\tilde{s}}\right)=\Pr\left(\sum_{i=1}^{N_r}|D_i(\ell,s)|^2>\sum_{i=1}^{N_r}\left|D_i(\tilde{\ell},\tilde{s})\right|^2\right) \quad (6)$$

where

$$D_i(\ell,s)=y_i-h'_{\ell,i}s, \quad (7)$$

and,

$$y_i=v_i+h'_{\ell,i}s, \quad (8)$$

where $v_i\sim\mathcal{CN}(0,\sigma_n^2)$. Substituting (8) into (7) result in,

$$D_i(\ell,s)=v_i \quad (9)$$

and

$$D_i(\tilde{\ell},\tilde{s})=v_i+h'_{\ell,i}s-h'_{\tilde{\ell},i}\tilde{s} \quad (10)$$

Hence, $D_i(\ell,s)\sim\mathcal{CN}(0,\sigma_n^2)$, $D_i(\tilde{\ell},\tilde{s})\sim\mathcal{CN}(0,\sigma^2_{D_{\tilde{\ell},\tilde{s}}})$, and,

$$\begin{aligned}\sigma^2_{D_{\tilde{\ell},\tilde{s}}} &= \sigma_n^2+\left(|s|^2+|\tilde{s}|^2\right)d(\ell,\tilde{\ell})+|s-\tilde{s}|^2\left(N_u-d(\ell,\tilde{\ell})\right)\\ &= \sigma_n^2+2\,\mathrm{Re}\{s\tilde{s}^*\}d(\ell,\tilde{\ell})+|s-\tilde{s}|^2N_u \quad (11)\end{aligned}$$

where $\mathrm{Re}(\cdot)$ is the real part of a complex variable and $d(\ell,\tilde{\ell})$ is the number of elements where ℓ and $\tilde{\ell}$ differ from each other.

Let,

$$\kappa_{D_{\ell,s}}=\sum_{i=1}^{N_r}\left|\frac{D_i(\ell,s)}{\sigma_n/\sqrt{2}}\right|^2 \quad (12)$$

and

$$\kappa_{D_{\tilde{\ell},\tilde{s}}}=\sum_{i=1}^{N_r}\left|\frac{D_i(\tilde{\ell},\tilde{s})}{\sigma_{D_{\tilde{\ell},\tilde{s}}}/\sqrt{2}}\right|^2 \quad (13)$$

be the summation of N_r squared complex Gaussian random variables, with zero mean and variance equal to 1, *i.e.* $\kappa_{D_{\ell,s}}$ and $\kappa_{D_{\tilde{\ell},\tilde{s}}}$ are a central chi–squared random variables with $2N_r$ degrees of freedom [11].

Substituting (12) and (13) in (6) gives,

$$\begin{aligned}\Pr\left(x_{\ell,s}\rightarrow x_{\tilde{\ell},\tilde{s}}\right) &= \Pr\left(\frac{\sigma_n^2}{2}\kappa_{D_{\ell,s}}>\frac{\sigma^2_{D_{\tilde{\ell},\tilde{s}}}}{2}\kappa_{D_{\tilde{\ell},\tilde{s}}}\right)\\ &= \Pr\left(\frac{\kappa_{D_{\tilde{\ell},\tilde{s}}}}{\kappa_{D_{\ell,s}}}<\frac{\sigma_n^2}{\sigma^2_{D_{\tilde{\ell},\tilde{s}}}}\right) \quad (14)\end{aligned}$$

Both $\kappa_{D_{\tilde{\ell},\tilde{s}}}$ and $\kappa_{D_{\ell,s}}$ are chi–square distributed random variables and have the same degree of freedom. Let,

$$\varphi=\frac{\kappa_{D_{\tilde{\ell},\tilde{s}}}}{\kappa_{D_{\ell,s}}} \quad (15)$$

which follows an F–distribution with degrees of freedom $\varsigma_1=\varsigma_2=2N_r$. Substituting (15) in (14),

$$\begin{aligned}\Pr\left(x_{\ell,s}\rightarrow x_{\tilde{\ell},\tilde{s}}\right) &= \Pr\left(\varphi<\frac{\sigma_n^2}{\sigma^2_{D_{\tilde{\ell},\tilde{s}}}}\right)\\ &= F_\varphi\left(\frac{\sigma_n^2}{\sigma^2_{D_{\tilde{\ell},\tilde{s}}}}\right). \quad (16)\end{aligned}$$

$F_\varphi(\cdot)$ is the cumulative distribution function (CDF) of the F–distributed random variable given by,

$$F_\varphi(x)=I_{\frac{\varsigma_1 x}{\varsigma_1 x+\varsigma_2}}\left(\varsigma_1/2,\varsigma_2/2\right), \quad (17)$$

where $I_x(a,b)$ is the regularised incomplete beta function given by,

$$I_x(a,b)=\frac{B(x;a,b)}{B(a,b)}=\frac{1}{B(a,b)}\int_0^x t^{(a-1)}\left(1-t\right)^{(b-1)}dt \quad (18)$$

with

$$B(a,b)=\int_0^1 t^{(a-1)}\left(1-t\right)^{(b-1)}dt \quad (19)$$

From (16) and (17) it follows that,

$$\Pr\left(x_{\ell,s}\rightarrow x_{\tilde{\ell},\tilde{s}}\right)=I_{\frac{\sigma_n^2}{\sigma_n^2+\sigma^2_{D_{\tilde{\ell},\tilde{s}}}}}(N_r,N_r) \quad (20)$$

Substituting (20) in (5) yields,

$$\begin{aligned}\Pr_{\text{e,bit}} &\leq \mathrm{E}_{\mathbf{x}}\left[\sum_{\tilde{\ell},\tilde{s}}\frac{N\left(x_{\ell,s},x_{\tilde{\ell},\tilde{s}}\right)I_{\frac{\sigma_n^2}{\sigma_n^2+\sigma^2_{D_{\tilde{\ell},\tilde{s}}}}}(N_r,N_r)}{2^m}\right]\\ &\leq \sum_{\ell,s}\sum_{\tilde{\ell},\tilde{s}}\frac{N\left(x_{\ell,s},x_{\tilde{\ell},\tilde{s}}\right)I_{\frac{\sigma_n^2}{\sigma_n^2+\sigma^2_{D_{\tilde{\ell},\tilde{s}}}}}(N_r,N_r)}{2^{2m}} \quad (21)\end{aligned}$$

It is shown later in section V, that (21) gives a tight approximation to the GSM BER performance.

B. Optimal set of antenna combinations selection

The optimal antenna combination Φ_{opt} is found by minimising the average BER given in (21).

$$\tilde{\Gamma}_{\text{opt}} = \arg\min_{\Gamma} \Pr_{\text{e,bit}} \tag{22}$$

where Γ is the set of parameters (N_t, N_u, Φ).

From (21), it can be noted that only $N(x_{\ell,s}, x_{\tilde{\ell},\tilde{s}})$ and $\sigma^2_{D_{\tilde{\ell},\tilde{s}}}$ depend on Γ. Moreover, it can be found that the relation between I and $\sigma^2_{D_{\tilde{\ell},\tilde{s}}}$ is,

$$I_{\frac{\sigma_h^2}{\sigma_n^2+\sigma^2_{D_{\tilde{\ell},\tilde{s}}}}}(N_r, N_r) \propto \frac{1}{\sigma^2_{D_{\tilde{\ell},\tilde{s}}}} \tag{23}$$

Hence, the optimisation in (22) can be simplified to,

$$\tilde{\Gamma}_{\text{opt}} = \arg\min_{\Gamma} \sum_{\ell,s} \sum_{\tilde{\ell},\tilde{s}} \frac{N\left(x_{\ell,s}, x_{\tilde{\ell},\tilde{s}}\right)}{\sigma^2_{D_{\tilde{\ell},\tilde{s}}}} \tag{24}$$

Fig. 2 shows GSM BER performance using (21) for different set of parameters (Γ), where $m = 5$ and $N_r = 8$. On the one hand, it can be seen from Fig. 2 that the larger N_t is, the better the performance. On the other hand, as it will be shown in the next section, increasing N_t increases the complexity. Furthermore, increasing N_u increases the possibility of having the same antenna in different antenna combinations, which will reduce $d(\ell, \tilde{\ell})$, and consequently degrades GSM performance.

To further elaborate on this, it can be seen from Fig. 2 that there is an optimum number of transmit antennas. Generally a low number of transmit antennas (*e.g.* $N_t = 4$) results in a worse performance. However, increasing the number of transmit antennas does not necessarily improve the performance. For example, the performance of GSM with $N_t = 5$ is better than with $N_t = 6, 7$ or 8.

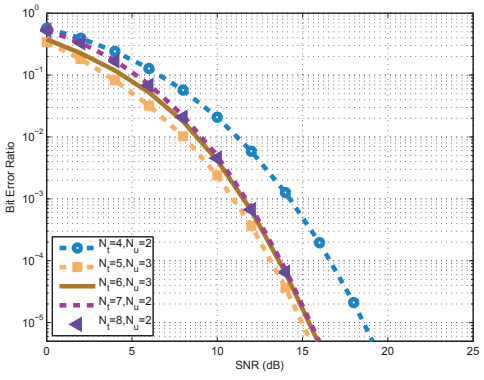

Fig. 2. GSM BER bounds for different Γ

Another interesting observation in Fig. 2 is that a different set of parameters might give very similar performance. In other words, there might not be a unique solution for the optimisation problem in (24) which provides useful flexibility for choosing Γ.

IV. Receiver Complexity

In this section the receiver complexity for GSM is compared to the complexity of the SM optimal decoder given in [4, eq. (4)], using the number of complex operations needed at the receiver. A complex operation is a complex multiplication or addition.

The optimum SM receiver is given by,

$$[\tilde{\ell}_{\text{SM}}, \tilde{s}_{\text{SM}}] = \arg\min_{\ell,s} ||\mathbf{g}_{\ell s}||^2 - 2\,\text{Re}\{\mathbf{y}^H \mathbf{g}_{\ell s}\} \tag{25}$$

where $\mathbf{g}_{\ell s} = \mathbf{h}_{\ell} s$. The complexity of SM optimal decoder in (25) is equal to $N_t M(3N_r + 1)$, where the first term $||\mathbf{g}_{\ell s}||^2$ needs $N_r + 1$ complex operations, and the second term $\mathbf{y}^H \mathbf{g}_{\ell s}$ needs $2N_r$ complex operations, giving a total of $3N_r + 1$ complex operations to compute the equation $(||\mathbf{g}_{\ell s}||^2 - 2\,\text{Re}\{\mathbf{y}^H \mathbf{g}_{\ell s}\})$, which is evaluated $N_t M$ times.

The GSM receiver has a complexity of $N_r N_c M(N_u + 2)$ complex operations, where the squared euclidean distance $|y_i - h'_{\ell,i} s|^2$ needs $N_u + 2$ complex operations, which is calculated $N_r N_c M$ times. Note that $h'_{\ell,i}$ requires a $N_u - 1$ complex summations.

The ratio of GSM receiver complexity to the complexity of SM optimal decoder for the same m_ℓ is,

$$R = \frac{N_r N_C M(N_u + 2)}{N_t M(3N_r + 1)} = \frac{N_r(N_u + 2)}{3N_r + 1} \tag{26}$$

where $N_t = N_c = 2^{m_\ell}$. This is plotted in Fig. 3 for $N_r = 8$. It can be seen that the complexity of GSM increases with the increase of N_u, but this increase is compensated by the substantial reduction in the number of transmit antennas.

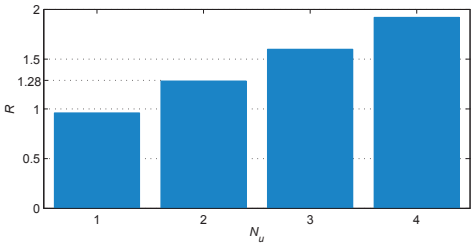

Fig. 3. The ratio of GSM receiver complexity to the complexity of SM optimal decoder

For example, let $m = 6$ bis/s/Hz, $M = 4$ and $N_r = 8$. GSM would have $\sim 28\%$ increase in complexity in comparison to SM, when $N_u = 2$. However, the number of transmit antennas required by GSM is less than half the number of transmit antennas required for SM, where $N_t = 7$ for GSM, and $N_t = 16$ for SM.

Another observation which can be made from Fig. 3 is that for $N_u = 1$ the complexity of GSM is less than the complexity of SM. This is because, the GSM ML receiver proposed here

is less complex than the SM optimal decoder. Note that, GSM with only one active antenna resembles traditional SM.

V. Simulation Results

In the following, Monte Carlo simulation results for at least 10^6 channel realisations are considered in order to compare the performance of GSM with the performance of SM. In the analysis, two different set of parameters (Γ) are considered, to achieve a spectral efficiency of $m = 6$ bits/s/Hz, using $M = 4$ and $M = 8$ QAM and $N_r = 4$.

The BER performance versus signal to noise ratio (SNR) for $M = 4$ is depicted in Fig. 4, where for GSM $N_t = 7$ and $N_u = 2$ and for SM $N_t = 16$. The performance of GSM is nearly identical to the performance of SM. The better performance of SM is mainly due to the higher probability of error when detecting two active antennas instead of only one. However, SM requires more than twice the number of transmit antennas to achieve the same spectral efficiency as compared to GSM. The result also validates the derived analytical bound and shows that, indeed, it is very tight.

The results for $M = 8$ are depicted in Fig. 5 where $N_t = 5$ and $N_u = 2$ are considered for GSM and $N_t = 8$ for SM. Again, GSM and SM have nearly the same performance, with a slightly better performance of SM at high SNR.

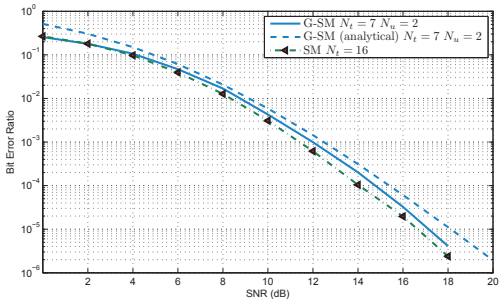

Fig. 4. BER performance versus SNR, for M=4

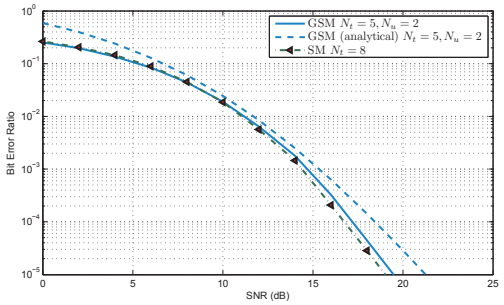

Fig. 5. BER performance versus SNR, for M=8

VI. Summary and Conclusions

In this paper SM was generalised by sending the same symbol from more than one transmit antenna at a time. Hence, SM is no longer limited to a number of transmit antennas which strictly has to follow a power of two. Instead an arbitrary number of transmit antennas can be used. Moreover, higher spectral efficiency can be achieved with a much lower number of transmit antennas, as compared to SM. These, enhancements are achieved at the cost of a slight increase in the complexity. This complexity increase depends on the number of active antennas. The smaller the number of active transmit antennas the less the complexity increase. In general, however, the increase in complexity is outweighed by the significant reduction in the number of transmit antennas. In this context, it is important to highlight that the BER performance of SM and GSM are almost identical. Moreover, GSM retains one of the key advantages of SM, namely that ICI is avoided while spatial multiplexing gains are obtained. Furthermore, this paper proposed a novel receiver based on the ML principle to determine the complete information bits, *i.e.*, the antenna combination used and the transmitted complex symbol. In addition, an algorithm to optimise the selection of the set of antenna combinations, was proposed. Finally, the analytical BER performance for GSM was derived, along with its complexity.

References

[1] E. Telatar, "Capacity of Multi-Antenna Gaussian Channels," *European Transaction on Telecommunication*, vol. 10, no. 6, pp. 585–595, November / December 1999.

[2] G. J. Foschini, "Layered Space-Time Architecture for Wireless Communication in a Fading Environment when Using Multi-Element Antennas," *Bell Labs Technical Journal*, vol. 1, no. 2, pp. 41–59, 1996.

[3] R. Mesleh, H. Haas, S. Sinanović, C. W. Ahn, and S. Yun, "Spatial modulation," *IEEE Trans. Veh. Technol.*, vol. 57, no. 4, pp. 2228 – 2241, July 2008.

[4] J. Jeganathan, A. Ghrayeb, and L. Szczecinski, "Spatial Modulation: Optimal Detection and Performance Analysis," *IEEE Commun. Lett.*, vol. 12, no. 8, pp. 545–547, 2008.

[5] R. Mesleh, M. Di Renzo, H. Haas, and P. M. Grant, "Trellis Coded Spatial Modulation," *IEEE Trans. on Wireless Commun.*, vol. 9, no. 7, pp. 2349–2361, July 2010.

[6] M. Di Renzo and H. Haas, "Space shift keying (ssk) modulation with partial channel state information: Optimal detector and performance analysis over fading channels," *IEEE Trans. on Commun.*, vol. 58, no. 11, pp. 3196 –3210, 2010.

[7] ——, "A general framework for performance analysis of space shift keying (ssk) modulation for miso correlated nakagami-m fading channels," *IEEE Trans. on Commun,*, vol. 58, no. 9, pp. 2590 –2603, 2010.

[8] N. Serafimovski, M. D. Renzo, S. Sinanović, R. Y. Mesleh, and H. Haas, "Fractional Bit Encoded Spatial Modulation (FBE–SM)," *IEEE Commun. Lett.*, vol. 14, no. 5, pp. 429–431, May 2010.

[9] J. Jeganathan, A. Ghrayeb, and L. Szczecinski, "Generalized space shift keying modulation for MIMO channels," in *Proc. IEEE 19th International Symposium on Personal, Indoor and Mobile Radio Communications PIMRC 2008*, Cannes, France, 15–18 September 2008, pp. 1–5.

[10] V. Tarokh, N. Seshadri, and A. Calderbank, "Space-Time Codes for High Data Rate Wireless Communication: Performance Criterion and Code Construction," *IEEE Trans. on Inform. Theory*, vol. 44, no. 2, pp. 744–765, 1998.

[11] J. G. Proakis, *Digital Communications*, 4th ed., ser. McGraw-Hill Series in Electrical and Computer Engineering, S. W. Director, Ed. McGraw-Hill Higher Education, December 2000.

Performance of Spatial Modulation using Measured Real–World Channels

A. Younis[(1)], W. Thompson[(2)], M. Di Renzo[(3)], C.-X. Wang[(4)], M. A. Beach[(2)], H. Haas[(1)], and P. M. Grant[(1)]
[(1)] *Institute for Digital Communications, The University of Edinburgh*
King's Buildings, Mayfield Road, Edinburgh. EH9 3JL, UK
[(2)] *The University of Bristol, Bristol, BS8 1UB, UK*
[(3)] *École Supérieure d'Électricité (SUPÉLEC), University of Paris–Sud XI (UPS)*
3 rue Joliot–Curie, 91192 Gif–sur–Yvette (Paris), France
[(4)] *School of Engineering & Physical Sciences*
Heriot-Watt University, Edinburgh, EH14 4AS, UK
E–Mail: {a.younis, h.haas, p.grant}@ed.ac.uk, {w. thompson, m.a.beach}@bristol.ac.uk,
marco.direnzo@lss.supelec.fr, cheng-xiang.wang@hw.ac.uk

***Abstract*—In this paper, for the first time real–world channel measurements are used to analyse the performance of spatial modulation (SM), where a full analysis of the average bit error rate performance (ABER) of SM using measured urban correlated and uncorrelated Rayleigh fading channels is provided. The channel measurements are taken from an outdoor urban multiple input multiple output (MIMO) measurement campaign. Moreover, ABER performance results using simulated Rayleigh fading channels are provided and compared with a derived analytical bound for the ABER of SM, and the ABER results for SM using the measured urban channels. The ABER results using the measured urban channels validate the derived analytical bound and the ABER results using the simulated channels. Finally, the ABER of SM is compared with the performance of spatial multiplexing (SMX) using the measured urban channels for small and large scale MIMO. It is shown that SM offers nearly the same or a slightly better performance than SMX for small scale MIMO. However, SM offers large reduction in ABER for large scale MIMO.**

***Index Terms*—Spatial modulation (SM), multiple–input multiple–output (MIMO), experimental results, large scale MIMO.**

I. Introduction

Multiple input multiple output (MIMO) systems offer a significant increase in spectral efficiency in comparison to single antenna systems [1]. An example is spatial multiplexing (SMX) [2]. SMX achieves a spectral efficiency that increases linearly with the number of transmit antennas, by transmitting simultaneously over all the transmit antennas. However, SMX cannot cope with the exponential increase of wireless data traffic, and a larger number of transmit antennas (large scale MIMO) should be used. Large scale MIMO systems studied in [3], offers a higher data rate and better average bit error performance (ABER). However, this comes at the expense of an increase in i) hardware complexity, where the number of radio frequency (RF) chains is equal to the number of transmit antennas, ii) receiver computational complexity, where the SMX complexity increases exponentially with the number of transmit antennas. Thus, SMX may not be always feasible and a cheaper solution should be used.

Spatial Modulation (SM) is a transmission technology proposed for MIMO wireless systems. It aims to increase the spectral efficiency, of single–antenna systems while avoiding Inter–Channel Interference (ICI) [4]. This is achieved by i) the activation of a single antenna at each time instance which transmits a given data symbol (*constellation symbol*), and ii) the exploitation of the spatial position (index) of the active antenna as an additional dimension for data transmission (*spatial symbol*). The receiver applies the Maximum Likelihood optimum decoder for SM (SM–ML), which performs an exhaustive search over the whole *constellation symbol* and *spatial symbol* space. Activating only one antenna at a time means that only one RF chain is needed, which significantly reduces the hardware complexity of the system [5]. It also offers a significant reduction in the energy needed. This reduction increases linearly with the number of transmit antennas, as only one antenna needs to be powered at a time, *i.e.*, "green" technology. Moreover, as it will be shown in this paper the computational complexity of SM–ML is equal to the complexity of single–antenna systems, *i.e.*, the complexity of SM–ML does not depend on the number of transmit antennas. Accordingly, SM is an attractive candidate for large scale MIMO.

In this paper, for the first time real-world channel measurements are used to analyse the performance of SM, where a full analysis of the ABER of SM using measured urban correlated and uncorrelated Rayleigh fading channels is provided. The channel measurements are taken from an outdoor urban MIMO measurement campaign. Moreover, an analytical bound for the ABER of SM is derived and performance results using simulated Rayleigh fading channels are provided. It is shown that the results using the measured urban channels validate the derived analytical bound and the results using the simulated channels. Furthermore, the ABER of SM is compared with the performance of SMX using the measured urban channels for small and large scale MIMO. It is shown that SM offers nearly the same or a slightly better performance than SMX for small scale MIMO. However, SM offers large reduction in ABER for large scale MIMO.

The remainder of this paper is organised as follows. In Section II, the system model and the ML–optimum receiver are summarised. In Section III, the channel measurements are introduced. In Section IV, an analytical bound for SM over correlated and uncorrelated Rayleigh channels is derived. The complexity of SM and SMX is discussed and compared in V. Finally, the results are presented in Section VI, and the paper is concluded in Section VII.

II. System Model

In SM, the bit stream emitted by a binary source is divided into blocks containing $m = \log_2(N_t) + \log_2(M)$ bits each, where m is the spectral efficiency, N_t is the number of transmit antennas and M is the signal constellation size. Then the following mapping rule is used [4]:

- The first $\log_2(N_t)$ bits are used to select the antenna that is switched on for data transmission, while all the other transmit–antennas are kept silent. In this paper, the actual transmit–antenna that is active for transmission is denoted by ℓ_t, with $\ell_t \in \{1, 2, \ldots, N_t\}$.
- The second $\log_2(M)$ bits are used to choose a symbol in the signal–constellation diagram. Without loss of generality, Quadrature Amplitude Modulation (QAM) is considered. In this paper, the actual complex symbol emitted by the transmit–antenna ℓ_t is denoted by s_t, with $s_t \in \{s_1, s_2, \ldots, s_M\}$.

Accordingly, the $N_t \times 1$ dimensional transmit vector is:

$$\mathbf{x}_{\ell_t, s_t} = \left[\mathbf{0}_{1\times(\ell_t-1)}, s_t, \mathbf{0}_{1\times(N_t-\ell_t)}\right]^T \tag{1}$$

where $[\cdot]^T$ denotes transpose operation, and $\mathbf{0}_{p\times q}$ is a $p \times q$ matrix with all–zero entries.

The transmitted vector, $\mathbf{x}_{\ell_t, s_t}$, in (1) is transmitted over a flat fading $N_r \times N_t$ MIMO channel with transfer function $\mathbf{H}$, where N_r is the number of receive antennas. The Kronecker channel model [6], with an exponential correlation profile for both the transmitter correlation matrix ($\mathbf{R}_{\text{Tx}}$) and receiver correlation matrix ($\mathbf{R}_{\text{Rx}}$), is used to model channel correlation [7],

$$\mathbf{H} = \mathbf{R}_{\text{Rx}}^{\frac{1}{2}} \bar{\mathbf{H}} \mathbf{R}_{\text{Tx}}^{\frac{1}{2}} \tag{2}$$

where $\bar{\mathbf{H}}$ has independent and identically distributed (i.i.d.) entries according to $\mathcal{CN}(0, 1)$.

Thus, the $N_r \times 1$ dimensional receive vector can be written as follows:

$$\mathbf{y} = \mathbf{H}\mathbf{x}_{\ell_t, s_t} + \mathbf{n} \tag{3}$$

where $\mathbf{n}$ is the N_r–dimensional Additive White Gaussian Noise (AWGN) with zero–mean and variance σ^2 per dimension at the receiver input.

At the receiver the ML optimum detector for MIMO systems is used,

$$\hat{\mathbf{x}}_t = \underset{\mathbf{x}\in\mathcal{Q}^m}{\arg\min} \left\{ \|\mathbf{y} - \mathbf{H}\mathbf{x}\|_{\text{F}}^2 \right\} \tag{4}$$

where $\mathcal{Q}^m$ is a 2^m space containing all possible $(N_t \times 1)$ transmitted vectors, $\|\cdot\|_{\text{F}}$ is the Frobenius norm, and $\hat{\cdot}$ denotes the estimated spatial and constellation symbols.

In SM only one transmit antenna is active at a time. Therefore, the optimal receiver in (5) can be simplified to,

$$\begin{aligned} \left[\hat{\ell}_t, \hat{s}_t\right] &= \underset{\substack{\ell\in\{1,2,\ldots N_t\} \\ s\in\{s_1,s_2,\ldots s_M\}}}{\arg\min} \left\{ \|\mathbf{y} - \mathbf{h}_\ell s\|_{\text{F}}^2 \right\} \\ &= \underset{\substack{\ell\in\{1,2,\ldots N_t\} \\ s\in\{s_1,s_2,\ldots s_M\}}}{\arg\min} \left\{ \sum_{r=1}^{N_r} |y_r - h_{\ell,r} s|^2 \right\} \end{aligned} \tag{5}$$

where y_r and $h_{\ell,r}$ are the r–th entries of $\mathbf{y}$ and $\mathbf{h}_\ell$ respectively.

III. Channel Measurement and Model

The channel measurements used within this paper were acquired within the Mobile VCE MIMO elective [8]. MIMO channel measurements were taken around the centre of Bristol in the United Kingdom, using a MEDAV RUSK channel sounder, a 4×4 antenna configuration, with 20 MHz bandwidth centred at 2 GHz. The transmitter consisted of a pair of dual polarised ($\pm45^\circ$) Racal Xp651772 antennas [9] separated by 2 m, positioned atop a building, providing elevated coverage of the central business and commercial districts of Bristol city. At the receiver two different receiver devices are used, both equipped with four antennas.

The two receiver devices are a reference headset and a laptop. The reference antenna design is based on 4-dipoles mounted on a cycle helmet, thus avoiding any shadowing by the user. The laptop is equipped with 4 PIFA elements, both devices are detailed in [8]. Fifty–eight measurement locations were chosen around the city. At each location the user walked, holding the laptop in front of them and the reference device on their head, in a straight line roughly 6 m long, until 4096 channel snapshots have been recorded. A second measurement was then taken with the user walking a second path perpendicular to the first. As the measurement speed is significantly faster than the coherence time of the channel, the measurements are averaged in groups of four to reduce measurement noise.

One set of measurement results with the laptop and reference device, and a second set of only the reference device measurements taken at the same locations, but on different days, is also included in the measurement data for analysis. This provides a total of 348 different measurement sets, each containing 1024 snapshots of a 4×4 MIMO channel, with 128 frequency bins spanning the 20 MHz bandwidth. As the simulations are carried out using flat fading channels, a single frequency bin centred around 2 GHz, is chosen from each measurement snapshot to create the narrowband channel.

A. Small Scale MIMO

For small scale MIMO, Rayleigh fading channels were distinguished using the Chi-squared goodness of fit test, with a significance level of 1%, where of the 348 measurements, only 20 measurements fulfilled this requirement. For each measurement the transmit and receive correlation matrices are estimated, then the decay of the correlation, based on the antenna indices, is fitted to an exponential decay model [7],

$$\mathbf{R}_c = \begin{bmatrix} 1 & r_c & r_c^2 & \cdots & r_c^{n-1} \\ r_c & 1 & r_c & \ddots & \vdots \\ \vdots & \ddots & \ddots & \ddots & r_c \\ r_c^{n-1} & \cdots & r_c^2 & r_c & 1 \end{bmatrix} \tag{6}$$

where $r_c = \exp(-\beta)$, β is the correlation decay coefficient, and n is the number of antennas. Two channels with the lowest mean square error between the exponential decay in (6) and the actual correlation matrices are chosen for the two correlated channel results. Both of the chosen channels are from measurements taken using the laptop device, and the measured decay coefficients for the transmitter and receiver

are 0.5 and 0.8 for the first channel and 0.7 and 0.4 for the second channel respectively.

For the uncorrelated channels, the two channels with the lowest average correlation coefficient between their MIMO channels were chosen. One is from the laptop measurements, and the other from the reference headset device measurements. Selecting the channels in this manner may not provide completely uncorrelated channels per say, as there may still be a small correlation between the channels. However, it will provide the channel measurements that experienced the lowest spatial correlations.

B. Large scale MIMO

The original measurements were taken using 4×4 system. However, by manipulating the measurements we are able to create much larger virtual MIMO systems.

The following steps are taken in order to create the large scale channel array:

1) Channel measurements from the reference device is used to exclude the body shadowing effects.
2) The original channels are reversed, such that the mobile station becomes the transmitting device. The reason for that is that the transmitters of the original channel measurements are fixed on top of a building, while the receiver device moved.
3) The first channel from each snapshot, from the walking measurements, was chosen to form each of the virtual array transmitters, resulting in a virtual array with 1024 elements.
4) To reduce the correlation between adjacent channels, every fourth element of this array was chosen, forming a maximum array size of 256 antennas. These are equally spaced along a path of about 6 m in length.
5) The locations with good fitting to Rayleigh fading distributions were first chosen, and then those that showed the lowest variation in their Rayleigh fading statistics between each virtual spatial channel were selected. This is done to avoid the scenario where the user experienced significant channel shadowing along part of the walking measurement, as this would introduce a significant power imbalance in the virtual MIMO channel.

The Rayleigh fading mean statistic of the normalised constructed virtual MIMO channel has an average of 0.70, and a variance of 0.16.

IV. Analytical Modelling of SM–ABER over Correlated and Uncorrelated Channels

The ABER for SM system can be approximated by using the union bound [10], which can be expressed as follows,

$$\underset{\text{SM}}{\text{ABER}} \leq \sum_{\ell_t,s_t} \sum_{\ell,s} \frac{N\left(\mathbf{x}_{\ell_t,s_t}, \mathbf{x}_{\ell,s}\right)}{m} \frac{\mathrm{E}_{\mathbf{H}}\left\{\Pr\left(\mathbf{x}_{\ell,s} \neq \mathbf{x}_{\ell_t,s_t}\right)\right\}}{2^m} \tag{7}$$

where $N\left(\mathbf{x}_{\ell_t,s_t}, \mathbf{x}_{\ell,s}\right)$ is the number of bits in error between $\mathbf{x}_{\ell_t,s_t}$ and $\mathbf{x}_{\ell,s}$, $\mathrm{E}_{\mathbf{H}}\{\cdot\}$ is the expectation across $\mathbf{H}$ and $\Pr\left(\mathbf{x}_{\ell,s} \neq \mathbf{x}_{\ell_t,s_t}\right)$ is the conditional pairwise error probability (PEP) of deciding on $\mathbf{x}_{\ell,s}$ given that $\mathbf{x}_{\ell_t,s_t}$ is transmitted,

$$\begin{aligned} \Pr\left(\mathbf{x}_{\ell,s} \neq \mathbf{x}_{\ell_t,s_t}\right) &= \Pr\left(\left\|\mathbf{y} - \mathbf{H}\mathbf{x}_{\ell_t,s_t}\right\|^2 > \left\|\mathbf{y} - \mathbf{H}\mathbf{x}_{\ell,s}\right\|^2\right) \\ &= Q\left(\sqrt{\frac{\left\|\mathbf{H}\Psi\right\|^2}{2\sigma_n^2}}\right) \\ &= \frac{1}{\pi}\int_0^{\frac{\pi}{2}} \exp\left(-\frac{\left\|\mathbf{H}\Psi\right\|^2}{4\sigma_n^2 \sin^2\theta}\right) d\theta \end{aligned} \tag{8}$$

where $\Psi = \left(\mathbf{x}_{\ell_t,s_t} - \mathbf{x}_{\ell,s}\right)$, and the alternative integral expression of the Q-function is given in [11].

Taking the expectation of (8), we have,

$$\mathrm{E}_{\mathbf{H}}\left\{\Pr\left(\mathbf{x}_{\ell,s} \neq \mathbf{x}_{\ell_t,s_t}\right)\right\} = \frac{1}{\pi}\int_0^{\frac{\pi}{2}} \Phi\left(-\frac{1}{4\sigma_n^2 \sin^2\theta}\right) d\theta \tag{9}$$

where $\Phi\left(\cdot\right)$ is the moment-generation function (MGF) of the random variable $\left\|\bar{\mathbf{H}}\Psi\right\|^2$.

From [12], and noting that in SM only one antenna is active at a time, the MGF in (9) for quasi–static fading with spatial correlation is equal to,

$$\Phi\left(s\right) = \prod_{j=1}^{N_r} \left(1 - s\lambda_j\mu\right)^{-1} \tag{10}$$

where λ_j are the eigenvalues of $\mathbf{R}_{\text{Rx}}$ and $\mu = |s_t|^2 + |s|^2 - 2\text{Re}\{s_t s^*\}\mathbf{R}_{\text{Tx}}(\ell_t, \ell)$.

Substituting (10) and (9) in (7) and using the Chernoff bound, the ABER for SM over Rayleigh channels is,

$$\underset{\text{SM}}{\text{ABER}} \leq \frac{1}{2\pi} \sum_{\ell_t,s_t} \sum_{\ell,s} \prod_{j=1}^{N_r} \frac{N\left(\mathbf{x}_{\ell_t,s_t}, \mathbf{x}_{\ell,s}\right)}{m} \frac{1}{2^m} \left(1 + \frac{\lambda_j\mu}{4\sigma_n^2}\right)^{-1} \tag{11}$$

In Section VI, we show that the two bounds; for uncorrelated and correlated Rayleigh channels, i) are tight upper bounds for SM, and ii) they validate the experimental results.

V. Complexity Analysis

In this section the receiver complexity for SM–ML is compared to the complexity of SMX–ML. The complexity is computed as the number of real multiplicative operations $(\times, \div)$ needed by each algorithm [13].

- SM–ML: The computational complexity of the SM–ML receiver in (5) is equal to

$$\mathcal{C}_{\text{SM–ML}} = 8N_r 2^m \tag{12}$$

  as the ML detector searches through the whole transmit and receive search spaces. Note, evaluating the Euclidean distance $\left(\left|y_r - h_{\ell,r}s\right|^2\right)$ requires 2 complex multiplications, where each complex multiplication requires 4 real multiplications.
- SMX–ML: The computational complexity of SMX–ML is equal to,

$$\mathcal{C}_{\text{SMX–ML}} = 4\left(N_t + 1\right)N_r 2^m \tag{13}$$

  Note, $\left(\left|\mathbf{y} - \mathbf{H}\mathbf{x}\right|^2\right)$ in (4) requires $(N_t + 1)$ complex multiplications.

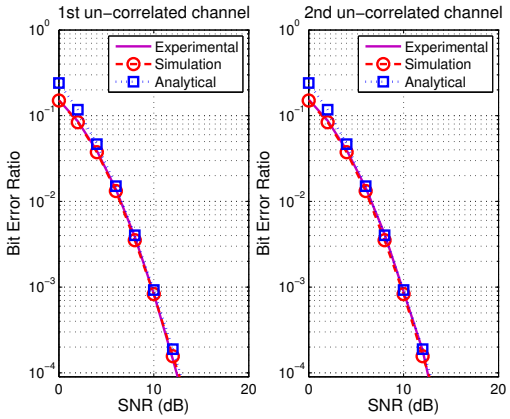

Fig. 1. ABER versus the SNR for SM over an uncorrelated channel. $m = 4$, $N_t = N_r = 4$.

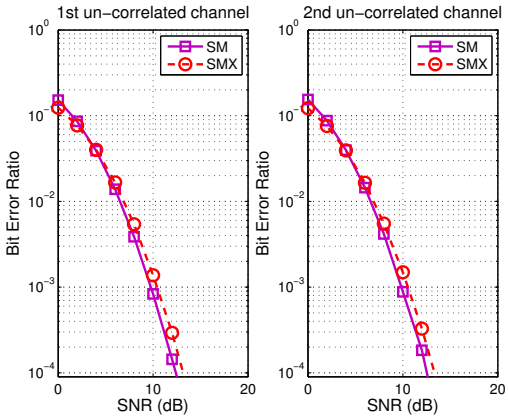

Fig. 3. ABER versus the SNR for SM and SMX over an uncorrelated channel. $m = 4$, $N_t = N_r = 4$.

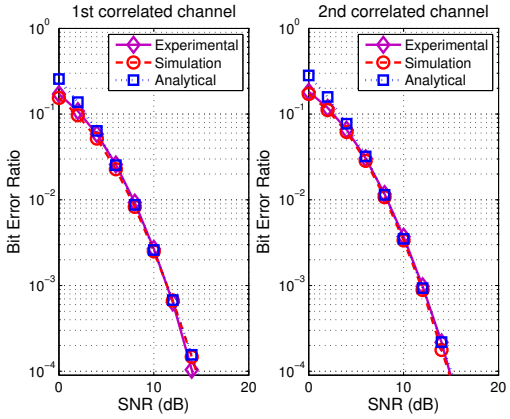

Fig. 2. ABER versus the SNR for SM over a correlated channel. $m = 4$, $N_t = N_r = 4$.

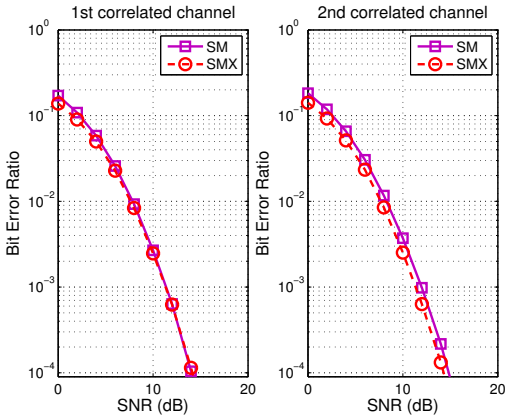

Fig. 4. ABER versus the SNR for SM and SMX over a correlated channel. $m = 4$, $N_t = N_r = 4$.

From (12) and (13), the reduction of SM–ML receiver complexity relative to the complexity of the SMX–ML decoder for the same spectral efficiency is given by,

$$\mathcal{C}_{\text{rel}} = 100 \times \left(1 - \frac{2}{N_t + 1}\right) \tag{14}$$

From (12), the complexity of SM does not depend on the number of transmit antennas, and it is equal to the complexity of single–input multiple–output (SIMO) systems. Hence, the reduction in complexity offered by SM increases with the increase in the number of transmit antennas. However, the complexity of SMX increases linearly with the number of transmit antennas. For example from (14), for $N_t = 4$, SM offers a 60% reduction in complexity, and as the number of transmit antennas increase the reduction increases. For $N_t = 128$, SM offers 98% reduction in complexity.

VI. Results

In the following, Monte Carlo simulation results for the ABER performance of SM using the measured urban channels and simulated Rayleigh channels are compared with the derived analytical bound. Note, each channel of the measured urban channels contains 1024 snapshots. Furthermore, the performance of SM using the measured urban channel is compared with the performance of SMX over the same channels for small and large scale MIMO.

A. Validation of SM analytical ABER performance using experimental results

Fig. 1 and Fig. 2 show the ABER performance of SM using the measured urban channels (solid line) and using simulated Rayleigh channels (red dashed line). The results are compared with the derived analytical bound (blue dotted line), for $m = 4$ and $N_t = N_r = 4$. Fig. 1 shows the ABER for uncorrelated

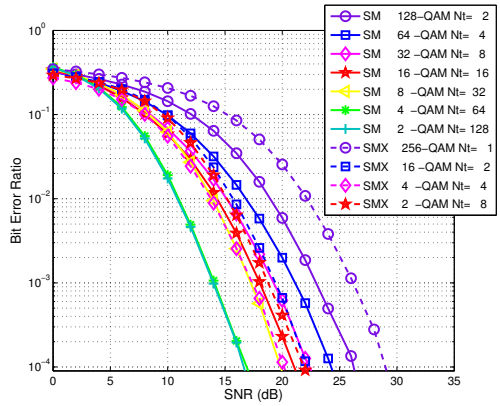

Fig. 5. ABER versus the SNR for SM and SMX over real measured channels. $m = 8$, $N_r = 4$.

channels and Fig. 2 shows the ABER for correlated channels. As can be seen from the figures, the experimental results closely match the simulation and analytical curves for ABER $< 10^{-2}$. In Fig. 1 we can see that SM offers the same performance for both chosen channels, where both channels are uncorrelated. However, in Fig. 2, there is a slight difference in the performance, since the two chosen correlated channels have different correlation matrices. Moreover, if we compare the results for uncorrelated channels in Fig. 1 with those correlated channels in Fig. 2, we see that SM performs better when the channels are uncorrelated channels, as it is easier to distinguish the different channel paths.

B. Comparison in the ABER performance of SM and SMX

1) Small Scale MIMO: Figs. 3 and 4 compare the ABER between SM (solid line) and SMX (dashed line) using the measured urban channels for $m = 4$ and $N_t = N_r = 4$. From both figures, we can see that SM offers almost the same as or slightly better performance than SMX. In Fig. 3, the performance of both systems does not change for both channels since the channels are uncorrelated. However, as shown in Fig. 4, this is not the case for the correlated channels, where the performance is different due to the different correlation coefficients.

2) Large Scale MIMO: Fig. 5 compares the ABER between SM (solid line) and SMX (dashed line) using the virtual large scale MIMO channel created using the measured urban channels as explained in Sec.III-B, where $m = 8$, $N_r = 4$. For $m = 8$ the maximum number of transmit antennas that SMX can use is $N_t = 8$, where $m = N_t \log_2(M)$. However, for SM the maximum number of antennas that can be used is $N_t = 128$, making it possible to exploit the advantages of large scale MIMO. Note that for SM it holds that: $m = \log_2(N_t) + \log_2(M)$. Finally, in Fig. 5 we can see that SM with $N_t = 128$ and $N_t = 64$ offers 6 dB and 4 dB better performance than SMX with $N_t = 8$ and $N_t = 4$ respectively. Note that the constellation size is the same for both SM with $N_t = 128$ and SMX with $N_t = 8$, as is for SM with $N_t = 64$ and SMX with $N_t = 4$. As the number of transmit antennas decreases, the ABER of SM and SMX increases, *i.e.*, moving to $N_t = 16$ for SM we see that SM offers only a 1 dB performance increase relative to SMX with $N_t = 2$. Note, the number of bits sent per transmission for both SM and SMX for all the scenarios is equal, $m = 8$.

VII. Summary and Conclusion

In this paper, performance analysis of SM using urban Rayleigh channel measurements for both correlated and uncorrelated scenarios has been carried out. An analytical bound has been derived and performance results using simulated channels have been provided. An important observation is that experimental results confirm the analytical bound as well as computer simulations of the system. The performance of SM has been compared with the performance of SMX using the same urban channels. It has been demonstrated that for small scale MIMO, SM offers similar or slightly better ABER performance. However, for large scale MIMO, SM exhibits a significant enhancement in the ABER performance at no increase in complexity. This makes SM an ideal candidate for future large scale MIMO systems.

Acknowledgement

This work has been partially funded by the University of Edinburgh Initiating Knowledge Transfer Fund (IKTF), RCUK (EP/G042713/1, UK-China Science Bridges "R&D on (B)4G Wireless Mobile Communications") and the European Union (PITNGA2010264759) "GREENET" project.

References

[1] E. Telatar, "Capacity of Multi-Antenna Gaussian Channels," *European Trans. on Telecommun.*, vol. 10, no. 6, pp. 585–595, Nov. / Dec. 1999.
[2] G. J. Foschini, "Layered Space-Time Architecture for Wireless Communication in a Fading Environment when Using Multi-Element Antennas," *Bell Labs Tech. J.*, vol. 1, no. 2, pp. 41–59, 1996.
[3] B. Cerato and E. Viterbo, "Hardware implementation of a low-complexity detector for large MIMO," in *IEEE Int. Symp. on Circuits and Systems (ISCAS 2009)*, May 2009, pp. 593 –596.
[4] R. Mesleh, H. Haas, S. Sinanović, C. W. Ahn, and S. Yun, "Spatial Modulation," *IEEE Trans. on Veh. Tech.*, vol. 57, no. 4, pp. 2228 – 2241, Jul. 2008.
[5] J. Jeganathan, A. Ghrayeb, L. Szczecinski, and A. Ceron, "Space Shift Keying Modulation for MIMO Channels," *IEEE Trans. on Wireless Commun.*, vol. 8, no. 7, pp. 3692–3703, Jul. 2009.
[6] J. P. Kermoal, L. Schumacher, K. I. Pedersen, P. E. Mogensen, and F. Frederiksen, "A Stochastic MIMO Radio Channel Model with Experimental Validation," *IEEE Journal on Selected Areas in Communications*, vol. 20, no. 6, pp. 1211 – 1226, Aug. 2002.
[7] A. V. Zelst and J. S. Hammerschmidt, "A Single Coefficient Spatial Correlation Model for Multiple-Input Multiple-Output (MIMO) Radio Channels," in *27th General Assembly of the International Union of Radio Science (URSI)*, 2002, pp. 1–4.
[8] M. Hunukumbure and M. Beach, "MIMO Channel Measurements and Analysis with Prototype User Devices in a 2GHz Urban Cell," in *2006 IEEE 17th International Symposium on Personal, Indoor and Mobile Radio Communications (PIMRC)*, Sept. 2006, pp. 1 –5.
[9] INOTEK Antennas, "Single Band, Dual Polarised Antenna UMTS XP/65/17.5/2, 4, 6, 8 or 10 Type 2209," http://www.inotekantennas.com/pdf/2209.pdf.
[10] J. G. Proakis, *Digital Communications*, 4th ed. McGraw–Hill, 2000.
[11] M. K. Simon and M.-S. Alouini, *Digital Communication over Fading Channels: A Unified Approach to Performance Analysis*, 1st ed. John Wiley & Sons, Inc., 2000.
[12] A. Hedayat, H. Shah, and A. Nosratinia, "Analysis of space-time coding in correlated fading channels," *IEEE Transactions on Wireless Communications*, vol. 4, no. 6, pp. 2882 – 2891, Nov. 2005.
[13] G. H. Golub and C. F. van Loan, *Matrix Computations*. The John Hopkins University Press, 1996.

6th IEEE International Workshop on Heterogeneous, Multi-Hop, Wireless and Mobile Networks

2-User Multiple Access Spatial Modulation

Nikola Serafimovski*, Sinan Sinanović*, Abdelhamid Younis*, Marco Di Renzo†, and Harald Haas*

*Institute for Digital Communications
Joint Research Institute for Signal and Image Processing
School of Engineering
The University of Edinburgh
EH9 3JL, Edinburgh, UK
{n.serafimovski, s.sinanovic, a.younis, h.haas}@ed.ac.uk

†Laboratory of Signals and Systems (L2S),
French National Center for Scientific Research (CNRS)
École Supérieure d'Électricité (SUPÉLEC),
University of Paris–Sud XI (UPS)
3 rue Joliot–Curie, 91192 Gif–sur–Yvette (Paris), France
marco.direnzo@lss.supelec.fr

***Abstract*—Spatial modulation (SM) is a recently proposed approach to multiple–input–multiple–output (MIMO) systems which entirely avoids inter–channel interference (ICI) and requires no synchronisation between the transmit antennas, while achieving a spatial multiplexing gain. SM allows the system designer to freely trade off the number of transmit antennas with the signal constellation. Additionally, the number of transmit antennas is independent from the number of receive antennas which is an advantage over other multiplexing MIMO schemes. Most contributions thus far, however, have only addressed SM aspects for a point-to-point communication systems, *i.e.* the single-user scenario. In this work we seek to characterise the behaviour of SM in the interference limited scenario. The proposed maximum-likelihood (ML) detector can successfully decode incoming data from multiple sources in an interference limited scenario and does not suffer from the near-far problem.**

I. Introduction

Multiple-antenna systems are fast becoming a key technology for modern wireless systems. They offer improved error performance and higher data rates, at the expense of increased complexity and power consumption [1]. Spatial modulation (SM) is a recently proposed approach to multiple–input–multiple–output (MIMO) systems which entirely avoids inter–channel interference (ICI) and requires no synchronisation between the transmit antennas, while achieving a spatial multiplexing gain [2]. A spatial multiplexing gain is achieved by mapping a block of information bits into a constellation point in the signal and spatial domains [3]. In SM, the number of information bits, ℓ, encoded in the spatial domain can be related to the number of transmit antennas N_t as $N_t = 2^\ell$. This means that the number of transmit antennas must be a power of two unless fractional bit encoding is used [4]. Additionally, compared to other MIMO schemes, the spatial multiplexing gain *i.e.* the number of transmit antennas, is independent of the number of receive antennas. This offers the flexibility to trade off the number of transmit antennas with the modulation order in the signal domain to meet the desired data rate without regard for the number of receive antennas. It should also be noted that SM is shown to outperform other MIMO schemes in terms of bit-error-ratio (BER) [3].

A number of papers are available in the literature which are aimed at understanding and improving the performance of SM in various scenarios. Trellis coding on the transmit antenna is proposed in [5], a reduced complexity decoder is given in [6] and the performance of SM over a wide range of channels is presented in [7]. The optimal detector is known with and without channel state information at the receiver in [8–10]. The optimal power allocation problem for a 2 transmit with 1 receive antenna system is solved in closed form in [11] and the performance of SM in correlated fading channels is considered in [12]. Recent work has also shown that SM can be combined with space-time block codes to attain spectral efficiency gains [13]. SM has also been applied to relaying systems in [14] where it exhibits significant signal-to-noise-ratio (SNR) gains when compared to non-cooperative decode and forward.

Most contributions thus far, however, have only addressed SM aspects for a point-to-point communication systems, *i.e.* the single-user scenario. These scenarios include the application of SM in traditional orthogonal access systems such as frequency division multiple access (FDMA), time division multiple access (TDMA) or orthogonal frequency division multiple access (OFDMA) where co-channel interference is managed by ensuring orthogonal transmissions by all nodes in the system. A notable exception is given in [15], where the authors focus their analysis on a limited two user scenario employing only space-shift-keying (SSK). It should be noted, that SSK is similar to SM in that the antenna index is used for data transmission, but instead of a full signal-symbol only a reference signal is sent to enable channel estimation at the receiver.

In this work we seek to characterise the behaviour of SM in the interference limited scenario. In particular, we propose a maximum-likelihood (ML) detector which can successfully decode incoming data in the case of simultaneous transmission and does not suffer from the near-far problem, *i.e.* the detector can successfully decode data from a user with a lower signal-to-noise-ratio (SNR). The proposed jointly optimum multi-user detector minimises the BER for all users and does not suffer from the near-far problem.

The remainder of this work is organized as follows. In Section II, the system and channel models are introduced. In Section III, the performance of SM in the multiple access scenario is characterised and the analytical modelling for the multi-user detector is proposed. Section IV provides numerical and simulation results to substantiate the accuracy of the analytical framework developed. In Section V, we summarise and conclude the work.

978-1-4673-0040-7/11/$26.00 ©2011 IEEE

II. System Model

The basic idea of SM is to map blocks of information bits into two information carrying units [3]: i) a symbol, chosen from a complex signal–constellation diagram, and ii) a unique transmit–antenna, chosen from the set of transmit–antennas in the antenna–array, *i.e.* the spatial–constellation. The general SM constellation point is thus a combination of a signal-constellation point and a spatial-constellation point. The SM constellation diagram is presented in Fig. 1.

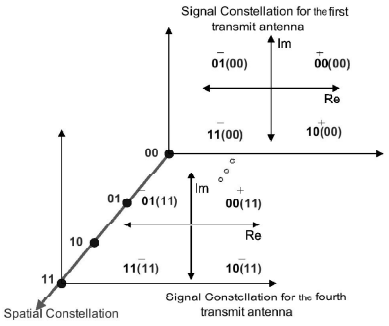

Fig. 1. A transmission of four bits is assumed. The first two bits from right to left define the spatial–constellation point identifying the active antenna, while the remaining two bits determine the signal–constellation point that will be transmitted. This scenario means that a single SM constellation point carries four information bits.

In the following work we assume a three node scenario as shown in Fig. 2 where we seek to characterise the behaviour of SM during simultaneous transmission *i.e.* in the presence of co-channel interference. We assume that the two transmit nodes, denoted as User1, node (U_1), and User2, node (U_2), in Fig. 2, transmit simultaneously to the receiver on the same time-frequency slot. Each node broadcasts a signal constellation symbol, x, from one of its available antennas.

The received signal is given by:

$$y_j = \sqrt{E_m \sigma^2_{(U_1)}}\, h_{i^{(U_1)}j} x^{(U_1)} + \sqrt{E_m \sigma^2_{(U_2)}}\, h_{k^{(U_2)}j} x^{(U_2)} + \eta \tag{1}$$

where:

- E_m is the average energy per symbol for both nodes,
- i and k are the indices of the transmit antennas from nodes 1 and 2 respectively,
- j is the index of the receive antenna from a total of N_r available,

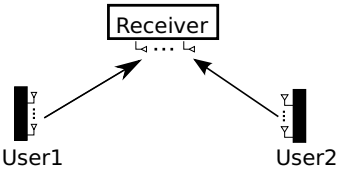

Fig. 2. Spatial modulation with simultaneous transmission. The receive cannot distinguish which is the desired and which is the interferencing user. Therefore, it must treat each users as its intended user.

- $\sigma^2_{(U_1)}$ and $\sigma^2_{(U_2)}$ are the channel attenuation coefficients on the U_1 to receiver and U_2 to receiver links in Fig. 2 respectively,
- $h_{i^{(U_1)}j}$ and $h_{k^{(U_2)}j}$ are the fast fading channel coefficients of the link between the active antennas (i, k) and the receiving antenna j, and
- η, is a complex normal random variable with zero mean and variance N_o, $\mathcal{CN}(0, N_o)$, and represents the additive white Gaussian noise (AWGN) at the receiver.

We note that all bold notations indicate vector notations. We now look at the analytical formulation of the system.

III. Analytical Modelling

In this section, we develop a ML detector for use in the presence of co-channel interference. The detector computes the Euclidean distance between the received vector signal $\bar{\mathbf{y}}$ and the set of all possible received signals, selecting the closest one. The mathematical formulation of the ML detector used in the system is given in (2). We note that this formulation is valid for any channel vectors and any transmitted symbols. In particular, if the channels are correlated *i.e.* non-orthogonal, then it will be more difficult for the receiver to distinguish the individual antennas used in the transmission, which will result in an increase of the BER.

Starting from the system model presented in Section II, the decoded pair $(x_{\text{est}}, n_t)^{(\xi)}$, formed from the estimated symbol x_{est} emitted from antenna n_t on node ξ, where $\xi \in \{(U_1), (U_2)\}$, is given by:

$$\begin{Bmatrix} (x_{\text{est}}, n_t)^{(U_1)}, \\ (x_{\text{est}}, n_t)^{(U_2)} \end{Bmatrix} = \text{argmin} \left\{ \left|\left| \bar{\mathbf{y}} - \sum_{u \in \{(U_1),(U_2)\}} x^{(u)} \mathbf{h}_{n_t^{(u)}} \right|\right|^2_{\text{F}} \right\} \tag{2}$$

$$x^{(u)} \in \mathcal{X}^{(u)} \qquad n_t^{(u)} \in \{1 \dots N_t^{(u)}\}$$

$\mathcal{X}^{(u)}$ is the set of all possible signal constellation points for node u with $M^{(u)}$ number of elements, $N_t^{(u)}$ is the number of available transmit antennas on node u and $||\cdot||_{\text{F}}$ is the Frobenius norm.

From here we can use techniques base on the union bound to describe the behaviour of the interference aware SM detector in the high SNR regions. The union bound for the interference aware SM detector, which estimates the average bit-error-ratio (ABER) for node ξ, can be expressed as given in (3) where $\mathcal{N}_\xi(b, \hat{b}) = \mathcal{N}_\xi(n_t, \hat{n}_t) + \mathcal{N}_\xi(x, \hat{x})$. $\mathcal{N}_\xi(n_t, \hat{n}_t)$ denotes the Hamming distance between the binary representations of the antenna indices n_t and $\hat{n}_t$ on node ξ. Similarly, $\mathcal{N}_\xi(x, \hat{x})$ denotes the Hamming distance between the binary representations of the symbols x and $\hat{x}$ on node ξ.

We define PEP $\left(x^{(U_1),(U_2)}, n_t^{(U_1),(U_2)}, \hat{x}^{(U_1),(U_2)}, \hat{n}_t^{(U_1),(U_2)}\right)$ to be the pairwise error probability between the symbol $x^{(U_1),(U_2)}$ emitted from antennas $n_t^{(U_1),(U_2)}$ being detected as symbol $\hat{x}^{(U_1),(U_2)}$ emitted by antenna $\hat{n}_t^{(U_1),(U_2)}$. It should be noted that the pairs, $\left(x^{(U_1),(U_2)}, n_t^{(U_1),(U_2)}\right)$ and $\left(\hat{x}^{(U_1),(U_2)}, \hat{n}_t^{(U_1),(U_2)}\right)$, come from the set of

$$\text{ABER}_{\xi} \leq \sum_{\substack{x^{(U_1),(U_2)},\\ n_t^{(U_1),(U_2)}}}^{M^{(U_1)}N_t^{(U_1)}} \sum_{\substack{\hat{x}^{(U_1),(U_2)},\\ \hat{n}_t^{(U_1),(U_2)}}}^{M^{(U_2)}N_t^{(U_2)}} \frac{\mathcal{N}_{\xi}(b,\hat{b})}{\log_2\left(M^{(\xi)}N_t^{(\xi)}\right)} \frac{\text{E}_{\mathbf{H}}\left[\text{PEP}\left(x^{(U_1),(U_2)},\, n_t^{(U_1),(U_2)},\, \hat{x}^{(U_1),(U_2)},\, \hat{n}_t^{(U_1),(U_2)}\right)\right]}{M^{(U_1)}N_t^{(U_1)}M^{(U_2)}N_t^{(U_2)}}. \quad (3)$$

$$\text{PEP}\left(\cdot\right) = Q\left(\sqrt{\frac{E_m}{2N_o}\left|\left|\sigma_{(U_1)}\left(\mathbf{h}_{n_t^{(U_1)}}x^{(U_1)} - \mathbf{h}_{\hat{n}_t^{(U_1)}}\hat{x}^{(U_1)}\right) + \sigma_{(U_2)}\left(\mathbf{h}_{n_t^{(U_2)}}x^{(U_2)} - \mathbf{h}_{\hat{n}_t^{(U_2)}}x^{(U_2)}\right)\right|\right|^2}\right) \quad (4)$$

all possible symbol-antenna pairs for both nodes, *i.e.* $\left(x^{(U_1),(U_2)}, n_t^{(U_1),(U_2)}\right) = \mathbf{h}_{n_t^{(U_1)}}x^{(U_1)} + \mathbf{h}_{n_t^{(U_2)}}x^{(U_2)}$ and $\left(\hat{x}^{(U_1),(U_2)}, \hat{n}_t^{(U_1),(U_2)}\right) = \mathbf{h}_{\hat{n}_t^{(U_1)}}\hat{x}^{(U_1)} + \mathbf{h}_{\hat{n}_t^{(U_2)}}\hat{x}^{(U_2)}$. $\text{E}_{\mathbf{H}}[\cdot]$ represents the expectation of the system with respect to the channel and $Q(\omega) = \frac{1}{\sqrt{2\pi}}\int_{\omega}^{\infty}\exp\left(-\frac{t}{2}\right)dt$.

The ABER for node ξ is shown in (3), where the pairwise error probability is given in (4). Due to space constraints, we omit the derivation of (4). We note that thus far no assumptions have been made as to the distribution of the channel.

If we consider a Rayleigh fading channel, then we can derive the closed form solution for $\text{E}_{\mathbf{H}}\left[\text{PEP}\left(\cdot\right)\right]$ in (3) by employing the solution to [16, eq. 62]. We note that by assuming a Rayleigh fading channel, the argument within (4) can be represented as the summation of $2N_r$ squared Gaussian random variables, with zero mean and variance equal to 1, which means that they can be described by a central Chi-squared distribution with $2N_r$ degrees of freedom and a probability density function of:

$$p_K(\kappa) = \frac{1}{2^{N_r}(N_r-1)!}\kappa^{N_r-1}\exp\left(-\kappa/2\right).$$

The result for $\text{E}_{\mathbf{H}}\left[\text{PEP}\left(\cdot\right)\right]$ is given as:

$$\text{E}_{\mathbf{H}}\left[\text{PEP}\left(\cdot\right)\right] = f(c)^{N_r}\sum_{r=0}^{N_r-1}\binom{N_r-1+r}{r}\left(1-f(c)\right)^r \quad (5)$$

such that

$$f(c) = \frac{1}{2}\left(1-\sqrt{\frac{c}{1+c}}\right)$$

where

$$c = \frac{E_m}{4N_o}\sum_{u\in\{U_1,U_2\}}\sigma_{(u)}^2\lambda_{(u)} \quad (6)$$

which is a quarter of the received SNR at the receiver, and

$$\lambda_{(u)} = \begin{cases} \left(|x_{(u)}|^2 + |\hat{x}_{(u)}|^2\right) & n_t^{(u)} \neq \hat{n}_t^{(u)}, \\ \left(|x_{(u)} - \hat{x}_{(u)}|^2\right) & n_t^{(u)} = \hat{n}_t^{(u)}, \\ 0 & n_t^{(u)} = \hat{n}_t^{(u)} \text{ and } x_{(u)} = \hat{x}_{(u)}. \end{cases}$$

IV. Simulation Results and Discussion

In this section we aim to show that the interference aware detector proposed in (2) can successfully decode the incoming streams for the two users. Numerical results are shown which demonstrate that (3) provides a tight upper bound for the BER of the interference aware detector at high SNR. The aim of this work is to develop and test a viable multi-user detector for SM.

A. Simulation Setup

A frequency-flat Rayleigh fading channel with no correlation between the transmitting antennas and AWGN is assumed. Perfect channel state information (CSI) is assumed at the receiving node, with no CSI at the transmitter. Only one of the available transmit antennas for each node is active at any transmitting instance. In theory each user independently decides the number of transmit antennas and the symbol modulation it uses. For use in the simulation we assume each node has the same number of transmit antennas as well as the same spectral efficiency target. In each figure, for each user, there are three presented results: i) the simulation results for the interference aware detector, denoted by `Sim(User`ξ`)`, ii) the theoretical results from (3) using (5), denoted by `Analytical(User`ξ`)`, and iii) the single-user-lower-bound (SULB), denoted by `SULB(User`ξ`)`. We define SULB as the system performance in a single-user-single-receiver scenario where the system performance is determined purely by its SNR, defined as $\frac{E_m}{2N_o}$. The theory behind SULB is well developed in [7].

B. Results

Fig. 3 and Fig. 4 clearly demonstrate that the analytical model presented in (3) represents a tight upper bound for the system in the high SNR region. Additionally, we can see that the system with the lowest SNR has similar performance to that predicted by its SULB. It should be noted that this is not the case for the node with the better SNR. This difference in performance of the two systems can be explained by looking at the error contribution of each element from each node in the analytical prediction.

We define two sets, one for every pairwise possibility within a particular user, given by $\Omega^{(U_1)}$ in (7) for User1. We can similarly define the set $\Omega^{(U_2)}$ for User2. If we now consider (3) and (4) we see that the overall error for each user is inevitably influenced by the errors from the other user. However, since each element from $\Omega^{(U_1)}$ is associated with the full set of possible errors from $\Omega^{(U_2)}$, then all erroneous terms from $\Omega^{(U_1)}$ will 'carry' the full error from the terms in $\Omega^{(U_2)}$ and vice versa. This means that besides the pairwise error associated with the mis-detection of the antenna-symbol combination of User1 alone, the error term for User1 is increased by the pairwise error of User2 and vice versa, *i.e.* the overall error for node 1 has $\left[\left(\texttt{card}\left\{\Omega^{(U_1)}\right\} - M^{(U_1)}N_t^{(U_1)}\right)\texttt{card}\left\{\Omega^{(U_2)}\right\}\right]$ number of error terms where $\texttt{card}\{\cdot\}$ denotes the cardinality of a given set.

We further note that each pairwise error from the user with

the worse SNR makes a bigger contribution to the overall BER than the pairwise error from the node with the better SNR. This can be shown if we look at the Euclidean distance between the different pairwise errors. We classify a pairwise error if the Euclidean distance between the symbol-antenna pairs being tested is greater than zero. In particular, the greater the Euclidean distance becomes, the smaller the error from that term. From (4) it is clear that the pairwise error depends on the SNR as well as the Euclidean distance. It thus follows that given pairwise error terms with the same Euclidean distance, the worse the SNR is for each term, the greater the absolute pairwise error. Considering the above, it is clear that the node with the better channel gain never performs close to its SULB, while the node with the worse channel gain does perform near its SULB.

Fig. 3 and Fig. 4 demonstrate this behaviour. The gap in performance with respect to the SULB for the main contributor to the overall user error, *i.e.* the node with the lower SNR, effectively increases the BER of the node with the higher SNR. To further elaborate, we note that the difference between the simulation BER curves of the two nodes when $N_r = 2$ and $N_r = 3$ increases as more receive antennas are added. This can be explained if we consider that by increasing the number of receive antennas, the diversity of the system increases and the pairwise error terms for each node approach zero more rapidly. This mean that the absolute pairwise error contributed to the overall BER is less for each node. As a consequence, the node with the better channel gain *i.e.* the node with higher SNR, will perform closer to its SULB.

On the one hand, moving from Fig. 3 and Fig. 4 to Fig. 5, we notice that for a fixed spectral efficiency and a fixed number of transmit antennas, the addition of more receive antennas results in an increasing gap between the average analytical BER curves of the two nodes. In particular, a gap of around 4 dB between the performance of User1 and User2 with $N_r = 2$ is increased to around 7 dB when $N_r = 4$ and further increased to around 9 dB for $N_r = 8$. On the other hand, given that the two nodes experience a channel gain difference of 10 dB, we know that the interference aware detector cannot reach the performance of independent detection and the SULB for the node with the better SNR. Nonetheless, the gap between their respective BER curves tends toward the difference between the channel attenuations of the two users as N_r grows to infinity but can never reach it *i.e.* the gap tends towards 10 dB.

The addition of more transmit antennas at each of the nodes results in SNR gains for each node as can be seen when we compare Fig. 4 and Fig. 6. Interestingly, however, increasing the number of transmit antennas does not change the relative behaviour of the system, *i.e.* the SNR difference between the BER curves of the two nodes remains constant. This behaviour is expected when we consider that (5) is independent of N_t and heavily influenced by N_r. In particular, the BER of both nodes is dependent on the variance of the channel coefficients in (4) which follow a central chi-squared distribution with $2N_r$ degrees of freedom. This variance is defined in (6).

At this point it should be noted that while the proposed detector is jointly optimum for both nodes and does not suffer from the near-far problem, it needs full CSI from

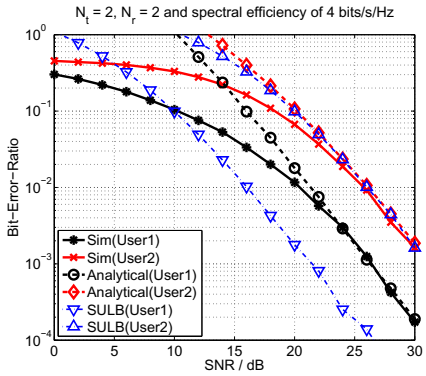

Fig. 3. BER for user 1 with $\sigma^2_{(U_1)} = 1$ and user 2 with $\sigma^2_{(U_2)} = 0.1$ using the interference aware detector.

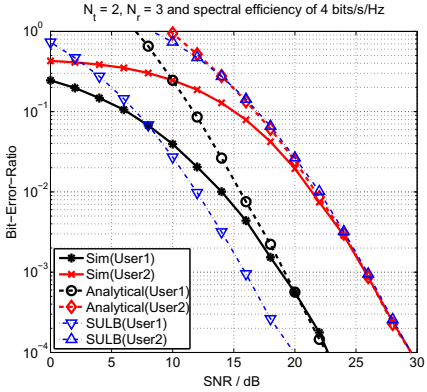

Fig. 4. BER for user 1 with $\sigma^2_{(U_1)} = 1$ and user 2 with $\sigma^2_{(U_2)} = 0.1$ using the interference aware detector.

all possible transmitting antennas to each receiving antenna. Additionally, finding the optimal solution is an exponentially complex problem, *i.e.* if we assume each node has the same number of transmit antennas and uses the same signal constellation, then the multi user ML detector has $\mathcal{O}\left((MN_t)^{N_u}\right)$ computational complexity which is proven to be NP-complete [17]. Fortunately, recent work on sphere detection algorithms may be used to alleviate this computational cost [18].

V. Conclusion

In this work the performance of SM with simultaneous transmission was analysed. A ML detector for SM in the interference limited scenario was proposed. Its performance over uncorrelated Rayleigh fading channels was studied and a closed form solution for the upper bound of the system was provided. Numerical results verified that the proposed analysis was fairly accurate for the high SNR regions. On the one hand, increasing the number of transmit antennas at each of the nodes from 2 to 4 resulted in SNR gains of around 2 dB. This measure did not, however, have any effect on the

$$\Omega^{(U_1)} = \{(\mathbf{h_1}x_1, \mathbf{h_1}x_1), (\mathbf{h_1}x_1, \mathbf{h_2}x_2), \ldots, (\mathbf{h_1}x_1, \mathbf{h_{N_t}}x_M),\ (\mathbf{h_2}x_1, \mathbf{h_1}x_1), \ldots, (\mathbf{h_{N_t}}x_M, \mathbf{h_{N_t}}x_M)\} \quad (7)$$

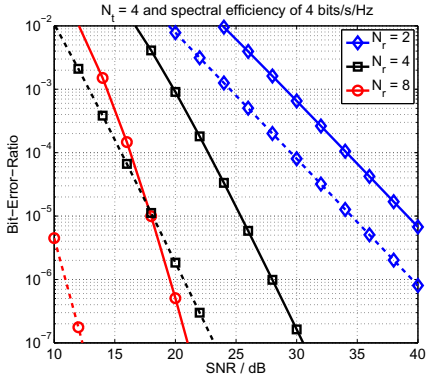

Fig. 5. BER for user 1 with $\sigma^2_{(U_1)} = 1$ and user 2 with $\sigma^2_{(U_2)} = 0.1$. Solid lines denote the performance of user 2 with a varying number of receive antennas while dashed lines denote the performance of user 1 with a varying number of receive antennas.

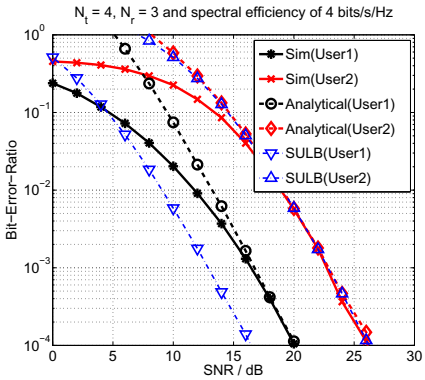

Fig. 6. BER for user 1 with $\sigma^2_{(U_1)} = 1$ and user 2 with $\sigma^2_{(U_2)} = 0.1$ using the interference aware detector.

relative coding gain between the BER curves of the two nodes *i.e.* the two nodes improved their performance by the same amount. On the other hand, increasing the number of receive antennas increased the diversity of the system and decreased the error contribution of each node, thus increasing the SNR gap between the BER curves of the two nodes.

The generalization of this work to a system with an arbitrary number of nodes, along with further investigation on the performance of SM in an interference limited scenario will be considered in the future.

Acknowledgement

We gratefully acknowledge support from the Engineering and Physical Sciences Research Council (EP/G011788/1) in the United Kingdom for this work. Professor Harald Haas acknowledges the Scottish Funding Council support of his position within the Edinburgh Research Partnership in Engineering and Mathematics between the University of Edinburgh and Heriot Watt University. Nikola Serafimovski would like to acknowledge Harald Burchardt for his advice.

References

[1] J. Mietzner, R. Schober, L. Lampe, W. H. Gerstacker, and P. A. Hoeher, "Multiple-antenna techniques for wireless communications - a comprehensive literature survey," *Communications Surveys Tutorials, IEEE*, vol. 11, no. 2, pp. 87 –105, 2009.

[2] R. Mesleh, H. Haas, Y. Lee, and S. Yun, "Interchannel Interference Avoidance in MIMO Transmission by Exploiting Spatial Information," in *Proc. of the 16th IEEE International Symposium on Personal, Indoor and Mobile Radio Communications (PIMRC)*, vol. 1, Berlin, Germany, 11-14 Sep. 2005, pp. 141–145.

[3] R. Mesleh, H. Haas, S. Sinanović, C. W. Ahn, and S. Yun, "Spatial Modulation," *IEEE Trans. Veh. Technol.*, vol. 57, no. 4, pp. 2228 – 2241, July 2008.

[4] N. Serafimovski, M. Di Renzo, S. Sinanović, R. Y. Mesleh, and H. Haas, "Fractional Bit Encoded Spatial Modulation (FBE–SM)," *IEEE Commun. Lett.*, vol. 14, no. 5, pp. 429–431, May 2010.

[5] R. Mesleh, M. Di Renzo, H. Haas, and P. M. Grant, "Trellis Coded Spatial Modulation," *IEEE Trans. on Wireless Commun.*, vol. 9, no. 7, pp. 2349–2361, July 2010.

[6] A. Younis, R. Mesleh, H. Haas, and P. Grant, "Reduced Complexity Sphere Decoder for Spatial Modulation Detection Receivers," in *2010 IEEE Global Telecommunications Conference GLOBECOM 2010*, Miami, USA, 2010, pp. 1 –5.

[7] M. Di Renzo and H. Haas, "Performance analysis of spatial modulation," in *5th International ICST Conference on Communications and Networking in China*, August 2010.

[8] J. Jeganathan, A. Ghrayeb, and L. Szczecinski, "Spatial Modulation: Optimal Detection and Performance Analysis," *IEEE Commun. Lett.*, vol. 12, no. 8, pp. 545–547, 2008.

[9] S. U. Hwang, S. Jeon, S. Lee, and J. Seo, "Soft-Output ML Detector for Spatial Modulation OFDM Systems," *IEICE Electronics Express*, vol. 6, no. 19, pp. 1426–1431, Oct. 2009.

[10] M. Di Renzo and H. Haas, "Spatial modulation with partial-csi at the receiver: optimal detector and performance evaluation," in *Proceedings of the 33rd IEEE conference on Sarnoff*, ser. Sarnoff'10. Piscataway, NJ, USA: IEEE Press, 2010, pp. 58–63. [Online]. Available: http://portal.acm.org/citation.cfm?id=1843486.1843498

[11] ——, "Improving the performance of space shift keying (SSK) modulation via opportunistic power allocation," *Communications Letters, IEEE*, vol. 14, no. 6, pp. 500 –502, 2010.

[12] T. Handte, A. Muller, and J. Speidel, "BER analysis and optimization of generalized spatial modulation in correlated fading channels," in *Vehicular Technology Conference Fall (VTC Fall-2009)*, Sep. 2009, pp. 1 –5.

[13] E. Basar, U. Aygolu, E. Panayirci, and V. H. Poor, "Space-time block coded spatial modulation," *Communications, IEEE Transactions on*, vol. 59, no. 3, pp. 823 –832, 2011.

[14] N. Serafimovski, S. Sinanovic, M. Di Renzo, and H. Haas, "Dual-hop Spatial Modulation (Dh-SM)," in *IEEE 73rd Vehicular Technology Conference: VTC2011-Spring*, Budapest, Hungary, May 2011.

[15] M. Di Renzo and H. Haas, "On the performance of ssk modulation over multiple-access rayleigh fading channels," in *GLOBECOM 2010, 2010 IEEE Global Telecommunications Conference*, dec. 2010, pp. 1 –6.

[16] M.-S. Alouini and A. Goldsmith, "A Unified Approach for Calculating Error Rates Of Linearly Modulated Signals over Generalized Fading Channels," *IEEE Transactions on Communications*, vol. 47, no. 9, pp. 1324–1334, 1999.

[17] S. Verdu, "Computational complexity of optimum multiuser detection," *Algorithmica*, vol. 4, pp. 303–312, 1989, 10.1007/BF01553893. [Online]. Available: http://dx.doi.org/10.1007/BF01553893

[18] A. Younis, M. Di Renzo, R. Mesleh, and H. Haas, "Sphere Decoding for Spatial Modulation," in *IEEE International Conference on Communications (IEEE ICC 2011)*, Kyoto, Japan, 5–9 Jun. 2011.

Bibliography

[1] E. Telatar, "Capacity of Multi-Antenna Gaussian Channels," *European Trans. on Telecommun.*, vol. 10, no. 6, pp. 585–595, Nov. / Dec. 1999.

[2] G. J. Foschini, "Layered Space-Time Architecture for Wireless Communication in a Fading Environment when Using Multi-Element Antennas," *Bell Labs Tech. J.*, vol. 1, no. 2, pp. 41–59, 1996.

[3] J. Hoydis, S. ten Brink, and M. Debbah, "Massive MIMO: How many antennas do we need?" in *2011 49th Annual Allerton Conf. on Commun., Control, and Computing (Allerton)*, Sept. 2011, pp. 545 –550.

[4] B. Cerato and E. Viterbo, "Hardware implementation of a low-complexity detector for large MIMO," in *IEEE Int. Symp. on Circuits and Systems (ISCAS 2009)*, May 2009, pp. 593 –596.

[5] A. Chockalingam, "Low-complexity algorithms for large-MIMO detection," in *4th Int. Symp. on Commun., Control and Sig. Process. (ISCCSP)*, Mar. 2010, pp. 1 –6.

[6] S. Mohammed, A. Chockalingam, and B. Sundar Rajan, "A Low-complexity near-ML performance achieving algorithm for large MIMO detection," in *IEEE Int. Symp. on Inf. Theory (ISIT 2008)*, Jul. 2008, pp. 2012 –2016.

[7] S. Mohammed, A. Chockalingam, and B. Rajan, "High-Rate Space-Time Coded Large MIMO Systems: Low-Complexity Detection and Performance," in *IEEE Global Telecommun. Conf. (GLOBECOM)* , Dec. 2008, pp. 1 –5.

[8] S. Mohammed, A. Zaki, A. Chockalingam, and B. Rajan, "High-Rate Space-Time Coded Large-MIMO Systems: Low-Complexity Detection and Channel Estimation," *IEEE J. of Selected Topics in Sig. Process.* , vol. 3, no. 6, pp. 958 –974, Dec. 2009.

[9] E. Viterbo and E. Biglieri, "A universal lattice decoder," in *14 eme Colloque GRETSI*, France, sept. 1993, pp. 611–614.

[10] E. Viterbo and J. Boutros, "A Universal Lattice Code Decoder for Fading Channels," *IEEE Trans. on Inform. Theory*, vol. 45, no. 5, pp. 1639–1642, Jul. 1999.

[11] O. Damen, A. Chkeif, and J.-C. Belfiore, "Lattice Code Decoder for Space-Time Codes," *IEEE Commun. Lett.*, vol. 4, no. 5, pp. 161–163, May 2000.

[12] A. Molisch and M. Win, "MIMO systems with antenna selection," *IEEE Microwave Magazine*, vol. 5, no. 1, pp. 46–56, Mar. 2004.

[13] A. Stavridis, S. Sinanović, M. D. Renzo., H. Haas, and P. Grant, "An Energy Saving Base Station Employing Spatial Modulation," in *IEEE 17th Int. Workshop on Computer Aided Modeling and Design of Communication Links and Networks (CAMAD)*, Sep. 17–19 2012, pp. 231 –235.

[14] L. Correia, D. Zeller, O. Blume, D. Ferling, A. Kangas, I. Godor, G. Auer, and L. Van Der Perre, "Challenges and Enabling Technologies for Energy Aware Mobile Radio Networks," *IEEE Communications Magazine*, vol. 48, no. 11, pp. 66–72, Nov. 2010.

[15] R. Mesleh, H. Haas, Y. Lee, and S. Yun, "Interchannel Interference Avoidance in MIMO Transmission by Exploiting Spatial Information," in *Proc. of the 16th IEEE Int. Symp. on Personal, Indoor and Mobile Radio Commun. (PIMRC)*, vol. 1, Berlin, Germany, 11-14 Sep. 2005, pp. 141–145.

[16] R. Mesleh, H. Haas, S. Sinanović, C. W. Ahn, and S. Yun, "Spatial Modulation," *IEEE Trans. on Veh. Tech.*, vol. 57, no. 4, pp. 2228 – 2241, Jul. 2008.

[17] J. Jeganathan, A. Ghrayeb, and L. Szczecinski, "Spatial Modulation: Optimal Detection and Performance Analysis," *IEEE Commun. Lett.*, vol. 12, no. 8, pp. 545–547, 2008.

[18] J. Jeganathan, A. Ghrayeb, L. Szczecinski, and A. Ceron, "Space Shift Keying Modulation for MIMO Channels," *IEEE Trans. on Wireless Commun.*, vol. 8, no. 7, pp. 3692–3703, Jul. 2009.

[19] A. Stavridis, S. Sinanović, M. D. Renzo, and H. Haas, "A Power Saving Dual-Hop Architecture Based on Hybrid Spatial Modulation," in *2012 Conf. Record of the Forty Sixth Asilomar Conf. on Signals, Systems and Computers (ASILOMAR)*, Nov. 4–7 2012, pp. 1366–1370.

[20] M. Di Renzo and H. Haas, "Bit Error Probability of Spatial Modulation (SM) MIMO over Generalized Fading Channels," *IEEE Trans. on Veh. Tech.*, vol. 61, no. 3, pp. 1124 –1144, Mar. 2012.

[21] M. Di Renzo and H. Haas, "On Transmit-Diversity for Spatial Modulation MIMO: Impact of Spatial-Constellation Diagram and Shaping Filters at the Transmitter," in *IEEE Trans. on Veh. Tech.*, 2013, to appear. Available: IEEE Xplore Early Access.

[22] M. D. Renzo, D. D. Leonardis, F. Graziosi, and H. Haas, "Space Shift Keying (SSK) MIMO with Practical Channel Estimates," *IEEE Trans. on Commun.*, vol. 60, no. 4, pp. 998 –1012, Apr. 2012.

[23] M. Di Renzo and H. Haas, "Bit Error Probability of Space-Shift Keying MIMO Over Multiple-Access Independent Fading Channels," *IEEE Trans. on Veh. Tech.*, vol. 60, no. 8, pp. 3694 –3711, Oct. 2011.

[24] T. Handte, A. Müller, and J. Speidel, "BER Analysis and Optimization of Generalized Spatial Modulation in Correlated Fading Channels," in *Veh. Tech. Conf. Fall (VTC Fall-2009)*, Anchorage, AK, Sep. 20–23 2009, pp. 1 –5.

[25] M. Di Renzo, R. Mesleh, H. Haas, and P. Grant, "Upper Bounds for the Analysis of Trellis Coded Spatial Modulation over Correlated Fading Channels," in *IEEE 71st Vehicular Technology Conference (VTC 2010-Spring)*, May 2010, pp. 1 –5.

[26] A. Alshamali and B. Quza, "Spatial modulation: Performance Evaluation in Nakagami Fading Channels," in *5th IEEE GCC Conference Exhibition*, Mar. 2009, pp. 1 – 4.

[27] ——, "Performance of Spatial Modulation in Correlated and Uncorrelated Nakagami Fading Channel," *Journal of Communications*, vol. 4, no. 3, pp. 170–174, Apr. 2009.

[28] M. Di Renzo and H. Haas, "A General Framework for Performance Analysis of Space Shift Keying (SSK) Modulation for MISO Correlated Nakagami-m Fading Channels," *IEEE Trans. on Commun.*, vol. 58, no. 9, pp. 2590 –2603, Sep. 2010.

[29] M. Di Renzo and H. Haas, "Bit Error Probability of Space Modulation over Nakagami-m Fading: Asymptotic Analysis," *IEEE Commun. Lett.*, vol. 15, no. 10, pp. 1026 –1028, Oct. 2011.

[30] M. D. Renzo and H. Haas, "Performance analysis of Spatial Modulation," in *Int. ICST Conf. on Commun. and Networking in China (CHINACOM),*, Aug. 2010, pp. 1 –7.

[31] M. Yacoub, G. Fraidenraich, and J. Santos Filho, "Nakagami-m Phase-Envelope Joint Distribution," *Electronics Letters*, vol. 41, no. 5, pp. 259 –261, Mar. 2005.

[32] M. Yacoub, "Nakagami-m Phase-Envelope Joint Distribution: An Improved Model," in *IEEE MTT-S International Microwave and Optoelectronics Conference (IMOC)*, Nov. 2009, pp. 335 –339.

[33] ——, "Nakagami-m Phase-Envelope Joint Distribution: A New Model," *IEEE Transactions on Vehicular Technology*, vol. 59, no. 3, pp. 1552 –1557, Mar. 2010.

[34] R. Rajashekar and K. V. S. Hari, "Sphere Decoding for Spatial Modulation Systems with Arbitrary Nt," *CoRR*, vol. abs/1202.5187, 2012.

[35] ——, "Low Complexity Maximum Likelihood Detection in Spatial Modulation Systems," *CoRR*, vol. abs/1206.6190, 2012.

[36] A. Younis, M. Di Renzo, R. Mesleh, and H. Haas, "Sphere Decoding for Spatial Modulation," in *Proc. of IEEE Int. Conf. on Commun. (ICC)*, Kyoto, Japan, 5–9 Jun. 2011, pp. 1 –6.

[37] N. Serafimovski, M. Di Renzo, S. Sinanović, R. Y. Mesleh, and H. Haas, "Fractional Bit Encoded Spatial Modulation (FBE–SM)," *IEEE Commun. Lett.*, vol. 14, no. 5, pp. 429–431, May 2010.

[38] A. Younis, N. Serafimovski, R. Mesleh, and H. Haas, "Generalised Spatial Modulation," in *Asilomar Conf. on Signals, Systems, and Computers*, Pacific Grove, CA, USA, Nov. 2010.

[39] J. Fu, C. Hou, W. Xiang, L. Yan, and Y. Hou, "Generalised spatial modulation with multiple active transmit antennas," in *IEEE Global Communications Conference (GLOBECOM 2010) Workshops*, Miami, FL, 6-10 Dec. 2010, pp. 839–844.

[40] N. Serafimovski, A. Younis, and H. Haas, "Spatial Modulation," Oct. 2012. [Online]. Available: http://youtu.be/cPKIbxrEDho

[41] J. G. Proakis and M. Salehi, *Communication System Engineering*. Prentice Hall, 1994.

[42] G. Marconi, "Improvements in Transmitting Electrical impulses and Signals, and in Apparatus therefor," British Patent 12 039, Mar., 1897.

[43] R. Barrett, "Popov Versus Marconi: the Century of Radio," *GEC Review*, vol. 12, no. 2, pp. 107–116, 1997.

[44] L. Hanzo, M. El-Hajjar, and O. Alamri, "Near-Capacity Wireless Transceivers and Cooperative Communications in the MIMO Era: Evolution of Standards, Waveform Design, and Future Perspectives," *Proceedings of the IEEE*, vol. 99, no. 8, pp. 1343 –1385, Aug. 2011.

[45] G. D. Durgin, *Space-Time Wireless Channels*, ser. Prentice Hall communications engineering and emerging technologies series. Upper Saddle River, NJ : Prentice Hall PTR, c2003., 2003.

[46] (1987, May) Milestones:one-way police radio communication, 1928. IEEE Southeastern Michigan Section. Detroit, MI. [Online]. Available: http://www.ieeeghn.org/wiki/index.php/Milestones:One-Way_Police_Radio_Communication,_1928

[47] (1988, May) Milestones:two-way police radio communication, 1933. IEEE North Jersey Section. Bayonne, NJ. [Online]. Available: http://www.ieeeghn.org/wiki/index.php/Milestones:Two-Way_Police_Radio_Communication,_1933

[48] C. Shannon, "A Mathematical Theory of Communication," *Bell System Technical Journal*, vol. 27, pp. 379–423 & 623–656, Jul. & Oct. 1948.

[49] R. Mesleh, "Spatial Modulation: A Spatial Multiplexing Technique for Efficient Wireless Data Transmission," Ph.D. dissertation, Jacobs University, Bremen, Germany, Jun. 2007.

[50] D. Tse and P. Viswanath, *Fundamentals of Wireless Communication*. Cambridge University Press, 2005.

[51] C. Shannon, "Communication in the Presence of Noise," in *Proc. of the IRE*, vol. 37, no. 1, Jan. 1949, pp. 10–21.

[52] BROADCOM Corporation, "802.11n: Next-Generation Wireless LAN Technology," White paper, BROADCOM Corporation, Tech. Rep., Apr. 2006, retrieved Aug. 4, 2006 http://www.broadcom.com/docs/WLAN/802-11n-WP100-R.pdf.

[53] D. Steinbock, *The Mobile Revolution : the Making of Mobile Services Worldwide*. Kogan Page Limited, 2005.

[54] X. Wang and H. V. Poor, *Wireless Communication Systems: Advanced Techniques for Signal Reception*. Prentice Hall Communications Engineering and Emerging Technologies Series, 2002.

[55] O. Billstrm, L. Cederquist, M. Ewerbring, G. Sandegren, and J. Uddenfeldt, "Fifty years with mobile phones From novelty to no. 1 consumer product," *Ericsson Review*, no. 3, pp. 101–106, 2006.

[56] J. E. Padgett, C. G. Gunther, and T. Hattori, "Overview of Wireless Personal Communications," *IEEE Communications Magazine*, vol. 33, no. 1, pp. 28–41, Jan. 1995.

[57] W. Erdman, "Wireless Communications: a Decade of Progress," *IEEE Communications Magazine*, vol. 31, no. 12, pp. 48 –51, Dec. 1993.

[58] R. Steele and L. Hanzo, *Mobile Radio Communications: Second and Third Generation Cellular and WATM Systems*, 2nd ed. IEEE Press - John Wiley, 1999.

[59] T. K. Sarkar, R. J. Mailloux, A. A. Oliner, M. Salazar-Palma, and D. L. Sengupta, *History of Wireless*. JOHN WILEY & SONS, INC., 2006.

[60] T. Halonen, J. Romero, and J. Melero, *GSM, GPRS and EDGE Performance*. John Wiley & Sons Ltd.; Second Edition, 2003.

[61] D. Cox, "Wireless Personal Communications: What is it?" *IEEE Personal Communications*, vol. 2, no. 2, pp. 20–35, Apr. 1995.

[62] J. Rizzo and N. Sollenberger, "Multitier Wireless Access," *IEEE Personal Communications*, vol. 2, no. 3, pp. 18–30, Jun. 1995.

[63] H. Schulze and C. Lüders, *Theory and Applications of OFDM and CDMA*. John Wiley & Sons Ltd., 2005.

[64] A. J. Viterbi and R. Padovani, "Implications of Mobile Cellular CDMA," *IEEE Communications Magazine*, vol. 30, no. 12, pp. 38–41, Dec. 1992.

[65] A. Technologies, *LTE and the Evolution to 4G Wireless: Design and Measurement Challenges*, M. Rumney, Ed. Agilent Technologies, 2009.

[66] ITU-R, "Requirements Related to Technical Performance for IMT-Advanced Radio Interface(s)," ITU, Tech. Rep. ITU-R M.2134, Retrieved Jan. 22, 2010 from http://www.itu.int/dms_pub/itu-r/opb/rep/R-REP-M.2134-2008-PDF-E.pdf, 2008.

[67] E. Seidel, "Progress on "LTE Advanced" – the New 4G Standard," Nomor Research GmbH, Münich, Germany, Newsletter, Jul. 24, 2008. [Online]. Available: www.nomor.de/uploads/_c/V1/_cV1fTZl6MtFnAHVXltStg/LTEAdvanced_2008-07.pdf

[68] ——, "The way of LTE towards 4G," Nomor Research GmbH, Münich, Germany, Newsletter, Dec. 2009. [Online]. Available: http://www.nomor-research.com/uploads/5O/Ge/5OGeGN5_731KWhm3m0JgDQ/Nomor_3GPP_Newsletter_2009-12_v1-0.pdf

[69] I.-R. S. W. 5D, "Acknowledgment of Candidate Submission from 3GPP Proponent (3GPP Organization Partners of ARIB, ATIS, CCSA, ETSI, TTA AND TTC) under Step 3 of the IMT-Advanced Process (3GPP Technology)," ITU, Doc. IMT-ADV/4-E, Oct. 2009.

[70] ——, "Acknowledgment of Candidate Submission from IEEE under Step 3 of the IMT-Advanced Process (IEEE Technology)," ITU, Doc. IMT-ADV/4-E, Oct. 2009.

[71] J. Mietzner, R. Schober, L. Lampe, W. H. Gerstacker, and P. A. Höeher, "Multiple-Antenna Techniques for Wireless Communications - A Comprehensive Literature Survey," *IEEE Commun. Surveys Tutorials*, vol. 11, no. 2, pp. 87 –105, 2009.

[72] Q. Li, G. Li, W. Lee, M. il Lee, D. Mazzarese, B. Clerckx, and Z. Li, "MIMO techniques in WiMAX and LTE: A Feature Overview," *IEEE Communications Magazine*, vol. 48, no. 5, pp. 86 –92, May 2010.

[73] Cisco Visual Networking Index, "Global Mobile Data Traffic Forecast Update, 2011-2016," Cisco, White Paper, Feb. 2012. [Online]. Available: http://www.cisco.com/en/US/solutions/collateral/ns341/ns525/ns537/ns705/ns827/white_paper_c11-520862.pdf

[74] 3GPP, "Requirements for Evolved UTRA (E-UTRA) and Evolved UTRAN (E-UTRAN)," 3GPP TS 25.913 V 8.0.0 (2008-12), Dec. 2008. Retrieved Oct. 10, 2009 from www.3gpp.org/ftp/Specs/.

[75] S. Sesia, I. Toufik, and M. Baker, *LTE - The UMTS Long Term Evolution: From Theory to Practice*, 1st ed., S. Sesia, I. Toufik, and M. Baker, Eds. Wiley, 2009.

[76] Z. R. Bharucha, "Ad Hoc Wireless Networks with Femto-Cell Deployment: A Study," Ph.D. dissertation, Univeristy of Edinburgh, 2010.

[77] L. Hanzo, L. Yang, E. Kuan, and K. Yen, *Single and Multi-Carrier DS-CDMA: Multi-User Detection, Space-Time Spreading, Synchronisation, Networkingand Standards*. Wiley, 2003.

[78] L. Hanzo, T. Liew, and B. Yeap, *Turbo Coding, Turbo Equalisation and Space-Time Coding for Transmission over Fading Channels*. John Wiley & Sons, 2002.

[79] L. Hanzo, S. X. Ng, T. Keller, and W. Webb, *Quadrature amplitude modulation: from basics to adaptive trellis-coded, turbo-equalised and space-time coded OFDM, CDMA and MC-CDMA systems*. IEEE Press, 2004.

[80] B. Vucetic and J. Yuan, *Space-Time Coding*. Wiley, 2003. [Online]. Available: http://books.google.co.uk/books?id=qeFT2eLZH-UC

[81] L. Hanzo, O. Alamri, M. El-Hajjar, and N. Wu, *Near-Capacity Multi-Functional MIMO Systems: Sphere-Packing, Iterative Detection and Cooperation*, ser. Wiley - IEEE. Wiley, 2009.

[82] D. George, "Matched filters for interfering signals," *IEEE Transactions on Information Theory (Correspondence)*, vol. 11, no. 1, pp. 153 – 154, Jan. 1965.

[83] D. Tufts, "Nyquist's problem - The joint optimization of transmitter and receiver in pulse amplitude modulation," *Proceedings of the IEEE*, vol. 53, no. 3, pp. 248 – 259, Mar. 1965.

[84] A. Kaye, "Reception of pulse-amplitude-modulated signals transmitted over a dispersive fading channel with nonstationary statistics," *Proceedings of the IEEE*, vol. 56, no. 6, pp. 1087 – 1088, Jun. 1968.

[85] A. Kaye and D. George, "Transmission of Multiplexed PAM Signals Over Multiple Channel and Diversity Systems," *IEEE Transactions on Communication Technology*, vol. 18, no. 5, pp. 520 –526, Oct. 1970.

[86] N. Serafimovski, "Extension and Practical Evaluation of the Spatial Modulation Concept," Ph.D. dissertation, The University of Edinburgh, Edinburgh, UK, Aug. 8 2012.

[87] S. M. Alamouti, "A Simple Transmit Diversity Technique for Wireless Communications," *IEEE Journal on Selected Areas in Communications*, vol. 16, no. 8, pp. 1451–1458, Oct. 1998.

[88] V. Tarokh, H. Jafarkhani, and A. Calderbank, "Space-time Block Codes from Orthogonal Designs," *IEEE Transactions on Information Theory*, vol. 45, no. 5, pp. 1456–1467, Jul. 1999.

[89] J.-C. Guey, M. Fitz, M. Bell, and W.-Y. Kuo, "Signal Design for Transmitter Diversity Wireless Communication Systems over Rayleigh Fading Channels," *IEEE Transactions on Communications*, vol. 47, no. 4, pp. 527–537, Apr. 1999.

[90] T. Eng, N. Kong, and L. Milstein, "Comparison of iversity combining techniques for Rayleigh-fading channels," *IEEE Trans. on Commun.*, vol. 44, no. 9, pp. 1117–1129, 1996.

[91] A. Wittneben, "Basestation Modulation Diversity for Digital SIMULCAST," in *IEEE 41st Vehicular Technology Conference, 1991. 'Gateway to the Future Technology in Motion'*, 19-22 May 1991, pp. 848–853.

[92] D. Brennan, "Linear diversity combining techniques," *Proceedings of the IEEE*, vol. 91, no. 2, pp. 331 – 356, Feb. 2003.

[93] ——, "Linear diversity combining techniques," *Proc. IRE*, vol. 47, no. 6, pp. 1075–1102, Jun. 1959.

[94] V. Tarokh, N. Seshadri, and A. Calderbank, "Space-Time Codes for High Data Rate Wireless Communication: Performance Criterion and Code Construction," *IEEE Trans. on Inform. Theory*, vol. 44, no. 2, pp. 744–765, 1998.

[95] V. Tarokh, H. Jafarkhani, and A. R. Calderbank, "Space-Time Block Coding for Wireless Communications: Performance Results," *IEEE Journal on Selected Areas in Communications*, vol. 17, no. 3, pp. 451–460, Mar. 1999.

[96] V. Tarokh, A. Naguib, N. Seshadri, and A. Calderbank, "Space-time codes for high data rate wireless communication: performance criteria in the presence of channel estimation errors, mobility, and multiple paths," *IEEE Transactions on Communications*, vol. 47, no. 2, pp. 199 –207, feb 1999.

[97] H. Jafarkhani, "A Quasi-Orthogonal Space-Time Block Code," *IEEE Transactions on Communications*, vol. 49, no. 1, pp. 1 –4, jan 2001.

[98] B. Hassibi and B. Hochwald, "High-rate codes that are linear in space and time," *IEEE Transactions on Information Theory*, vol. 48, no. 7, pp. 1804 –1824, jul 2002.

[99] V. Tarokh and H. Jafarkhani, "A Differential Detection Scheme for Transmit Diversity," in *IEEE Wireless Communications and Networking Conference (WCNC)*, 1999, pp. 1043 –1047 vol.3.

[100] ——, "A Differential Detection Scheme for Transmit Diversity," *IEEE Journal on Selected Areas in Communications*, vol. 18, no. 7, pp. 1169 –1174, july 2000.

[101] C.-S. Hwang, S. H. Nam, J. Chung, and V. Tarokh, "Differential Space Time Block Codes using QAM Constellations," in *14th IEEE Proceedings on Personal, Indoor and Mobile Radio Communications, 2003. PIMRC 2003.*, vol. 2, sept. 2003, pp. 1693 – 1697 vol.2.

[102] ——, "Differential Space Time Block Codes using Nonconstant Modulus Constellations," *IEEE Transactions on Signal Processing* , vol. 51, no. 11, pp. 2955 – 2964, nov 2003.

[103] A. Jamalipour, T. Wada, and T. Yamazato, "A Tutorial on Multiple Access Technologies for beyond 3G Mobile Networks," *IEEE Communications Magazine*, vol. 43, no. 2, pp. 110 –117, feb. 2005.

[104] V. Seba and B. Modlic, "Multiple Access Techniques for Future Generation Mobile Networks," in *47th International Symposium ELMAR*, june 2005, pp. 339 –344.

[105] J. S. Blogh and L. Hanzo, *Third-Generation Systems and Intelligent Wireless Networking*, ser. Wiley Interscience. West Sussex, UK: John Wiley & Sons, Ltd, May 2002.

[106] L. Godara, "Applications of Antenna Arrays to Mobile Communications. I. Performance Improvement, Feasibility, and System Considerations," *Proceedings of the IEEE*, vol. 85, no. 7, pp. 1031 –1060, jul 1997.

[107] ——, "Application of Antenna Arrays to Mobile Communications. II. Beam-forming and Direction-of-arrival Considerations," *Proceedings of the IEEE*, vol. 85, no. 8, pp. 1195 –1245, Aug. 1997.

[108] A. Paulraj, D. GORE, R. Nabar, and H. Bolcskei, "An Overview of MIMO Communications - A Key to Gigabit Wireless," *Proceedings of the IEEE*, vol. 92, no. 2, pp. 198 – 218, Feb. 2004.

[109] P. Wolniansky, G. Foschini, G. Golden, and R. Valenzuela, "V-BLAST: an Architecture for Realizing very High Data Rates over the Rich-Scattering Wireless Channel," in *Unino Radio-Scientifique Internationale (URSI) Intern. Symp. on Signals, Systems, and Electronics (ISSSE)*, Sep. 29–Oct. 2, 1998, pp. 295–300.

[110] J. G. Proakis, *Digital Communications*, 4th ed. New York, NY, USA: McGraw–Hill, 2000.

[111] H. Haas, E. Costa, and E. Schulz, "Increasing Spectral Efficiency by Data Multiplexing using Antenna Arrays," in *Proc. of the 13th IEEE International Symposium on Personal, Indoor and Mobile Radio Communications (PIMRC)*, vol. 2, Sep. 2002, pp. 610–613.

[112] M. Di Renzo, H. Haas, and P. M. Grant, "Spatial Modulation for Multiple-Antenna Wireless Systems: A Survey," *IEEE Commun. Mag,*, vol. 49, no. 11, pp. 182–191, Nov. 2011.

[113] V. Tarokh, A. Naguib, N. Seshadri, and A. Calderbank, "Combined Array Processing and Space-Time Coding," *IEEE Transactions on Information Theory*, vol. 45, no. 4, pp. 1121 –1128, may 1999.

[114] E. Basar, U. Aygolu, E. Panayirci, and H. Poor, "Space-Time Block Coding for Spatial Modulation," in *IEEE 21st International Symposium on Personal Indoor and Mobile Radio Communications (PIMRC)*, sept. 2010, pp. 803 –808.

[115] E. Basar, U. Aygolu, E. Panayirci, and V. H. Poor, "Space-Time Block Coded Spatial Modulation," *IEEE Trans. on Commun.*, vol. 59, no. 3, pp. 823 –832, Mar. 2011.

[116] E. C. V. D. Meulen, "Three-Terminal Communication Channels," *Advances in Applied Probability*, vol. 3, no. 1, pp. pp. 120–154, 1971.

[117] T. Cover and A. Gamal, "Capacity Theorems for The Relay Channel," *IEEE Transactions on Information Theory*, vol. 25, no. 5, pp. 572 – 584, sep 1979.

[118] A. Sendonaris, E. Erkip, and B. Aazhang, "User Cooperation Diversity. Part I. System Description," *IEEE Transactions on Communications*, vol. 51, no. 11, pp. 1927–1938, Nov. 2003.

[119] ——, "User Cooperation Diversity. Part II. Implementation Aspects and Performance Analysis," *IEEE Transactions on Communications*, vol. 51, no. 11, pp. 1939 – 1948, Nov. 2003.

[120] S. Ma, Y. Yang, and H. Sharif, "Distributed MIMO Technologies in Cooperative Wireless Networks," *IEEE 63rd Vehicular Technology Conference (VTC) SpringCommunications Magazine*, vol. 49, no. 5, pp. 78 –82, may 2011.

[121] A. Paulraj, R. Nabar, and D. Gore, *Introduction to Space-Time Wireless Communications*. U.K.: Cambridge University Press, 2003.

[122] R. B. Ertel, P. Cardieri, K. W. Sowerby, T. S. Rappaport, and J. H. Reed, "Overview of Spatial Channel Models for Antenna Array Communication Systems," *IEEE Personal*

Communications [see also IEEE Wireless Communications], vol. 5, no. 1, pp. 10–22, Feb. 1998.

[123] D. Gesbert, H. Bolcskei, D. Gore, and A. Paulraj, "Outdoor MIMO Wireless Channels: Models and Performance Prediction," *IEEE Transactions on Communications*, vol. 50, no. 12, pp. 1926–1934, Dec. 2002.

[124] T. S. Rappaport, *Wireless Communications: Principles and Practice*. Prentice Hall PTR, 1996.

[125] ——, *Wireless Communications: Principles and Practice*, 2nd ed. Prentice Hall PTR, 2002.

[126] L. Rayleigh, "On the Resultant of a Large Number of Vibrations of the Same Pitch and of Arbitrary Phase," *Phil. Mag.*, vol. 10, pp. 73–78, Aug. 1880.

[127] U. Charash, "Reception Through Nakagami Fading Multipath Channels with Random Delays," *IEEE Trans. on Commun.*, vol. 27, no. 4, pp. 657 – 670, Apr. 1979.

[128] S. O. Rice, "Mathematical Analysis of Random Noise," *Bell System Technical*, vol. 23, pp. 282–332, 1944. [Online]. Available: http://adsabs.harvard.edu/cgi-bin/nph-bib_query?bibcode=1944BSTJ...23..282R

[129] M. K. Simon and M. Alouini, *Digital Communication over Fading Channels*, 2nd ed., ser. Wiley series in telecommunications and signal processing. John Wiley & Sons, Inc., 2005, ISBN: 978-0-471-64953-3.

[130] R. Mesleh, M. Di Renzo, H. Haas, and P. M. Grant, "Trellis Coded Spatial Modulation," *IEEE Trans. on Wireless Commun.*, vol. 9, no. 7, pp. 2349–2361, Jul. 2010.

[131] M. Nakagami, "The m-distribution – A General Formula of Intensity Distribution of Rapid Fading," in *Statistical Methods in Radio Wave Propagation*, W. C. Hoffmann, Ed., Elmsford, NY, 1960.

[132] N. Beaulieu and C. Cheng, "Efficient Nakagami-m fading channel Simulation," *IEEE Transactions on Vehicular Technology*, vol. 54, no. 2, pp. 413 – 424, Mar. 2005.

[133] K. Pedersen, P. Mogensen, and B. Fleury, "Spatial Channel Characteristics in Outdoor Environments and their Impact on BS Antenna System Performance," in *Proc. of the 1998 48th IEEE Vehicular Technology Conference*, vol. 2, 18-21 May 1998, pp. 719–723.

[134] L. Schumacher, K. Pedersen, and P. Mogensen, "From Antenna Spacings to Theoretical Capacities - Guidelines for Simulating MIMO Systems," in *Proc. of the 13th IEEE International Symposium on Personal, Indoor and Mobile Radio Communications (PIMRC)*, vol. 2, 15-18 Sep. 2002, pp. 587–592.

[135] J. P. Kermoal, L. Schumacher, K. I. Pedersen, P. E. Mogensen, and F. Frederiksen, "A Stochastic MIMO Radio Channel Model with Experimental Validation," *IEEE Journal on Selected Areas in Communications*, vol. 20, no. 6, pp. 1211 – 1226, Aug. 2002.

[136] K. Yu, M. Bengtsson, B. Ottersten, D. McNamara, P. Karlsson, and M. Beach, "Second order statistics of NLOS indoor MIMO channels based on 5.2 GHz measurements," in *IEEE Global Telecommunications Conf. (GLOBECOM '01)*, vol. 1, 2001, pp. 156–160 vol.1.

[137] A. V. Zelst and J. S. Hammerschmidt, "A Single Coefficient Spatial Correlation Model for Multiple-Input Multiple-Output (MIMO) Radio Channels," in *27th General Assembly of the International Union of Radio Science (URSI)*, Maastricht, The Netherlands, Aug. 17–24 2002, pp. 1–4.

[138] G. Auer, V. Giannini, C. Desset, I. Godor, P. Skillermark, M. Olsson, M. Imran, D. Sabella, M. Gonzalez, O. Blume, and A. Fehske, "How Much Energy is Needed to Run a Wireless Network?" *IEEE Wireless Commun.*, vol. 18, no. 5, pp. 40–49, 2011.

[139] C. Desset, B. Debaillie, V. Giannini, A. Fehske, G. Auer, H. Holtkamp, W. Wajda, D. Sabella, F. Richter, M. J. Gonzalez, H. Klessig, I. Godor, M. Olsson, M. A. Imran, A. Ambrosy, and O. Blume, "Flexible Power Modeling of LTE Base Stations," in *IEEE Wireless Commun. and Networking Conf. (WCNC)*, Shanghai, China, Apr. 1–4 2012, pp. 2858 –2862.

[140] B. Hassibi and H. Vikalo, "On the Sphere-Decoding Algorithm I. Expected Complexity," *IEEE Trans. on Signal Process.*, vol. 53, no. 8, pp. 2806–2818, Aug. 2005.

[141] T. Cui and C. Tellambura, "An Efficient Generalized Sphere Decoder for Rank-Deficient MIMO Systems," *IEEE Commun. Lett.*, vol. 9, no. 5, pp. 423 – 425, May 2005.

[142] P. Wang and T. Le-Ngoc, "A Low-Complexity Generalized Sphere Decoding Approach for Underdetermined Linear Communication Systems: Performance and Complexity Evaluation," *IEEE Trans. on Commun.*, vol. 57, no. 11, pp. 3376 –3388, Nov. 2009.

[143] N. Serafimovski, A. Younis, R. Mesleh, P. Chambers, M. D. Renzo, C.-X. Wang, P. M. Grant, M. A. Beach, and H. Haas, "Practical Implementation of Spatial Modulation," *IEEE Trans. on Veh. Tech.*, vol. 62, no. 9, pp. 4511–4523, 2013.

[144] Y. A. Chau and S.-H. Yu, "Space Modulation on Wireless Fading Channels," in *IEEE Vehicular Technology Conference (VTC Fall 2001)*, vol. 3, 7–11 Oct. 2001, pp. 1668–1671.

[145] S. Song, Y. Yang, Q. Xionq, K. Xie, B.-J. Jeong, and B. Jiao, "A Channel Hopping Technique I: Theoretical Studies on Band Efficiency and Capacity," in *IEEE International Conference on Communications, Circuits and Systems*, vol. 1, Jun. 2004, pp. 229 –233 Vol.1.

[146] Y. Yang, S. Song, K. Xie, B.-J. Jeong, and B. Jiao, "A Channel Hopping Technique II: Simulation Result," in *IEEE International Conference on Communications, Circuits and Systems*, vol. 1, Jun. 2004, pp. 234 –237 Vol.1.

[147] Y. Yang and B. Jiao, "Information-Guided Channel-Hopping for High Data Rate Wireless Communication," *IEEE Communications Letters*, vol. 12, no. 4, pp. 225 –227, Apr. 2008.

[148] R. Mesleh, H. Haas, C. W. Ahn, and S. Yun, "Spatial Modulation – A New Low Complexity Spectral Efficiency Enhancing Technique," in *IEEE International Conference on Communication and Networking in China (CHINACOM)*, Beijing, China, Oct. 25–27, 2006, pp. 1–5.

[149] S. Ganesan, R. Mesleh, H. Haas, C. W. Ahn, and S. Yun, "On the Performance of Spatial Modulation OFDM," in *Asilomar Conference on Signals, Systems, and Computers*, Pacific Grove, CA, USA, 29 Oct. - 1 Nov. 2006, pp. 1825–1829.

[150] J. Jeganathan, A. Ghrayeb, and L. Szczecinski, "Generalized Space Shift Keying Modulation for MIMO Channels," in *Proc. IEEE 19th International Symposium on Personal, Indoor and Mobile Radio Communications PIMRC 2008*, Cannes, France, 15–18 Sep. 2008, pp. 1–5.

[151] M. Di Renzo and H. Haas, "Space Shift Keying (SSK) Modulation with Partial Channel State Information: Optimal Detector and Performance Analysis over Fading Channels," *IEEE Trans. on Commun.*, vol. 58, no. 11, pp. 3196 –3210, Nov. 2010.

[152] M. Di Renzo, D. De Leonardis, F. Graziosi, and H. Haas, "On the Performance of Space Shift Keying (SSK) Modulation with Imperfect Channel Knowledge," in *IEEE Proc. of the Global Telecommunications Conference (GLOBECOM)*, Houston, Texas, USA, Dec. 5–9, 2011, pp. 1–6.

[153] M. Di Renzo and H. Haas, "Space Shift Keying (SSK-) MIMO over Correlated Rician Fading Channels: Performance Analysis And a New Method for Transmit-Diversity," *IEEE Trans. on Commun.* , vol. 59, no. 1, pp. 116–129, Jan. 2011.

[154] M. Di Renzo and H. Haas, "On the Performance of Space Shift Keying MIMO Systems Over Correlated Rician Fading Channels," in *ITG International Workshop on Smart Antennas (WSA 2010)*, Bremen, Germany, Feb. 23–24 2010.

[155] M. Di Renzo and H. Haas, "Improving the Performance of Space Shift Keying (SSK) Modulation via Opportunistic Power Allocation," *IEEE Commun. Lett.*, vol. 14, no. 6, pp. 500 –502, 2010.

[156] M. Di Renzo and H. Haas, "Performance Comparison of Different Spatial Modulation Schemes in Correlated Fading Channels," in *IEEE International Conference on Communications (ICC)*, May 2010.

[157] R. Mesleh, S. Gansean, and H. Haas, "Impact of Channel Imperfections on Spatial Modulation OFDM," in *IEEE 18th International Symposium on Personal, Indoor and Mobile Radio Communications (PIMRC)*, Athens, Greece, Mar. 2007, pp. 1–5.

[158] S. U. Hwang, S. Jeon, S. Lee, and J. Seo, "Soft-Output ML Detector for Spatial Modulation OFDM Systems," *IEICE Electronics Express*, vol. 6, no. 19, pp. 1426–1431, Oct. 2009.

[159] M. Di Renzo and H. Haas, "Spatial Modulation with Partial-CSI at the Receiver: Optimal Detector and Performance Evaluation," in *IEEE Sarnoff Symposium*, Princeton, NJ, Apr. 12–14 2010, pp. 1 –6.

[160] E. Basar, U. Aygolu, E. Panayirci, and H. V. Poor, "Performance of Spatial Modulation in the Presence of Channel Estimation Errors," *IEEE Commun. Lett.*, vol. 16, no. 2, pp. 176 –179, Feb. 2012.

[161] R. Mesleh and S. Ikki, "On the Effect of Gaussian Imperfect Channel Estimations on the Performance of Space Modulation Techniques," in *IEEE 75th Vehicular Technology Conference (VTC Spring)*, May 2012, pp. 1 –5.

[162] R. Mesleh, I. Stefan, H. Haas, and P. Grant, "On the Performance of Trellis Coded Spatial Modulation," in *ITG International Workshop on Smart Antennas (WSA'09)*, Berlin, Germany, Feb. 16–19 2009. [Online]. Available: http://www.mk.tu-berlin.de/wsa2009/

[163] S. M. Alamouti, V. Tarokh, and P. Poon, "Trellis- Coded Modulation and Transmit Diversity: Design Criteria and Performance Evaluation," in *Proc. IEEE 1998 International Conference on Universal Personal Communications ICUPC '98*, vol. 1, Florence, Italy, 5–9 Oct. 1998, pp. 703–707.

[164] A. Stefanov and T. M. Duman, "Turbo-Coded Modulation for Systems with Transmit and Receive Antenna Diversity over Block Fading Channels: System Model, Decoding Approaches, and Practical Considerations," *IEEE Journal on Selected Areas in Communications*, vol. 19, no. 5, pp. 958–968, May 2001.

[165] E. Basar, U. Aygolu, E. Panayirci, and H. V. Poor, "New Trellis Code Design for Spatial Modulation," *IEEE Transactions on Wireless Communications*, vol. 10, pp. 2670 – 2680, Aug. 2011.

[166] L. Hanzo, H. Haas, S. Imre, D. O'Brien, M. Rupp, and L. Gyongyosi, "Wireless Myths, Realities and Futures: From 3G/4G to Optical and Quantum Wireless," *Proc. IEEE*, vol. 100, pp. 1853–1888, May 2012.

[167] R. Mesleh, R. Mehmood, H. Elgala, and H. Haas, "Indoor MIMO Optical Wireless Communication Using Spatial Modulation," in *IEEE International Conference on Communications (ICC)*, Cape Town, South Africa, May 22–27 2010, pp. 1–5.

[168] T. Fath, H. Haas, Marco Di Renzo, and R. Mesleh, "Spatial Modulation Applied to Optical Wireless Communications in Indoor LOS Environments," in *IEEE Proc. of the Global Commun. Conf. (GLOBECOM)*, Houston, Texas, USA, 5–9 Dec. 2011, pp. 1–5, 5 pages.

[169] T. Fath, J. Klaue, and H. Haas, "Coded Spatial Modulation applied to Optical Wireless Communications in Indoor Environments," in *IEEE Proc. of the Wireless Communications and Networking Conference (WCNC)*. Paris, France: IEEE, Apr. 1–4 2012, pp. 1000 – 1004.

[170] E. Poves, W. Popoola, H. Haas, J. Thompson, and D. Cárdenas, "Experimental results on the performance of Optical Spatial Modulation," in *Proc. of the IEEE Vehicular Technology Conference (IEEE VTC Fall)*. Quebec City, Canada: IEEE, Sep. 3–6 2012.

[171] J. W. Craig, "A New, Simple and Exact Result for Calculating the Probability of Error for Two-Dimensional Signal Constellations," in *Proc. of the IEEE Military Communications Conference (MILCOM)*, McLean, USA, Nov. 1991, pp. 571–575.

[172] M. K. Simon and M.-S. Alouini, *Digital Communication over Fading Channels: A Unified Approach to Performance Analysis*, 1st ed. John Wiley & Sons, Inc., 2000.

[173] A. Hedayat, H. Shah, and A. Nosratinia, "Analysis of space-time coding in correlated fading channels," *IEEE Transactions on Wireless Communications*, vol. 4, no. 6, pp. 2882 – 2891, Nov. 2005.

[174] G. L. Turin, "The Characteristic Function of Hermitian Quadratic Forms in Complex Normal Variables," *Biometrika*, vol. 47, no. 1/2, pp. pp. 199–201, Jun. 1960.

[175] G. H. Golub and C. F. van Loan, *Matrix Computations*. The John Hopkins University Press, 1996.

[176] H. V. T. Kailath and B. Hassibi, *Space-Time Wireless Systems: From Array Processing to MIMO Communications*, C. P. H. Bolcskei, D. Gesbert and A. J. van der Veen, Eds. Cambridge University Press, 2006.

[177] J. Jalden, L. Barbero, B. Ottersten, and J. Thompson, "The error probability of the fixed-complexity sphere decoder," *IEEE Trans. on Signal Process.*, vol. 57, no. 7, pp. 2711 –2720, Jul. 2009.

[178] X. Xia, H. Hu, and H. Wang, "Reduced Initial Searching Radius for Sphere Decoder," in *Proc. IEEE 18th Int. Symp. on Personal, Indoor and Mobile Radio Commun. (PIMRC)*, Athens, Greece, Sep. 3–7, 2007, pp. 1–4.

[179] M.-S. Alouini and A. Goldsmith, "A Unified Approach for Calculating Error Rates Of Linearly Modulated Signals over Generalized Fading Channels," *IEEE Trans. on Commun.*, vol. 47, no. 9, pp. 1324–1334, 1999.

[180] A. Younis, S. Sinanovic, M. Di Renzo, R. Mesleh, and H. Haas, "Generalised Sphere Decoding for Spatial Modulation," *IEEE Trans. on Commun.*, vol. 61, no. 7, pp. 2805–2815, 2013.

[181] M. Hunukumbure and M. Beach, "MIMO Channel Measurements and Analysis with Prototype User Devices in a 2GHz Urban Cell," in *2006 IEEE 17th International Symposium on Personal, Indoor and Mobile Radio Communications (PIMRC)*, Sept. 2006, pp. 1 –5.

[182] INOTEK Antennas, "Single Band, Dual Polarised Antenna UMTS XP/65/17.5/2, 4, 6, 8 or 10 Type 2209," http://www.inotekantennas.com/pdf/2209.pdf.

[183] W. Thompson, M. Beach, J. McGeehan, A. Younis, H. Haas, P. Grant, P. Chambers, Z. Chen, C.-X. Wang, and M. D. Renzo, "Spatial Modulation Explained and Routes for Practical Evaluation," in *European Cooperation in the Field of Scientific and Technical Research (COST)*, Lisbon, Portugal, 19-21 Oct. 2011.

[184] A. Younis, W. Thompson, M. D. Renzo, C.-X. Wang, M. A. Beach, H. Haas, and P. M. Grant, "Performance of Spatial Modulation using Measured Real-World Channels," in *Proc. of the 78th IEEE Veh. Tech. Conf. (VTC)*, Las Vegas, USA, Sep. 2–5 2013.

[185] National Instruments, *NI PXIe-5622 Specifications*, 2011, 16-Bit IF Digitizer with Onboard Signal Processing.

[186] S. Tiiro, J. Ylioinas, M. Myllyla, and M. Juntti, "Implementation of the Least Squares Channel Estimation Algorithm for MIMO-OFDM Systems," in *Proc. of the International ITG Workshop on Smart Antennas (WSA 2009)*, Berlin, Germany, 16–18 Feb. 2009.

[187] L. Lo Presti and M. Mondin, "Design of optimal FIR raised-cosine filters," *Electronics Lett.*, vol. 25, no. 7, pp. 467 –468, Mar. 1989.

[188] J. L. Massey, "Optimum Frame Synchronization," *IEEE Transactions on Communications*, vol. 20, pp. 115–119, 1972.

[189] H. Xuefei and C. Jie, "Implementation Frame Synchronization for MIMO-OFDM System with ZCZ-codes," in *IEEE Int. Symp. on Microwave, Antenna, Propagation and EMC Tech. for Wireless Commun. (MAPE)*, vol. 1, Aug. 8–12 2005, pp. 241 – 244 Vol. 1.

[190] J.-J. van de Beek, M. Sandell, M. Isaksson, and P. Ola Borjesson, "Low-complex Frame Synchronization in OFDM Systems," in *IEEE Int. Conf. on Universal Personal Commun.*, Tokyo, Japan, Nov. 6–10 1995, pp. 982 –986.

[191] H. Hashemi, "The Indoor Radio Propagation Channel," *Proceedings of the IEEE*, vol. 81, no. 7, pp. 943 –968, Jul. 1993.

[192] D. McNamara, M. Beach, and P. Fletcher, "Experimental Investigation of the Temporal Variation of MIMO Channels," in *IEEE 54th Veh. Tech. Conf. (VTC 2010-Fall)*, vol. 2, Atlantic City, USA, Oct. 7–11 2001, pp. 1063 –1067 vol.2.

[193] F. Quitin, C. Oestges, F. Horlin, and P. D. Doncker, "Multipolarized MIMO Channel Characteristics: Analytical Study and Experimental Results," *IEEE Trans. on Antennas and Propagation*, vol. 57, no. 9, pp. 2739 –2745, 2009.